Techno-Economic Analysis of Sour Gas Oxy-Fuel Combustion Power Cycles for Carbon Capture and Sequestration

by

Nadim Walid Chakroun

B.S., Mechanical Engineering,
Purdue University (2012)
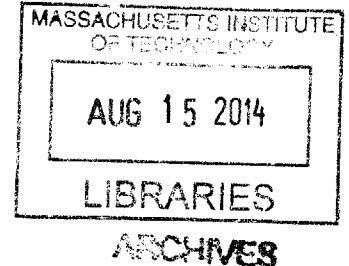
Submitted to the Department of Mechanical Engineering
in partial fulfillment of the requirements for the degree of

Master of Science in Mechanical Engineering

at the

MASSACHUSETTS INSTITUTE OF TECHNOLOGY

June 2014

© Massachusetts Institute of Technology 2014. All rights reserved.

Signature redacted

Author . . . .
Department of Mechanical Engineering

Signature redacted May 9, 2014

Certified by . . . .
Ahmed F. Ghoniem
Ronald C. Crane Professor, Department of Mechanical Engineering

Signature redacted Thesis Supervisor

Accepted by . . . .
David E. Hardt
Professor, Department of Mechanical Engineering
Chairman, Department Committee on Graduate Students

Techno-Economic Analysis of Sour Gas Oxy-Fuel Combustion Power Cycles for Carbon Capture and Sequestration

by

Nadim Walid Chakroun

Abstract

The world's growing energy demand coupled with the problem of global warming have led us to investigate new energy sources that can be utilized in a way to reduce carbon dioxide emissions than traditional fossil fuel power plants. One of these unconventional fuels is sour gas. Sour gas consists of mainly methane, containing large concentrations of hydrogen sulfide and carbon dioxide. Over 30% of the world's natural gas reserves are considered sour. However this unusual fuel poses many challenges due to the toxic and corrosive nature of the combustion products.

One of the most promising technologies for carbon capture and sequestration is oxy-fuel combustion. This involves separating the nitrogen from air prior to the combustion itself. Then, after combustion, we separate the water and other substances and can use the resulting carbon dioxide stream for enhanced oil recovery representing an added economic benefit of this system. Firing temperatures for pure oxygen combustion can reach values up to 2500°C, which is well above what the combustor can handle. Therefore a diluent has to be added to reduce the temperature back to appropriate levels, but the key question is how this impacts the efficiency and performance of the entire cycle. Hence, if feasible, the use of sour gas in an oxy-fuel power plant could potentially allow us to harness the economic and environmental potential of this unconventional fuel.

Depending on the cycle configuration, water or carbon dioxide can be used as diluents to control the flame temperature in the combustion process. All of these cycle types were modeled and the cycles' performances and emissions were studied. When the working fluid condenses in the cycle, sulfuric acid is formed due the presence of SO_x compounds, which causes corrosion and can damage power plant components. Therefore, either expensive acid resistant materials should be used, or a redesign of the cycle is required to overcome this challenge. Different options were explored for each of the cycle types mentioned to help in the visualization and performance prediction of possible sour gas oxy-fuel power cycle configurations. A cost analysis

of the proposed systems was also conducted in order to provide preliminary levelized cost of electricity estimates.

Thesis Supervisor: Ahmed F. Ghoniem
Title: Ronald C. Crane Professor, Department of Mechanical Engineering

Acknowledgments

First and foremost, I would like to express my sincere gratitude to my advisor, Prof. Ghoniem, for all the continuous support and guidance throughout my Masters program.

I am also grateful to Chukwunwike for all the valuable and helpful support that he provided along with Randall Field and Navid Seifkar who were always available whenever I needed their inputs.

I also would like to thank my colleagues working on the Sour Gas Oxy-Combustion project, Santosh Shanbhogue and Dominik Bongartz, for their feedback and assistance. My gratitude also goes out to my lab-mates in the Reacting Gas Dynamics group and Lorraine Rabb who have all been very helpful and supportive.

A big thanks to my sponsors, Siemens, for their generous support and contributions to this work.

There are countless friends who have been there for me throughout this time at MIT and I thank you all for all the experiences we shared and great times we had.

To my family, especially my parents, brother and sister, I thank you endlessly for all your unwavering support and sacrifices along this great journey. My dad, Walid, for being my idol, friend and someone who I will always look up to and try to emulate. My mom, May, for being the compassionate and loving mother that you are and who I always try to make proud through my life achievements. Rami and Leah, I love you both greatly and I look forward to the day where I can just sit back and marvel in your accomplishments and successes in this life. I would also have to thank my grandmother for being a second mother to me and always keeping me humble and grounded, and making me remember where I came from. This thesis is dedicated to all of you.

A final thanks to God for giving me strength and care that I can always rely on throughout my research work.

I end this section with one of my favorite quotes from the best there ever was:

"If you're trying to achieve, there will be roadblocks. I've had them; everybody has had them. But obstacles don't have to stop you. If you run into a wall, don't turn around and give up. Figure out how to climb it, go through it, or work around it."

–Michael Jordan

Contents

List of Figures

12

13

15

16

List of Tables

Chapter 1

Introduction

1.1 The Global Warming Problem

In the late 1950s, a scientist by the name of Charles Keeling first started measuring atmospheric concentrations of CO_2 in Mauna Loa, Hawaii. He found that the mean CO_2 concentrations and the average surface temperature were correlated and were both increasing over time. These curves (see Figure 1-1) have become one of the major icons of global warming and since then the debate of whether CO_2 emissions affect the earth's surface temperature, has never been the same.

Before the 1800s, average atmospheric CO_2 concentrations remained fairly constant at around 280 ppm [35]. But since the industrial revolution there has been a rapid increase in the CO_2 levels, and this has consequently corresponded to an increase in the average surface temperature. Keeling's data further reinforced this idea and Figure 1-1 below shows how the increase in the atmospheric CO_2 concentrations corresponds to an increase in the global temperature anomaly.

Despite the rise in the average surface temperatures, some people still believed that natural variations in the earth's atmosphere could be responsible for this. It took until the 1980s for the whole world to eventually accept the theory of global warming and that increased manmade CO_2 emissions were mainly responsible for this. Efforts to solve this problem within the global community began to arise and the Intergovernmental Panel on Climate Change (IPCC) was founded by the United
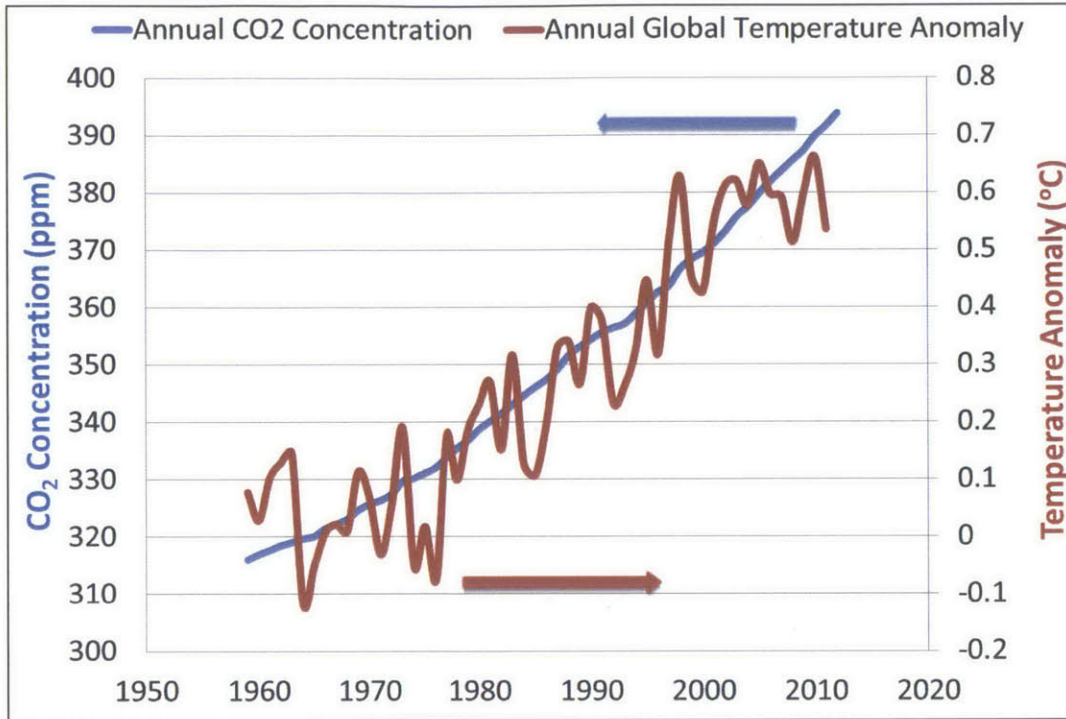
Figure 1-1: Correlation between the annual mean atmospheric CO_2 concentrations at Mauna Loa and the annual global temperature anomaly [1] [36, 37]

Nations Environmental Programme (UNEP). The Panel consists of scientists and experts from all around the world with the purpose of studying the impacts of human induced climate change and measures for mitigation [35].

The data collected by the IPCC on global warming and their future projections on the impact on climate change, prompted the United Nations Framework Convention on Climate Change (UNCC) to adopt the Kyoto Protocol in Kyoto, Japan in 1998. This is an international agreement which requires participating countries to reduce their manmade greenhouse gas (GHG) emissions in an effort to stabilize the problem of global warming [38]. This has stimulated extensive research on the topic of storing or capturing the CO_2 released from various sources, or commonly known as carbon capture and sequestration (CCS).

---

[1] Anomalies are provided as departures from the 20th century average (1901-2000)

1.2   Carbon Capture and Sequestration (CCS)

CO_2 is the primary GHG released into the atmosphere by humans. At the global scale, CO_2 emissions accounted for approximately 77% of all GHG emissions in 2007 [1]. According to the Environmental Protection Agency (EPA), about 26% of all the global GHG emissions were from the energy supply sector (see Figure 1-2). It is also estimated that the world CO_2 emissions from energy production will increase by approximately 43% by 2035, from 30.2 billion metric tons in 2008 to 43.2 billion metric tons in 2035 [2]. As can be seen from Figure 1-3, much of this growth in emissions is attributed to the developing non-OECD countries which continue to rely on fossil fuels to meet their growing energy demand. By 2040, these non-OECD countries are expect to contribute as much as 69% of the world's total emissions, whereas the OECD emissions will total about 14 billion metric tons which is 31% of the world total [2]. Therefore, it can be concluded that the important issue of GHG emissions is a truly global one and more specifically emissions reductions are vital for the developing nations with their ever increasing populations and energy demand.

One strategy to reduce the emissions from this source is through Carbon Capture and Sequestration (CCS). This is a type of technology that captures the CO_2 from power plants, compresses and transports the stream to the site for underground injection in secure geological formations. These formations include natural underground reservoirs, for permanent storage, and oil and gas fields, for enhanced oil recovery (EOR). Figure 1-4 below shows the possible CO_2 storage options.

1.2.1   Enhanced Oil Recovery

EOR increases the amount of oil that can be recovered from an oil reservoir (see Figure 1-5 below). The natural pressure in an oil reservoir pushes the oil to the surface and allows for the recovery of about 30-35% of the well's oil reserves. This means that 65-70% of the oil is still in the ground. EOR further increases the amount of oil that can be recovered by 5-15% [39]. This is because EOR with CO_2 accomplishes three things: reduces the viscosity of the oil, acts as a pressurizing agent inside the well,
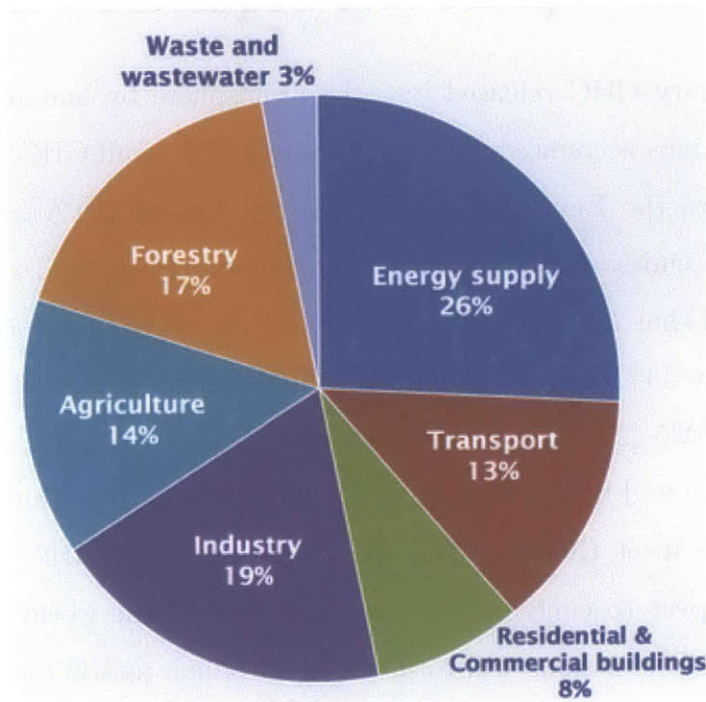
Figure 1-2: Global greenhouse gas emissions by source [1]
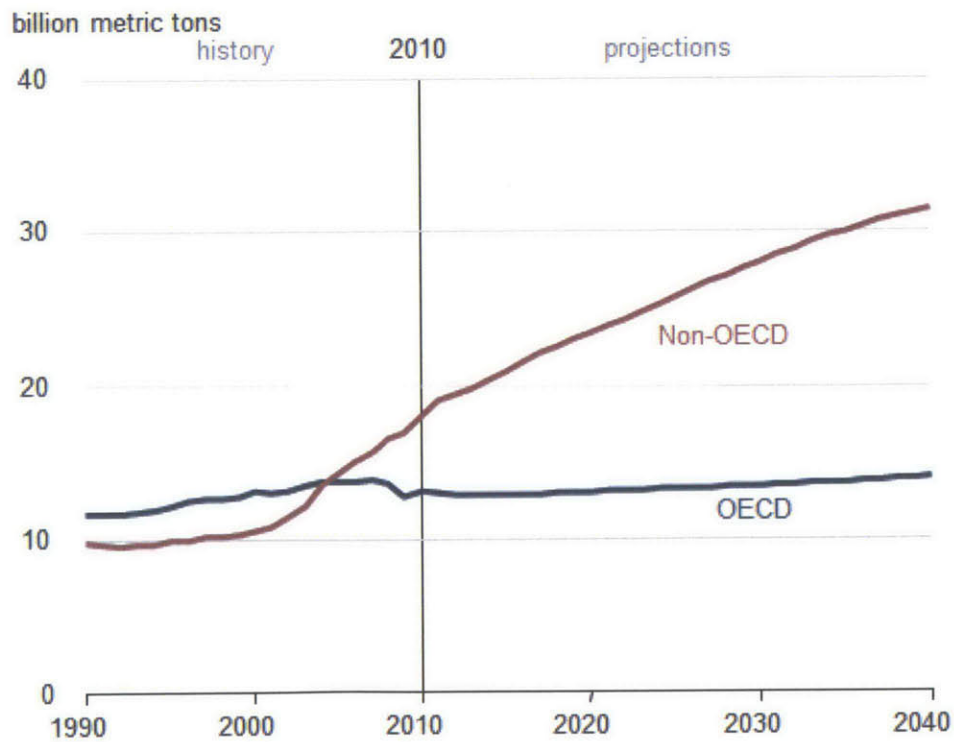
Figure 1-3: World energy-related carbon dioxide emissions, 1990-2040 [2]
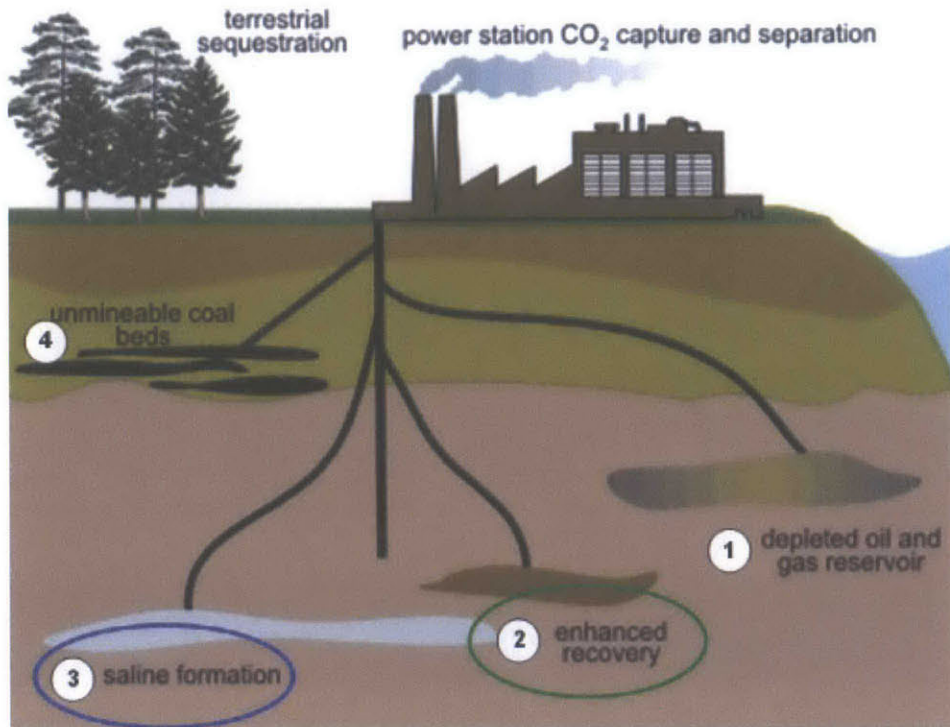
Figure 1-4: Geological CO_2 storage options [3]

and helps free oil trapped in between the reservoir's rocks (see Figure 1-6).

However there are certain purity requirements for the CO_2 stream that can be transported from power plants and pumped underground for EOR. These impose limits on the concentrations of contaminants allowable in that stream. These restrictions aim to prevent issues like corrosion in the pipelines, miscibility problems, and health and safety problems. The presence of non-condensable contaminants increase the compression work per kg of CO_2 transported and increases the minimum miscibility pressure for EOR. The minimum miscibility pressure (MMP) is defined as the minimum pressure at which the CO_2 can achieve multiple-contact miscibility with the reservoir oil. So naturally we would want to try and reduce the minimum miscibility pressure because if the MMP becomes greater than the well fracture pressure, this can be a very big problem and can cause serious damage.

Corrosion due to water and acid condensation, are also big problems. Water corrosion hasn't been much of an issue specifically for Kinder-Morgan, but the presence
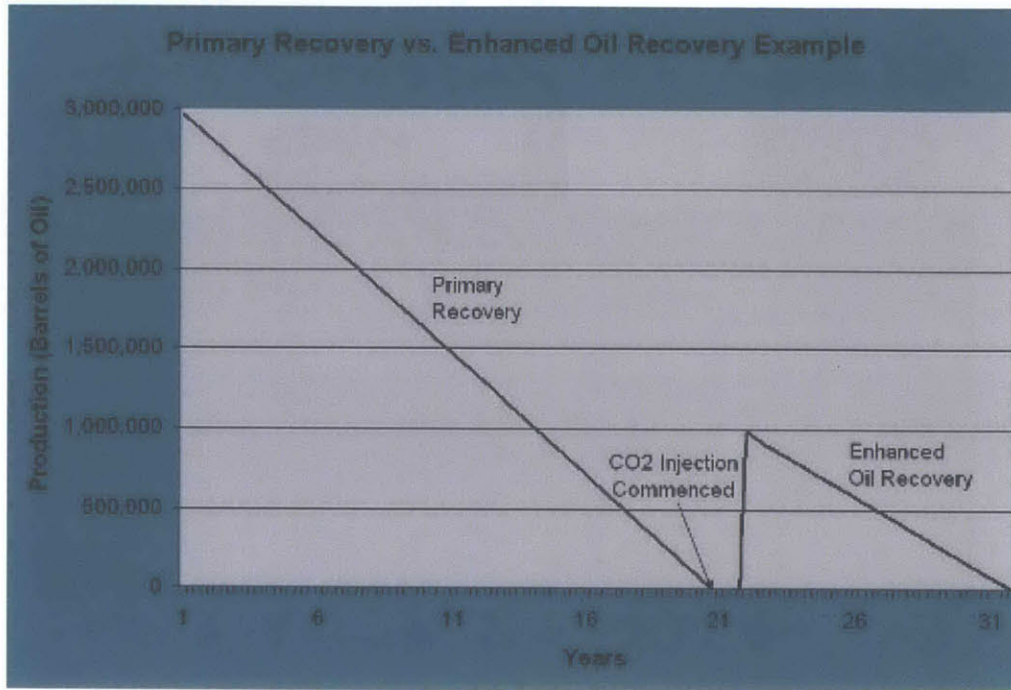
Figure 1-5: Example of the effect of EOR on oil production [3]
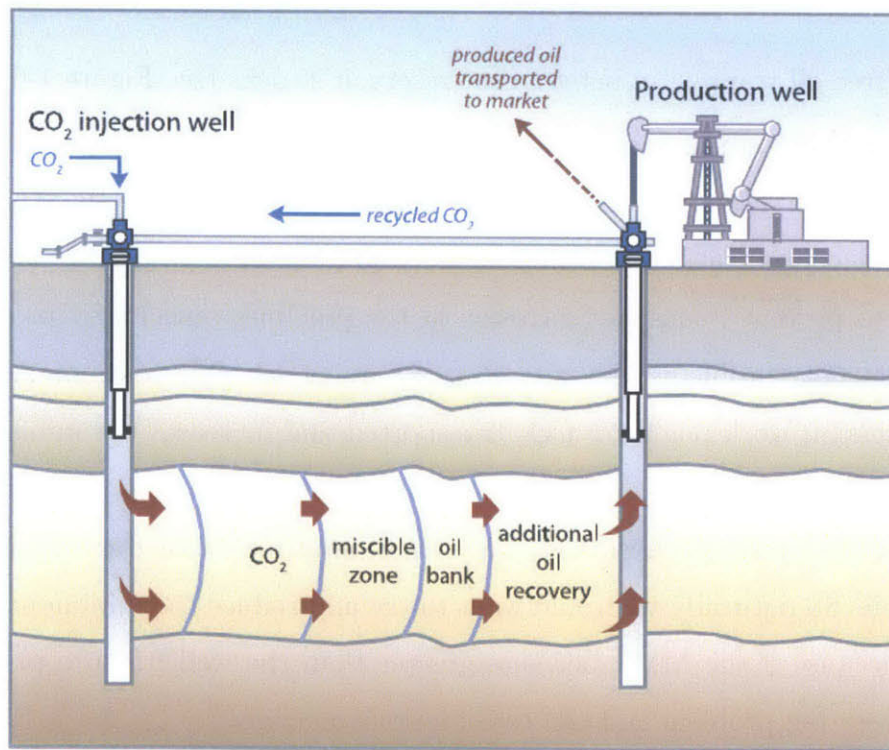
Figure 1-6: Injection of CO_2 for enhanced oil recovery [4]

Compound	Kinder-Morgan EOR	Weyburn EOR
CO_2	> 95% (vol)	> 96% (vol)
H_2S	10-200 ppm	9000 ppm
O_2	< 10 ppm	< 50 ppm
CO	-	< 1000 ppm
H_2O	< 690 ppm	< 20 ppm

Table 1.1: Pipeline specifications from two existing projects [31]

of SO_x in the compressed stream has the potential to form sulfuric acid (H_2SO_4). Unfortunately though, the effects of SO_x on EOR are not as well documented [4]. Although it is known that SO_2 increases the miscibility of CO_2 with the oil, thus improving oil recovery. On the other hand impurities such as O_2 and CO are immiscible with oil and increase the MMP. Finally, high O_2 concentrations can result in overheating at the injection point and oxidation in the reservoir can lead to increases in the oil's viscosity thus increasing extraction costs. Table 1.1 shows the pipeline specifications of certain compounds for two examples just to give an idea of what their safe, maximum concentrations might be [31].

In 2011, there were over 110 EOR operations that existed in the United States with more than 3,900 miles of CO_2 pipeline. In 2010, the US consumed about 19 million barrels of oil per day and it was found that EOR accounted for 281,000 barrels per day, or six percent of the total US oil production [40]. Therefore, you can see the impact that EOR is slowly starting to have on the oil production sector. However, EOR development is constrained by the insufficient supply of CO_2. Most companies tend to buy the CO_2 for EOR, and CO_2 prices are usually indexed to oil prices. Purchasing CO_2 can account for around 68% of the total cost of EOR [4]. Consequently the benefits of implementing CCS technologies (especially oxy-fuel combustion) on current power plants for EOR applications are great. For example, oil companies would be able to use the CO_2 stream from an oxy-fuel power plant, for instance, and use that for EOR to increase their revenues. While at the same time, the energy companies would be able to deliver a near carbon-free form of electricity to their customers which will increase their tax credits and boost their reputation
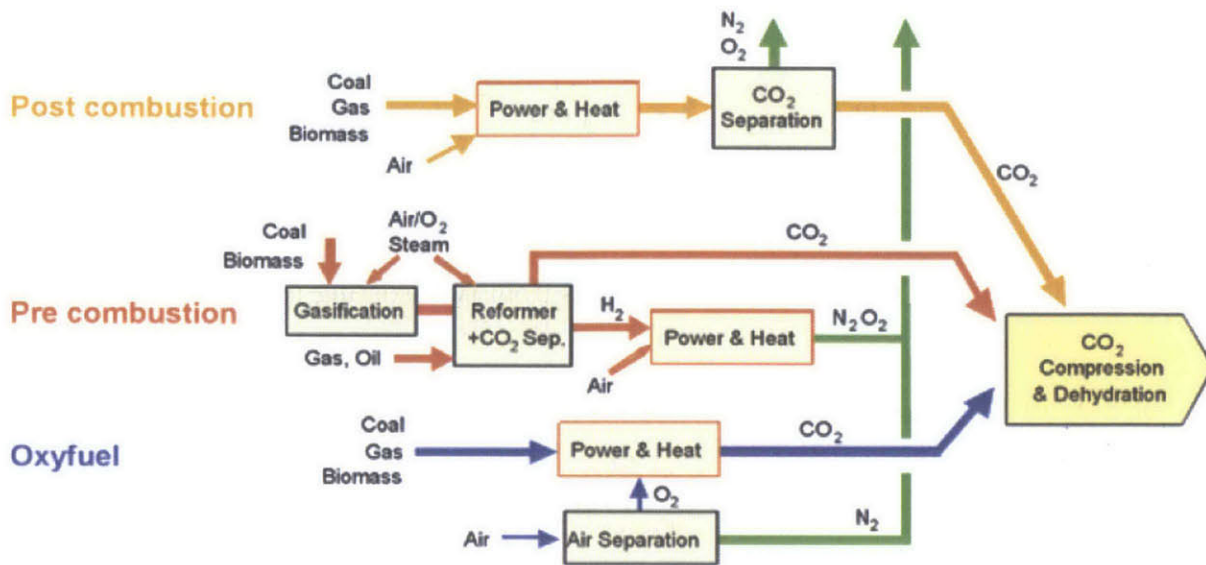
Figure 1-7: The three different CCS technologies [4]

around the world. So it is a win-win situation!

The three main technologies for carbon capture in power plants are: post-combustion CO_2 capture, pre-combustion CO_2 capture and oxy-fuel combustion. The main difference between these technologies is the location at which the CO_2 is removed in the cycle. These three systems are shown in simplified form in Figure 1-7 and explained in greater detail in the forthcoming sections.

1.2.2   Post-Combustion

In post combustion cycles, the CO_2 is removed from the flue gases of a traditional power plant through the use of an added carbon dioxide stripping plant, as shown in Figure 1-8. The most commonly used stripper system is the monoethanolamine absorption cycle. The amine based solution chemically reacts with the CO_2 in the exhaust stream and helps pull it out from the flue gases, the remaining flue gases are then discharged to the atmosphere.

The efficiency penalties associated with using these amine stripping techniques for post combustion carbon dioxide removal were found to be around 8.5% when
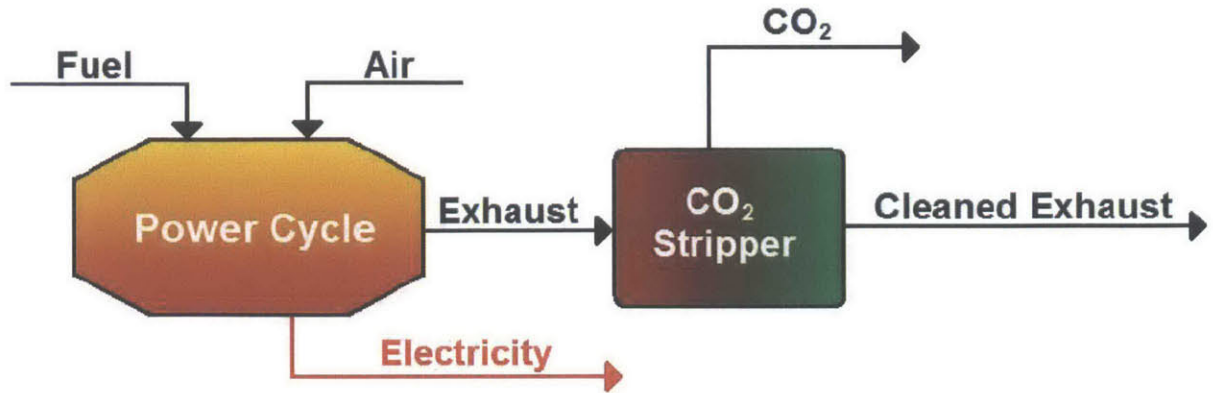
Figure 1-8: A post combustion power cycle [5]

using natural gas as the fuel and around 11.6% when using coal as the fuel [5]. The difference between these two is from the gas cleanup that is required on the flue gases of the coal power plant to remove impurities such as sulfur compounds before they enter the stripping plant. A study by Bolland et al. [41], places the efficiency of a post combustion cycle at 49.6% when using natural gas as the fuel in a traditional air-fired combined cycle with amine absorption. The estimated cost of electricity (COE) for post combustion cycles was found to be around $58/MWh, a 53% increase in the COE over the reference plant without CCS. The capital costs of the cycle also increased by about 80% over the reference plant [4].

The big advantage this cycle has is that the components needed to upgrade existing power plants are commercially available and may be considered to be off the shelf. The original power cycles can be used in their current design with minor modifications. But the limitations of the amine stripping units are that they have yet to be proven for large scale applications. Also as mentioned, post combustion cycles substantially increase the cost of electricity and the absorption cycle requires a high heat input which is a non-trivial loss to the overall energy output of the plant. Another problem lies in the efficiency of the carbon capture process as it is only capable of removing around 90% of the CO_2 from the flue gases compared to almost 100% capture in oxy-fuel cycles [41]. Finally the amine solution that is used in the carbon stripper can be corrosive and reactive, damaging equipment and internal piping systems so it

requires a dilute solution further increasing the capitol costs of the cycle. To conclude, this technology can be regarded as commercially available, but should be developed somewhat further before large-scale applications.

1.2.3   Pre-Combustion

The second type of CCS technology is pre-combustion capture. This type of system removes the carbon as carbon dioxide from the fuel source (typically coal) before the fuel is combusted in the power cycle. The fuel is first gasified to form syngas, a mixture of carbon monoxide and hydrogen. This is done in a gasifier (see Figure 1-9) where the fuel is oxidized in an oxygen deprived environment which does not allow for complete combustion to occur, thus producing syngas. The syngas is then mixed with steam and passed through a water-gas shift reactor which produces carbon dioxide and hydrogen. The CO_2 stream is then separated and compressed for sequestration, and the H_2 stream is sent to the burner of a regular combined cycle. An example of the pre-combustion capture system is the Integrated Gasification Combined Cycles (IGCC) for coal [42].

The efficiency of the pre-combustion cycle with natural gas as the fuel with an auto-thermal reformer (ATR), was found to be 45.3% [41]. Compared to the reference plant which had an efficiency of 58%, the pre-combustion cycle had almost a 13% efficiency drop. This was mainly due to the loss in heating value of the fuel in the reforming process ($\approx$6%-points) and also from the air separation unit needed to produce the oxygen stream. A coal based plant (similar to the one shown above) would have an even lower efficiency due to the efficiency losses from the required gas cleanup to remove sulfur compounds.

This cycle has many components which can be regarded as proven technologies but natural gas pre-combustion cycles have not been demonstrated. They require minor modifications to current gas turbine designs due to the burning of the hydrogen based fuel in the combined cycle. The COE for a natural gas based pre-combustion cycle was found to be around $34.4/MWh, a 60% increase over the reference plant. The capital costs of the plant also increased by about 120% over the reference plant [4].
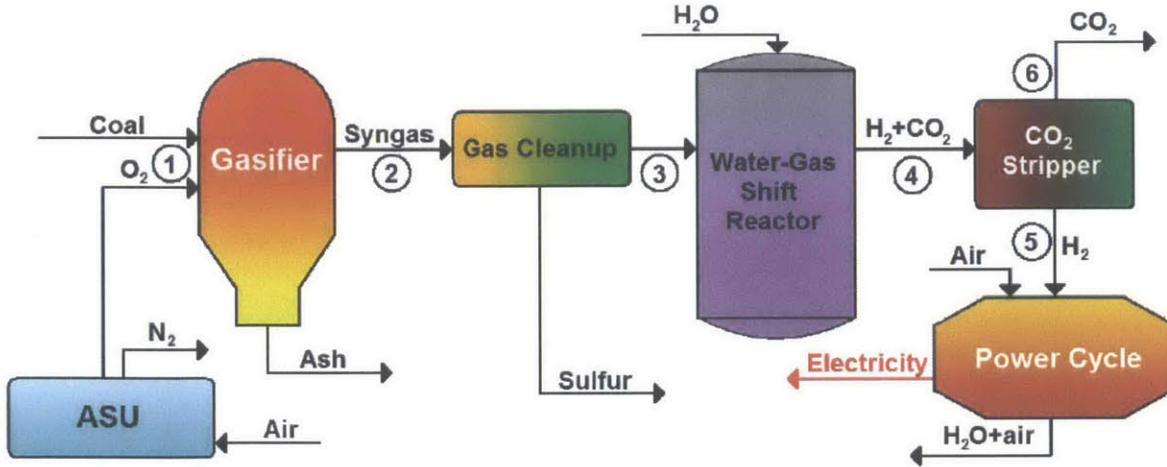
Figure 1-9: A coal pre-combustion power cycle [5]

However IGCC plants are large scale, near commercial examples of pre-combustion cycles being implemented today. The DOE Clean Coal Demonstration Project helped construct 3 IGCC plants: Wabash River Power Station in Indiana, Polk Power Station in Florida (online since 1996), and Pinon Pine in Nevada [43].

1.2.4 Oxy-Fuel Combustion

The third type of CCS technology is oxy-fuel combustion. In oxy-fuel combustion, the fuel is burned in pure oxygen rather than in air, in near stoichiometric conditions so that the products consist of only carbon dioxide and water. The water in the products can easily be separated from the carbon dioxide through condensation and the remaining concentrated carbon dioxide stream can then be used for sequestration. This process has a 99% capture rate, with the only carbon dioxide released being dissolved in the rejected water. Combustion in pure oxygen alone results in very high flame temperatures, due to the removal of the inert nitrogen from air which acts as a heat sink. These temperatures are well above the material limits of some of the components in the cycle such as the turbine blades. Therefore a diluent is commonly added to the fuel and oxidizer to moderate the temperatures in the combustion chamber (see Figure 1-10). Since the products consist of carbon dioxide and water, either of these or both are used as diluents in the combustion process.

31
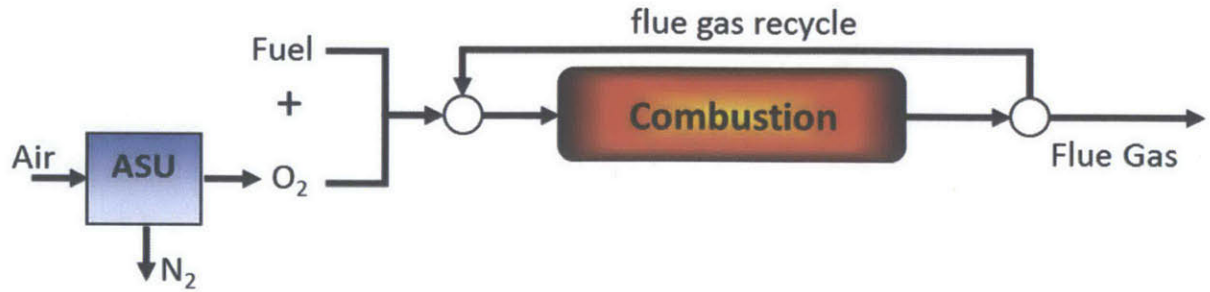
Figure 1-10: The oxy-fuel combustion process

In oxy-fuel combustion cycles, the main technical challenges arise from the high energy penalty and extra cost which comes from producing the pure oxygen stream from the air, and the problems associated with successfully integrating this air separation with the rest of the power plant. The air separation is done in an air separation unit (ASU) which generally utilizes a cryogenic distillation process to separate the air. This is an energy intensive process, consuming about 0.25 kWh/kgO$_2$ with 95% oxygen purity [42]. For a natural gas oxy-fuel cycle, the oxygen production and compression process usually results in an efficiency penalty of approximately 9% [34]. There other advanced air separation technologies still under development, such as the ion-transport membranes (ITM) and chemical looping air separation (CLAS). A more in depth look into the oxygen production is provided in section 1.2.5.

Oxy-fuel combustion offers significant advantages than the other two CCS methods. It doesn't require as expensive and complex retrofits to existing power plants than the other two CCS technologies. However the main obstacle to its implementation is the development of new components such as the CO_2 and H_2O based turbines with blade cooling that handle very high inlet temperatures (1300°C). The flue gas in oxy-fuel combustion (mainly CO_2 and H_2O) is much denser ($\approx$50% higher) than air combustion, therefore this means that the volume of the flue gases decrease, which leads to employing smaller equipment within power plants. In addition, the oxy-combustion environment produces higher gas emissivities and heat capacities which improve the overall heat transfer. Also the specific heat ratio of the new working fluid is lower than air, resulting in a smaller temperature change during adiabatic expan-

32

sion or compression. This is the reason why oxy-fuel gas turbines in combined cycle arrangements have higher optimal pressure ratios (as will be explained in chapter 2) of 30-35 compared to 15-18 with air fired cycles. A final and important advantage of oxy-fuel combustion is the significant reduction in NO_x emissions due to the absence of N_2 in the oxidizer.

For coal combustion, the capital cost for retrofits with oxy-fuel is \$867/kWe, which is significantly lower than the capital cost of post-combustion retrofits (\$1314/kWe) and that of IGCC plants (\$1890/kWe) [42]. There are many different configurations of natural gas oxy-fuel cycles which will be described later on, but their average efficiency was placed at around 47% in a study by Bolland et al. [41]. The estimated COE for natural gas oxy-fuel cycles was found to be around \$50/MWh and the capital costs of the cycle increased by 72% over the reference plant.

The figure below compares all of the three CCS technologies by looking at their efficiencies, COE and the increase in capital cost required. From an efficiency point of view, post combustion cycles seem the most attractive but its COE is higher than the other two and has a high capital cost increase. The oxy-fuel combustion cycles seem like the best bet since they have relatively high efficiencies and low COEs and capital costs. One thing to note in the figure is that the data for COE and capital costs were from a 2005 report by the Intergovernmental Panel on Climate Change (IPCC), and so since then the efficiencies and costs of the ASUs have been significantly improved. This will reduce the COE for the oxy-fuel cycle making it comparable to the pre-combustion cycles. The pre-combustion cycle has a low COE but a very high capital cost increase over the reference plant and relatively low efficiency, all of these make it seem somewhat unattractive compared to the other two. However the remaining focus of this work will be on natural gas oxy-fuel cycles specifically with sour gas as the fuel (see section 1.3).
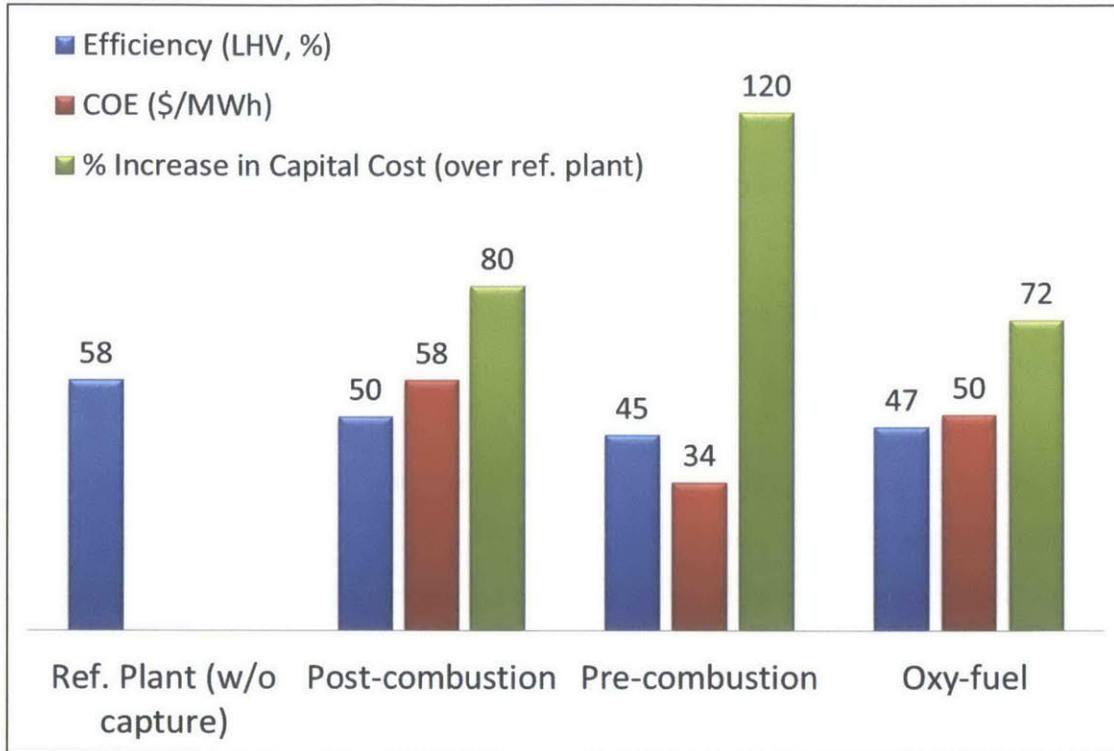
Figure 1-11: Comparison of the different CCS technologies w.r.t net efficiency and COE

1.2.5 Oxygen Production

A critical aspect of oxy-fuel combustion is the production process of the oxygen stream. In a 500 MW oxy-fuel power plant, over 10,000 tons of oxygen are consumed per day [44]. For such large scale applications, cryogenic separation using distillation columns is the only proven and available option that meets the volume and purity demand. This is a technology that has been practiced for over 100 years. An alternative technology that promises a lower energy penalty and lower cost is ion transport membranes (ITM), although this technology is still being developed.

Cryogenic Oxygen Production

The air separation unit, based on cryogenic distillation, in an oxy-fuel cycle accounts for around an 8% efficiency loss [34]. Therefore it is crucial to optimize the integration of the ASU with the cycle and find a way to increase its exergetic efficiency to improve
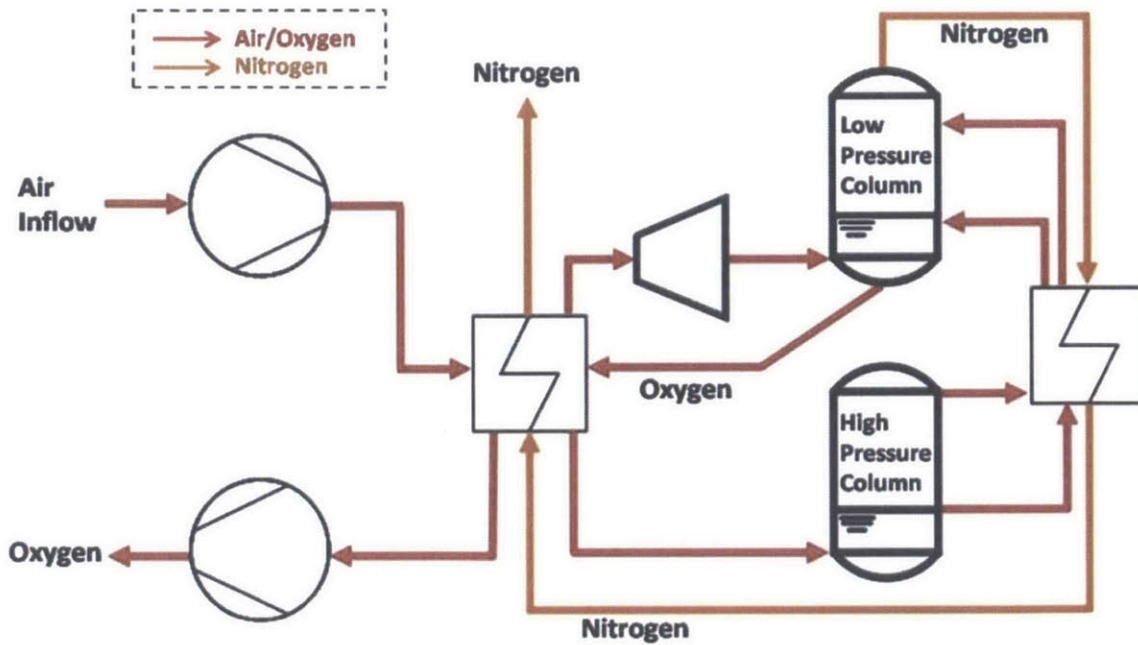
Figure 1-12: The process layout for oxygen production using cryogenic distillation [6]

the overall efficiency of the cycle. In a two distillation column system (see Figure 1-12), the ASU delivers an oxygen stream with 95% (vol.) purity and with the specific energy of production of 0.245 kWh/kg-O_2 [6]. The ASU's power requirement is quite sensitive to the oxygen purity (see Figure 1-13), as the oxygen purity decreases from 97% to 90%, the energy requirement also decreases by about 3%.

The air separation process is shown in the figure above. The feed air is first compressed up to a pressure of 5.5 bars by a two stage air compressor. Then the pressurized air passes through the regenerator to remove impurities such as water and CO_2 which could cause problems in the distillation columns, and then cooled against the returning products (oxygen and nitrogen). The resulting air is separated into pure oxygen and nitrogen in the double-column distillation system and the oxygen stream is then compressed up to the desired level and sent to the combustor of the oxy-fuel cycle.
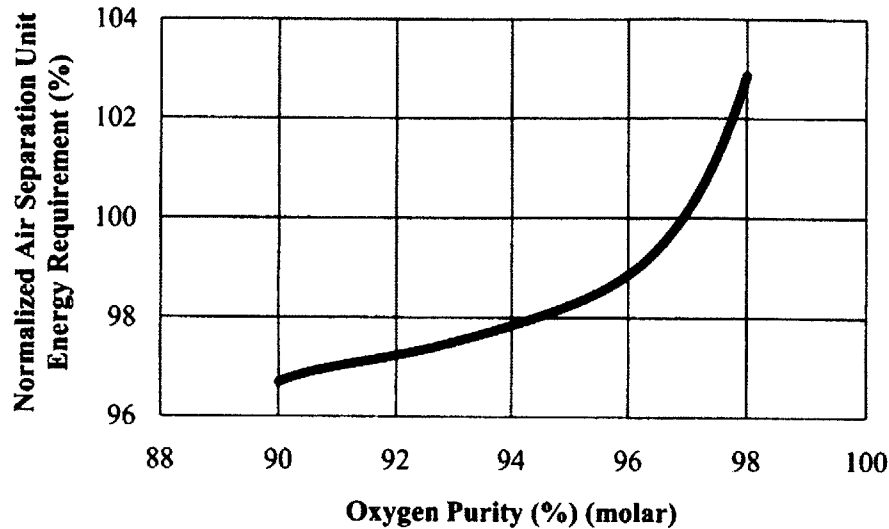
Figure 1-13: Normalized energy requirement of cryogenic air separation unit based on oxygen purity (100%-energy at 97%-oxygen purity) [7]

Ion Transport Membranes (ITM)

ITM's are another way to separate the oxygen from air, by exploiting the oxygen partial pressure gradient across a ceramic membrane. These thin non-porous, mixed-conducting membranes promise lower efficiency penalties and lower costs than traditional cryogenic air separation methods, when they are successfully developed for large scale applications. The temperatures in the ITMs are usually very high compared to traditional air-fired cycles, about 800-900°C [45].

Ceramic mixed metal oxides exhibit simultaneous oxygen ion and electron conduction at the high temperatures mentioned above. The difference in oxygen partial pressure across the membrane will cause the oxygen molecule to ionize, and pass into the crystal structure on the ceramic surface. While at the same time, on the permeate side of the membrane, the oxygen ions will give up their electrons and leave the ceramic structure as a molecule. One problem with these types of membrane configuration is that the oxygen can accumulate on the sweep side of the membrane, thus decreasing the oxygen flux. Hong et al. [8] have a proposed a system shown in Figure 1-14 that allows oxygen to pass through the membrane to the sweep side and then mix with the fuel stream and generate heat through the combustion process.
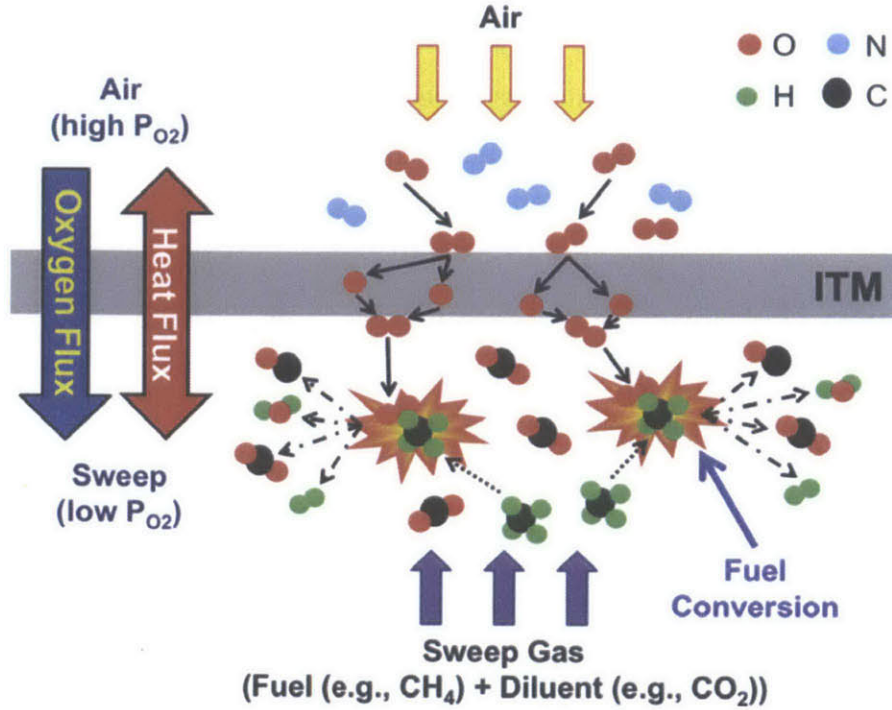
Figure 1-14: Diagram showing the process of oxygen separation and fuel conversion simultaneously [8]

The combustion of the fuel burns the oxygen away, decreasing the partial pressure, thus allowing room for more oxygen to flow through. The combustion products can then be used to drive a turbine in an oxy-fuel cycle. This system would be more compact and less complex than having the oxygen separation and combustion processes separate.

The formula governing the oxygen flux through the membrane is [45]:

$$j_{O_2} = \frac{\sigma_i RT}{4Ln^2 F^2} ln\frac{P'_{O_2}}{P''_{O_2}} \tag{1.1}$$

where j_{O_2} is the oxygen ionic flux, σ_i is the ionic conductivity (material property), R is the ideal gas constant, T is the absolute temperature, L is the membrane thickness, n is the charge of the charge carrier (=2), F is Faraday's constant, P'_{O_2} is the oxygen partial pressure at the air side of the membrane, and P''_{O_2} is the oxygen partial pressure at the sweep side of the membrane.

Therefore as you can see from this equation, the partial pressure ratio across the

membrane is the main driving force for the oxygen flux. Also the flux is inversely proportional to the membrane thickness, therefore the membrane should be as thin as possible to maximize the oxygen flux, but also be capable of supporting the pressure gradient necessary.

When these ITMs are integrated with the rest of the cycle for large scale applications, their performance is very comparable to cycles with cryogenic ASUs. Currently IGCC systems seem like the best fit for ITMs since they already operate at the high pressure required by ITM technology. In a study by Dyer et al. [45] comparing the two different air separation methods, it was found that the ITM system saved about one-third of the installation cost of cryogenic ASUs. When looking at the whole cycle, an IGCC plant with ITM had a 1-3% point efficiency increase with about a 6.5% reduction in the cost of electricity [45].

Oxy-fuel cycles with ITMs have also been studied in the literature mainly for methane as the fuel. An example of one is the advanced zero emission power plant (AZEP), shown in the figure below. The cycle incorporates an ITM operating at about $800\text{-}1000°C$ in a standard air-based combined cycle arrangement. The combustion chamber has been replaced by an ITM reactor that separates the oxygen from the hot air, combusts the fuel with the oxygen while simultaneously heating up the oxygen depleted air that will be used to run the gas turbine combined cycle. The combustion products are then partially recycled to moderate the temperatures in the ITM reactor, and the remaining is expanded in the turbine to produce work. The net efficiency of this type of cycle was calculated to be between 49-50% including the efficiency penalty of the CO_2 compression. This is a 1-3% point increase over the other oxy-fuel cycles with cryogenic ASUs [34]. The main challenge with cycle, other than the development of the ITM reactor, is the CO_2/steam turbine which has not been developed yet for commercial applications and remains in the design stage. This will be discussed further in section 2.2.1. Therefore there is a great potential for ITMs to be used in oxy-fuel cycles and IGCC plants if they are successfully developed and are able to handle large scale applications.
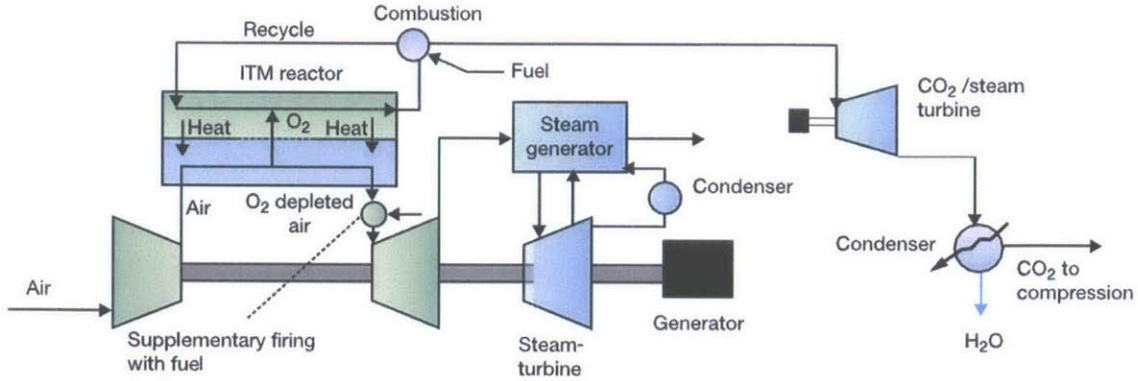
Figure 1-15: The advanced zero emission power plant (AZEP) cycle [4]

1.3   Why Sour Gas?

Oxy combustion has usually been associated with coal because it is considered dirtier than natural gas, and coal power plants produce about two times as much CO_2 per MWh than natural gas power plants [1]. Natural gas' share of the world's electricity generation is expected to grow from 22% in 2010 to 24% in 2040 [2]. Natural gas is also predicted to be one of the fastest-growing sources of electric power in the future. Therefore as we move away from coal and petroleum and towards renewables, natural gas is the natural stepping stone in this slow transition. From Figure 1-16 below, which shows the estimated cost of electricity by source, it is clear that natural gas cycles for CCS are much more economical than solar and wind energy technologies in the short run and so efforts have now been shifted towards developing these cycles further. However for our analysis we will be focusing on a special form of natural gas called sour gas.

Sour gas consists of three major components: hydrogen sulfide (H_2S), methane (CH_4) and CO_2. This is the main form of natural gas extracted from gas fields before any major purifications are done. Example compositions of these components for a couple of different wells are shown in Table 1.2 below. These may not be the typical compositions for a gas well as the composition values may change depending on the life of the well, location and geography.

When sour gas is burnt in the combustor with pure oxygen, the products will

Figure 1-16: Estimated levelized cost of electricity generation in 2018 [9]

Gas Field	Compositions (% vol.)		
	CH_4	H_2S	CO_2
South Pars, Iran	97%	1%	2%
Lacq, France	69%	16%	10%
LaBarge, Wyoming, USA	21%	5%	65%

Table 1.2: Three examples of sour gas compositions at different gas fields [32, 33]

	Temp. (K)	Press. (bar)	R_{gas} (J/kg-K)	Density (kg/m^3)	C_p (J/kg-K)	Specific Heat Ratio, γ
Air	1500	40	288.2	9.291	1217.7	1.31
CO_2	1500	40	188.9	14.12	1327	1.166
H_2O	1500	40	461.5	5.778	2628	1.219
SO_2	1500	40	129.8	20.55	887	1.171
SO_3	1500	40	103.8	25.68	995.2	1.117

Table 1.3: Typical thermodynamic properties of gases in the working fluid after the sour gas oxy-combustion at the sample operating conditions shown [2]

mainly consist of CO_2, H_2O, SO_2 and SO_3. H_2SO_4 will also form downstream as the working fluid is expanded and cooled in the turbines and the SO_3 reacts with the H_2O. This will be discussed later on. Some thermodynamic properties of these gases are shown in the table above for a sample temperature and pressure, at the exit of the combustor. For an oxy-fuel cycle with CO_2 recycle (see section 2.2.1), the working fluid is mainly CO_2 and a preliminary observation of the sour gas working fluid properties shows that the sulfur byproducts of combustion have some similar properties to the CO_2. For example the average density of the sulfur-based gases is about 60% higher than that of CO_2, also the specific heat ratio is very close to the CO_2. Therefore when designing compressors and turbines for this new working fluid, they can benefit from the turbo machinery development of the CO_2 based working fluid. However the exact compositions of these gases, and hence the working fluid properties, will depend on what type of reaction mechanism is employed in the oxy-fuel combustor to simulate the combustion process (this will be developed in a separate work). It will also depend on the operating conditions of the combustor and turbines, which will be determined from this cycle analysis of sour gas oxy-combustion.

Nearly 40% of the world's gas reserves can be classified as being sour [32]. The levels of CO_2 and H_2S in the wells pose obstacles for the extraction and development of the gas reservoirs due to safety and practical considerations. After a certain concentration, companies can no longer extract the gas as it becomes too sour and the difficulties of extraction outweigh the benefits.

---

[2]Properties evaluated using Engineering Equation Solver (EES)

The main objective of this work is to use sour gas directly as the fuel in an oxy-combustion power plant for CCS which can then be used for enhanced oil recovery (EOR). The big benefits of using this unusual fuel, is that it saves on the energy consumed by the natural gas purification plant (see Figure 1-17). We can now send the gas directly from the well or reservoir to the power plant and then use the CO_2 stream for injection back into the well thus eliminating the CO_2 emissions of the power plant. As previously mentioned CO_2 injection can greatly increase the life of the reservoir and so this will result in increased revenues for companies. However it is not going to be that simple since sour gas combustion produces various harmful pollutants (H_2SO_4, SO_x) which can damage equipment (corrosion) and also affect the transportation and storage of the CO_2 stream for EOR, as mentioned in the previous section. Therefore an important part of the analysis is limiting the concentrations of these harmful emissions. Since sour gas combustion, specifically for oxy-combustion, has not been studied before in the literature, the way to proceed with this issue is to study the natural gas oxy-cycles and also the sulfur chemistry and then find a way to connect them together.
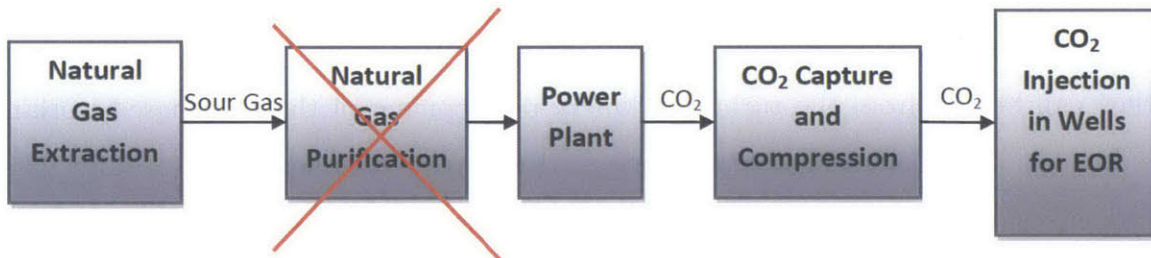
Figure 1-17: Natural gas life cycle process

1.4 Conclusions

Global warming and climate change are becoming important world-wide issues that need to be tackled. CO_2 emissions from burning fossil fuels will continue to increase and contribute to global warming if nothing is done about it. Since fossil fuel consumption is still expected to grow in the near future, one option to reduce these

42

emissions is by carbon capture and storage. More specifically oxy-fuel combustion in power plants is emerging as an important technology that can deliver a purified CO_2 stream to be used for sequestration or EOR. Also since natural gas is predicted to be one of the fastest-growing sources of electric power in the future, this type of fuel will be studied in this work but looking at a more specific type which is called "Sour Gas".

In the next chapter, a thorough literature review will be presented looking at all the common oxy-fuel combustion power cycles that are modeled in the literature. This will help us in constructing the sour gas cycles later on in this thesis. In Chapter 3, the base-case cycles are discussed along with all the important modeling assumptions and cycle components that are critical in oxy-combustion cycles. Then the two types of sour gas cycles are discussed and explained along with sensitivity studies that were done looking at the effects of pressure in Chapters 4 and 5. Finally, cost estimates for the various sour gas cycle configurations developed are presented in Chapter 6 and then Chapter 7 wraps up with the summary and conclusions of this work.

.

Chapter 2

Literature Review

Unfortunately there is a lack of research in the area of sour gas oxy-combustion explicitly but there has been work done on the oxy-combustion of coal, looking at the impacts of sulfur in the fuel specifically [10, 46]. Once again this isn't exactly the same as what would happen in sour gas because the sulfur compound present in the natural gas is in the form of H_2S. There is also a lot of work that has been done on the cycle analyses of different oxy-fuel cycles that use pure natural gas (mainly methane) as the fuel. So by combining these two types of works, a decent idea can be obtained about how to design a sour gas oxy-combustion cycle that meets most of the constraints described previously.

2.1 Sulfur Chemistry

The presence of sulfur in the fuel poses many challenges, mainly due to SO_x and sulfuric acid (H_2SO_4) formation. Sulfuric acid is a highly corrosive substance which can cause severe problems if it comes into contact with metal materials in the turbines, heat exchangers, pumps... etc. Therefore once we know where sulfuric acid might form in the cycle, care must be taken to ensure that the operating conditions at that point are well above the acid dew point temperature to prevent corrosion issues. This will especially be a problem in the low pressure components of the cycle (i.e. condenser and low pressure turbine). SO_x formation (mainly SO_2 and SO_3) is also a

45

major problem as these compounds can also cause corrosion but they can cause issues in the CO_2 compression, transportation and underground injection; as well as some being toxic chemicals if leaked into the atmosphere. The isothermal compression and purification energy consumption of the flue gas stream was found to be most sensitive to changes in SO_x compared to the other impurities [47]. Another problem found after the compression stage, was that NO_x species can almost completely catalytically convert the SO_2 to H_2SO_4; which is potentially corrosive [46].

During transportation of the CO_2 stream for sequestration there are certain pipeline specifications for the maximum concentration of SO_2 in the flue gas, an example recommendation from the European 6th Framework Programme, Dynamis is 100 ppm due to the toxicological health effects in the event of a leak [31]. There are similar concentration limits given by Dynamis for the moisture content in the pipelines to prevent corrosion from carbon and sulfur based acids. When transported to the site, there are also limits on the impurities in the CO_2 stream that can be pumped into the ground for EOR. However SO_2 injection with CO_2 is not as established and documented as H_2S injection, but SO_2 does have the advantage in that it increases the miscibility of CO_2 with the oil when injected underground in the CO_2 stream [46]. On the other hand there is a limit on the concentration of SO_2 that can be injected since it is very toxic if there are any leakages and it can alter the acidity of the well, decreasing the well's life.

At high temperatures (usually $>1000°C$) and oxygen-rich conditions, SO_2 is the thermodynamically favored SO_x. As the temperature goes down, the equilibrium shifts towards SO_3 but the reaction rate decreases with temperature so the concentration of SO_3 is low compared to SO_2 in the exiting flue gas stream. Nonetheless, there is a sufficient concentration of SO_3 that will react with the water in the flue gases to form sulfuric acid, at temperatures below $500°C$, which can damage metal equipment in the combustion system if allowed to condense [10]. Therefore studying SO_3 formation is also an important issue. The relevant reactions for the formation of SO_3 are:

$$SO_2 + O \longrightarrow SO_3 \qquad (2.1)$$

$$SO_2 + OH \longrightarrow HOSO_2 \qquad (2.2)$$

$$HOSO_2 + O_2 \longrightarrow SO_3 + HO_2 \qquad (2.3)$$
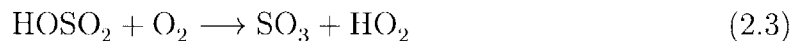
In a recent study by Fleig et al. [46] on the oxy-fuel combustion of lignite, a kinetic model was used to simulate the conversion of SO_2 to SO_3 during cooling of the flue gases. The model assumed a plug flow reactor with the predefine temperature profile and it was assumed that the flue gases after complete combustion, were at their equilibrium compositions and at the peak temperature ($\sim$1600 °C). Their modeling results found that SO_3 was primarily formed during cooling in the temperature range of 600-1400 °C, over a one second period. Reaction 2.1 above was mainly responsible for the formation over the higher temperature range of 1000-1400°C, and the two step lower temperature path (reactions 2.2 and 2.3) accounted for the remaining over a temperature range of 600-1000°C. Reactions 2.2 and 2.3 are also influenced by the reaction below; the amount of CO_2 present affects the concentration of the OH-radical (reaction 2.4) which in turn affects reaction 2.2.

$$CO_2 + H \longrightarrow CO + OH \qquad (2.4)$$

Another problem that can occur from sulfur compounds, as previously mentioned, is the sulfuric acid formation and condensation that can occur as the flue gases go through the cycle and cool down. It is vital to keep the temperature of the gases above the sulfuric acid dew point temperature in order to prevent condensation of the acid, which can then cause corrosion problems when it comes into contact with metal equipment in the cycle components. The concentrations of both SO_3 and H_2O are of importance for the acid dew point temperature. In the figure below, the acid dew point temperature is plotted as a function of the SO_3 concentration for three different water concentrations. It shows that the acid dew point temperature increases with the concentrations of SO_3 and H_2O in the flue gas. The influence of the

H_2O content in the flue gas is significant because by wet flue gas recycling, the dew point temperature increases by about 20°C depending on the SO_3 concentration in the flue gases, compared to dry recycling [10]. This means that we have to be careful in choosing and designing the best cycle to use for sour gas combustion. A drawback of a cycle with wet recycling would be that the operating conditions of the cycle would have to be at higher temperatures to prevent sulfuric acid condensation, affecting the system performance and cycle complexity. However there are other factors which influence the acid dew point temperature which still need to be explored in order to properly predict the dew point at different points in the cycle. Some of these factors include but are not limited to: pressure, equivalence ratio, dilution ratio in combustor and the type of diluent. After this analysis, a better design of the cycle can be made that would prevent or minimize sulfuric acid condensation and also help determine the optimal operating conditions.
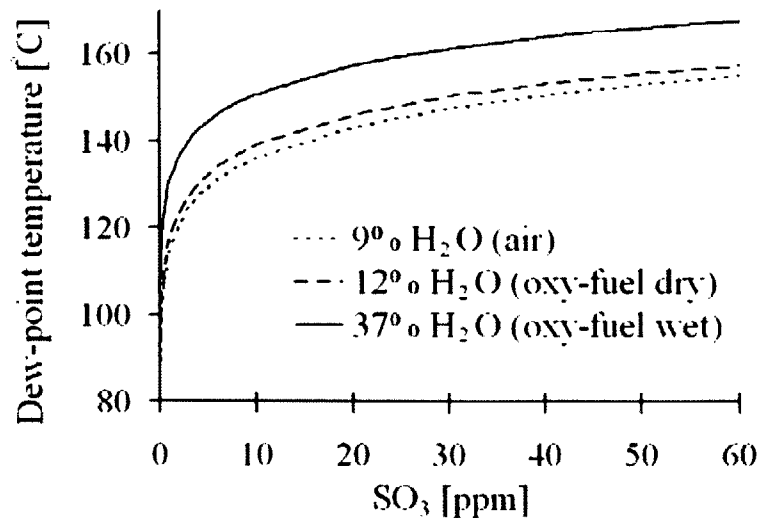
Figure 2-1: Acid dew-point temperature as a function of SO_3 concentration for 3 water concentrations (P= 1 atm) [10]

48

2.2 Methane Oxy-Fuel Cycles

Oxy-fuel cycles have the great advantages of almost eliminating NO_x emissions, and also providing a simpler mechanism to capture CO_2 since the flue gases consist of only CO_2 and H_2O. But due to the fact that combustion of the fuel is in pure oxygen, the flame temperature is very high and so a diluent is needed to absorb some of that heat and moderate the temperatures in the combustor. The diluent used is usually some form of the recycled flue gases. Semi-Closed Oxy-fuel Combustion Combined Cycles (SCOC-CC) [12, 14, 15, 34] recycle part of the CO_2 and use it as the diluent. In Water cycles (also called CES cycles) [34, 48, 49], the H_2O is separated from the flue gases in the condenser and then recycled back to the combustor. The Graz cycle [12, 22, 34] on the other hand, adopts both CO_2 and H_2O recirculations. These three cycles are the main arrangements for natural gas oxy-fuel power cycles in the literature and will be used in the analysis of determining and designing the best cycle for sour gas combustion.

2.2.1 Semi-Closed Oxy-fuel Combustion Combined Cycle

Cycle Description

The SCOC-CC is similar to a traditional combined cycle with the important difference being that the combustor burns the input fuel in an oxygen rich environment. It consists of a high temperature Brayton cycle and a conventional bottoming steam turbine cycle (Rankine Cycle) with an unusual working fluid consisting of mainly CO_2 [15]. As mentioned before, compressed CO_2 gas is supplied to the combustor as a diluting medium. Figure 2-2 below depicts the form of the cycle and its components. The compressed fuel along with a nearly stoichiometric mass flow of oxygen is supplied to the combustor and burned. The exhaust gases are used to drive a turbine and then flow to a heat recovery steam generator (HRSG) to produce the high pressure steam for the bottoming cycle. The bottoming cycle consists of a steam turbine, a condenser and pumps. After the HRSG, the working fluid passes through a condenser which condenses and separates the liquid H_2O from the CO_2 rich working fluid. A certain
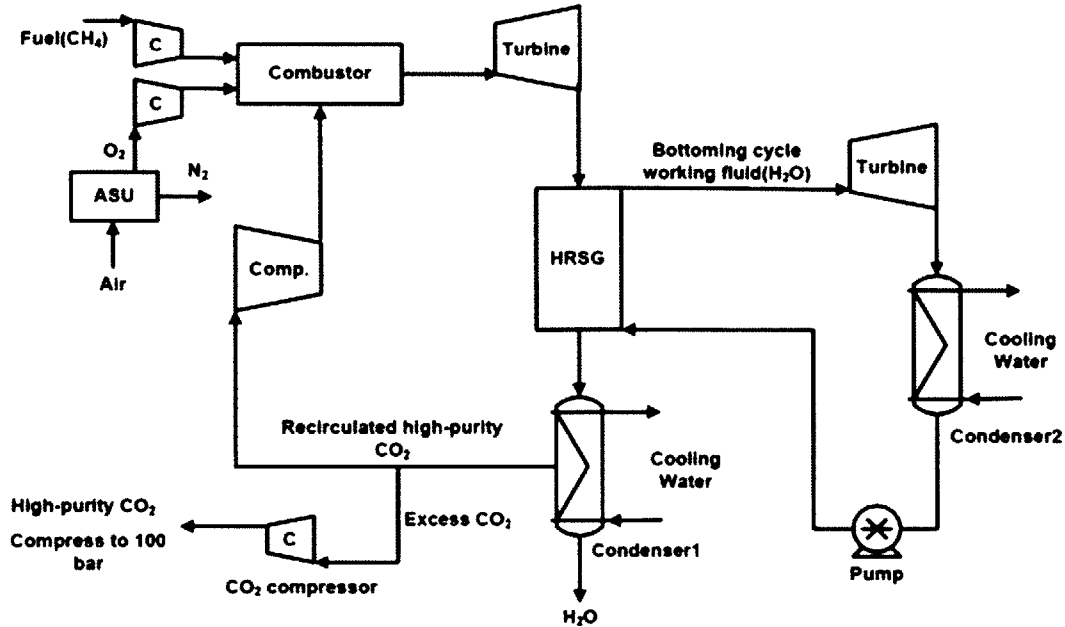
Figure 2-2: SCOC-CC simple cycle diagram [11]

amount of the CO_2 is extracted for CCS and the remaining is then recirculated back to the compressor and combustor to close the cycle. The amount of recirculation fluid is decided in order to meet the desired turbine inlet temperature for the cycle.

Most of the SCOC-CC's are modeled with a standard operating pressure of 40 bars (pressure of the topping cycle) and topping cycle turbine inlet temperatures (TIT) of around 1400 °C [11, 12, 14]. Some of the differences between the cycles are the number of turbines in the bottoming steam cycle, the pressures of the bottoming cycle, and the TIT's of the bottoming cycle. One SCOC-CC configuration is shown in Figure 2-3 below [12], with the corresponding T-s diagram shown in Figure 2-4. The composition of the working fluid at the exit of the HTT consists mainly of 94% CO_2 and 6% H_2O (mass fractions) at a pressure of 1.06 bar and a temperature of 618°C. These hot exhaust gases are then cooled down to 65°C in the HRSG, superheating the steam for the bottoming steam cycle. In the atmospheric condenser, the working fluid is cooled to 18°C which allows the H_2O to be extracted in the liquid state, leaving a near pure CO_2 stream for compression and EOR or for recirculation in the cycle. The CO_2-rich working fluid then flows into the compressor, C1 and then part of it flows

50
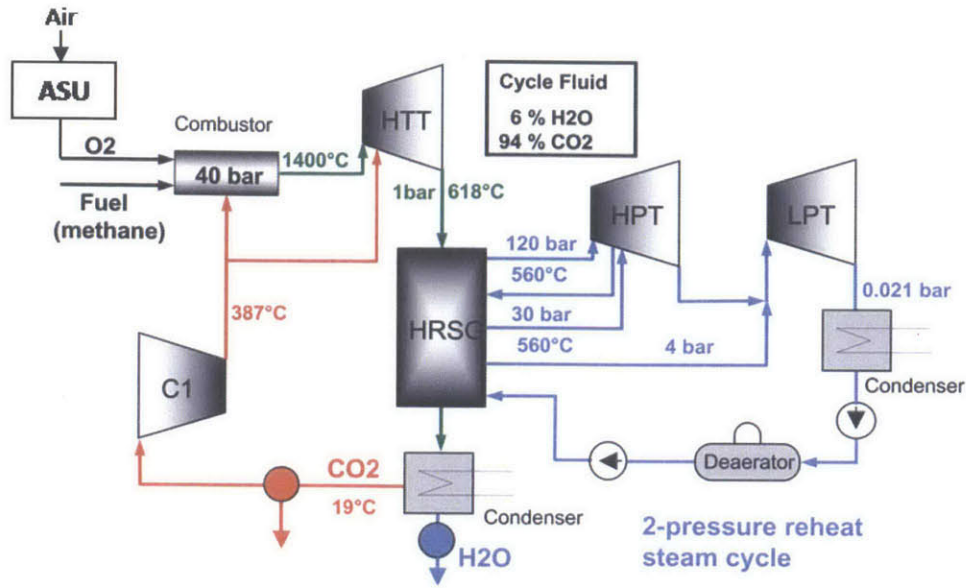
Figure 2-3: SCOC-CC cycle diagram showing operating conditions [12]

to the combustor and then the rest goes to the HTT for cooling at a temperature of 387°C. The necessary cooling mass flow is 30.5% of the HTT inlet mass flow, this high percentage is due to the low heat capacity of the CO_2. The bottoming steam cycle in this case is a double pressure reheat process for a better cycle efficiency. The reheat temperature is 560°C and steam expands from a pressure of 120 bar down to 0.021 bar.

The overall net efficiency of the SCOC-CC with the operating conditions shown in Figure 2-3, including CO_2 compression and O_2 production and compression, is 49.75% [12]. The power breakdown of the cycle components for this calculation is shown in Table 2.1. 25% of the total turbine power comes from the turbines in the bottoming steam cycle. The high cooling mass flow rate for the HTT results in a decrease in the percentage of the turbine power provided by the HTT compared to that of the Graz cycle, which has a lower cooling mass flow. The O_2 generation and compression accounts for an efficiency penalty of 9.7%, and the CO_2 compression accounts for about a 2% efficiency penalty.

There are many other studies which model the SCOC-CC, but with slightly different configurations and assumptions, and they place the efficiency of this cycle in
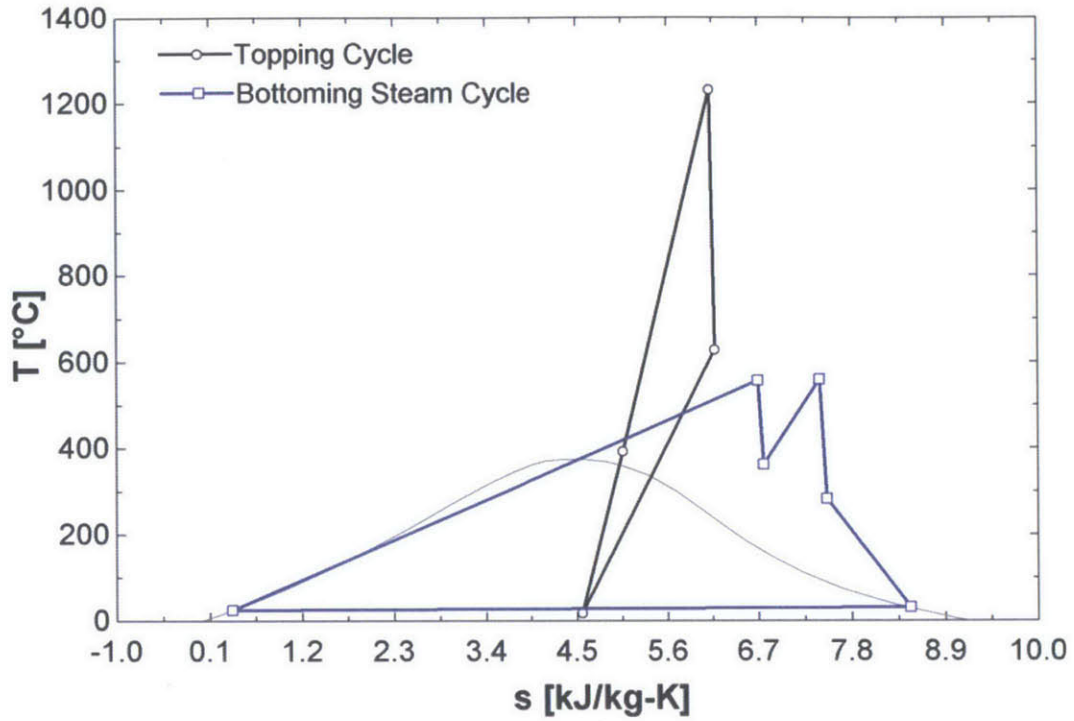
Figure 2-4: T-s diagram of the SCOC-CC, drawn using EES (grey line is the water vapor dome)

	Power (MW)
HTT power	557
HPT power	95
LPT power	95
Total turbine power	**747**
C1 power	235
Pump power	3.5
Total compression power	**238.5**
Electrical power output[a]	**494.5**
O_2 generation and compression	78.6
CO_2 compression to 100 bar	15.5
Net power	**400**
Total heat input	**804.6**

Table 2.1: SCOC-CC power balance for the cycle in Figure 2-3 [12]

[a]includes mechanical, electrical and auxiliary losses

the range 47-54% [34, 14, 12, 15, 11]. The important assumptions and configurations used in some of these studies are summarized in Table 2.2 below to show how the efficiency changes depending on how the cycle is modeled. Unfortunately not all of the assumptions were given in the literature that might explain the efficiency differences between the different studies. For example, as will be explained later, the ASU energy consumption is an important parameter that affects the net efficiency of the cycle, along with the oxygen purity exiting the ASU. Also all three of the SCOC-CC's in the literatures below used different simulation software and probably modeled the working fluid properties with slightly different equations of state and property methods.

	Tak et al. [11]	Kvamsdal et al. [34]	Sanz et al. [12]
Number of turbines in topping cycle	1	1	1
Number of turbines in bottoming cycle	1	3	2
Combustor pressure (bar)	40	40	40
TIT of the topping cycle (°C)	1400	1328	1400
Turbine inlet pressure of the bottoming cycle (bar)	100	111	120
TIT of the bottoming cycle (°C)	560	560	560
Topping cycle condenser exit temperature (°C)	25	not given	19
Topping cycle condenser pressure (bar)	1	1.01	1.01
Bottoming cycle condenser pressure (bar)	0.05	0.04	0.021
Gas turbine isentropic (polytropic) efficiency (%)	90	(87)	90
Steam turbine isentropic efficiency (%)	90	92, 92, 89[a]	90
Compressor isentropic (polytropic) efficiency (%)	87	(87)	88
Heat exchangers pressure drop (%)	not given	3	not given
ASU Power (kWh/kg-O_2)	not given	0.23	0.25
ASU O_2 Purity (mol%)	not given	95	not given
Modeling Software	HYSYS	PRO/II (SIMSCI, Inc.)	IPSEPRO by SIMTECH
Net Efficiency (%)	53.9	47	49.75

Table 2.2: Main assumptions made and how the calculations were performed for some SCOC-CC's studied in the literature

[a] bottoming cycle is a triple pressure, reheat steam cycle

Technology Availability & Turbo-Machinery Design

The layout of this cycle is very similar to conventional combined cycles and so any modifications from an existing combined cycle plant may be quite practicable and feasible, and the high composition of CO_2 in the working fluid ($\sim$95 %vol.) results in a simple carbon capture system (see later section) because only condensation is required to purify the stream for EOR. However current gas turbine technology is designed for streams with nitrogen based working fluids, and a new design is needed for the compressors and turbines in order to handle the SCOC-CC's unusual working fluid (CO_2 & H_2O) and high temperatures [12]. This is one of the reasons why this type of cycle has not been implemented in real life yet.

As mentioned before, the working fluid in the SCOC-CC has significantly lower gas constant and specific heat ratio compared to air. Thus to achieve dynamic similarity with an air compressor, an SCOC-CC compressor should run with a 25% reduction in the blade tip speed and a 15% increase in the mass flow. The rotational speed is usually 3000 rpm for SCOC-CC's (the same value as that of existing gas turbine compressors), while the mass flow is lower. Therefore the diameter of the SCOC-CC compressor has to be reduced, compared to an air compressor, to decrease the blade speed and associated Mach numbers. Also the pressure ratio of SCOC-CC's ($\sim$40) is much higher than current air-fired gas turbine plants and at this high exit pressure; the density of the gas (mainly CO_2) is significantly higher than air. This eventually means that the unusual working fluid of the SCOC-CC necessitates a novel compressor design which is different than those used in current gas turbine plants; where more stages are required for the SCOC-CC compressor (around 24), a lower exit radius (0.64m), and a very long (6.65m) and slender rotor [50]. Figure 2-5 below shows the annulus of the conceptual design of the SCOC-CC compressor. The long rotor can cause rotor dynamics problems and the high number of stages results in an end wall boundary layer growth that leads to reduced flow efficiency. Finally, another risk for the operation of the SCOC-CC compressors is with the H_2O present in the working fluid, which can cause the formation of water droplets and may lead to blade
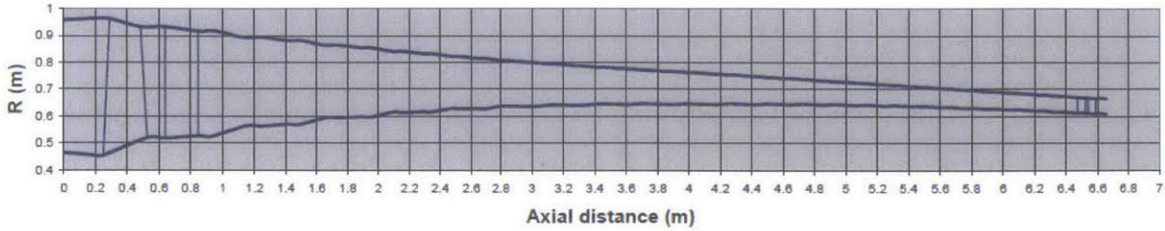
Figure 2-5: Annulus of the initial conceptual design of the SCOC-CC compressor [13]

erosion if the inlet temperature of the fluid is near saturation. This corrosion effect will be severely magnified when sour gas is used as the fuel due to the formation and condensation of sulfuric acid.

A similar analysis was done for the SCOC-CC turbine, and since the maximum speed of the compressor was 3000 rpm, this leads to a one-shaft design for the turbine running at the same speed. This rotational speed leads to a total stage number of 8. The main issue with the SCOC-CC turbines is the blade cooling that is required since they operate at very high temperatures (1400°C). The total cooling flow demand was calculated to be 30.5% of the inlet mass flow to the turbine. This value is almost twice that required for the Graz cycle. This is mainly because of three reasons: unfavorable properties of the SCOC-CC working fluid (small heat capacity), higher cooling flow temperature, and the increased turbine stage numbers [12]. One important aspect that has not been fully analyzed in the literature is the expected lifetime of the proposed cycle components once they are built and running because if they are not durable and reliable then the power plant's payback period will be seriously extended. Also it has not been mentioned if the blade material in current gas turbine technology needs to be changed to handle the new working fluid and similarly how this will affect the design of the combustor.

Therefore to conclude, from the analyses shown above it can be determined that completely new designs of the turbines and compressors for the SCOC-CC are needed before a feasible pathway to commercialization can be developed. The flow area, number of stages and possibly blade materials are some of the variations to current gas turbine designs. On the other hand the cycle is simple enough and there are

56

no major technical barriers for development so many studies suggest that we could probably expect the implementation of this cycle in the near future. NET Power recently announced that they are going to start developing a new gas-fired power generation technology that uses an oxy-fuel, high pressure, supercritical CO_2 cycle to produce pipeline-ready CO_2 for sequestration or EOR [51]. A small-scale 25 MW pilot plant is expected start construction by 2015 and a full-scale commercial 250 MW will consequently follow. This will be discussed further in the next section on Matiant cycles, but this project should help in the development of the CO_2 based turbines and compressors and hopefully pave the way for the implementation of SCOC's.

Sensitivity Analyses

The optimal operating conditions for this cycle are an important issue which has partially been looked at in the literature [11, 14, 15]. Sensitivity analyses were done to determine the optimal overall pressure ratio for the cycle based on efficiencies [14, 15], and a study was done to investigate the integration of the carbon capture process with the SCOC-CC, by looking at the condenser operating conditions [11]. An optimization analysis should be done to look at the best operating conditions that minimize emissions as well as maximizing the cycle performance. This analysis would especially be vital with sour gas oxy-combustion cycles due to the harmful substances that can form, including SO_2 and H_2SO_4.

For an SCOC-CC with a single steam turbine (similar to the configuration in Figure 2-2) and a gas TIT of 1319°C, the influence of the gas turbine pressure ratio on the cycle performance was investigated by Bolland et al. [15]. A similar analysis was done by Corchero et al. [14], but by modeling the cycle with a 2 gas turbine expansion, a single steam turbine and with the combustion temperature at 1327°C. The results of these analyses are shown in Figures 2-6 and 2-7 below. The optimal gas turbine pressure ratio, based on the net cycle efficiency (see Figure 2-6), was found to be approximately 30 for the cycle modeled by Bolland et al. [15] (single gas and steam turbine) and 35 for the cycle modeled by Corchero et al. [14] (2 gas turbines and 1 steam turbine). As the pressure ratio is increased, the efficiency peaks at a certain

ratio and then starts going back down due to the effects of a decreasing enthalpy gain by the steam in the HRSG which decreases the power output of the steam turbine cycle and decreases the overall efficiency. The difference in efficiencies between these two cycles can mainly be attributed to the difference in their configurations, and also because the ASU's were modeled with different specific powers (0.25 vs. 0.21 kWh/kg-O_2) and this has been known to greatly affect the net cycle efficiency (see Figure 2-8). Therefore these two effects combined to give the cycle with 2 gas turbines, an efficiency gain of about 2% over the other one.

The effect of the pressure ratio on the specific power of the cycle, gas and steam turbines was also looked at (Figure 2-7). The specific power of the gas turbine increases with the pressure ratio as expected. This is counteracted by a decrease in the steam turbine power due to the reason described above of the exhaust temperature of the gas turbine decreasing. The overall combined effects of these two, results in the net plant specific power decreasing as the pressure ratio increases. However, a smaller specific power will translate into a larger system size which means that the system costs will go up. Therefore, when choosing the best pressure ratio for the cycle there is a tradeoff between efficiency and system size. The ASU electricity consumption also affects the plant power output and efficiency. They both decrease linearly with increases in the energy consumption (see Figure 2-8). This is because the ASU power affects the work output of the cycle, which is the numerator in the net efficiency equation. In terms of the ASU power, the cycle power output would always be a constant minus the ASU power multiplied by the oxygen mass flow rate. An increase of the ASU energy consumption by only 0.1 kWh/kg-O_2 results in an efficiency drop of 3% and a power decrease of about 7% [15].

Corchero et al. [14], also investigated the effects of modeling the working fluid as pure CO_2 compared to the actual flue gases (see Figure 2-9). It was found that the optimal pressure ratio was about 28% lower when using the actual working fluid composition compared to pure CO_2. However there were no significant differences in the maximum cycle efficiency for both cases.

One final thing that was analyzed by Tak et al. [11] was how the condenser
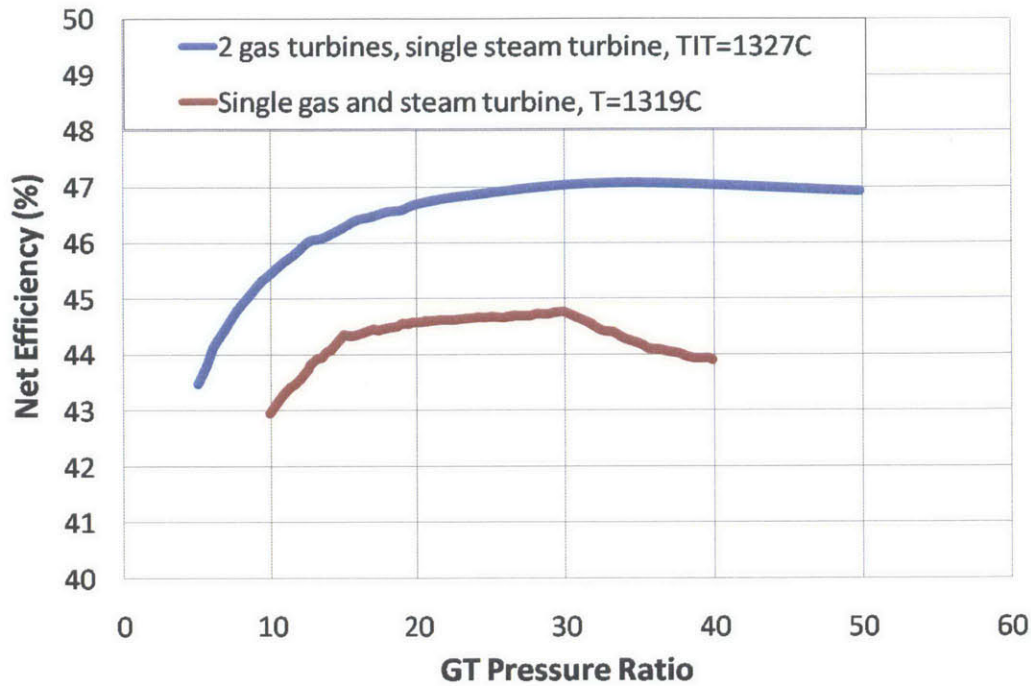
Figure 2-6: Effect of the gas turbine pressure ratio on the net cycle efficiency (includes O_2 production and CO_2 compression), for two cycles modeled in the literature [14, 15]

exit temperature influenced the concentration of CO_2 in the working fluid, at the condenser exit, which would then influence the compression power for CCS. Figure 2-10 depicts this relation for the cycle shown in Figure 2-2. At 25°C, the CO_2 mole fraction is 96.8% and it remains over 95%, the typical concentration for EOR, up to about 33°C. Therefore this would mean that the condenser can operate at higher temperatures and still provide a suitable stream for CCS. It was also found that at higher temperatures, the CO_2 compression work also increases slightly which would affect the efficiency of the cycle [11]. The configuration of this cycle is shown before in Figure 2-2.
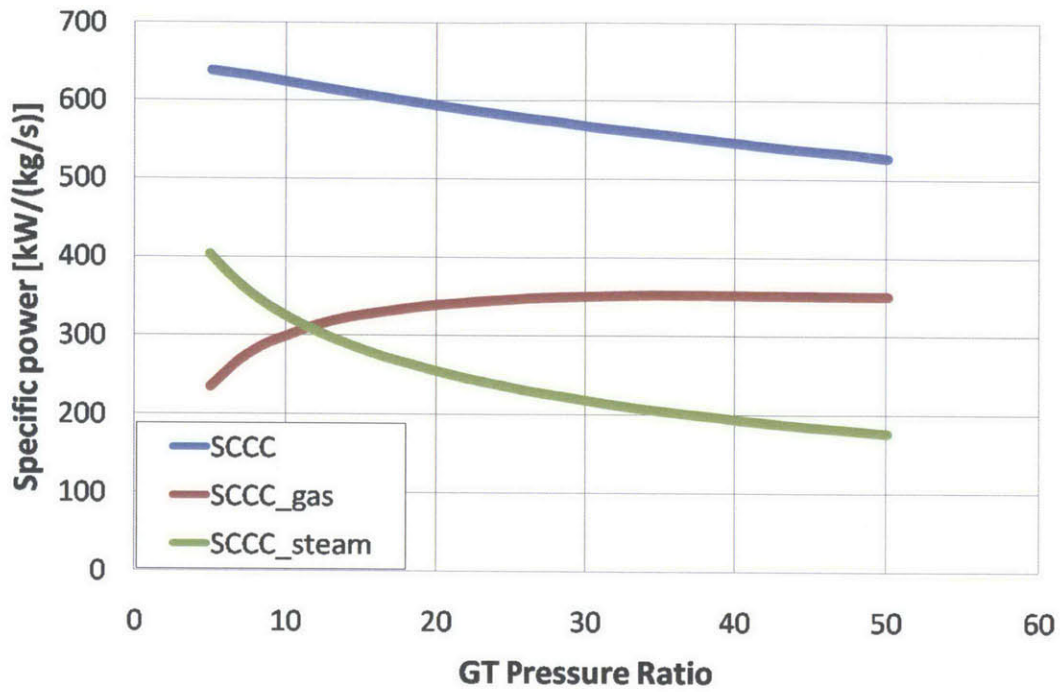
Figure 2-7: Effects of the gas turbine pressure ratio on the specific power output of the cycle, gas and steam turbines [14]
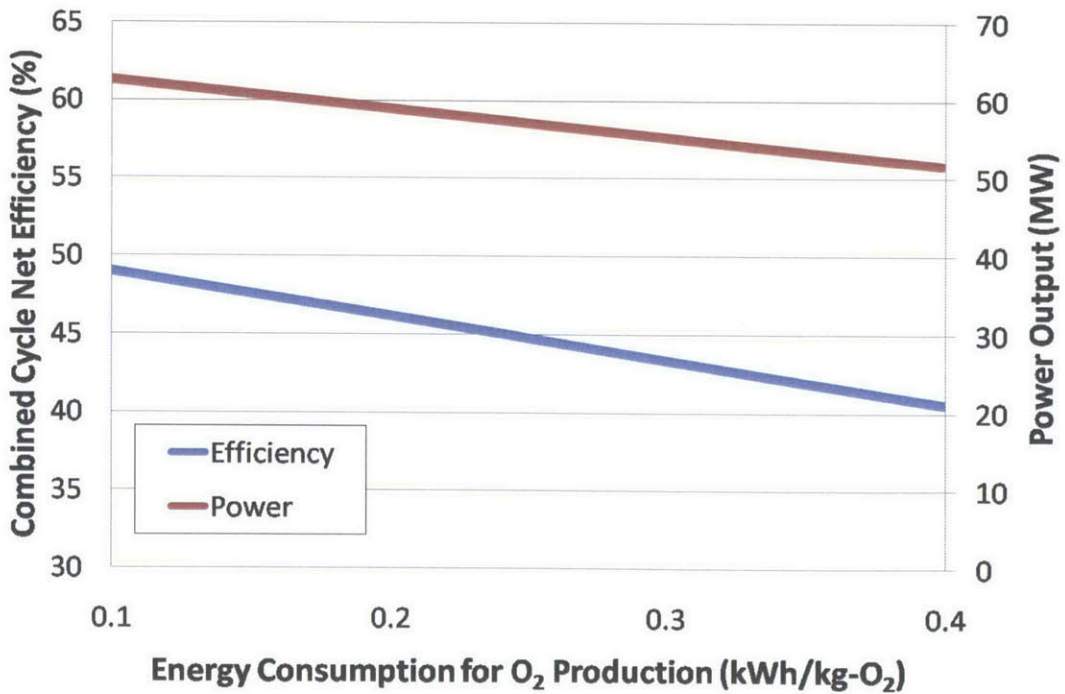
Figure 2-8: Sensitivity of the cycle performance on the ASU energy consumption [15]
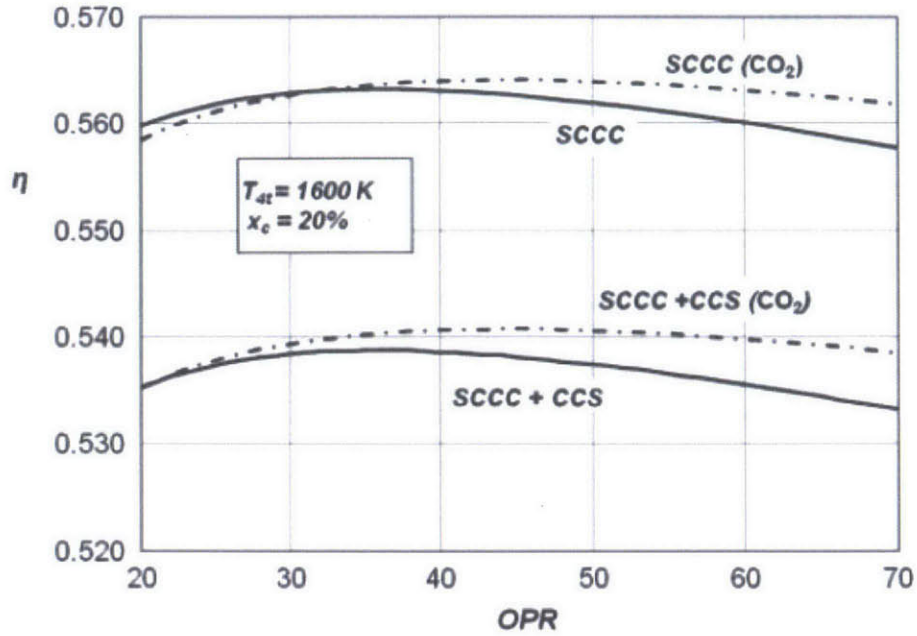
Figure 2-9: Efficiency of the SCOC-CC comparing the working fluid as the dry flue gases vs. pure CO_2 [14]
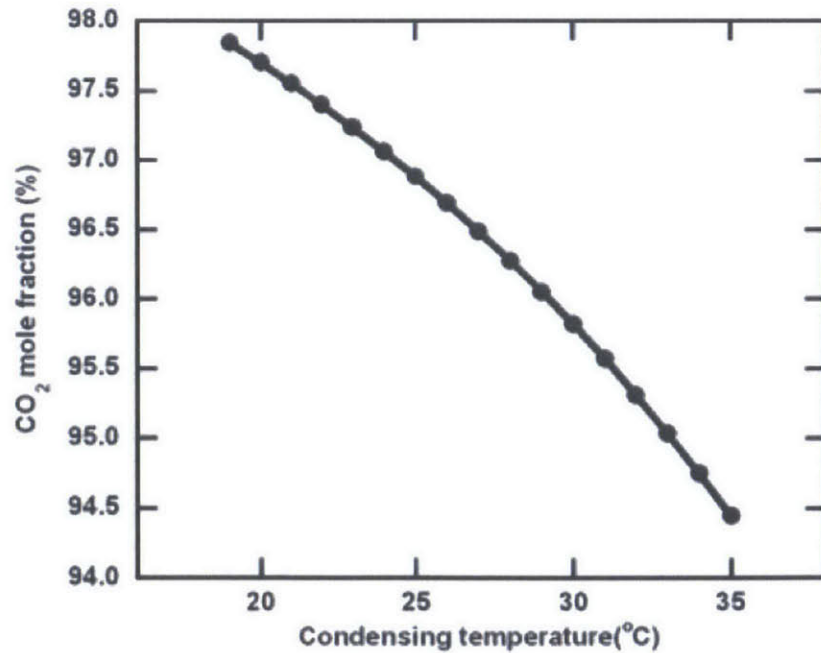
Figure 2-10: Variation in the CO_2 mole fraction of the working fluid, at the condenser exit, with the exit temperature for an SCOC-CC with the condenser operating at 1 bar [11]

2.2.2 Matiant Cycle

Cycle Description

Another cycle that utilizes mainly CO_2 as the working fluid is the Matiant cycle. This cycle was first presented by Professor Iantovski of the Moscow Institute of Energy Research about 20 years ago [52] after originating from a Russian patent [53]. It is mainly based on a recuperative Brayton-like cycle with a supercritical CO_2 Rankine-like cycle. The cycle diagram is shown in Figure 2-11 and the corresponding T-s diagram in Figure 2-13. The working fluid containing 97% (vol.) CO_2 is first compressed in compressors C1-C3 up to 75 bar. Then it liquefies in the condenser (streams 8-9) and is pumped further to 300 bar. After the excess working fluid is removed, it enters the recuperator to become superheated and supercritical CO_2 stream. This stream at a temperature of 600°C and a pressure of 285 bar is expanded in the turbine and to 42 bar then reenters the recuperator to increase its temperature up to 700°C before being sent to the combustor. The combustion product gases then drive the IPT and expand the gas down to 9.03 bars before being reheated in the second combustor to 1300°C and then finally expanded in the LPT. The exit fluid is sent to the recuperator to heat up both streams 13 and 14 and then finally to the condenser for separation.

Using the assumptions in the table below, the efficiency of this cycle was calculated to be 44.06% [16]. To give an idea of where the irreversibilities are in the cycle, the distribution of the exergy losses was also analyzed. The results of this are shown in Figure 2-14. The combustors, heat exchangers and air separation process clearly had the most losses and these are the major sources of irreversibilities within the cycle. Since there are large temperature differences in the heat exchangers, entropy generation is inevitable.

Technology Availability & Turbo-Machinery Design

In terms of technical feasibility, the Matiant cycle faces the most challenges out of all the oxy-fuel cycles. The complexity of the cycle along with the many internal
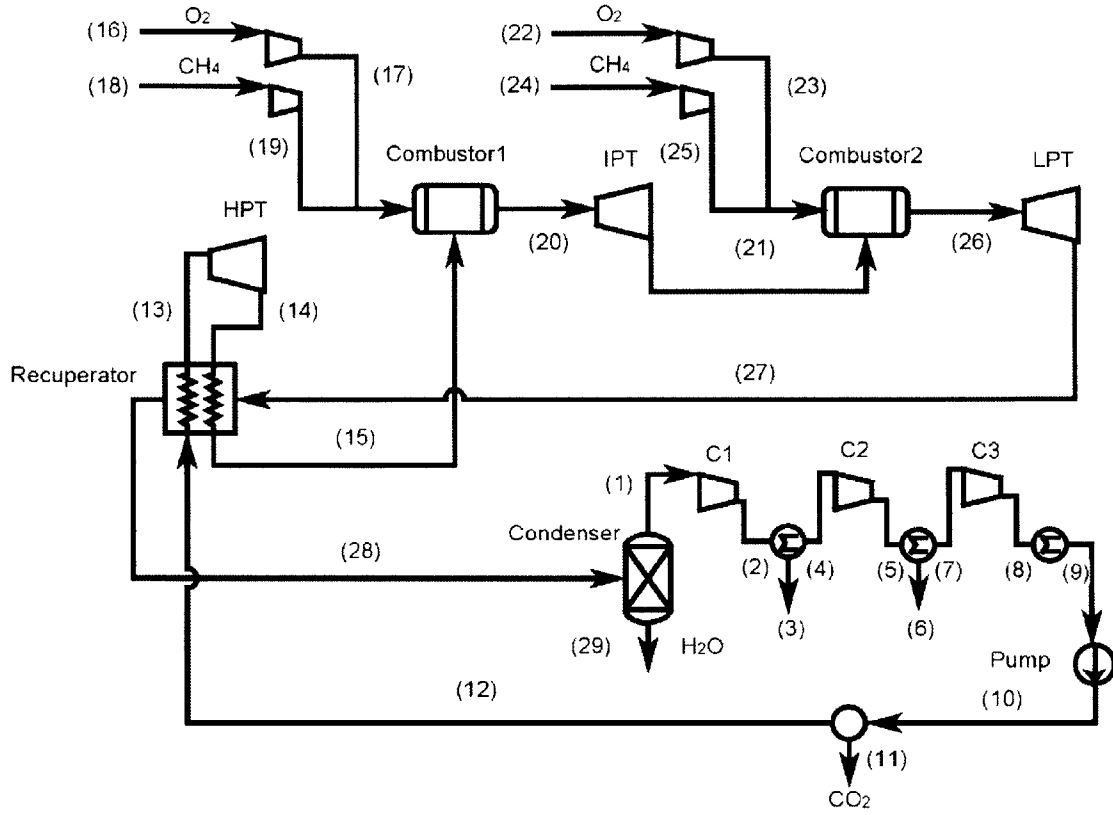
Figure 2-11: Matiant cycle flowsheet diagram [16]

Isentropic efficiency of compressors	87%
Isentropic efficiency of CH_4 and O_2 compressors	75%
Isentropic efficiency of the pumps	75%
Isentropic efficiency of the HPT	85%
Isentropic efficiency of the IPT and LPT	90%
Compressor intercooler and condenser temperature	27°C
Blade cooling efficiency penalty	2%
Combustor pressure drop	3%
Heat exchangers pressure drop	5%
Heat exchanger ΔT_{min}	30°C
Specific ASU Power (kWh/kg-O_2)	0.25
Property method	PENG-ROB Equation
Modeling Software	Aspen Plus

Table 2.3: Computational assumptions made for the Matiant cycle [16]

Points	Temperature (°C)	Pressure (bar)	Vapour fraction	Mole fraction of CO_2
(1)	27	1	1	0.97
(2)	151.5	4.36	1	0.97
(3)	27	4.142	0	0
(4)	27	4.142	1	0.993
(5)	153.7	18.059	1	0.993
(6)	27	17.156	0	0
(7)	27	17.156	1	0.998
(8)	163.1	75	1	0.998
(9)	27	71.25	0	0.998
(10)	73.4	300	1	0.998
(11)	73.4	300	1	0.998
(12)	73.4	300	1	0.998
(13)	600	285	1	0.998
(14)	390.4	42.1	1	0.998
(15)	700	40	1	0.998
(16)	15	5	1	0
(17)	311.2	40	1	0
(18)	15	3	1	0
(19)	281.5	40	1	0
(20)	1300	38.8	1	0.908
(21)	1029.2	9.03	1	0.908
(22)	15	5	1	0
(23)	84.7	9.03	1	0
(24)	15	3	1	0
(25)	121.8	9.03	1	0
(26)	1300	8.76	1	0.87
(27)	925.8	1.1	1	0.87
(28)	103.4	1.05	1	0.87
(29)	27	1	0	0

Figure 2-12: Table showing the thermal parameters at each point in the cycle [16]
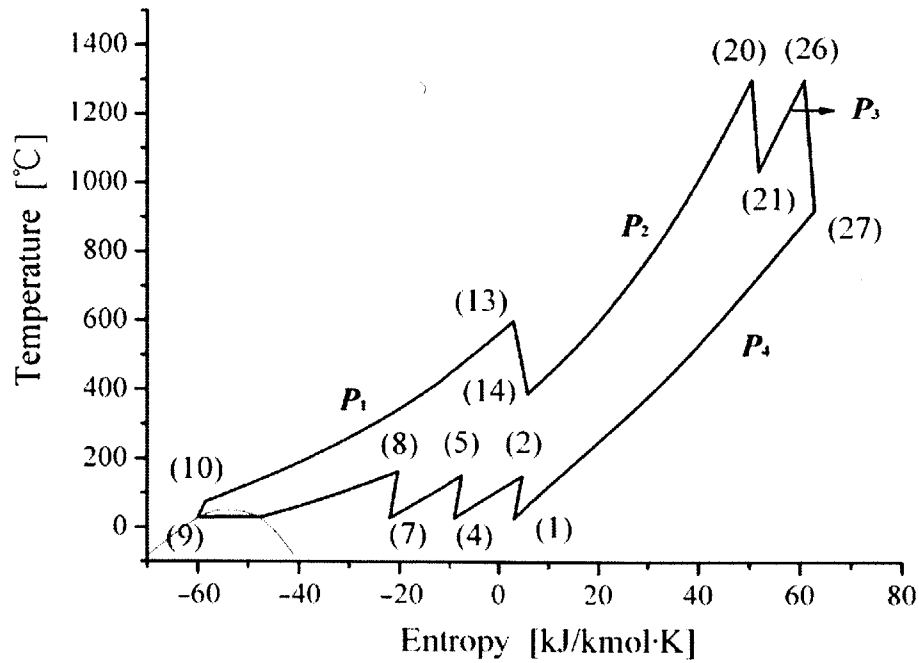
Figure 2-13: T-s diagram of the Matiant cycle with the CO_2 vapor dome shown [16]
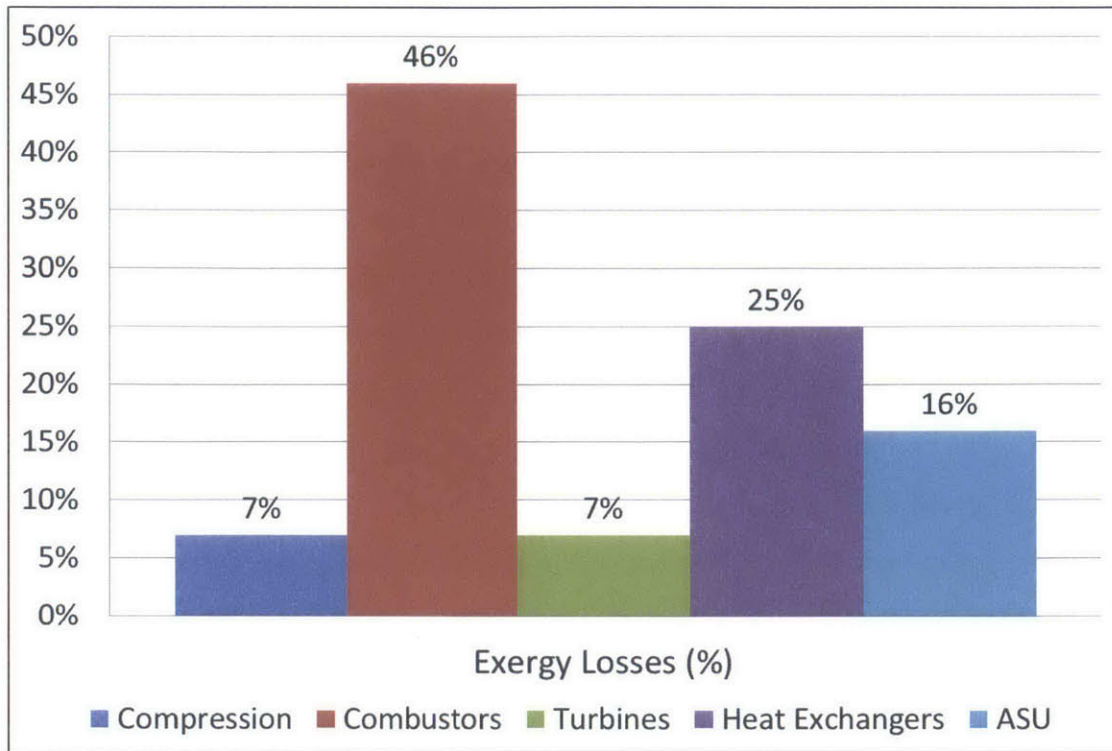
Figure 2-14: Distribution of exergy losses within cycle [16]

heat exchange process are a big challenge for power plant construction. Along with the technical challenges mentioned above for the SCOC-CC with regards to CO_2 turbines and compressors, the Matiant cycle requires a completely new turbine design to be able to handle the supercritical CO_2 at temperatures of around 700°C and pressures of 300 bars. The recuperator also poses a challenge because the exhaust stream needs to be cooled down from a temperature of about 926°C which implies problems for the heat exchanger technology. They would likely require cooling to control the temperature of the heat exchanger equipment and this will definitely introduce additional efficiency penalties which have not been accounted for thus far. The size, materials and capital costs of these heat exchangers could also prove to be problematic. The extremely high pressures in the cycle (300 bar) can also cause leakage and sealing issues and since the working fluid is predominantly CO_2, leakages can defeat the purpose of these carbon capture cycles and also decrease mass flow rates which can affect the cycle performance.

As mentioned before this cycle has not been implemented in real life, however a company called NET Power is teaming up with Toshiba Corporation, The Shaw Group and Exelon Corporation to develop a new gas-fired oxy-fuel power plant. This high pressure plant is a supercritical CO_2 cycle and produces pipe-line ready CO_2 for EOR (due to the high pressures). The brief layout of the cycle is shown below. Its simplicity is a big advantage for the manufacturers and designers. It doesn't require a carbon capture system since the working fluid is mainly CO_2 which is already at a high pressure. The combustor pressure is very high, at 300 bar, and with temperatures of $1150°C$ to produce an estimated efficiency of 59-62% [51]. It is not mentioned what the pressure drops are in the combustors and heat exchangers, and whether the efficiency accounts for the O_2 production and compression (very unlikely). The combustor and turbine is being designed, tested and manufactured by Toshiba so preliminary details about these should be forthcoming. The construction of a small-scale 25MW natural gas plant is expected to begin in late 2014, while a larger commercial 250 MW plant is also expected by 2017. As previously noted, the technology being developed for this project will be the breakthrough needed to further motivate the construction and development of CO_2 based natural gas oxy-fuel cycles (ex. SCOC-CC, Matiant cycle). It will help improve turbine, compressor, combustor and heat exchanger designs and also help in visualizing the impact of the CO_2/H_2 working fluid on blade materials, pressure drops, plant sizes and many other important aspects that have not yet been explored in the literature, but are crucial for extensive cycle evaluations. For the remainder of this literature review, the focus will mostly be on the other three cycles (Water, SCOC-CC and Graz) just because they are the most technologically feasible and the literature also mostly focuses on these three in their thermodynamic analyses.

2.2.3   Water Cycle (CES Cycle)

Cycle Description

The water cycle was first suggested by Clean Energy Systems (CES) in 1998 at the Fourth International Conference on Greenhouse Gas Control Technologies in Switzer-
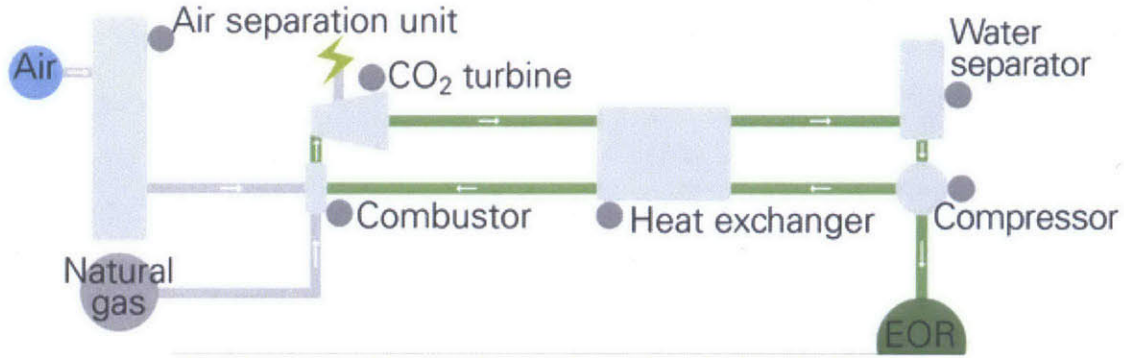
Figure 2-15: Supercritical CO_2 cycle being developed by NET Power [17]

land, as a new way to minimize the cost of CCS in power plants [48]. The water cycle can be categorized as a Rankine-type power cycle with a single reheat and regeneration. The working fluid consists mainly of H_2O and some CO_2 (90/10 %vol.), due to the fact that this cycle uses liquid H_2O as the diluting medium to moderate the combustion temperatures. Figure 2-16 below shows the components of the water cycle. The oxygen stream from the air separation unit and the natural gas are compressed and burned stoichiometrically in the combustor along with the liquid H_2O as a diluent. The exhaust gas from the combustor (H_2O and CO_2) drives the high pressure turbine (HPT), and then is sent to the reheat combustor where it is burned with additional fuel and oxygen to raise the temperature of the fluid. Then it drives the low pressure turbine (LPT), cooled in the regenerator and then condensed. In the condenser liquid H_2O is separated from the CO_2 because of their different boiling points, and then the CO_2 stream is compressed and purified before being used for EOR. The excess liquid water is extracted and the remaining is pumped up to the combustor pressure, before being preheated in the recuperator and then sent to the combustor to complete the cycle.

An example of this cycle is shown in Figure 2-16 with the pressures and temperatures of each point given in Figure 2-17 and the T-s diagram of the cycle shown in Figure 2-18. The HPT inlet temperature for the water cycle is taken to be 900°C and the reheat temperature is 1300°C [16]. However the combustor operating pressure is modeled with two different pressures in the literature, 83 bar and 100 bar [11, 16, 34].

The reheat pressure is usually chosen around 8-10 bar. These combustor pressures are attainable in the gas generator designed by CES and the reheat pressures and temperatures are also realistic in the two turbines designed by CES (see next section on technology availability). It was found that the overall net efficiency of the cycle to be highly sensitive to the HPT inlet temperature [20]. For every 100°C increase in temperature, the efficiency increased by 0.7-1.3%. But more about this sensitivity analysis will be discussed later. For the cycle shown below, the composition of the working fluid at the exit of the first combustor consists of 94% H_2O and 6% CO_2 (mole fractions) at a temperature of 900°C and a pressure of 103 bar. Then after expansion in the HPT to 9.9 bar, the working fluid is reheated to 1300°C and the mole fraction of CO_2 increases to 10%. The fluid is then expanded to 0.1 bar in the LPT before being cooled to 58°C in the regenerator and then sent to the condenser. Part of the H_2O is separated as a liquid and then sent to the pump and combustor to complete the cycle. The remaining working fluid (CO_2 & H_2O 71/29 %vol.) is then compressed and condensed several times to extract the liquid H_2O, leaving a stream with 99.6% CO_2 purity which is then used for sequestration. The condenser pressure affects the CO_2 composition at the exit of the cycle and also the CO_2 compression work which then directly affects the system efficiency. This issue was investigated by Tak et al. [11] and will be further analyzed later.

The overall net efficiency of this cycle (including CO_2 compression and O_2 production) was determined to be 44.6% [34]. The power breakdown of the cycle components for this calculation is shown in Table 2.4. The turbine work is significantly lower than that of the other two cycles (SCOC-CC and Graz cycle) because **liquid** water is fed to the gas generator so some of the fuel's LHV is used to produce steam. Whereas in the other cycles the diluent to the combustor is preheated from the exhaust gases of the low pressure turbine and this generates the steam in the working fluid. The working fluid compression work is also very small because it is mainly due to water pumping, which doesn't require a lot of work.
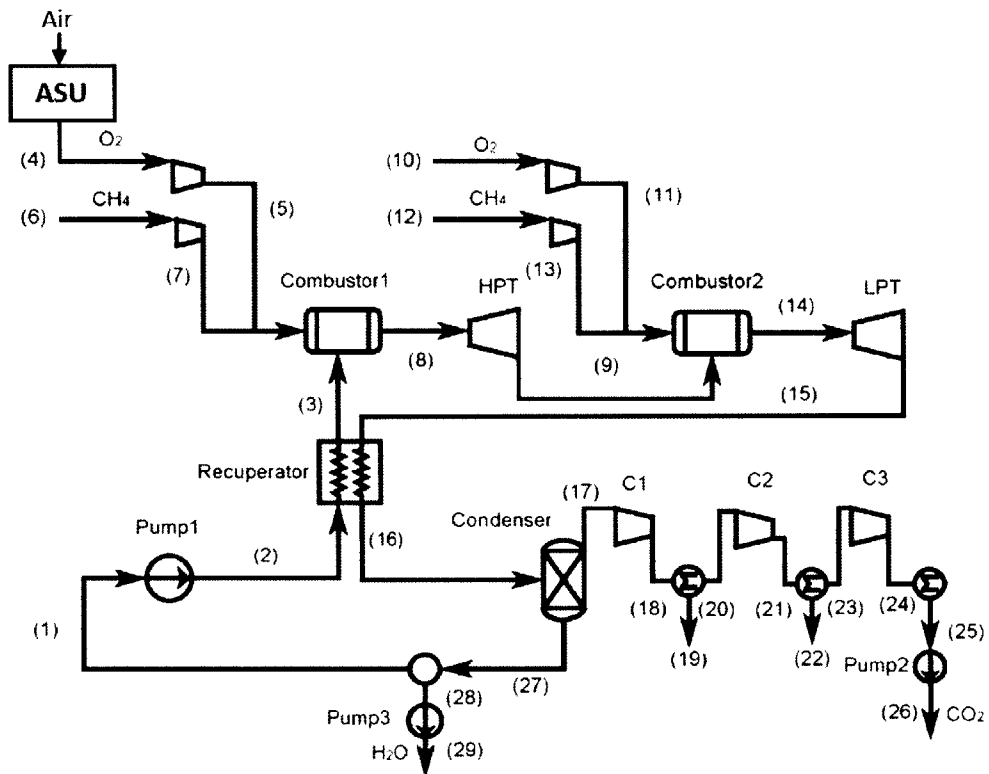
Figure 2-16: Cycle diagram of the water cycle [16]

	Power (MW)
Total turbine power	**556**
Compressor power	1
Auxiliaries	6
Pumps power	2
Total compression power	**9**
Electrical power output[a]	**536**
O_2 generation and compression	82
CO_2 compression to 200 bar	55
Net power	**400**
Total heat input	**897**

Table 2.4: Water cycle power balance [34]

[a]includes mechanical, electrical and auxiliary losses

69

Points	Temperature (C)	Pressure (bar)	Vapour fraction	Mole fraction of CO_2
(1)	27	0.1	0	0
(2)	28	112.2	0	0
(3)	283.3	106.6	0	0
(4)	15	5	1	0
(5)	506.2	106.6	1	0
(6)	15	3	1	0
(7)	394.7	106.6	1	0
(8)	900	103.4	1	0.061
(9)	509	9.9	1	0.061
(10)	15	5	1	0
(11)	96.6	9.9	1	0
(12)	15	3	1	0
(13)	131.2	9.9	1	0
(14)	1300	9.603	1	0.099
(15)	493.3	0.11	1	0.099
(16)	58	0.105	1	0.099
(17)	27	0.1	1	0.707
(18)	249.4	1.05	1	0.707
(19)	27	1	0	0
(20)	27	1	1	0.97
(21)	221.8	8.88	1	0.97
(22)	27	8.436	0	0
(23)	27	8.436	1	0.996
(24)	233.6	75	1	0.996
(25)	27	71.25	0	0.996
(26)	72.6	300	1	0.996
(27)	27	0.1	0	0
(28)	27	0.1	0	0
(29)	27	1	0	0

Figure 2-17: Table showing the temperatures, pressures and compositions of each point in the water cycle [16]

70
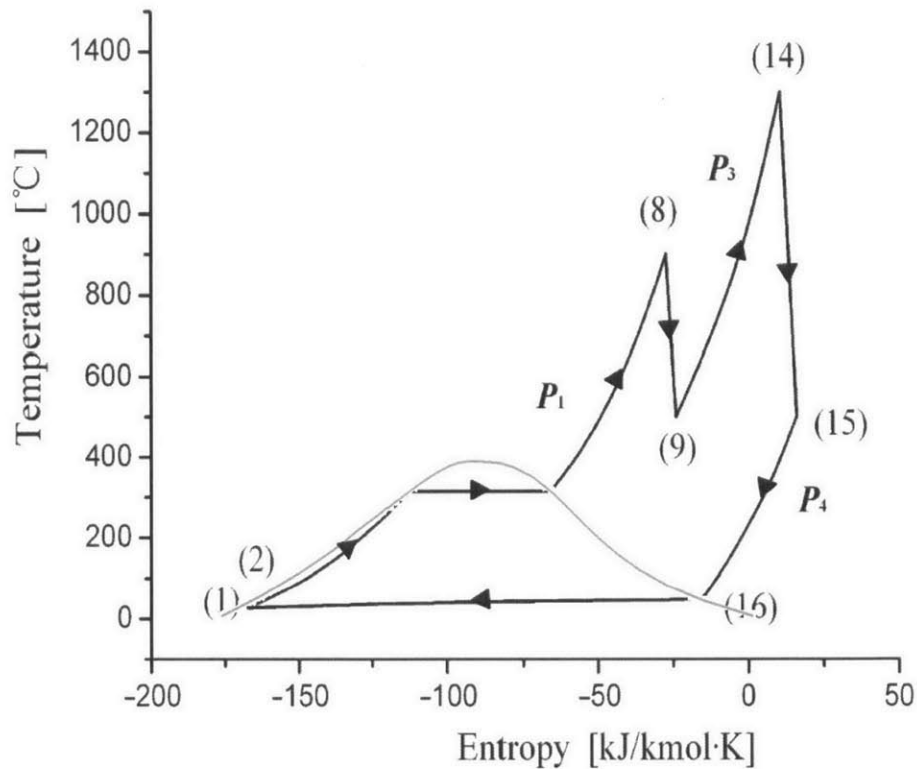
Figure 2-18: T-s diagram of the water cycle (for actual working fluid of CO_2 & H_2O) [16]

Multiple studies place the efficiency of the water cycle between 40-49% [16, 34, 48, 49]. The reason for this range is due to different assumptions made on isentropic efficiencies, pressure drops and also because the cycle configurations are slightly different. Table 2.5 below summarizes the computational assumptions made for some of these cycles and how they compare to each other. It is not that obvious to see why the cycle modeled by Tak et al. had a higher efficiency than the other two cycles because not all of the cycle assumptions were given especially the ASU specific power and pressure drops, and so it is not easy to extract the exact computational assumptions used in the publications. The O_2 production and compression accounted for only a 6% efficiency penalty for this model of the cycle, compared to almost 10% for the other two cycles. Also different simulation softwares were used which could have also made a difference to the calculations.

71

	Tak et al. [11]	Kvamsdal et al. [34]	Gou et al. [16]
Number of turbines	2	2	2
Combustor pressure (bar)	100	83	103
TIT's (°C)	815, 1400	900, 1328	900, 1300
Combustor reheat pressure (bar)	20	8.3	9.9
Condenser exit temperature (°C)	25	not given	27
Condenser pressure (bar)	0.1	0.045	0.1
Turbine isentropic efficiencies (HPT & LPT) (%)	90, 90	92, 89	87, 90
Pump efficiency (%)	87	75	75
Combustor pressure drop	not given	5%	3%
Heat exchangers pressure drop (%)	not given	3	5
Heat exchanger ΔT_{min} (°C)	not given	20	30
ASU Power (kWh/kg-O_2)	not given	0.23	0.25
ASU O_2 Purity (mol%)	not given	95	not given
CO_2 Transport Pressure (bar)	100	200	300
Modeling Software	HYSYS	PRO/II (SIMSCI, Inc.)	Aspen Plus
Net Efficiency (%) (includes ASU power and CO_2 compression)	48.9	44.6	44.4

Table 2.5: Main assumptions and cycle configurations for comparing three water cycles modeled in the literature
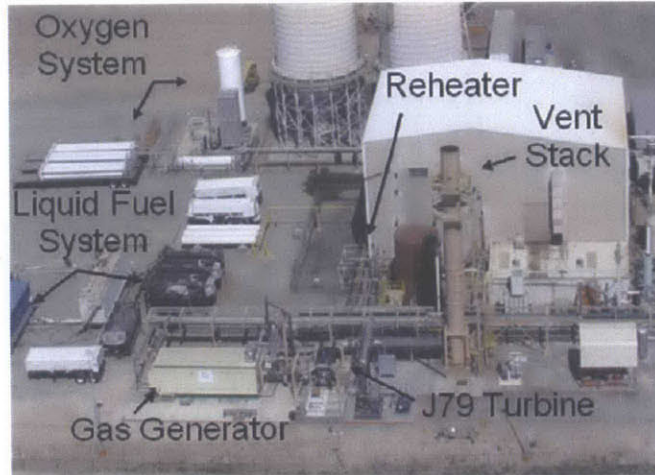
Figure 2-19: Kimberlina test facility [18]

Technology Availability & Turbo-Machinery Design

A big advantage this cycle has over other natural gas oxy-fuel cycles is that this cycle has been built and implemented in real life by Clean Energy Systems at the Kimberlina Power Plant in Bakersfield, CA. In 2005, CES successfully converted the former 5 MW biomass power plant into the world's largest oxy-fuel combustion facility [18]. The figure above shows the plant layout. It includes: two CES 4"& 12" Gas Generators, a CES OFJ-79 30MWe expander turbine and a CES OFT-900 150MWe expander turbine (Added June 2012).

CES has been successful in reengineering rocket engines to act as the combustors or Gas Generators which are able to reach the very high pressures and temperatures associated with this cycle. They have platelet-based fuel injectors (see Figure 2-20) which basically are hundreds of individual platelets stacked together and have intricate pathways that channel bulk fuel, oxygen and water into hundreds of small combustors and allow for stoichiometric mixing for complete combustion. Liquid water is run through the walls of the combustor to help keep the temperatures in the range which the material can handle and also help in extending the life the gas generator. A description of the gas generator is shown in Figure 2-21 below. A 0.102m (4" inside diameter) gas generator was designed and testing was completed in 2003.
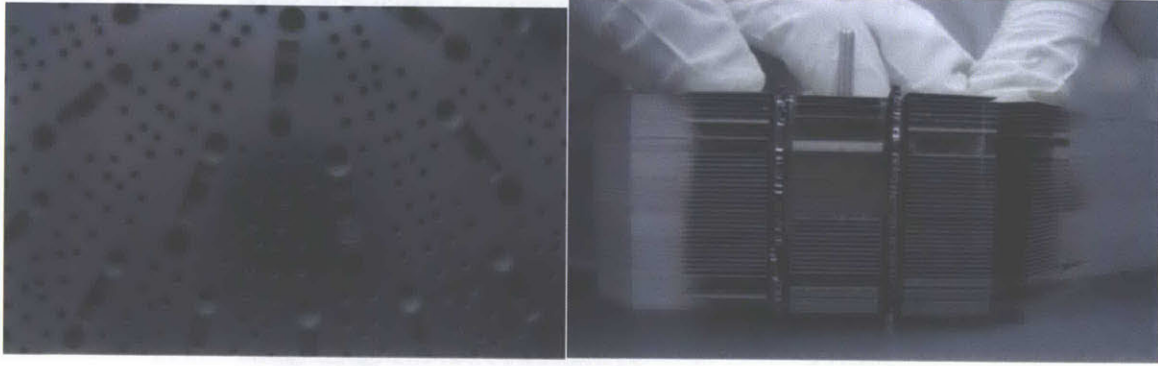
Figure 2-20: The CES platelet based fuel injectors for the gas generators [19]

Temperatures up to 1650°C were tested with pressures up to 106 bar. The combustor successfully functioned at a range of power settings from 20% of rated power to full load (20 MWth) in more than 95 tests [18]. This gas generator has about 2300 total run hours and 1600 starts.

In 2008 a larger (200 MWth) gas generator was built and tested with a 12" internal diameter and has been run for a total of 36 hours and can handle pressures of up to 55 bar and temperatures of 700°C so far [19]. These gas generators might seem like the perfect answer for oxy-fuel cycles since they can handle very high temperatures and pressures and also achieve near-stoichiometric combustion; however the pressure drops in these combustors have not been looked at with great detail. In the literature, the combustor pressure drops for the water cycle were usually 3-5% (see Table 2.5) but CES rates the gas generators on their website with a pressure drop of ~15%. This will significantly affect the efficiency of the cycle and it is one important issue which has not been analyzed.

Since the working fluid is mostly steam, current steam turbine technologies are mature and able to handle the high pressures associated with the cycle but not the high temperatures. The HPT can be based on current technologies, but the high temperature, intermediate pressure turbine needs advanced turbine materials and cooling technology, in order to tolerate the higher reheater temperatures which result in higher efficiencies (see Figure 2-22). CES has mainly focused on developing these high temperature IPT's from current gas turbine technologies and adapting them to

74
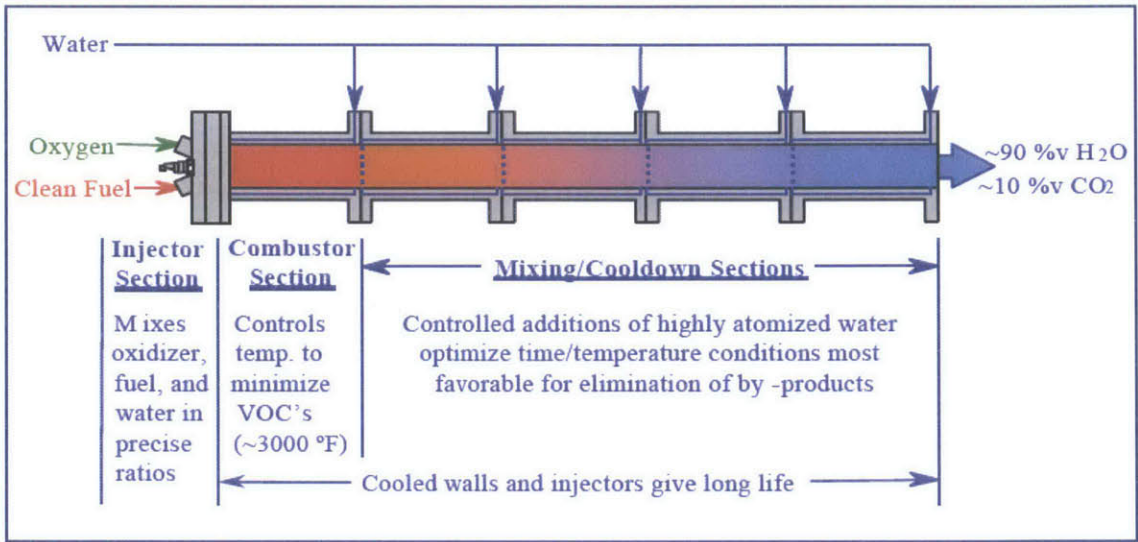
Figure 2-21: CES gas generator [19]
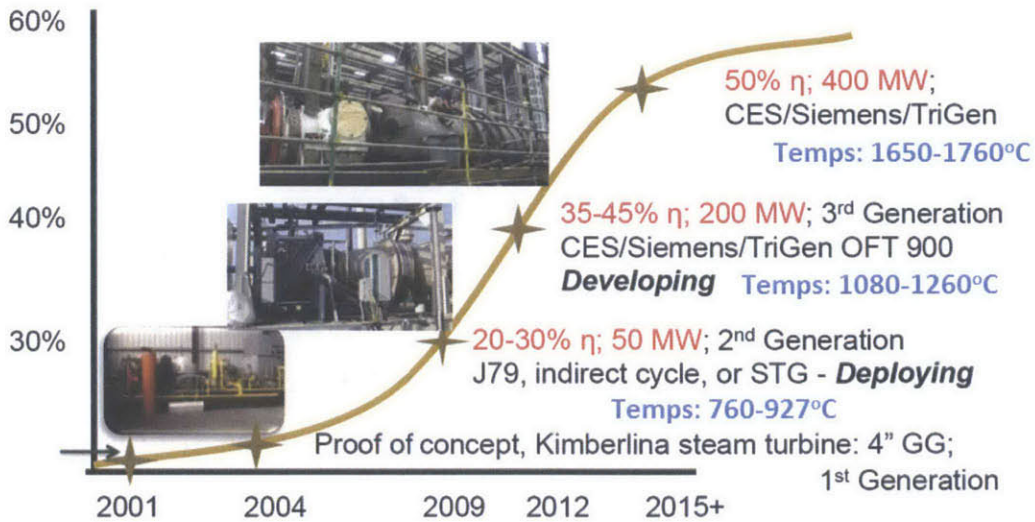
Figure 2-22: Development of turbines for the Kimberlina Plant [19]

Main Turbine	Modified J79	Original J79
Inlet Temp., °C	760	927
Inlet Pressure, bar	11.6	12.3
Exhaust Temp., °C	480	635
Exhaust Pressure, bar	2.14	2.28
Mass Flow, kg/s	62.7	73.6
Shaft Speed, rpm	7460	7460
Shaft Power, MWe	32.5	32.5
Exhaust Turbine		
Inlet Temp., °C	480	635
Inlet Pressure, bar	2.14	2.28
Exhaust Temp., °C	400	465
Exhaust Pressure, bar	1.10	1.07
Mass Flow, kg/s	62.7	73.6
Shaft Speed, rpm	5500	5500
Shaft Power, MWe	10.9	10.5

Table 2.6: Comparison of the modified J79 turbines to the original design [18]

the new working fluid. This development is being done in stages with each stage linked to a specific IPT with a progressively higher inlet temperature to improve the cycle efficiency. These technology stages generations are shown in the figure above. As can be seen, with each stage the efficiency of the cycle increases as the turbines are developed and the reheat temperatures are increased.

For the second generation systems, CES redesigned the GE J79 (gas turbine) into a steam turbine. They removed the 17-stage axial compressor from the engine since the working fluid is already at a high pressure, and they also set the design inlet temperature of the new turbine to be 760°C rather than the 925°C it usually operates at to eliminate the need for blade cooling. Table 2.6 compares the operating parameters of the J79 for the modified and original case. The J79 turbine consists of main turbine and a separate, single-staged exhaust turbine. The main turbine has an exhaust temperature of 480°C (for an inlet of 760°C) and this temperature is well below the design capability of the exhaust turbine, 635°C. Therefore these lowered operating conditions should result in a long-life, low-risk power plant.

When the above turbine was incorporated back into the cycle and tested with
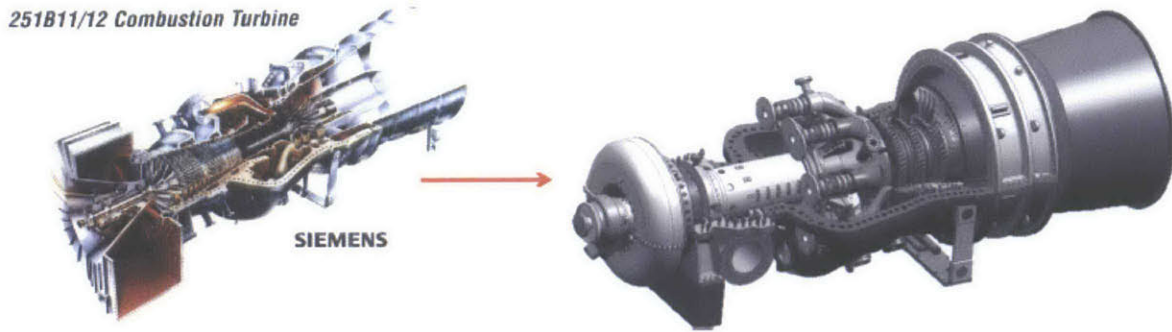
Figure 2-23: SGT-900 turbine modification [19]

a reheat temperature of 760°C, the plant had an efficiency of only around 30% [49]. The details of this calculation are not given but the main reason for this low efficiency was due to the decreased reheater temperature. To improve the efficiency, a third generation turbine is currently being developed to increase temperatures and pressures of the IPT and integrating a reheater into the turbo-machinery system. This new turbine is expected to handle temperatures of around 1300°C and will place the efficiency of the cycle in the 40-45% range [49]. The turbine selected for this modification is the Siemens Energy SGT-900. This original gas turbine configuration contains an axial compressor driven by 3 turbine stages coupled to can-annular combustion system. Some of the modifications made were (see Figure 2-23): replacing compressor with a new thrust balance system (this increases the power output from 50MW to 150MW), replacing the air intake with an inlet steam flow system, and converting the air-breathing combustors to oxy-fuel reheaters.

The SGT-900 was designed for products of natural gas combustion in air therefore the effect of the new CO_2/steam working fluid on the turbine materials were studied to assess the life of the cycle components. Oxidation and mechanical testing was performed in order to study the behavior of the alloy systems in an oxy-fuel environment. The gas composition tested was 90% steam and 10% CO_2 by volume. The results indicated that, for all alloys tested, the oxidation is more aggressive in a steam/CO_2 environment than in a typical gas turbine. This can be seen from Figure 2-24 where the sample exposed to the oxy-fuel working fluid showed increase weight gain and

**Beta Depletion of Bond Coat on Co-Base Substrate
After 500 Hours**
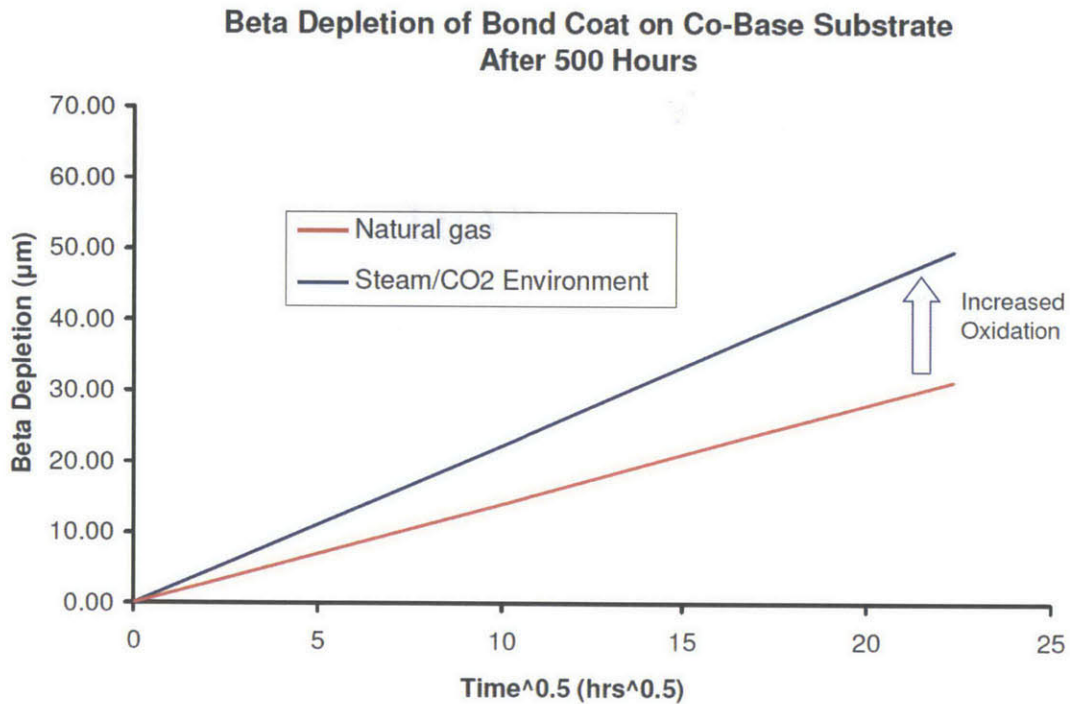
Figure 2-24: Beta phase depletion on a cobalt substrate in a gas turbine and steam/CO_2 environment [18]

increased bond coat beta depletion (measure of oxidation). The higher water vapor of the drive gas interfered with the formation of the protective oxide layers (Cr_2O_3 and Al_2O_3) and helped in forming the less-protective transient oxides. The effect of the free oxygen was considered and determined to be negligible on the oxidation of the steam/CO_2 environment [18]. Further material tests are planned that will provide design life information for blade, vane and rotor materials in the oxy-fuel turbine, along with fracture toughness and fatigue crack growth tests on the rotor steel. These future tests and results will help in determining the effect, if any, of the oxy-fuel environment on these material and turbine properties and will help in the design of these higher temperature turbines.

Finally, another problem with this CES cycle, other than the high combustor pressure drops, is that reheating with different combustor outlet temperatures, increases the combustion exergy losses (loss of useful work) and also increases the CH_4 and O_2 compression works [16]. Another problem with the water cycle is that when using

sour gas as the fuel, due to the high H_2O content in the working fluid, sulfuric acid formation is more likely and this can cause corrosion problems with metal surfaces.

Sensitivity Analyses

The variation of the net cycle efficiency (including ASU + CO_2 Compression) was plotted versus the reheat pressure for the cycle described before, and it was found that the optimal pressure to be 9.9 bar [16]. However the reheat pressure variation did not have a significant effect on efficiency because a 6 bar change in pressure only resulted in a 0.2% efficiency change. The combustor outlet temperature was found to have a bigger effect on the efficiency sensitivity. This analysis on the water cycle was done by Bolland et al. [20] to determine the optimal operating conditions that maximize efficiency for a cycle similar to the one shown in Figure 2-16. The base case conditions for the cycle were: combustor pressure=82.7 bar, combustor temperature=871°C and condenser pressure=0.83 bar. The reheat temperature was kept constant at 1427°C and the pressure was also set to 8.27 bar, but throughout the analysis it was varied assuming constant HP and LP pressure ratios. For the base case conditions, the efficiency of the cycle was calculated to be 40.5%. The combustor pressure and temperature, and the condenser pressure were varied and their effects on efficiency are shown in Figures 2-25 and 2-26 below.

From Figure 2-25 below, it can be seen that the efficiency of the cycle increases with the turbine inlet temperature. So as long as the turbine materials can handle the high temperatures, the efficiency of the cycle can keep increasing. For every 100°C of increased temperature, the net plant efficiency increases by 0.7-1.3%. At a 1400°C combustor exit temperature, the net plant efficiency is maximized around 45.5%. The combustion pressure on the other hand affects the efficiency in a different way. The efficiency actually starts to level off at a pressure of about 200 bar. This is because, initially, increasing the combustor operating pressure increases the power output of the turbines and also the efficiency. But at higher pressures, the efficiency starts to level off and eventually decreases slowly as the parasitic compression power dominates the overall performance. The net plant efficiency increases by about 3% when
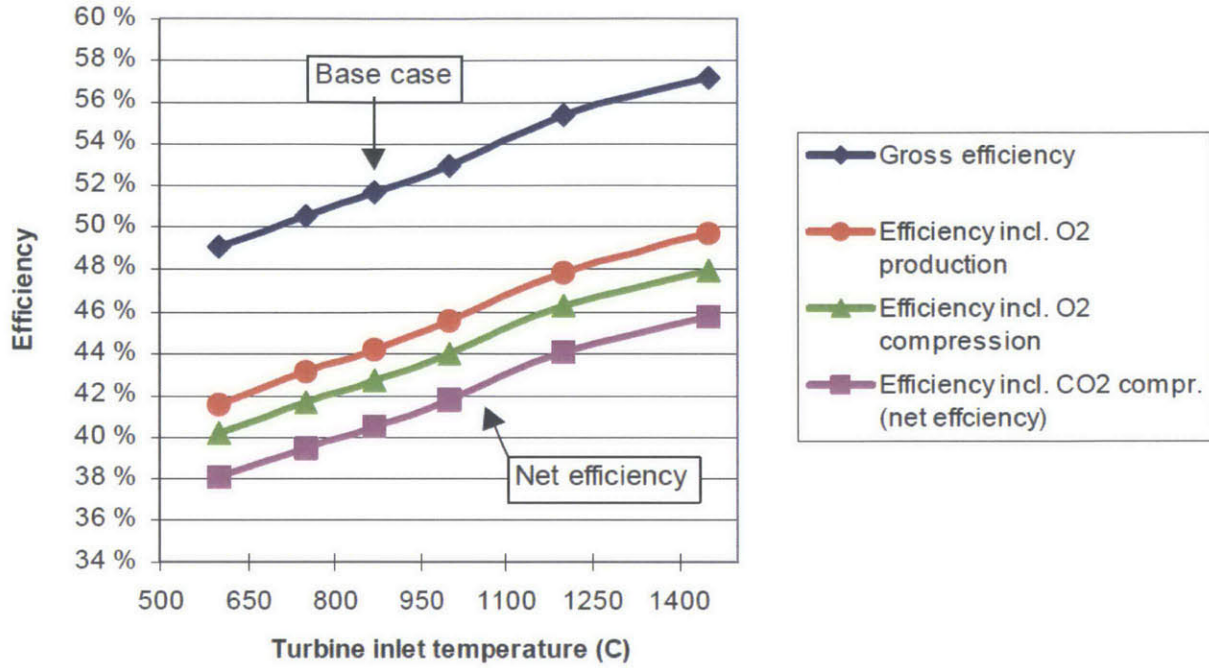
Figure 2-25: Efficiency of the water cycle vs. the turbine inlet temperature varied in the range of 600-1450°C [20]
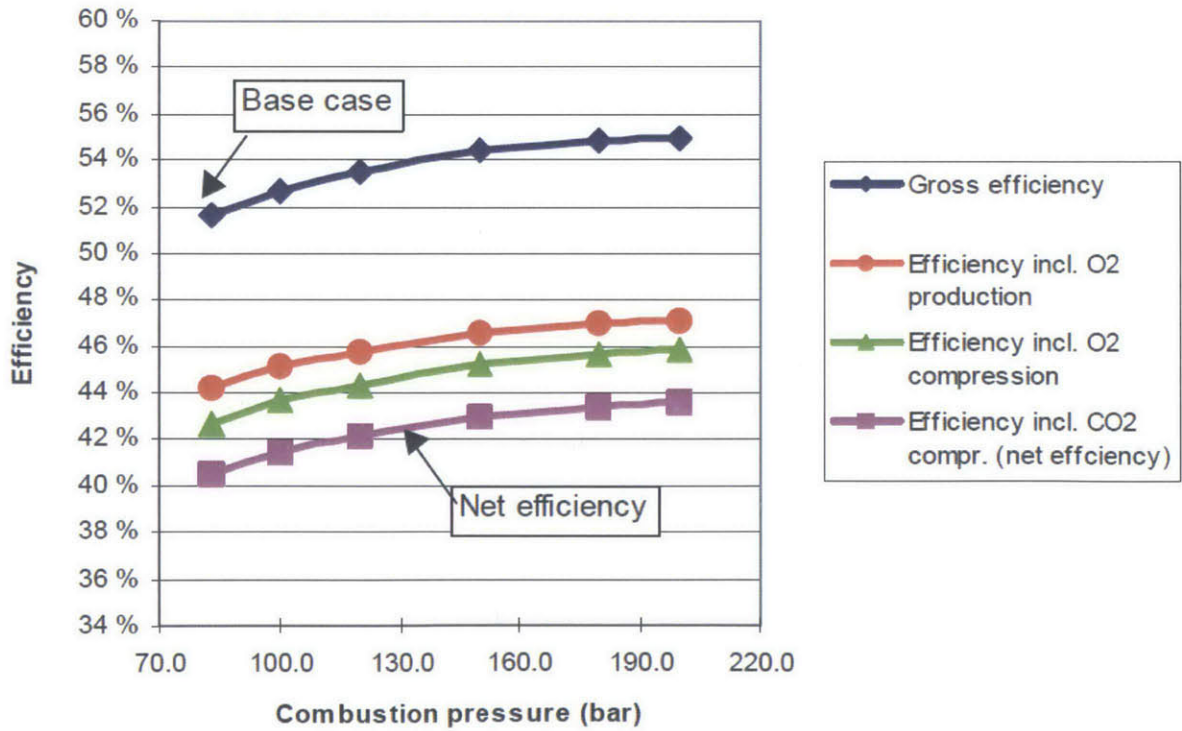
Figure 2-26: Efficiency of the water cycle vs. the high pressure combustor pressure varied in the range of 82.7-200 bar [20]

the combustor pressure increases from 82.7 bar to around 200 bar. At the maximum pressure of 200 bar, the net plant efficiency is maximized at 43.5%. The condenser pressure is also a factor that affects the net efficiency of the cycle. When the condenser pressure was decreased from 1 bar to 0.15 bar (condenser temperature not mentioned), the efficiency increased by about 8% points [20]. This result is further justified in Figure 2-29 below with a similar analysis done in a different publication. So from this analysis we can conclude that the net efficiency is most sensitive to variations in the combustor operating temperature and the condenser pressure. Combining the effects of all the previous parameters to maximize the efficiency, calculated net plant efficiencies of about 53% can be achieved for operating conditions of: combustor pressure=200 bar, combustor temperature=1400°C, condenser pressure=0.15 bar [20].

Another study was done by Tak et al. [11] on the integration of the CCS process with the power cycle similar to the one described previously for the SCOC-CC except that the condenser pressure was the main design variable. The condenser pressure was varied from 10 kPa (0.1 bar) to 100 kPa (1 bar) and its effect on the CO_2 composition for the vapor at the exit, the system efficiency and power output were analyzed. Given the condenser exit temperature (25°C), the compositions of the extracted vapor depend on the condensing pressure. Figure 2-27 below shows the CO_2 composition as a function of the condensing pressure at a fixed condensing temperature of 25°C. When the pressure was increased from 10 kPa to 100 kPa, the CO_2 mole fraction of the extracted vapor increased from 69% to 96.8% so the purity increases when the condensing pressure rises. The reason for this can be seen from Figure 2-28, which shows the properties of the CO_2/H_2O mixture at the condenser condition presented as a vapor-liquid equilibrium chart. For a constant temperature and increasing condenser pressure, the mole fraction of the CO_2 increases. At a condenser pressure of 65 kPa the CO_2 mole fraction is around 95%, the typical minimum concentration for EOR and storage. So for any pressure greater than 65 kPa, the CO_2 purity is high enough that a CO_2 recovery unit is not required for storage and transport. The effects of the concentrations of the non-condensable gases (ex. Ar, O_2) that would be

81
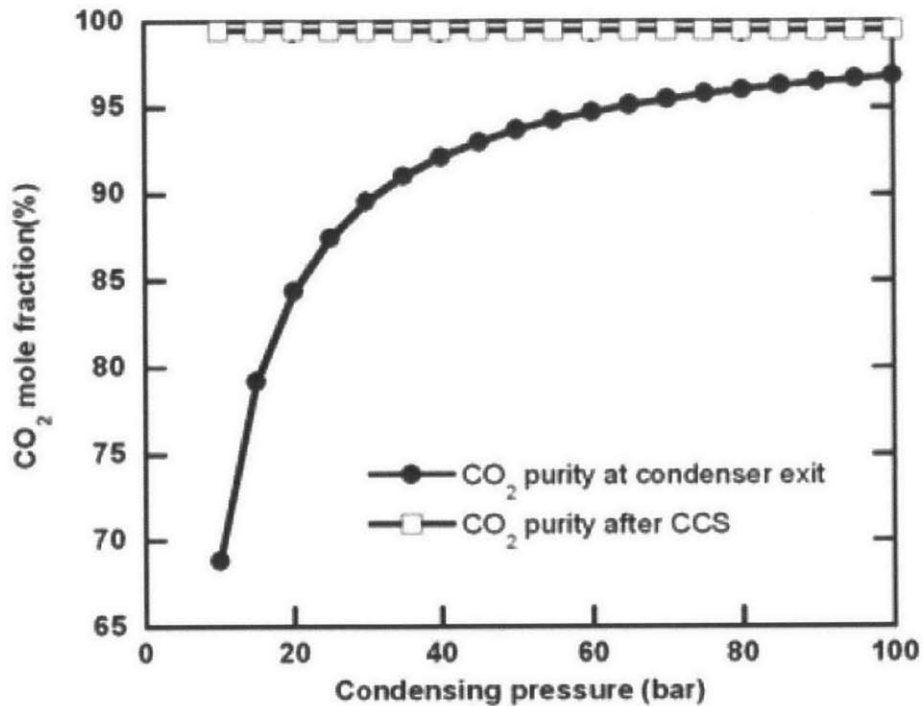
Figure 2-27: Variation in the CO_2 mole fraction of the exiting fluid with condensing pressure [11]

present in the exiting fluid have not been considered in this analysis and might be an important issue that needs to be looked at.

However the net power output of the cycle, and thus the net cycle efficiency (including CO_2 compression and O_2 production), increase with decreasing condenser pressure as seen in Figure 2-29 below. This is because the turbine power enhancement is much larger than the CO_2 compression power consumption. Therefore there is a tradeoff between efficiency and CO_2 purity. If higher condenser pressures (> 65 kPa) are used then this will make the CCS process much simpler thus reducing costs and system size. But this also reduces the efficiency of the cycle significantly which decreases the fuel economy of the entire system. When comparing this analysis on the water cycle to that done on the SCOC-CC, the efficiency penalty due to the CCS process (CO_2 compression) for each cycle were 7% and 5% respectively. Therefore in terms of the CCS process the SCOC-CC seems to be more advantageous as it has a lower efficiency penalty.
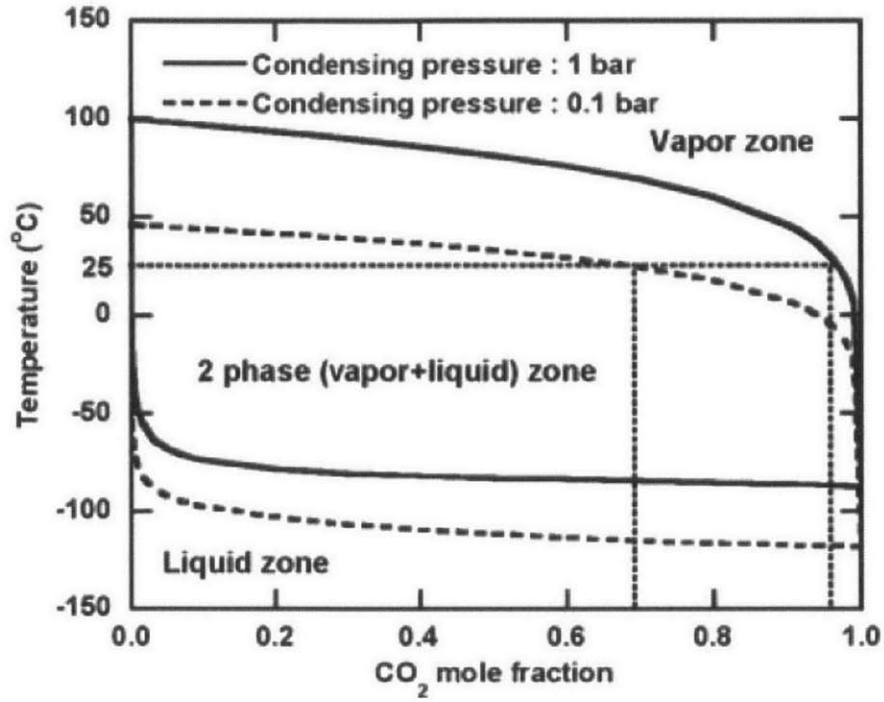
Figure 2-28: Vapor-liquid equilibrium chart [11]
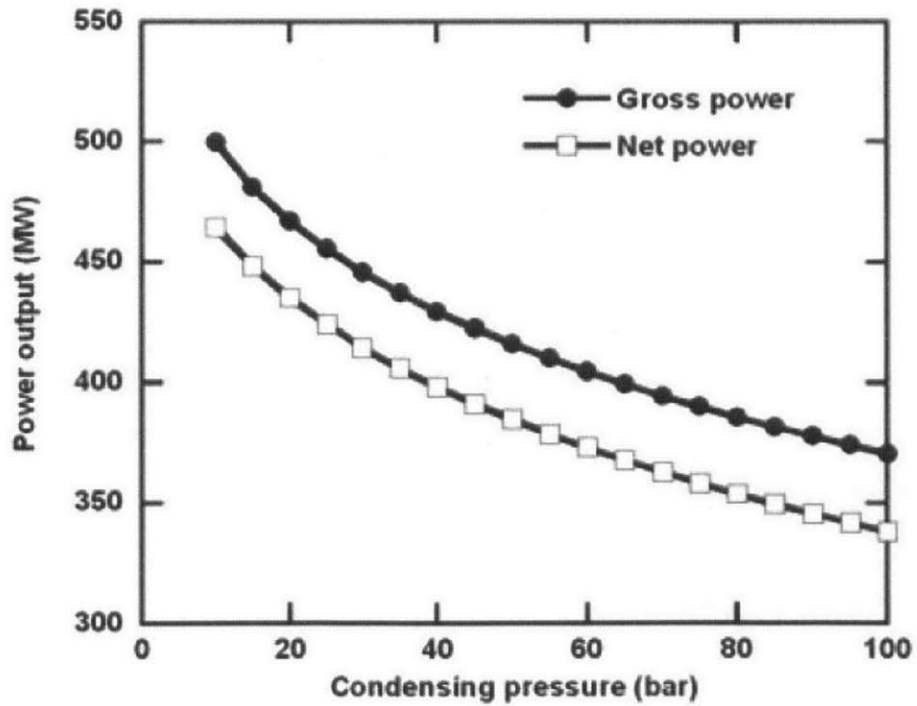
Figure 2-29: Variation in the system net efficiency with condensing pressure [11]

The Zeng Cycle

In 2004, the Zero Emission Norwegian Gas (ZENG) project team proposed a 40 MW Pilot & Demonstration Plant which was to be a modification of the water cycle developed by CES and utilizing the successful technologies that are being implemented at the Kimberlina facility in California [54]. The cycle being developed is shown in Figure 2-30. The cycle provides a better way to integrate the ASU with the cycle to increase efficiency and power output. Since the ASU produces high pressure N_2 as well as O_2, the N_2 flow can be used to increase the system's efficiency and power output. The cycle is a modification of the CES/water cycle with 2 reheaters and it includes the integration with a high pressure N_2 stream from the ASU. The high pressure N_2 stream is further compressed, heated and then expanded in the turbine to produce work. The heat of the exhaust of the N_2 turbine is recovered by a feedwater stream. The efficiency of this cycle is about 4% points higher than the water cycle proposed by CES; this is mainly due to the added power output of the high pressure N_2 stream [21]. The cycle has mostly the same advantages and disadvantages as the Water cycle with some modifications. Since the components of this cycle are very similar to the water cycle, the same turbines and combustors may be used and this technology mostly already exists (Clean Energy Systems). The N_2 stream offers a significant advantage over the regular water cycle because it combats the inability to recuperate the latent heat of water, by using the combustion gases to heat the N_2 and produce work, leading to a higher efficiency. Since the combustion gases are used as the energy input for the N_2 stream, the regular working fluid will have lower temperatures in the cycle and thus will exit the LPT at a lower temperature and this allows for less exergy losses in the condensers.

2.2.4 Graz Cycle

Cycle Description

The Graz cycle was first developed by Jericha et al. at a conference in Norway in 1985 and featured the internal combustion of hydrogen with oxygen stoichiometrically
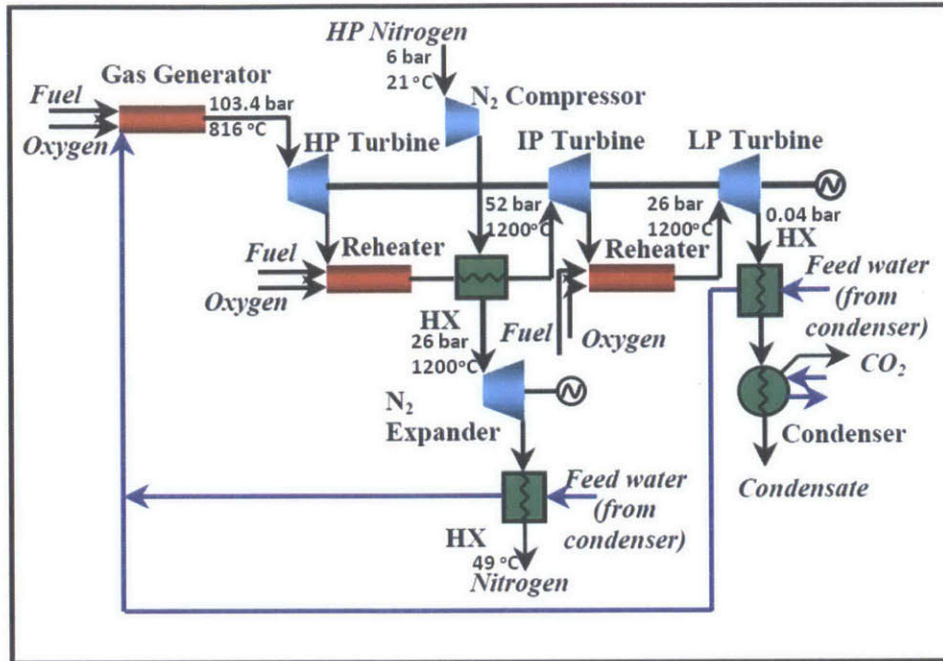
Figure 2-30: The ZENG cycle [21]

where the fuel is obtained from solar power plants by splitting the water into H_2 and O_2. But after hydrogen technology became less popular, the Graz cycle was adopted for fossil fuels in 1995. Since then the cycle has been improved and further developed at many conferences [22]. Burning the natural gas with pure oxygen instead of air allows a simple and cheap method for CO_2 separation by condensation of the cycle medium. The first version of the Graz Cycle is shown Figure 2-31 below and the T-s diagram in Figure 2-32:

It basically consists of a high temperature Brayton cycle and a low temperature steam cycle similar to the SCOC-CC, but with the main difference here being that both CO_2 and H_2O are used as the diluting medium in the combustor to moderate the temperatures. However this Graz cycle configuration has many difficulties that arise from the condensation of the working fluid. Research has shown that water films can form on the cooling tubes and a concentration of CO_2 can form a heat transfer hindering layer, which results in a low heat transfer coefficient for condensation. This will greatly increase the surface area needed for condensation which will result in a very large and expensive condenser. Another problem with this cycle is the expansion
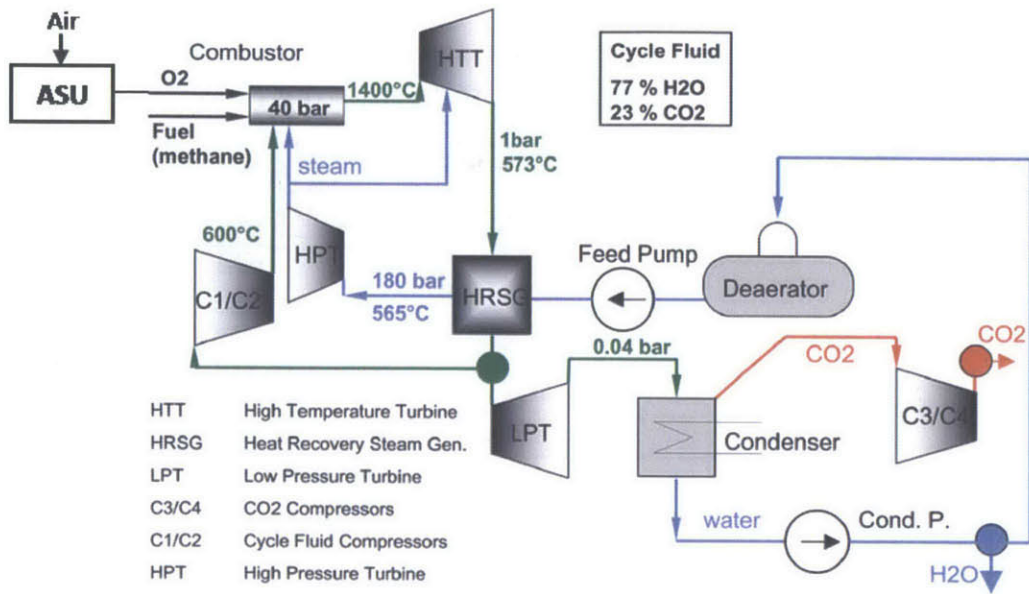
Figure 2-31: Principal flow scheme of the simple Graz Cycle power plant [22]
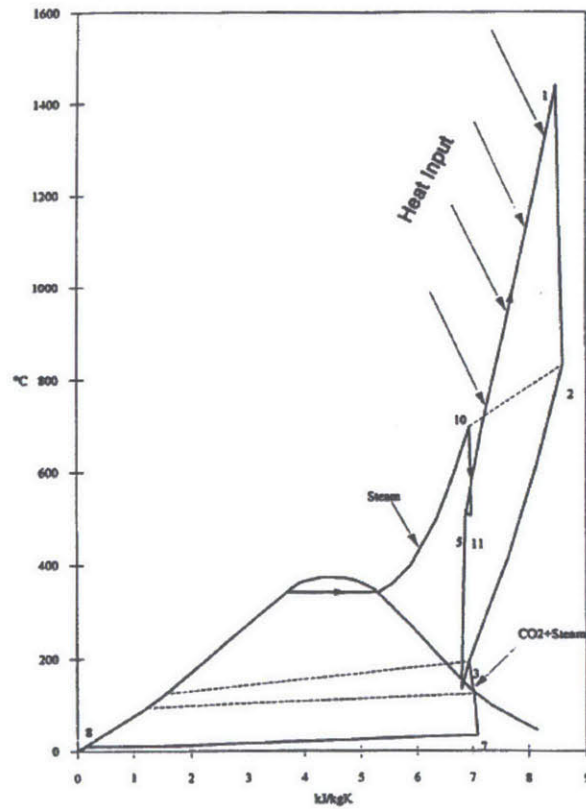
Figure 2-32: T-s diagram of the Graz cycle [23]
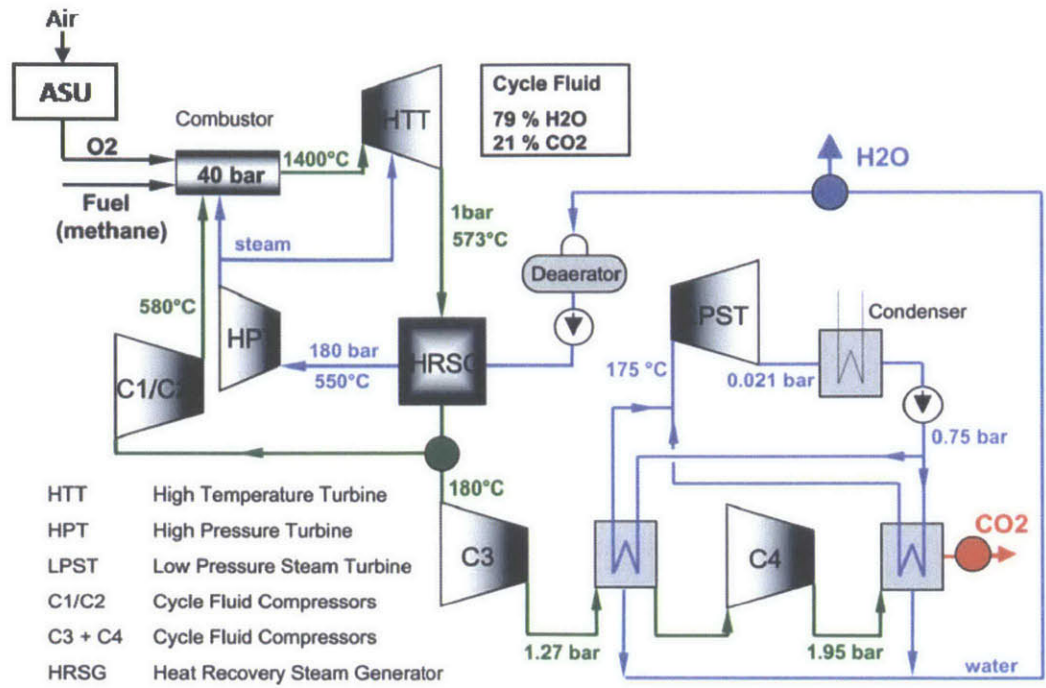
Figure 2-33: Principle flow scheme of the modified Graz Cycle power plant [12]

of the working fluid into vacuum conditions which can increase the corrosion risk for the LPT, if the exit temperature is below the dew point temperature. To solve these problems, the Graz cycle was modified and the new cycle diagram is shown in Figure 2-33 [12]. The working fluid is now condensed at atmospheric pressure, the excess CO_2 separated, and the condensation heat is used for evaporation in the bottoming steam cycle.

In this new cycle, the process is split into a high temperature cycle and a separate low temperature condensation process with a bottoming steam cycle. The high temperature cycle consists of HTT, HRSG, C1/C2 compressors and HPT. The low temperature cycle consists of LPST, condenser and C3/C4 compressors. In the combustor, which is operated at 40 bar, the fuel and a stoichiometric mass flow of oxygen is burned and the high flame temperature is reduced by the recycling of the working fluid stream and the steam exiting the HPT. The combustion gases consist of a mixture of about 76% H_2O and 25% CO_2 (mass fractions) at a temperature of 1400°C. This fluid is then expanded in the HTT down to a final pressure of 1.06 bar at a

temperature of 573°C. At an intermediate pressure of 10 bar in the HTT, steam from the HPT, at 330°C, is added for turbine cooling and then expanded further. The steam mass flow is 13.7% of the HTT inlet mass flow, and this cooling results in the steam content of the working fluid increasing to 79% (by mass). The hot gases at 573°C are used to produce steam for the HPT in the HRSG and are cooled to a temperature of 180°C. After the HRSG about half of the mass flow is sent back to the compressors to be recompressed back up to 40 bar and then sent to the combustor. The remaining fluid is sent to the condensation process in the 1 bar range to avoid the problems mentioned before of the cycle in Figure 2-31. The fluid still has a high heat content, so reevaporation and expansion in a bottoming cycle is necessary. At the pressure level of 1.27 bar, about 63% of the water content is extracted from the fluid and then a further 25% after C4. Throughout this two-step condensation process, the steam is evaporated for the LPST and enters at a pressure of 0.75 bar and 175°C. The water extracted from the condensation process is sent to the deaerator and then to the HRSG for vaporization and superheating. The steam is then delivered to the HPT at 180 bars and 550°C and the expanded steam is sent to the combustor to complete the cycle.

The net efficiency of the cycle (including CO_2 compression and O_2 production) in Figure 2-33 was calculated to be 53% [12]. The power breakdown of the cycle components for this calculation is shown in the table below. The HTT power output is much larger than that of the SCOC-CC due to the higher heat capacity of steam which is added to the HTT for cooling. The O_2 generation and compression accounts for an efficiency penalty of 9.8%, and the CO_2 compression accounts for about a 1.7% efficiency penalty.

In most of the literature, the net cycle efficiency was calculated to be between about 48-54% [12, 22, 34]. This is due to the different modeling assumptions made and the different software for simulations used. These are summarized in Table 2.8. It is not obvious to see why one cycle has a lower/higher efficiency than the other at first glance. A detailed analysis needs to be done given all the computational assumptions used in the literature. The different ASU powers could have played a

	Power (MW)
HTT power	623.6
HPT power	47
LPT power	72
Total turbine power	**743**
C1-C4 power	236.9
Pump power	4.3
Total compression power	**241.2**
Electrical power output[1]	**487.4**
O_2 generation and compression	74.3
CO_2 compression to 100 bar	13.1
Net power	**400**
Total heat input	**753.4**

Table 2.7: Power balance of the Graz cycle [12]

role although one of the cycles had a higher ASU specific work but still had a much higher efficiency. Finally the efficiencies might be affected by the different software used and the equations of state used to model the working fluid.

---

[1]includes mechanical, electrical and auxiliary losses

	Kvamsdal et al. [34]	Sanz et al. [12]
Combustor pressure (bar)	40	40
TIT of the HTT (°C)	1328	1400
Turbine inlet pressure of the HPT (bar)	180	180
TIT of the HPT (°C)	not given	550
Condenser pressure (bar)	0.021	0.046
Gas turbine isentropic (polytropic) efficiency (%)	(87)	90
Steam turbine isentropic efficiency (%)	92	90
Compressor isentropic efficiency (%)	85	88
Heat exchangers pressure drop (%)	3	not given
ASU Power (kWh/kg-O_2)	0.23	0.25
ASU O_2 Purity (mol%)	95	99
Modeling Software	PRO/II (SIMSCI, Inc.)	IPSEPRO by SIMTECH
Net Efficiency (%)	49	53

Table 2.8: Modeling assumptions of some Graz cycles analyzed in the literature
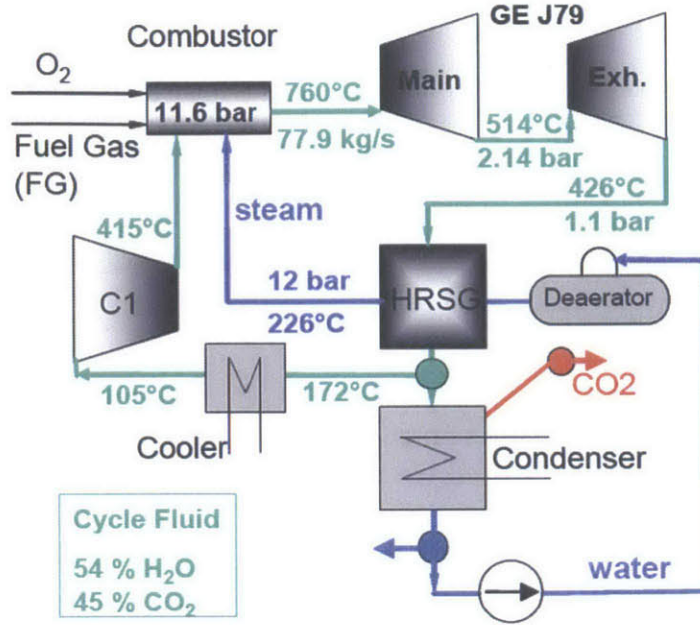
Figure 2-34: Cycle layout for a near-term basic Graz cycle [24]

Technology Availability

Since the working fluid of the Graz cycle consists of mainly steam, it has similar problems that are associated with the water cycle in terms of technological advancement. The problem with the water cycle's turbo-machinery blade materials is an important issue which also applies for the Graz cycle since there is also water present in the working fluid. The steam can cause oxidation and corrosion on the blades and therefore a special design is needed to prevent this which CES is currently working on. The design of the HTT has been a major issue since it needs to be able to handle the high temperatures around $1400°C$. But the HTT can benefit from the technology advancement being done by CES on their high temperature turbines with reheaters [49]. So once a high temperature turbine with a H_2O/CO_2 working fluid is designed and successfully demonstrated, this can pave the way for a future implementation of the Graz cycle in a power plant. In order to achieve near-term development of the Graz cycle for CCS it was suggested to utilize the existing hardware already proven by CES. The Graz cycle was tested with the GE J79 turbine data obtained from CES in a "basic" Graz cycle configuration shown above.

The working fluid has completely changed to almost equal fractions of water and carbon dioxide, and the HTT is replaced by the J79 turbine. The temperatures have also been changed (1440°C-760°C) to accommodate the J79 turbine's capabilities. These major changes resulted in net efficiencies of around 22% [24] which are significantly lower than what we would expect from regular Graz cycles, and also further justify the need for the turbo-machinery required by the Graz cycle in order to achieve respectable efficiencies.

There have been many studies on the designs of different Graz cycle power plants with different capacities [24, 55, 56]. It was suggested to increase the combustor pressure to 50 bar and the HTT inlet temperature to 1500°C to help increase the cycle efficiency and power output, and this resulted in a 1% efficiency gain [56]. However, these temperatures are very high and so far there are no known turbines that can handle those extreme conditions.

Despite all of these extensive studies, the main drawback of the Graz cycle is in its cycle complexity and it is not certain yet whether the actual capital costs of such a plant would make it economically viable and worthwhile, despite its efficiency advantage over the other oxy-fuel cycles (an approximate economic analysis is done in the next section). For these reason this cycle has not been implemented yet but could be within the next 5-10 years. Finally, another problem with the Graz cycle, similar to the water cycle, is that when using sour gas as the fuel, due to the high H_2O content in the working fluid, sulfuric acid formation is more likely and this can cause corrosion problems on metal surfaces.

Sensitivity Analyses

Unlike the previous two cycles, there have not been a lot of studies on the sensitivity of some of the cycle's operating conditions to the performance of the Graz cycle. The studies focused more on turbo-machinery optimization with regards to blade shapes, speeds, compression and expansion stages, which is not the main focus at this time for the system level analysis of sour gas combustion. In all of the Graz cycles in the literature, the combustor pressure was always chosen to be 40 bar for a 400 MW power
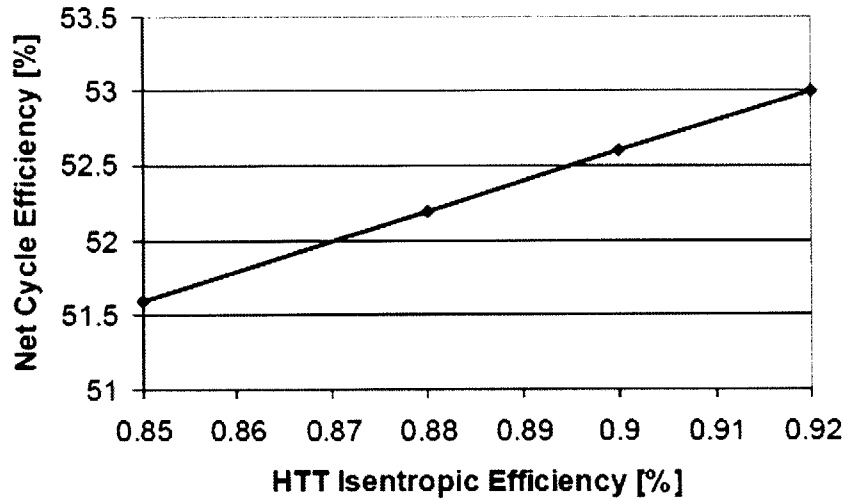
Figure 2-35: Influence of HTT isentropic efficiency on net cycle efficiency [22]

plant and the combustor exit temperature was always 1400°C. In one paper it was suggested to increase the operating pressure to 50 bar and the temperature to 1500°C in order to increase the power capacity of the power plant. But this only resulted in a 1% net efficiency gain. A thorough analysis was done by Brentan Alexander at MIT on the optimization of the Graz Cycle but using syngas as a fuel and including coal gasification. For this cycle, the optimal operating pressure was found to be in fact around 40 bar, the value currently used in Graz cycle analyses and the combustor exit temperature was calculated to be 1300°C. So we can safely assume that the net cycle efficiency is nearly maximized at an operating pressure of 40 bar.

The influence of the HTT isentropic efficiency on the net cycle efficiency was briefly studied for the original unmodified Graz cycle (see Figure 2-35). The results are shown below. As the isentropic efficiency went up, the net cycle efficiency also increased as we would expect. But there is a tradeoff because a higher isentropic efficiency results in a lower HTT outlet temperature which then decreases the HPT power output. For each 2% increase in the isentropic efficiency, the net cycle efficiency increases by 0.5%.

The effect of the condenser pressure, which has been studied a lot before for the other two cycles, was analyzed again for this cycle by Bolland et al. [20]. The Graz
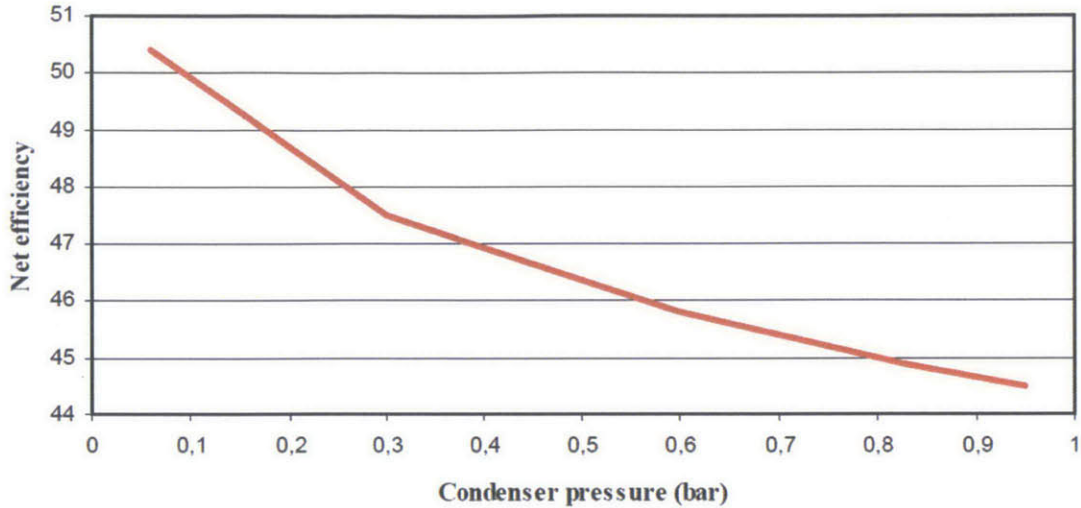
Figure 2-36: Net efficiency of the Graz cycle as a function of the condenser pressure in the range of 0.06-0.83 bar [20]

cycle configuration they used was the unmodified Graz cycle, similar to that shown in Figure 2-31. The results are shown in Figure 2-36.

As expected as the condenser pressure decreases, the efficiency of the cycle increases. The reason for this is that the LPT expansion work is higher than the CO_2 compression work such that the efficiency increase is mainly due to the increasing LPT work. The maximum net plant efficiency was calculated as 50.4% for a condenser pressure of 0.06 bar. But finally one key issue, when using sour gas as the fuel, is the condensation of the sulfuric acid in the low temperature components of the cycle, i.e. in the low pressure turbine and condenser. This is one of the major problems of the Graz cycle for sour gas combustion, since this cycle expands the working fluid down to very low pressures and temperatures.

2.2.5   Economic Evaluation

A study by Rezvani et al. [25] gives an overview of the cost estimation and economic evaluation of the SCOC-CC, Water, and Graz cycles using the ECLIPSE process simulation software. All the cycles were modeled similarly to how they have been modeled in the literature discussed above. The SCOC-CC was found to have an

Costs (M€)	SCOC-CC	WC	S-Graz
Waste Heat Boiler	16.03	22.35	5.63
HX + Cooling	11.57	8.65	9.21
Pumps	0.64	0.66	0.97
Piping	1.54	0.70	1.13
Compressor	0^2	5.53	74.91
Condenser	0.78	2.65	2.88
Gas Turbine	105.73	53.41	70.70
Steam Turbine	55.24	21.39	43.05
Burner	0	10.02	1.52
Misc	0	0.60	0
Indirect Costs	47.87	34.09	40.60
ASU	75.75	74.10	75.80
CO_2 Comp.	20.90	23.07	20.90
Total Cost (M€)	**336.02**	**257.23**	**347.30**
Specific Investment (€/kW net)	**1039**	**862**	**1042**

Table 2.9: Summary of the cycles' equipment costs

efficiency of 47.4%, the water cycle an efficiency of 43.74% and S-Graz cycle efficiency of 49%. The economic assessments of the cycles was performed in reference to year 2004. The results of this analysis are shown in the table above.

The economics of the studied power plants were strongly correlated to the cycle operating conditions. Since the SCOC-CC turbines and compressors need to be newly designed, it was estimated that the gas turbine cost increases over 22% over the traditional air-fired turbines. The plant complexity and usage of high quality materials also increase the cost of piping work by over 135%. For the water cycle, on the other hand, the high pressure areas and corrosion resistant materials place the cost of piping works comparable to the base case of a traditional combined cycle, mainly due to the simple cycle layout. But the Water and Graz cycles, require high tech materials to withstand the critical conditions such as corrosion and high pressures in some parts of the cycle. The low condensing pressures in the water and Graz cycles result in large heat exchanger surface area which will increase their size and thus cost. The low boiler costs of the Graz cycle are explained by the increased heat capacity

---

[2]This is zero because the gas turbine already accounts for the costs of the compressor and combustor
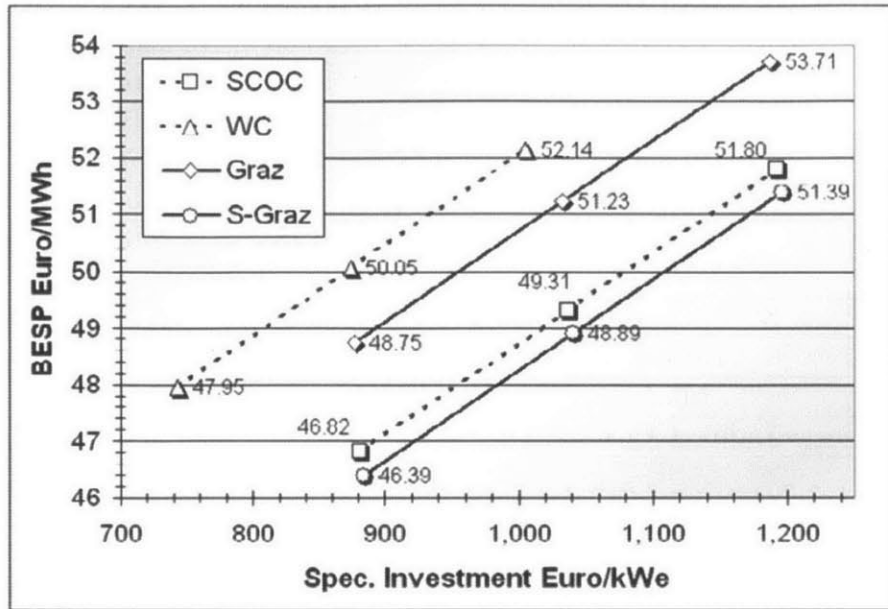
Figure 2-37: Electricity selling price versus the specific investment [25]

of the working fluid compared to the air-fired case. Finally it can be seen that the water cycle seems to be the best cycle since it has the lowest specific investment but this doesn't tell the whole story.

The figure above illustrates the typical breakeven selling prices of electricity for all of the cycles in relation to a specific investment variation of 15%. Due to the high efficiencies of the SCOC-CC and the Graz cycle, they deliver the best economic results, despite their higher specific investments and capital costs. The fuel price was also an important indicator of the economic viability of these cycles. Since the cycles with the lowest efficiencies consume the most fuel, the water cycle's overall fuel cost of 29.24 €/kWh is the highest among the systems. The electricity selling price was very sensitive to the fuel price fluctuations, with a 20% increase in the fuel price inflating the ESP at around 11%. To sum up these results, the Graz cycle was the most cost intensive process, but due to its high efficiency delivered the lowest electricity selling price. The water cycle on the other hand, is the least capital intensive technology but due to its poorer plant efficiency the economics of this cycle are not favorable.

96

2.3 Summary and Conclusions

The main results from this cycle review are summarized in the table below. The results from the literature are presented as advantages and disadvantages for each cycle while also incorporating the predicted effect from using sour gas as the fuel in oxy-combustion. The Combined Cycle (SCOC-CC) and Water Cycle seem like the best options to use as a basis for the sour gas cycles due to their simplicity and resemblance to conventional gas turbine cycle technologies. The Graz Cycle also has a major disadvantage in that at the exit of the HRSG, the working fluid is then expanded down to below-atmospheric pressures which would mean that there will be some sort of condensation occurring in the low pressure turbine. When using sour gas as the fuel, this would be disastrous since the condensed working fluid will contain sulfuric acid which will corrode the turbine blades and damage the cycle component. This notion was indeed verified when the Sour Gas Graz Cycle was modeled and in order to prevent condensation in that turbine, the cycle efficiency ended up being around 25%. This is much lower than the other sour gas cycles and thus making it not practical for this type of fuel. Therefore in the forthcoming chapters, the combined cycle and water cycle will be used as the basis for the sour gas cycles.

		SCOCC-CC	Water Cycle	Graz Cycle
Working Fluid Composition (% vol.)	CO_2	87%	6%	10%
	H_2O	13%	94%	90%
Operating Pressure (bar)		40	100	40
Efficiency Ranges		47-54%	40-49%	48-54%
Cycle Power Breakdown (% of heat input)	Turbine	89.7%	62%	102.7%
	Compressors, Pumps & Auxiliaries	30.8%	2.2%	39%
	ASU	8.8%	9.1%	9.2%
	CO_2 Compression	3%	6.1%	5.9%
Condensers		Working fluid has no major problem with equipment size	Working fluid expands to very low pressures: • Low heat transfer coefficient • Large equipment size • High capital costs	Working fluid expands to very low pressures: • Low heat transfer coefficient • Large equipment size • High capital costs
Potential Sulfuric Acid Formation with Sour Gas Oxy-Combustion		Sulfuric acid formation might not be as significant (due to low steam content in working fluid): • Simpler Cycle	High steam content in working fluid increases sulfuric acid formation: • Complex cycle	High steam content in working fluid increases sulfuric acid formation: • Complex cycle
Potential Condensation Problems with Sour Gas Oxy-Combustion		Water and sulfuric acid condensation may be possible but not significant	Need to operate condenser and LPT at higher temperatures and pressures to prevent water and sulfuric acid condensation: • Will impact cycle efficiency and complexity	Need to operate condenser and LPT at higher temps and pressures to prevent sulfuric acid condensation: • Will impact cycle efficiency and complexity

	SCOCC-CC	Water Cycle	Graz Cycle
CO₂ Capture Process	↗ CO_2 capture process is easier and simpler since working fluid has high CO_2 composition (87% vol.)	↗ CO_2 capture process is more complex since working fluid has low CO_2 composition (6% vol.), so more compression and condensation stages are needed to separate the H_2O	↗ CO_2 capture process is more complex since working fluid has low CO_2 composition (10% vol.), so more compression and condensation stages are needed to separate the H_2O
Turbine Technologies	↗ Needs new designs of current gas turbine machinery, for SCOC-CC compressors and turbines due to unusual working fluid (CO_2 &H_2O) and high temperatures	↗ Steam turbine technologies available for the HPT and LPT, from CES, for this cycle up to certain temperatures	↗ Needs development of advanced turbine technology, for HTT, due to unusual working fluid (H_2O & CO_2) and high temperatures
Cycle Implementation	↗ Cycle has not been implemented in real life but the layout of cycle is almost the same as a conventional combined cycle so modifications may be practicable. ↗ A new oxy-fuel gas-fired power generation technology with a supercritical carbon dioxide cycle is being developed by NET Power and a test plant should be completed by 2015	↗ Cycle has been built and implemented in real-life by CES at the Kimberlina Power Plant so it will be easier to analyze what would happen when using this new fuel (w.r.t. to efficiency, economics, corrosion issues...etc.)	↗ Cycle has not been implemented yet because of the complexity of the cycle and unusual working fluid makes it economically unviable (so far) and needs new turbo-machinery design (especially for HPT)

Chapter 3

Cycle Modeling and Base Cases

3.1   Methodology

Aspen Plus® [26] was used in all of the modeling for the cycles in this report. Its main strengths are in modeling chemical processes and non-standard components such as air separation units (ASUs) and acid removal systems. This software has been used many times in the literature for system analyses and it allows us to perform sensitivity analyses, generate graphs and conduct optimization studies.

The PR-BM property method [26] was used to model the components in the methane oxy-fuel cycles. It uses the Peng Robinson cubic equation of state with the Boston-Mathias alpha function for all thermodynamic properties. It can be applied for nonpolar or mildly polar mixtures (ex. hydrocarbons and light gases, such as carbon dioxide, hydrogen sulfide, and hydrogen). It is recommended for high-pressure hydrocarbon applications (ex. combustion and power generation). This was also used as the property method for the combustors in the sour gas cycles.

When modeling the cycle components in the sour gas cycles, a different property method had to be used due to the unusual components present in the working fluid (sulfur compounds). To determine which property method to be used, the flowchart shown in Fig. 3-1 provided by Aspen [26] was referenced. The SR-Polar property method was determined to be the best fit for our application. This is based on an equation-of-state model by Schwarzentruber and Renon, which is an extension of the
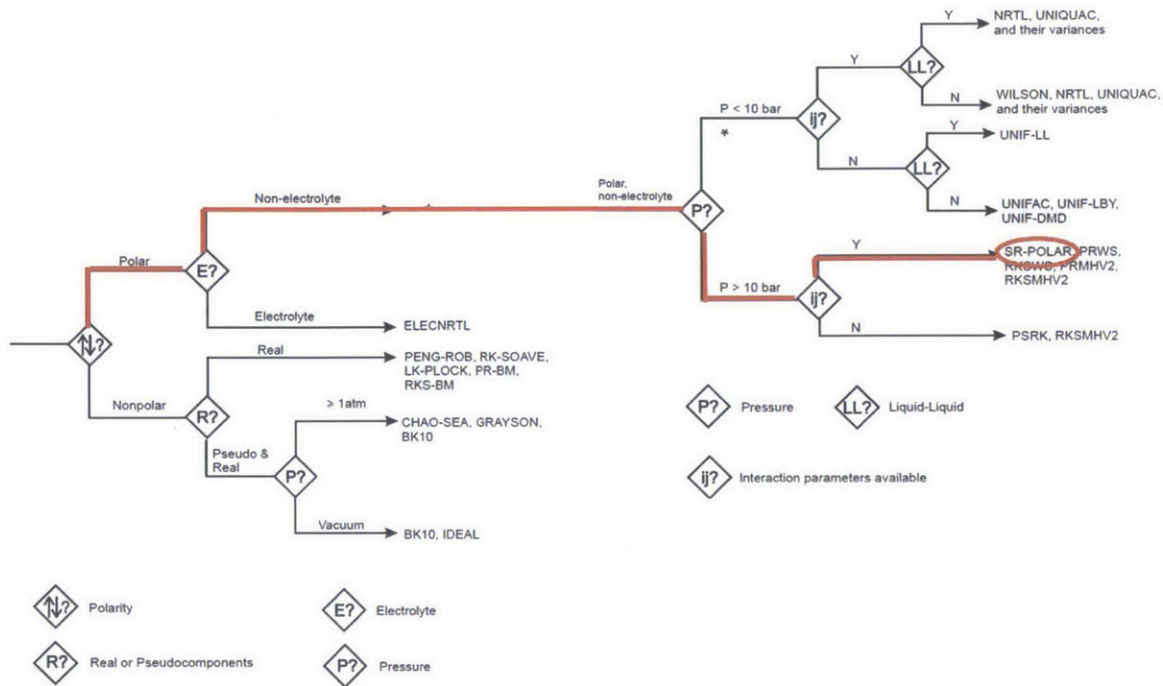
Figure 3-1: Aspen guidelines for choosing a property method [26]

Redlich-Kwong-Soave equation of state. It can be applied to highly polar components (ex. SO_2 and SO_3), and recommended for high temperature and pressure applications. This was used as the main property method for most of cycle components in the sour gas cycles.

Before we look into the structure of the sour gas oxy-fuel power cycles, the methane oxy-fuel cycles are described along with the cycle components and assumptions made, as these will serve as the base-case cycles in our future analyses for sour gas cycles.

3.2 Methane Oxy-Fuel Cycles

From the extensive literature review that was done on the methane oxy-fuel cycles, the water cycle and the oxy-fuel combined cycle were determined to be the most feasible, in terms of implementation and technology availability, of all the methane oxy-fuel power cycles, and so will serve as the basis when constructing the sour gas cycles. They also have some of the more simple cycle layouts and are similar to todays
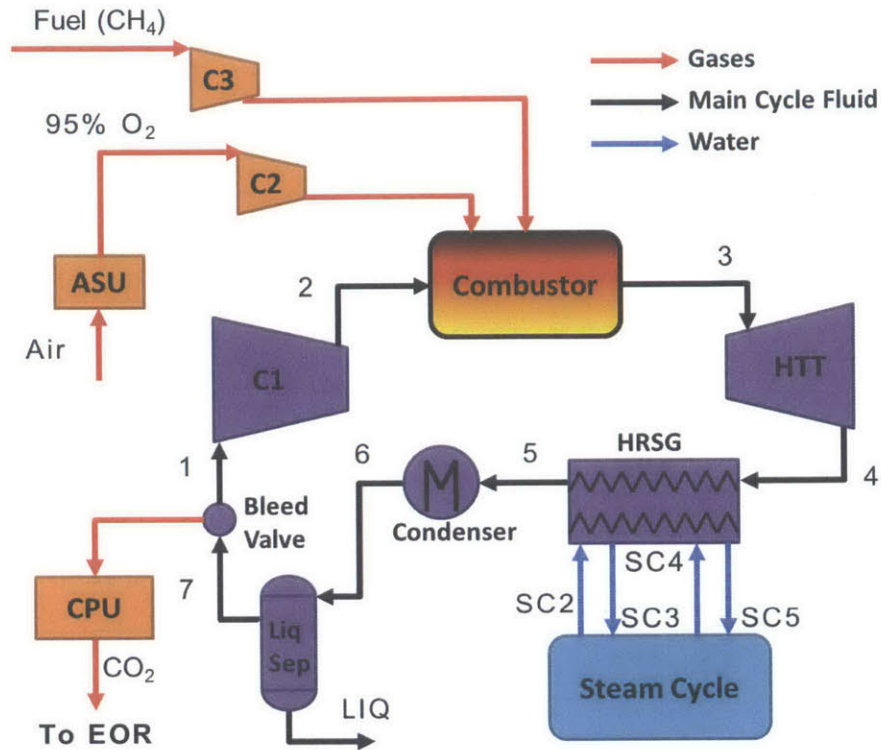
Figure 3-2: Overall process layout for the methane oxy-fuel combustion combined cycle

technologies of Combined Cycles and Steam Rankine Cycles.

3.2.1 Combined Cycle

Fig. 3-2 shows the cycle diagram of the oxy-fuel combined cycle with pure methane as the fuel, with the corresponding T-s diagram in Fig. 3-3. The cycle configuration is based on a Brayton combined cycle with a steam bottoming cycle.

The working fluid, consisting of about 88% CO_2 (by volume), enters the main compressor (C1) at state 1 and is compressed up to a pressure of 40 bar. On the gas side, the oxygen stream from the air separation unit is sent to the combustor along with the fuel (100% CH_4), and the recycled working fluid. The recycled working fluid acts as a diluent in the combustor, and so the recycle ratio of the working fluid fixes the combustor exit temperature at 1300°C. The combustor flue gases (78% CO_2, 14% H_2O by volume) at 1300°C, state 3, are next expanded in the turbine to 1.12 bars

103
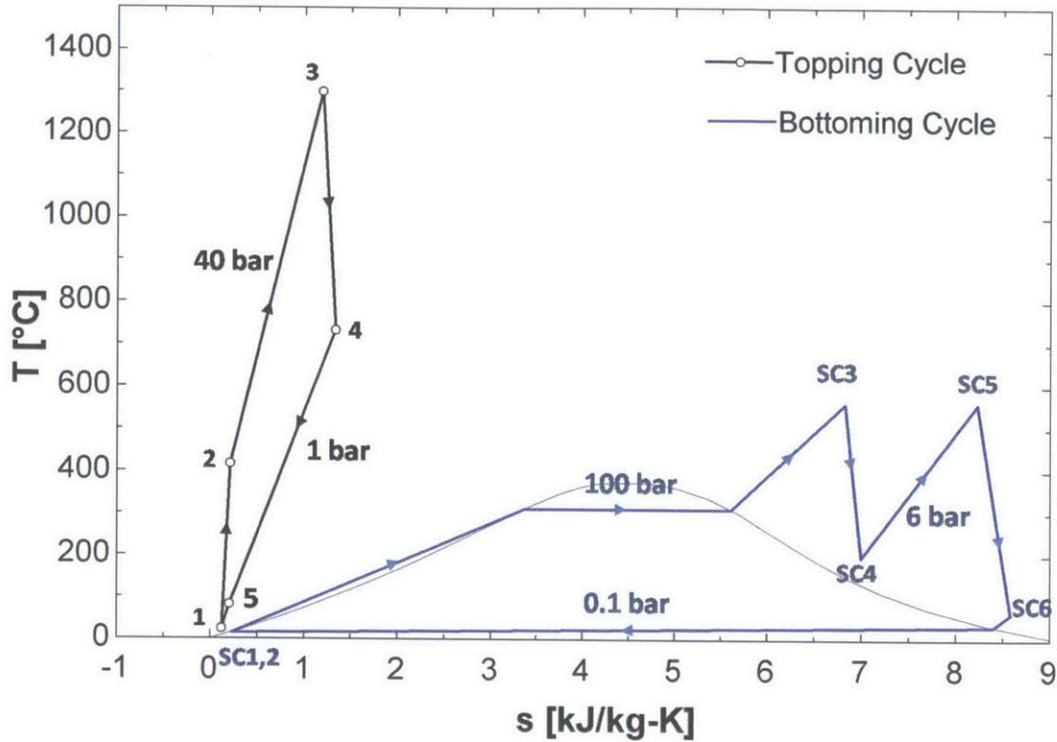
Figure 3-3: T-s diagram of the methane oxy-fuel combined cycle

to produce work. The lowest pressure in the cycle was chosen to be always greater than or equal to 1 atm to prevent any back flow when any of the fluid streams are extracted from the main cycle (ex. state 7).

Next, the main working fluid enters the HRSG at state 4 where it transfers thermal energy to the steam cycle while being cooled down to state 5. The steam bottoming cycle is quite similar to the steam turbine cycles of conventional combined cycle power plants. It is a double pressure Rankine cycle with reheat for a better efficiency. The two steam turbines operate at 100 bar and 6 bar respectively with inlet temperatures of 560°C. This is similar to those modeled in the literature as well [15, 11].

The remaining working fluid at state 5 is condensed to 25°C in the condenser and then the liquid (mostly water) is separated out to state 7. After that 93% of the working fluid is recycled back up to the compressor to be the diluting medium in the combustor. Then finally the excess working fluid is extracted in the bleed valve and sent to the CO_2 purification unit (CPU) and compressed up to 110 bars to yield a
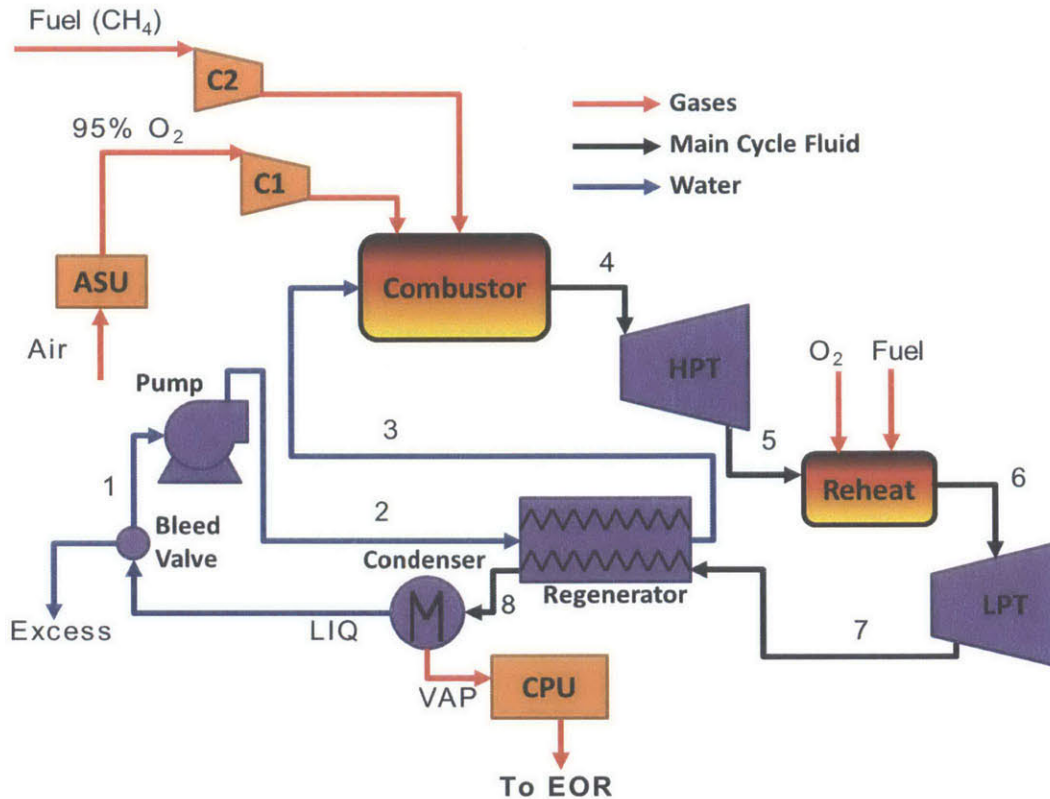
Figure 3-4: Overall process layout for the methane oxy-fuel combustion water cycle

capture-ready carbon dioxide stream for EOR. The efficiency of this cycle with these conditions was found to be 45.9%.

3.2.2 Water Cycle

The cycle layout for the methane oxy-fuel water cycle is shown in Fig. 3-4 along with its T-s diagram in Fig. 3-5. It is based on a Rankine Cycle with reheat and regeneration. Water is pumped up to a pressure of 100 bars where it is then preheated in the regenerator before entering the combustor where it is burned along with the fuel and oxidizer and exits at a temperature of 600°C. The main combustor flue gases (5% CO_2, 94% H_2O by volume), state 4, are then expanded in the turbine (HPT) to 15 bars to produce work. The fluid is then reheated to a temperature of 1200°C and then expanded again in the low pressure turbine (LPT) down to 0.1 bar.

In the regenerator, the working fluid transfers its thermal energy to the water
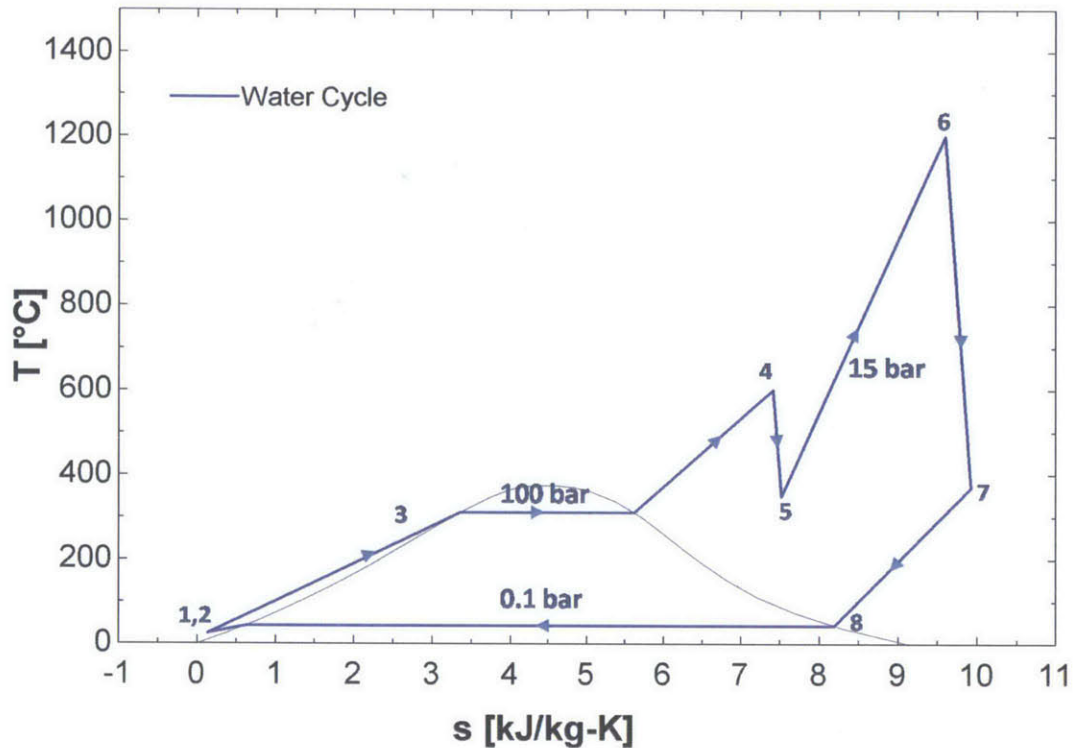
Figure 3-5: T-s diagram of the methane oxy-fuel water cycle

stream going to the combustor while being cooled down to state 8. The remaining working fluid at State 8 is condensed to 25°C in the condenser and then 83% of the water is pumped and recycled back up to the combustor. The vapor is sent to the CPU to produce an EOR ready CO_2 stream at 100 bars. The efficiency of this cycle with these conditions was found to be 41.4%.

3.2.3 Modeling Assumptions

The assumptions made when performing a thermodynamic analysis and modeling these two base-case cycles are shown in Table 3.1. The same assumptions were applied to the sour gas cycles but with additional modeling assumptions and components, as will be mentioned later on. Most of these assumptions and design variables are based on currently available commercial technologies and values common to what is seen in the literature.

	Combined Cycle	Water Cycle
Fuel		
Composition (mol%)	100% CH_4	
LHV[a] (MJ/kg)	50.1	
Combustors		
Operating Pressures (bar)	40	100 & 15 (Main & Reheater)
Pressure Drops (%)	5	10 & 6 (Main & Reheater)
Turbines		
TIT's[b] (°C)	1300	600 & 1200 (HPT & LPT)
Isentropic Efficiencies (%)	85	87 & 90 (HPT & LPT)
Compressors & Pumps		
Isentropic Efficiencies (%)	85 (Compressor)	75 (Pump)
Heat Exchangers		
MITA's[c] (°C)	20	20
Pressure Drops (%)	5	5
Steam Cycle		
HRSG Pressures (bar)	100 & 6	
TIT's (°C)	560	
Turbine Efficiencies (%)	90	N/A
Condenser Pressure (bar)	0.05	
Pump Efficiency (%)	75	
ASU		
Specific Power (kWh/kg-O_2)	0.225	
O_2 Stream Composition (mol%)	95% O_2, 4.2% Ar, 0.8% N_2	
O_2 Compression		
Isentropic Efficiency (%)	84	84
Compression Stages	3	3
Intercooler Temps (°C)	25, 50	25, 25
Max Exit Temp (°C)	200	200
CPU		
CO_2 Delivery Pressure (bar)	110	
Exit CO_2 Stream Composition (mol%)	> 99% CO_2 (EOR Ready)	

Table 3.1: Methane cycles modeling assumptions

[a]Lower Heating Value
[b]Turbine Inlet Temperature
[c]Minimum Internal Temperature Approach

3.2.4 Performance Analysis

The modeling assumptions listed in Table 3.1 were used to perform a thermodynamic analysis of the two types of methane oxy-fuel cycles shown in Figures 3-2 and 3-4.

First of all comparing the working fluids of the two cycles (measured at the exit of the combustors), as seen in Fig. 3-6, one can clearly see that the combined cycle has a much higher CO_2 content than the water cycle. But the water cycle has a much higher H_2O content than the combined cycle. This is because as was mentioned before, the methane oxy-fuel combined cycle recycles mostly CO_2 back to the combustor to act as a diluent, therefore resulting in higher amounts of CO_2 in the working fluid (78 vs 9%). On the other hand, the water cycle (as the name implies) recycles H_2O back to the combustor and so the working fluid contains much higher amounts of H_2O in the working fluid (90 vs 14%).

Details of the power generated and consumed by the different components in the cycles are shown in Fig. 3-7. The power outputs and inputs are expressed as a function of the (total) heat input to the cycle (based on the fuel's LHV) in order to non-dimensionalize the results. The heat inputs to both the combined and water cycles were 80.4 and 164.4 MW respectively. It can be seen that the turbine and compressor/pump works are significantly different for the two cycles. In the water cycle, since **liquid** water is being fed to the combustor, part of the fuel's heating value is being used for phase change. Whereas in the combined cycle, gaseous CO_2 is recycled back up to the combustor and so the heat input is only being used to raise the temperature of the working fluid. Therefore, for the water cycle, this results in a lower stream mass flow rate in order to keep the heat input constant which in turn decreases the turbine power output. The combustor and reheater pressure drops in the water cycle (10 & 6 %) are higher than those of the combustor in the combined cycle (5%), for reasons which are explained in section 3.3.2. This also helps contribute to the difference in turbine power outputs for the two cycle types. Since the compression and pumping requirement in the water cycle is mainly from liquid water pumping, the power consumption is much less than the combined cycle which
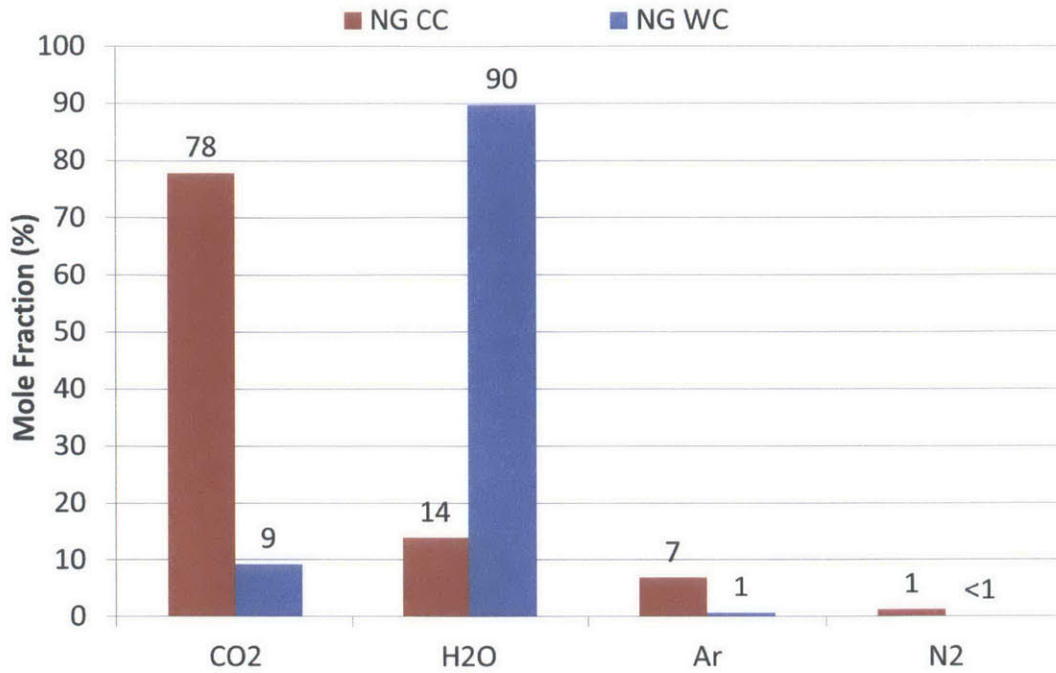
Figure 3-6: Working fluid comparison for the two methane cycles (Combined Cycle and Water Cycle)

requires an energy intensive gas compressor.

The ASU work is similar for both, but the CPU work is a bit higher for the water cycle because the condenser pressure in the water cycle is lower (0.05 vs 1 bar). Therefore it requires a larger compression work to recompress that stream up to the 110 bar needed for transportation for CO_2 sequestration. All of these above effects leads to the efficiency difference shown. The combined cycle has a 4.5% higher efficiency than the water cycle and this trend is seen regularly in our later analyses for the sour gas cycles.

3.2.5 Model Validation

When modeling these cycles in Aspen Plus, one can never be 100% certain that the pressures, temperatures and efficiencies reported by the Aspen Plus model is correct. Therefore some sort of model validation is required. However in most of the methane oxy-fuel cycles modeled in the literature, not enough assumptions were reported in
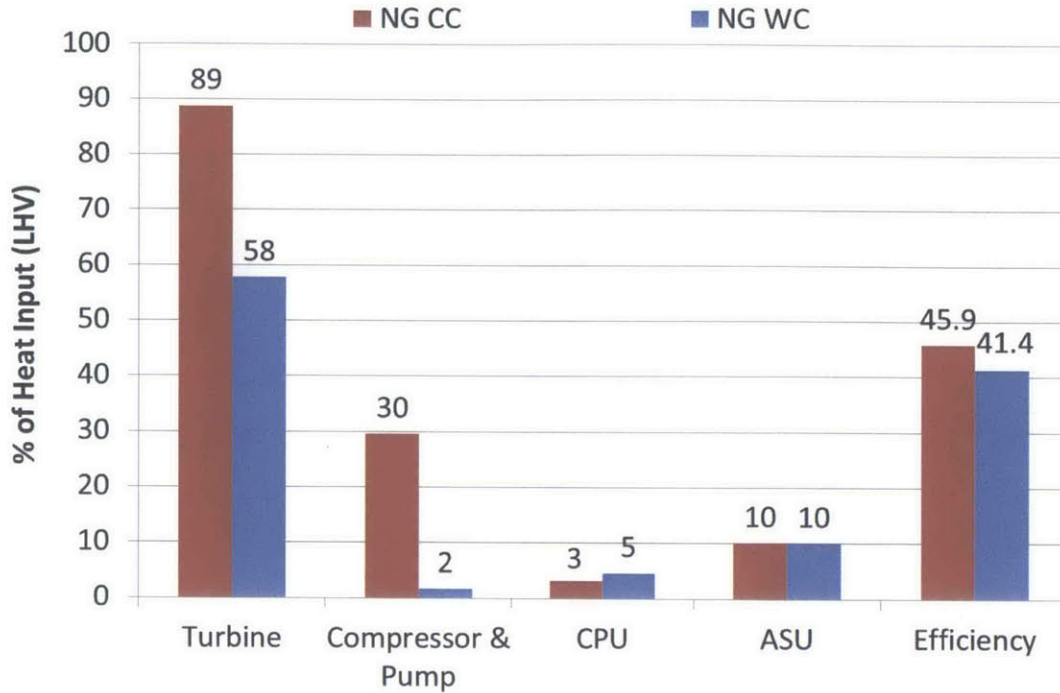
Figure 3-7: Power breakdown for the two methane cycles

order to replicate their results. The most information given about a cycle and the computational assumptions they made in the literature was the Water (CES) cycle modeled by Gou et al. [16]. The flowsheet diagram for that cycle is shown in Fig. 3-8. This cycle has the same layout as the water cycle but with a combustor temperature of 900°C and a reheat temperature of 1300°C. The cycle in the literature was also modeled in Aspen Plus which is another reason why this cycle was chosen.

Building on the existing model we had for the water cycle and using the assumptions given in the paper to modify the model's operating conditions, the cycle by Gou et al. was constructed and the results were compared to those given in the paper. The T-s diagrams were compared as these gave a good representation of the temperatures at certain points in the cycle. These are shown in Fig. 3-9 for both the Gou cycle and our model. The temperature and entropy values are almost identical and the shape of the T-s diagram is also very similar which is a good indication that our model is valid. We also wanted to compare the performance of the two cycles by looking at the efficiency values. Comparing the efficiencies reported both in the paper and the

Figure 3-8: Overall process layout for the Water Cycle modeled by Gou et al. [16]

	Gou et al. [16]	Our Model
Efficiency	44.4%	44.8%

Table 3.2: Efficiencies reported by Gou and the current model

one obtained in our model, there is about a 0.4% discrepancy, as evident by Table 3.2. Since all of the pressures, temperatures and stream compositions reported in the paper are very close to those obtained in our model, and the fact that the same computational assumptions were made, it can be safely assumed that our model functions well and can be relied on for future cycle modeling. This difference might have been due to the version of Aspen Plus used (since the paper was published in 2006), or the slight differences and updates to the property method (Peng-Rob) used since then.

(a) Gou et al.'s cycle [16]　　　(b) Our model's cycle

Figure 3-9: T-s diagrams for the water cycles modeled in the literature and in the current Aspen plus model

3.3　Cycle Components and Assumptions

Now that we know what the two main cycles look like, we will now discuss the important cycle components for oxy-fuel combustion and the assumptions we made while modeling them. The same assumptions and components were used for both the methane and sour gas oxy-fuel cycles. However, as will be described later on, the sour gas cycles will require some modifications and additional components due to the presence of sulfur compounds in the working fluid. These additional components will be talked about in Chapter 4 when we discuss the first of the sour gas cycles.

3.3.1　Air Separation Unit and Oxygen Compression

ASU

One key aspect of oxy-fuel combustion is the oxygen production process. As was described in section 1.2.5, air separation units (ASU) using cryogenic separation is the only available option to produce the large amounts of oxygen required by these plants. ASUs also have significant energy penalties of 7-8% as will be seen later on in the forthcoming chapters, and this is what distinguishes them from traditional

112
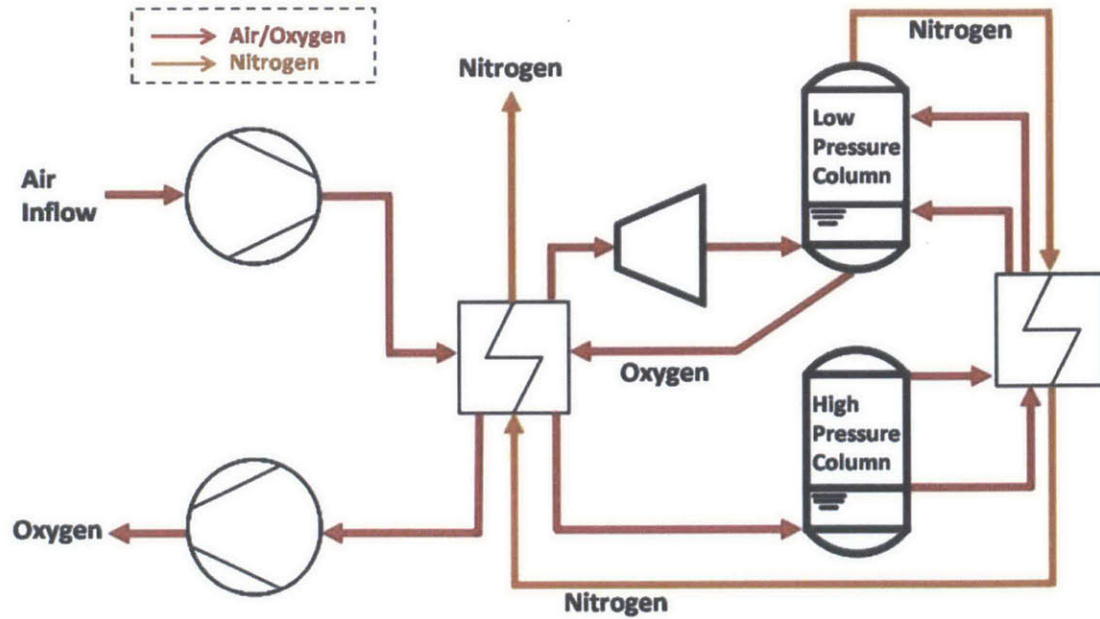
Figure 3-10: Process layout of the ASU [27]

air-fired power plants.

The air separation unit was modeled based on James Hong's model [27], also described in detail in section 1.2.5. The large amount of oxygen required by the oxy-fuel plant is produced using cryogenic separation processes. The process layout for the ASU is shown in Fig. 3-10. This ASU model produces an oxygen stream with an outlet oxygen purity (by volume) of 95% O_2, 4.2% Ar, 0.8% N_2 at a pressure of 1.24 bars, while requiring a specific power of 0.225 kWh/kg-O_2 (0.812 MJ/kg-O_2). This specific power value is also around what is being used in the literature [34] as the specific energy required to produce oxygen for oxy-fuel combustion.

In order to assess the impact of the specific power of the ASU on the whole cycle, a sensitivity analysis was done looking at different specific powers and their effect on efficiency. As can be seen from Fig. 3-11, changing the specific work by 0.1 kWh/kg-O_2, changes the efficiency by 3%. A similar analysis was done by Bolland et al. [15] and the same effect on efficiency was observed. Advances in cryogenic separation technologies could see this specific power decrease in the future and, as was seen from the previous analysis, significantly improve efficiency.
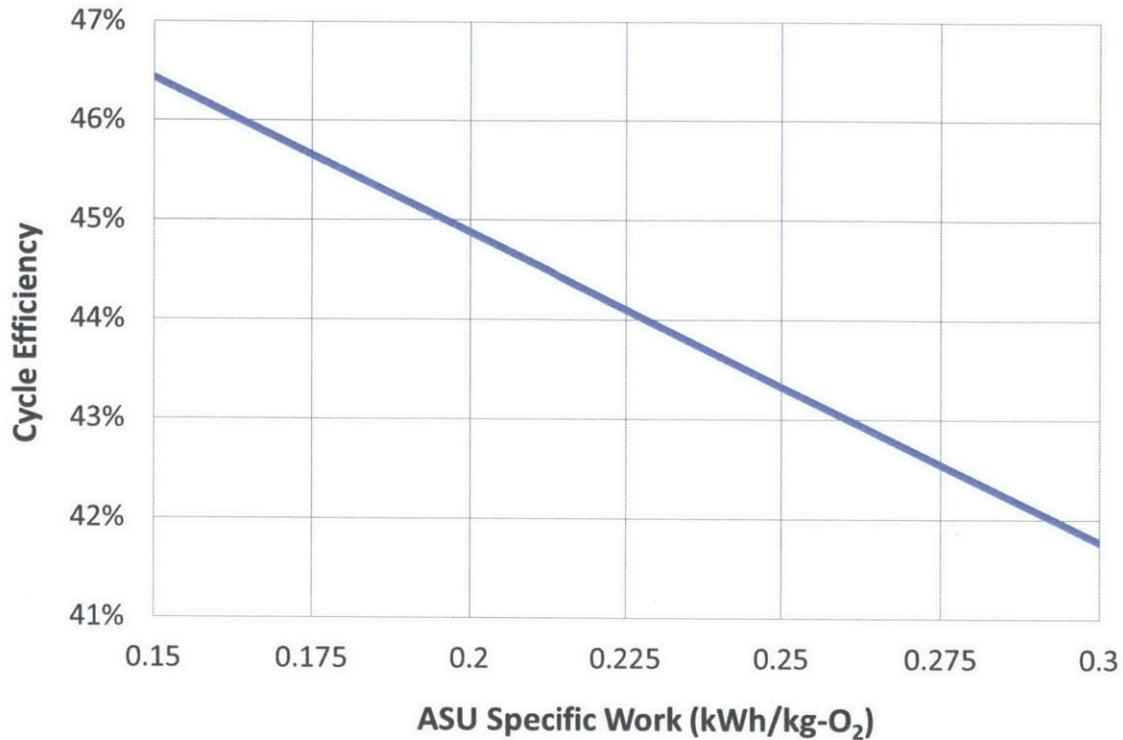
Figure 3-11: Effect of the ASU specific work on the cycle efficiency

O$_2$ Compression

At the exit of the ASU the O$_2$ stream is at a temperature of 17°C and pressure of 1.2 bar, therefore will require compression to increase the pressure up to the required combustor pressure (40 bar for the combined cycle and 100 bar for the water cycle). However there are tight constraints on the temperature of the stream in the compressors due to the high flammability of oxygen in the presence of any combustible material. Therefore a maximum temperature of 200°C of the stream was chosen based on DOE guidelines for energy system studies [57]. The isentropic efficiencies of the O$_2$ compressors, was also taken to be 84% based on those same guidelines. Fig. 3-12 shows the oxygen stream's compression process. In order to achieve the desired maximum temperature, compressors with intercooling had to be used with 3 compression stages because it was found that the temperature limit could not be achieved with just 2. So with this process there were two unknowns that had to be found: intercooler temperatures, 3 and 5. A temperature range of 25-50°C was tested
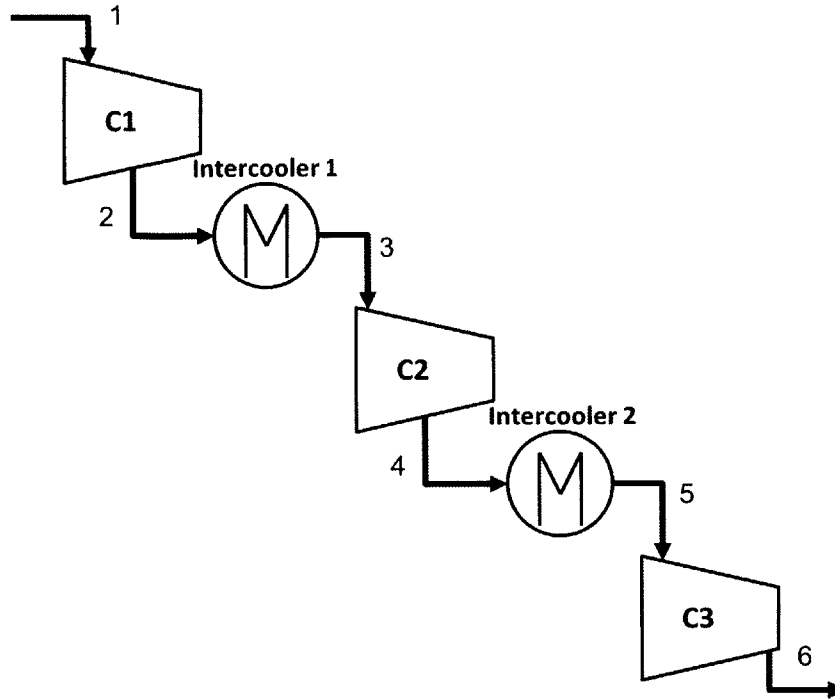
Figure 3-12: O_2 multi-stage compression process with intercooling

for each stream and its effect on cycle efficiency and the temperatures at the exit of the compressors was analyzed.

Fig. 3-13 shows the effect of changing both intercooler exit temperatures on the cycle efficiency. The results show that choosing the lowest temperature for intercooler 1 and the highest temperature for intercooler 2, gives the best combination to maximize efficiency. This is because there is a tradeoff between reducing the compressor power input and increasing the final compressor exit temperature (T_6). Both of these effects increase the cycle efficiency but choosing a certain intercooler temperature benefits one at the expense of the other. For example choosing 25°C vs 50°C reduces compressor power input, due to the lower input temperature, thus increasing efficiency. However this also decreases the final compressor exit temperature which lowers the cycle efficiency because of the increased temperature difference in the combustor. Therefore for this process choosing the lowest temperature for intercooler 1, increases efficiency due to the lowered compressor input temperature which in turn reduces the power required. Subsequently, choosing the highest temperature for in-
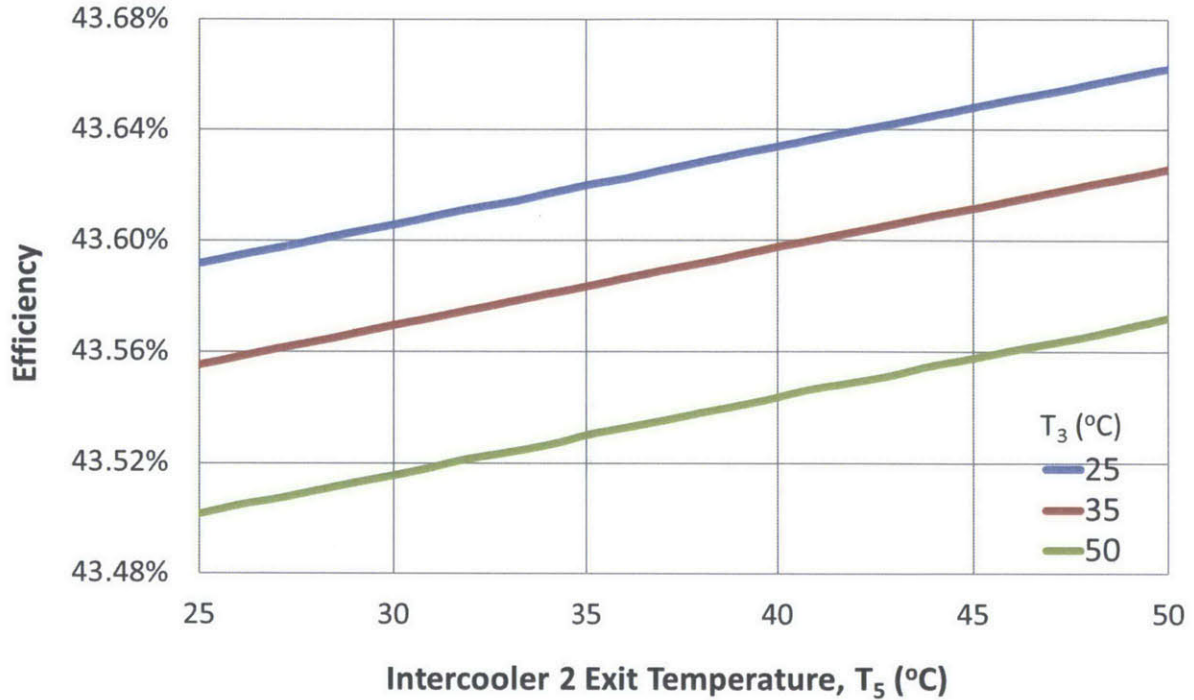
Figure 3-13: Effect of 3 stage O_2 compression on efficiency

tercooler 2 also increases efficiency because of the increase in the final compressor exit temperature. But now we need to see what happens to the temperatures of the compressors' exit temperatures when the intercooling temperature is changed.

Fig. 3-14 shows the effect of changing the 2nd intercooler's temperature on the compressors' exit temperatures. This was done by keeping the 1st intercooler's temperature fixed at 25°C as this was determined to be the best temperature from the preceding analysis. As we would expect, the compressor exit temperatures for C1 and C2 are fixed since their inlet temperatures are fixed. The final compressor, C3, exit temperature increased with increasing intercooler 2's temperature obviously since we are increasing that compressor's inlet temperature. But the main output from these results was to show that the temperatures never exceeded the 200°C limit we imposed earlier, throughout the whole compression process. Even at the point of maximum efficiency, $T_5=50°C$, the final exit temperature was still just under 200°C. This short compressor and intercooling analysis was used when modeling all of the cycles: methane and sour gas.

116
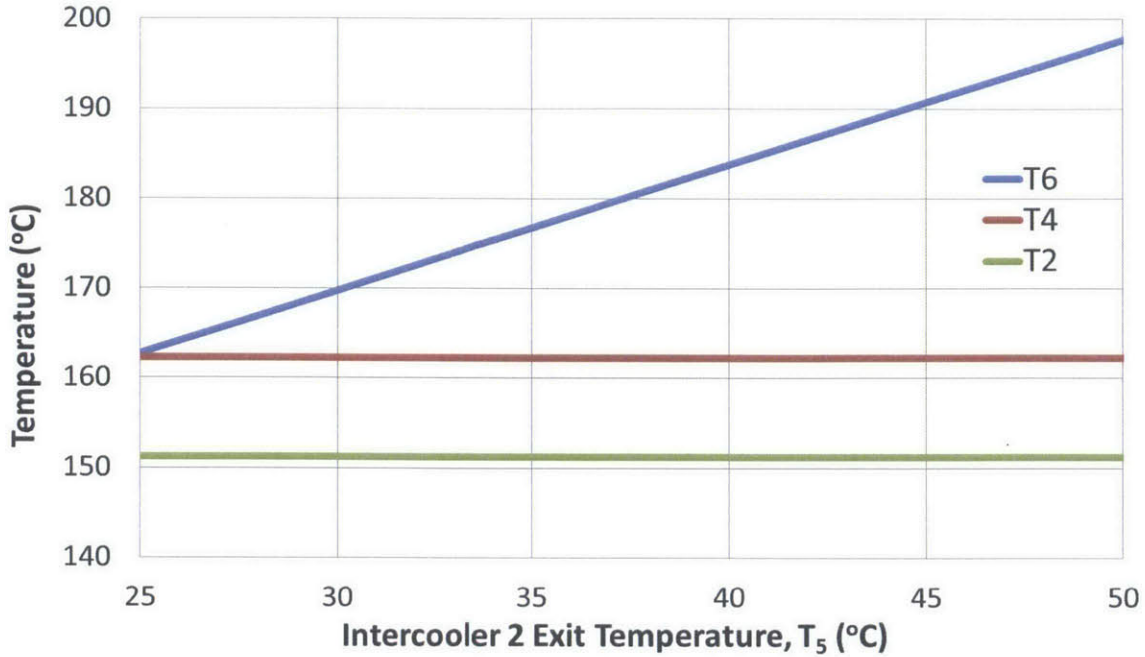
Figure 3-14: Effect of 3 stage O_2 compression on temperature's for $T_3 = 25°C$

3.3.2 Combustors

When modeling the combustor, the "RGibbs reactor" model was used [26]. RGibbs models single-phase chemical equilibrium, or simultaneous phase and chemical equilibria. The reaction kinetics are not taken into account. A Gibbs free energy minimization is done to determine the product composition. It is commonly used in the literature to model combustors when reactions occurring are not known, or are high in number due to the many components participating in the reactions.

The combustion was assumed to be stoichiometric. The way to control this was to adjust the mole flows of the oxygen and fuel streams to a certain ratio in according with the stoichiometric reaction below. Therefore in this case for every mole of methane we have, 2.105 moles of oxidizer is required. The fuel (100% methane in this case) was chosen to have a fixed mole flow of 100 mol/s and so the oxidizer streams mole flow is 210.53 mol/s (see figures 3-15 and 3-16).
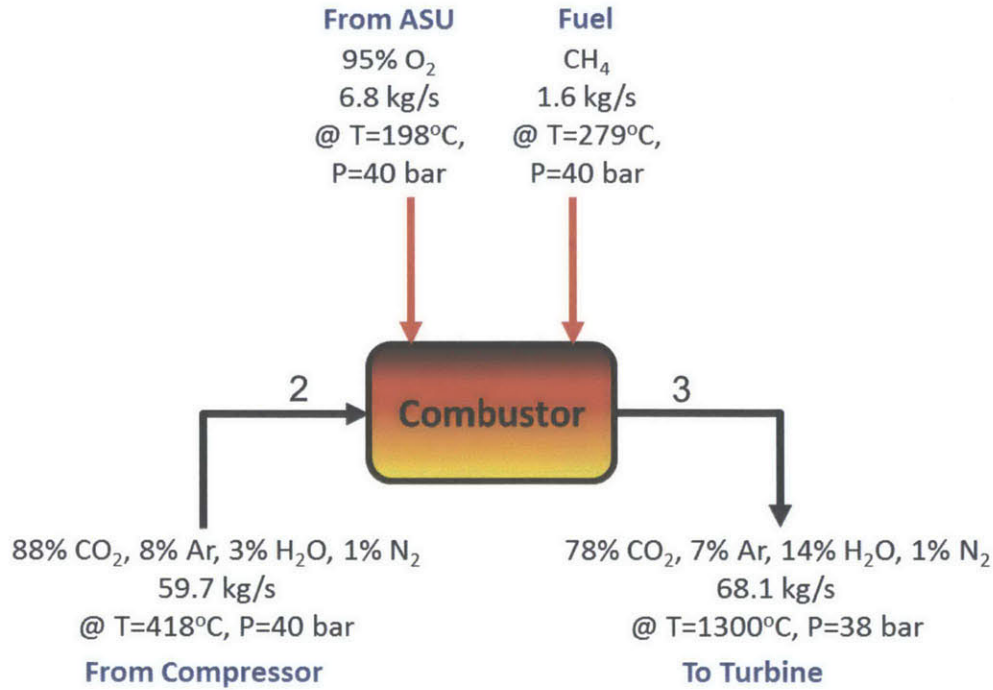
Figure 3-15: Mole fractions, mass flow rates, temperatures and pressures of streams across the combustor for the methane oxy-fuel combined cycle

$$CH_4 + \frac{2}{0.95}(0.95O_2 + 0.042Ar + 0.008N_2) \longrightarrow CO_2 + 2\,H_2O + 0.088Ar + 0.017N_2$$

(3.1)
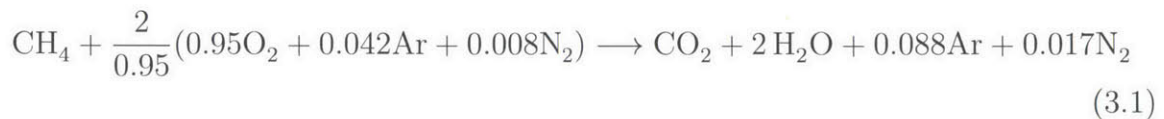
The combustor is also assumed to be completely adiabatic. The stoichiometric combustion of fuels with pure oxygen can reach temperatures around 3500°C [4], which is well above the design limits of typical power plant materials. Therefore a diluent is required to moderate the temperatures down to acceptable levels. In the combined cycles, mainly CO_2 is recycled to the combustor to act as the diluent. Whereas in the water cycles, as the name implies, H_2O is recycled back up to the combustor as the diluent.
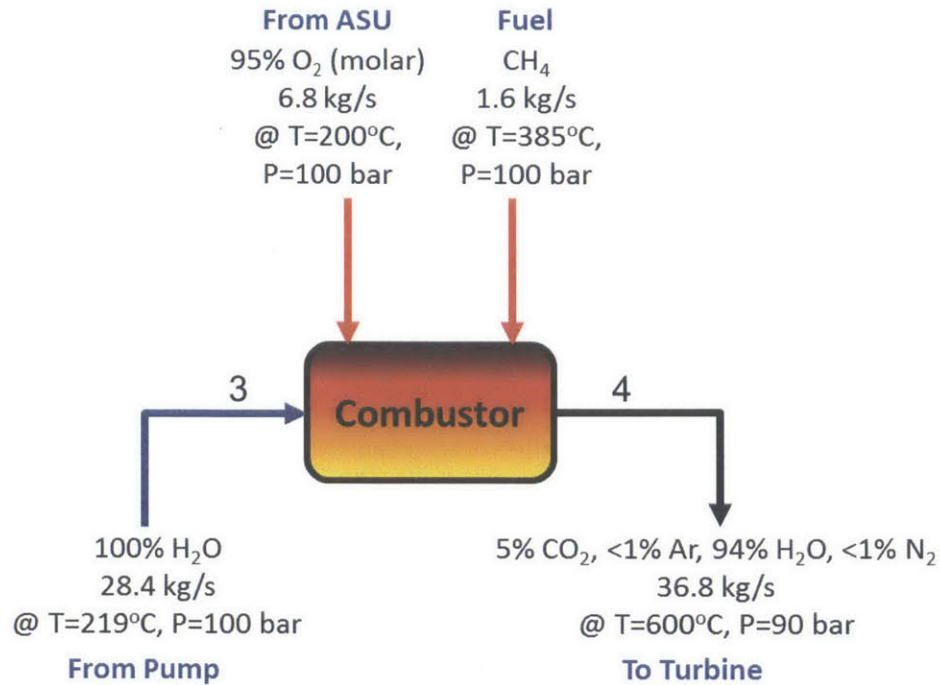
Figure 3-16: Mole fractions, mass flow rates, temperatures and pressures of streams across the combustor for the methane oxy-fuel water cycle

Combined Cycle

In gas combined cycles, typical combustor temperatures are between 1200-1400°C [34, 15, 13, 14]. Therefore in our analysis a fixed combustor exit temperature of 1300°C was chosen, and was controlled by the certain proportion of working fluid that was recycled back to the combustor (stream 1 in Fig. 3-2). For the base methane oxy-fuel combined cycle (Fig. 3-2), this recycle ratio was determined to be 93%. This is the ratio of stream 1 to stream 7, and was calculated using a design specification in Aspen Plus for maintaining the desired combustor temperature.

The operating pressure of the combustor for the combined cycle is 40 bars, which is also the typical combustor pressures for gas turbine combined cycles [34]. A pressure sensitivity analysis was done for the methane and sour gas combined cycles and the results are presented in section 4.2.2. A more conservative pressure drop of 5% was assumed compared to that of the literature. The compositions and operating conditions of the streams in the combustor for the methane combined cycle are shown

in Fig. 3-15.

Water Cycle

The oxy-fuel water cycle was developed by Clean Energy Systems (CES) back in 1999 [48]. As previously discussed in section 2.2.3, CES is one of the few companies that has implemented an oxy-fuel power cycle and has developed the combustor and turbines for this new working fluid (containing CO_2). Currently the turbines they've developed (for the LPT) can handle temperatures of 1080-1260°C [18, 49]. Therefore for the LPT, we have chosen the reheater exit temperature to be 1200°C. Since the LPT has a higher pressure ratio, advancing the turbine technology for this component to increase the temperatures it can handle, was the focus of CES.

It was found in pressure and temperature sensitivity studies discussed later, that increasing the LPT inlet temperature had a bigger impact on efficiency than increasing the HPT inlet temperature. Also since at the exit of the combustor the working fluid is mostly H_2O (see Fig. 3-16), it was assumed by CES that the HPT can be implemented using existing steam turbine technology [18]. Consequently, in our analysis a fixed combustor exit temperature of 600°C was chosen, and once again was controlled by the certain proportion of working fluid (water) that was recycled back to the combustor (stream 1 in Fig. 3-4). For the base methane oxy-fuel water cycle (Fig. 3-4), this recycle ratio was determined to be 83%. This is the ratio of stream 1 to stream 8, and once again was calculated using a design specification in Aspen Plus. It can be seen that the recycle ratio for the water cycle is lower than that of the combined cycle, due to the difference in the recycled stream. In the combined cycle mostly CO_2 is recycled, whereas in the water cycle H_2O is being recycled. The higher heat capacity of the water stream results in less of it being recycled in order to keep the combustor exit temperature fixed.

The operating pressure of the combustor for the water cycle is 100 bar, which is also the pressure commonly used for this type of cycle [11, 16] and based on CES's specifications. The reheater operates at 15 bar, which was found using a pressure sensitivity analysis (discussed later) to determine the optimum reheater pressure.

The pressure drops for these two burners were also based on CES's combustors and their specifications. CES's main combustor (or gas generator) has a pressure drop of 10-15% [58]. For our purposes a value of 10% was chosen. The compositions and operating conditions of the streams in the combustor for the methane water cycle are shown in Fig. 3-16. Finally, for the reheater the pressure drop used was 6%, the value given by CES [18].

3.3.3 Carbon Dioxide Purification and Compression Unit

The excess working fluid from the two cycles (red stream from the bleed valve for the CC in Fig. 3-2, 'VAP' stream in Fig. 3-4 for the WC), is sent to a CO_2 purification unit (CPU) where the non-condensable gases (Ar & N_2) are removed and the capture-ready CO_2 stream is compressed up to 110 bar for EOR.

The incoming stream (mostly CO_2) to the CPU has the inert gases removed using low temperature separation techniques and the purified CO_2 stream is extracted as a liquid and pumped up to the sequestration pressure, and an exhaust stream consisting of mainly the inert gases is also produced. The separation process was modeled based on Chukwunwike Iloeje' non-condensable gas removal configuration B [28]. This type of process was chosen because it delivers a liquid stream, thus eliminating the cost and energy penalty of gas phase compression of the purified stream. This separation technique also requires external refrigeration to provide the cooling load to the unit.

The process flowsheet is shown in Fig. 3-17. Initially the incoming stream is sent to regenerative dryer beds to remove the moisture in the gas. Next the gas which is at the cycles' respective condenser pressures (1 bar for the CC, 0.1 bar for the WC), is compressed up to 8 bar and cooled down to around -55°C by the external propane refrigeration cycle. The two phase stream is then sent to the distillation column where it interacts with the down-coming liquid and separation occurs. A high purity (99.1%) CO_2 stream is extracted from the bottom of the column and then pumped directly to the pipeline pressure of 110 bar. The exiting vapor stream from the top, still has CO_2 present (70%) which can be extracted further by repeating a similar process to before: compression, cooling (vapor fraction of 0.4 is achieved) and liquid
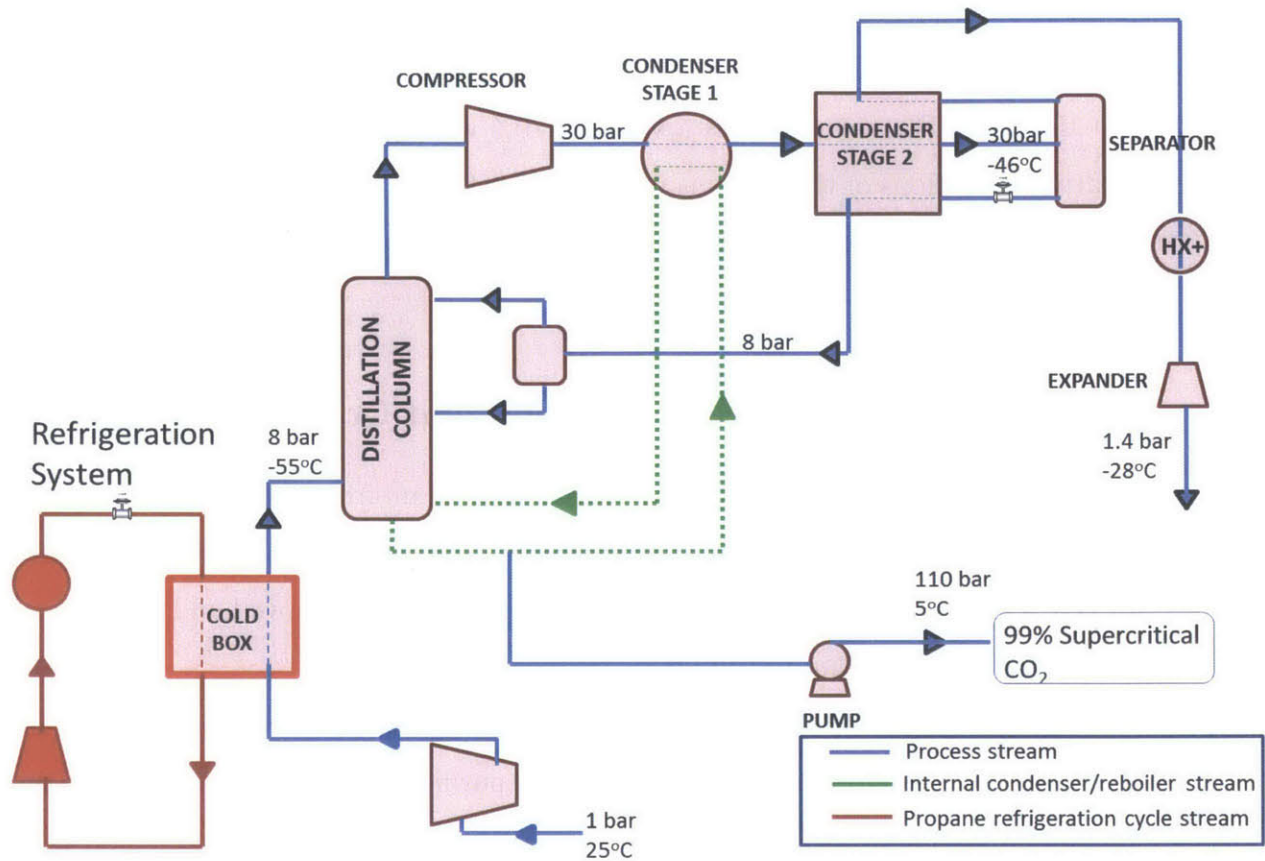
Figure 3-17: Process flow diagram of the CO_2 purification unit [28]

separation. This process is shown in the figure.

3.4   Sour Gas Cycle Modeling

After the extensive literature review that was done on the methane oxy-fuel power cycles, the questions and issues that might be encountered when using sour gas the fuel, helped in formulating a couple of different cycle possibilities to meet these challenges. The project statement, as stated previously is "How is the whole system and power cycle impacted when using sour gas as a fuel in oxy-combustion?". In order to answer that question and more importantly eventually decide what is the best cycle to use for this type of fuel, the issues that had to addressed along the way and the overall thought process for constructing these sour gas cycles are shown in Fig. 3-18.

Initially, we wanted to see what were the unwanted products present in the compressed CO_2 stream to be used for EOR. There are also constraints on what can be pumped into the ground for EOR as was shown in section 1.2.1 so after identifying the unwanted products we had to find a way to meet those EOR limits. Next, it was looked at when would sulfuric acid form in the cycle and how we could prevent it or neutralize it. Due to the H_2S present in the fuel, when it is combusted SO_x compounds are formed which when are allowed to condense and react with water, they form sulfuric acids. These acids are obviously a big problem because they can corrode the materials in the heat exchangers and other components that operate at low temperatures.

Additionally, the question of how does this working fluid affect cycle components modifications needs to be answered. Then once the modifications needed are known, the additional cycle complexities required for a more realistic cycle model can also be found. Importantly this all would then allow us to see how do those cycle modifications affect material selection and cost estimation. In the end we would want to compare the cycles using a techno-economic analysis, which would then allow us to have a better idea of what is the best cycle to use for this new working fluid and type of fuel.

This extensive analysis and thought process led us to model the following cycles, for both methane and sour gas, shown in Fig. 3-19. As was mentioned before, sour gas oxy-fuel cycles for CCS have not received any attention so far in the literature. On the other hand, the methane oxy-fuel cycles have been looked at. Therefore as a basis for comparison, we first modeled the natural gas (methane) oxy-fuel cycles, combined cycle and water cycle types, to better understand how they functioned and then used those to build on when the fuel was changed to sour gas. We adopted a similar approach to sour gas combustion cycles, in that we also modeled a combined cycle type and water cycle type. However, for sour gas due to the constraints and limitations from the presence of sulfur compounds in the cycle, 2-3 further configurations were considered pertaining to each of the combined cycle and water cycle.

123
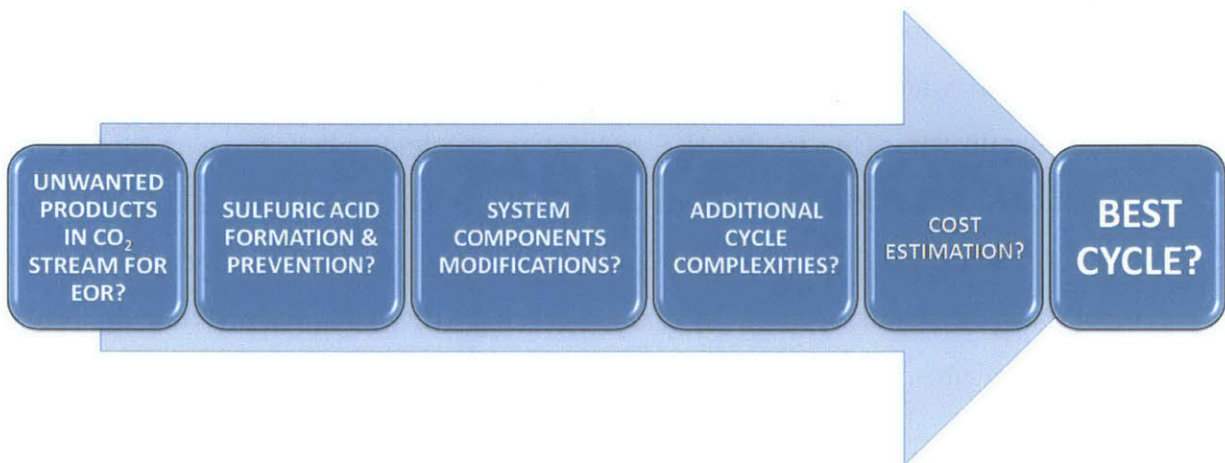
Figure 3-18: Project goals
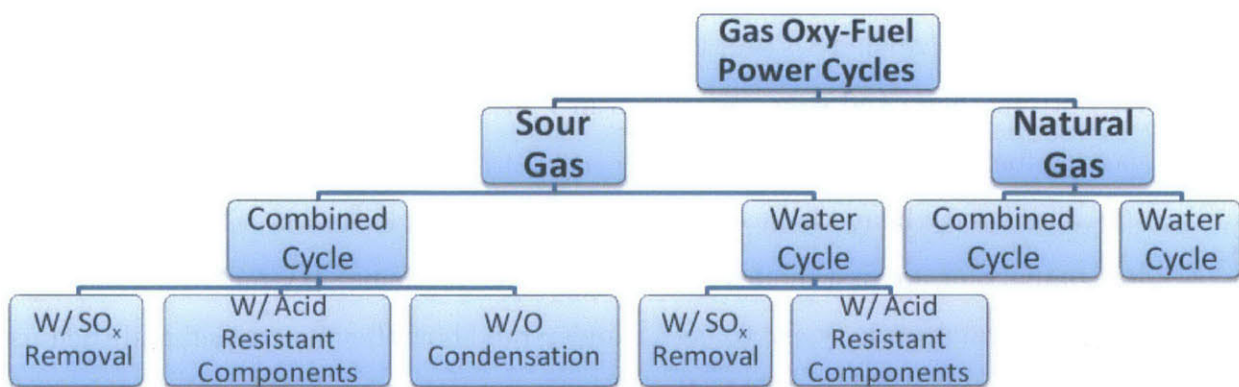
Figure 3-19: Flowchart showing all of the cycles that were modeled

3.4.1 Types of Sour Gas Cycles

The further configurations mentioned above and in the figure for the sour gas cycles, will be explained and presented in greater detail in the forthcoming chapters. But briefly as an overview, to start with, the cycles labeled "W/Acid Resistant Components" are meant to represent the cycles where we allow the working fluid (containing S-compounds) to condense in the main cycle. However this is a serious issue, because as mentioned before, acids form which can corrode the components. Therefore for these cycles, we assume that we use expensive acid-resistant materials in order to protect the components where the acid is present. Although this might appear as a solution to our problem with this type of fuel, the acid resistant materials represent a major economic burden and will significantly increase the cost of the cycle (as will be shown later in Chapter 6).

The second type of cycle that we have for sour gas, is one which is called "W/SO$_x$ Removal". This cycle has a SO$_x$ removal system just before the working fluid condenses in the main cycle. All of the sulfur compounds are removed in this system and the exiting gas stream contains only CO$_2$, Ar, N$_2$ and some H$_2$O (similar to the methane cycles). This gas stream is then used in the rest of the cycle and allowed to condense and everything. This cycle appears to solve the problem of acid condensation since we are removing the sulfur compounds before the working fluid condenses, but as will be shown later there is an efficiency penalty associated with this SO$_x$ removal process. The operation of this SO$_x$ removal system is described briefly in the next section and in depth in the next chapter.

The final type of cycle that was modeled for sour gas and more specifically only for the combined cycle type, is one called "No Condensation". To combat the problem of acid corrosion due to condensation, in this cycle the working fluid is not allowed to condense at all throughout the whole cycle. Therefore there is no condenser present and the working fluid remains at a temperature above the dew point throughout. As will be shown later on, there is a significant energy penalty that results from the inability to recuperate the latent enthalpy of the working fluid when it condenses.

3.4.2 SO_x Removal System

The SO_x removal system that was modeled for the sour gas cycles, was based on the wet flue gas desulfurization (FGD) techniques that are commonly used in coal combustion power plants [59]. As mentioned, this system removes SO_x from the working fluid resulting in a sulfur free gas stream that is used in the remainder of the cycle. The removal of these sulfur compounds prior to the working fluid condensing allows us to limit the use of expensive acid resistant materials in the remaining cycle components, thus reducing the overall cost of the power cycle.

This system removes the S-compounds from the working fluid by reacting it with lime solution ($CaO + H_2O$) and removing the byproducts as solid salts. The lime solution comes into direct contact with the working fluid and condenses the water and some SO_2 and SO_3. Then the SO_x compounds dissociate in the water to form ions and these react with the calcium ions present in the lime solution resulting in the formation of salts which eventually neutralize the effect of the acid. The salt formation creates a concentration gradient which drives more SO_2 and SO_3 to condense and dissolve in the water, thus furthering the flue gas desulfurization process. A more detailed analysis and description of the $deSO_x$ process will be described later in the next chapter.

3.5 Conclusions

The base-case cycles were described which had similar configurations to those in the previous chapter. Their modeling assumptions were chosen based on values commonly used in the literature and in industry and those same assumptions will be used later on for the sour gas cycles. The methane combined cycle was found to have a larger efficiency than the water cycle by almost 5% points. One reason for this was due to the fact that a liquid is being recycled to the combustor in the water cycle which eventually decreases the amount of power that can be produced in the turbines.

The important cycle components that are attributed with oxy-combustion cycles and specifically the sour gas cycles were also described in this chapter and those

126

were mainly the ASU, the combustor and the CPU. The ASU model used in this study was developed in a previous work but the oxygen compression process had to modified in order to meet the requirements and constraints in gas oxy-combustion cycles. The combustor was also modeled with the appropriate pressure drop for each of the two cycle types that are described in this work. The CPU was also modeled based on a model developed in a previous study but was modified for this type of cycle application.

After discussing the methane cycles, these two types of cycles (combined and water), were further subdivided into 2-3 more configurations, for the sour gas cycles, of addressing the issues and limitations due to the presence of sulfur compounds in these cycles. These sour gas cycles are explained in detail in the forthcoming chapters.

Chapter 4

Sour Gas Combined Cycles

4.1 Sour Gas Cycle Modeling

On top of the modeling assumptions made for the cycle components presented in section 3.3, when modeling the sour gas cycles, additional modeling assumptions and components had to be considered due to the presence of sulfur compounds (ex. SO_2, SO_3..) in the working fluid. These will be discussed in this section for both the combined and water cycles. When the sour gas water cycles are discussed in chapter 5, the same modeling assumptions were used for the sulfuric acid formation, additional combustor models and heat exchangers respectively as considered in this chapter.

4.1.1 Sulfuric Acid Formation

In order to accurately predict the sulfuric acid formation in the cycle components where the working fluid condenses, ionization reactions had to be modeled and included. The "ELECNRTL" property method [26] was used for all the cycle components where a liquid exists, in order to describe the liquid phase solution equilibrium. This method has been determined to be accurate for the moderately acidic conditions that is expected for this working fluid. This property method was used for the components shown in Figures 4-1 and 4-2 for the cycle types. The ionization reactions included with this property method, and that are relevant for the sour gas cycles'

Figure 4-1: Combined cycle components where condensation occurs

working fluid are shown in equations 4.1 to 4.6.

The first reaction is the general reaction for the formation of sulfuric acid from the SO_3 reaction with water. At temperatures below about $500^{\circ}C$, the reaction starts to shift to the right and gaseous sulfuric acid forms. Reaction 4.2 is the water dissociation reaction. Reactions 4.3 and 4.4 govern the dissociation of sulfuric acid into its respective ions, similarly reactions 4.5 and 4.6 are for sulfur dioxide. The resulting overall mixture of SO_2 and H_2SO_4 ions in water, is acidic and corrosive.

$$H_2O + SO_3 \longleftrightarrow H_2SO_4 \qquad (4.1)$$

$$H_2O \longleftrightarrow OH^- + H^+ \qquad (4.2)$$

$$H_2SO_4 \longleftrightarrow H^+ + HSO_4^- \qquad (4.3)$$

$$HSO_4^- \longleftrightarrow H^+SO_4^{2-} \qquad (4.4)$$

$$H_2O + SO_2 \longleftrightarrow H^+ + HSO_3^- \qquad (4.5)$$

$$HSO_3^- \longleftrightarrow H^+ + SO_3^{2-} \qquad (4.6)$$

The effect of including these reactions and applying this property method to those cycle components, shown in Figures 4-1 and 4-2, can be seen in the following plots in Figures 4-3 and 4-4. The figures show the concentration of the acid in the working

Figure 4-2: Water cycle components where condensation occurs

fluid (at exit of condenser) for the case with the ionization reactions and ELECNRTL property method included, and the case without plotted on a logarithmic scale to show the differences in orders of magnitude. Figure 4-3 also presents the results for the case with CO_2 recycle, whereas Figure 4-4 is for the H_2O recycle case. Both figures also have this mole fraction plotted for varying fuel compositions. The fuel composition was varied for H_2S from 0→30% with CO_2 varying from 30→0% simultaneously while keeping the 70% CH_4 in the fuel constant. One can deduce from the two figures that the concentrations of the acid for the cases with the reactions included, is orders of magnitudes higher than the one without those reactions. This further justifies the use of that property method with those reactions included in order to have a better estimate of the amount of acid formed. Another thing to notice is that the concentrations are higher for the H_2O recycle case than the CO_2 case. This also makes sense because the higher water content in the working fluid for the H_2O recycle case allows more of the SO_2 and SO_3 to react and dissolve in the water to form acids, therefore resulting in a higher acid concentration.

4.1.2 SO_3 Formation

As was mentioned before, the combustors were modeled as equilibrium type combustors. However this will grossly under-predict the SO_3 concentrations at the exit.

Figure 4-3: Mole fractions (ppm) of the total acidic components (mainly H_2SO_4) in the working fluid (at exit of condenser) when ionization reactions were included (red) and when they weren't (black) for the case with CO_2 recycle and for varying fuel composition

Figure 4-4: Mole fractions (ppm) of the total acidic components (mainly H_2SO_4) in the working fluid (at exit of condenser) when ionization reactions were included (red) and when they weren't (black) for the case with H_2O recycle and for varying fuel composition

Since the amount of SO_3 dictates how much acid forms in the latter stages of the cycle, it is important to try and improve the accuracy of the concentration of SO_3 in the working fluid. To do this, an additional reactor was added to model the SO_3 formation after the equilibrium combustor reactor as shown in Fig. 4-5. The second reactor was modeled as an "RStoic" reactor in Aspen Plus [26]. This reactor was used only to model the formation of SO_3 from SO_2 using the single reaction: $SO_2 + \frac{1}{2}O_2 \longrightarrow SO_3$ with a specified conversion rate (SO_2/SO_3) of 1.5%. This conversion percentage was obtained from Fleig et al. [29] where the SO_3/SO_x formation ratio was measured for different temperatures (see Fig. 4-5). The conditions that they tested were significantly different than ours (250-1000 ppm vs 11% SO_2), and so the conversion percentage chosen is really an upper limit and represents the most conservative estimate since the conversion ratio was found to decrease with increasing SO_2 concentration. However in our cycle since the combustors are stoichiometric, there is not enough excess oxygen for the SO_2 to react with to achieve that conversion percentage. Thus the SO_3 concentration only increases from about 48 to 60 ppm (by volume) across that second reactor.

4.1.3 Modeling Assumptions

The assumptions made when performing a thermodynamic analysis and modeling of the three sour gas combined cycles are shown in Table 4.1. Similar assumptions were made for the methane base-case combined cycle as mentioned previously. The same assumptions were applied to all three sour gas combined cycles: Acid-Resistance Cycle, No Condensation Cycle and SO_x Removal Cycle. The SO_x removal system assumptions details will be discussed further in section 4.4.1.

4.2 Acid Resistance Cycle

The first type of the sour gas combined cycles that was modeled, was one which we call the "Acid Resistance Cycle". This cycle has the exact same configuration as the methane combined cycle in section 3.2.1. The only difference is the fuel (70% CH_4,
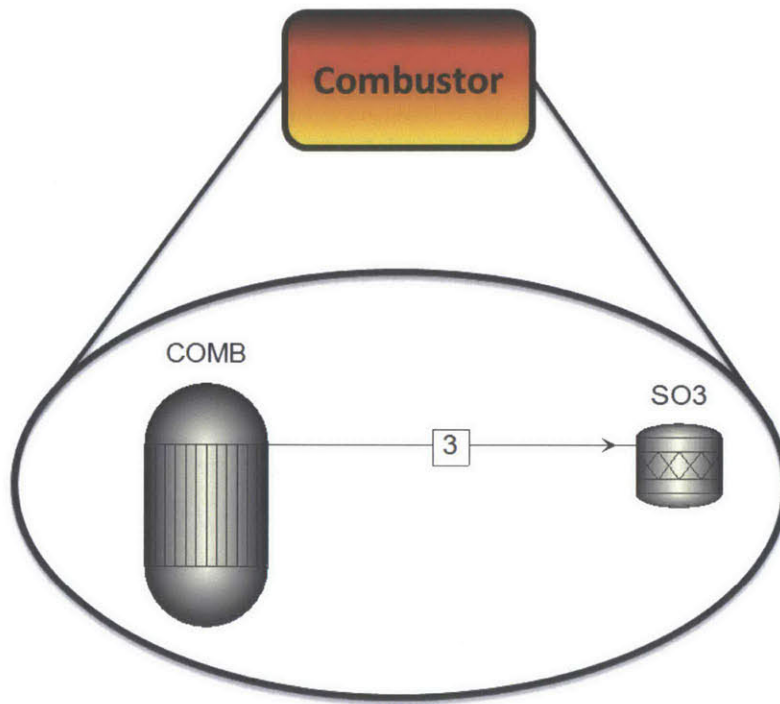
Figure 4-5: Modeling of the sour gas combustor using two reactors in series to better predict SO_3 concentrations
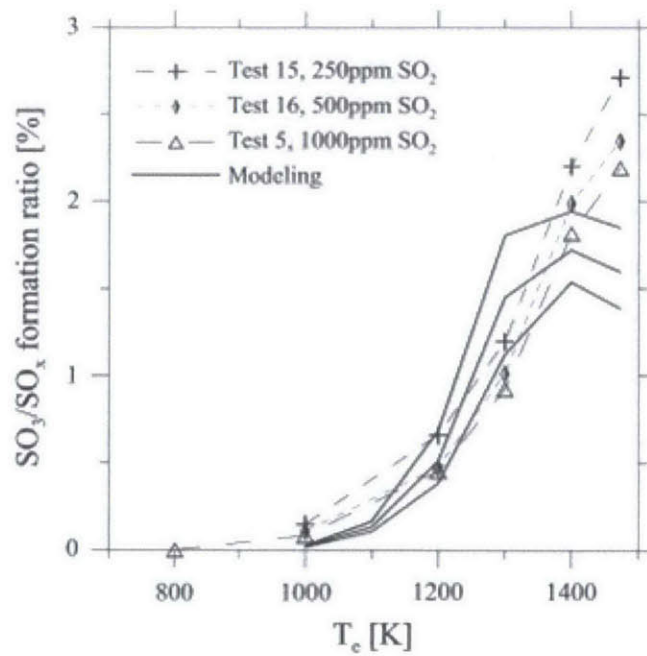
Figure 4-6: Measured SO_3/SO_x ratios for different SO_2 concentrations and different temperatures [29]

	Sour Gas Combined Cycles
Fuel	
Composition (mol%)	70% CH_4, 15% H_2S, 15% CO_2
LHV_{CH4}[a] (MJ/kg-CH_4)	50.1
LHV_{H2S} (MJ/kg-H_2S)	15.2
Combustor	
Operating Pressure (bar)	40
Pressure Drop (%)	5
Turbine	
TIT[b] (°C)	1300
Isentropic Efficiencies (%)	85
Compressor	
Isentropic Efficiency (%)	85
Heat Exchangers	
MITA's[c] (°C)	20
Pressure Drops (%)	5
Steam Cycle	
HRSG Pressures (bar)	100 & 6
TIT's (°C)	560
Turbine Efficiencies (%)	90
Condenser Pressure (bar)	0.05
Pump Efficiency (%)	75
ASU	
Specific Power (kWh/kg-O_2)	0.225
O_2 Stream Composition (mol%)	95% O_2, 4.2% Ar, 0.8% N_2
O_2 Compression	
Isentropic Efficiency (%)	84
Compression Stages	3
Intercooler Temps (°C)	25, 50
Max Exit Temp (°C)	200
SO_x Removal System	
Gas Exit SO_2 Concentration	< 100 ppm
Liquid Exit pH	≈ 7
CPU	
CO_2 Delivery Pressure (bar)	110
Exit CO_2 Stream Composition (mol%)	> 99% CO_2 (EOR Ready)

Table 4.1: Sour gas combined cycles modeling assumptions

[a]Lower Heating Value
[b]Turbine Inlet Temperature
[c]Minimum Internal Temperature Approach
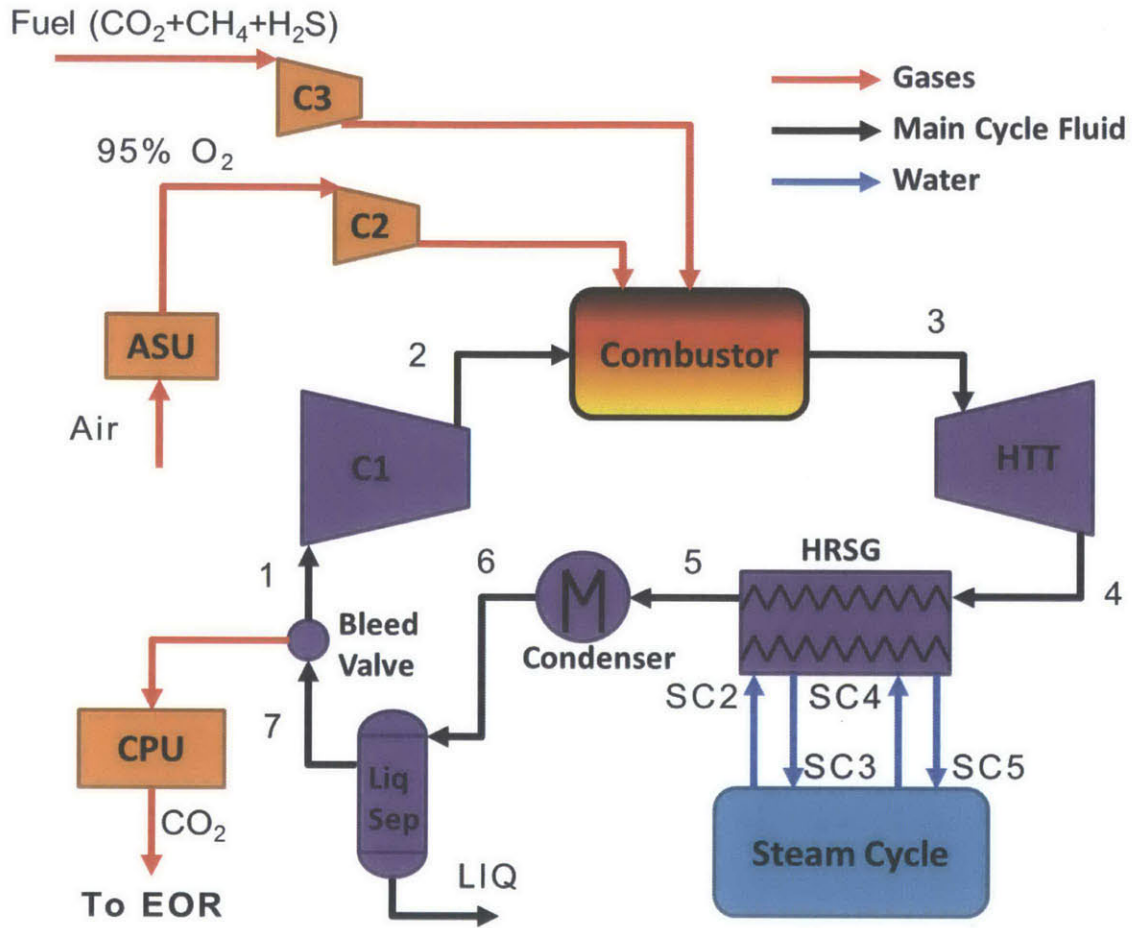
Figure 4-7: Overall process layout for the sour gas combined cycle with acid resistance

15% H_2S, 15% CO_2) and the fact that acid resistant materials are used for all the cycle components where condensation occurs. Fig. 4-7 shows the cycle diagram and components for the acid resistance sour gas combined cycle, with the corresponding T-s diagram in Fig. 4-8.

The working fluid, consisting of about 76% CO_2, 3% H_2O, 13% SO_2 (by volume), enters the main compressor (C1) at state 1 and is compressed up to a pressure of 40 bar. On the gas side, the oxygen stream from the air separation unit is sent to the combustor along with the fuel (70% CH_4, 15% H_2S, 15% CO_2), and the recycled working fluid. The recycled working fluid acts as a diluent in the combustor, and so the recycle ratio ($\dot{m}_1/\dot{m}_7$) of the working fluid fixes the combustor exit temperature at 1300°C. The combustor flue gases (68% CO_2, 14% H_2O, 12% SO_2 by volume) at

136
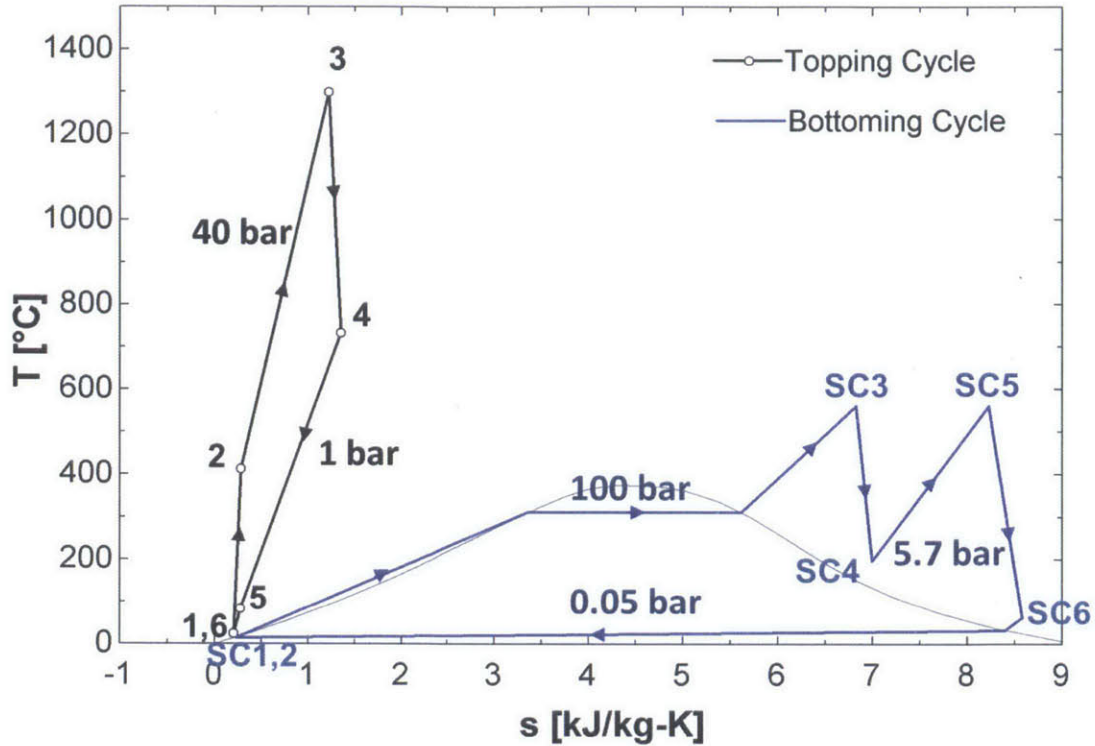
Figure 4-8: T-s diagram of the sour gas combined cycle with acid resistance

1300°C, state 3, are next expanded in the turbine to 1.12 bars to produce work. The lowest pressure in the cycle was chosen to be always greater than or equal to 1 atm to prevent any back flow when any of the fluid streams are extracted from the main cycle (ex. state 7).

Next, the main working fluid enters the HRSG at state 4 where it transfers thermal energy to the steam cycle while being cooled down to state 5. The steam bottoming cycle is quite similar to the steam turbine cycles of conventional combined cycle power plants. It is a double pressure Rankine cycle with reheat for better efficiency.

The remaining working fluid at state 5 is condensed to 25°C in the condenser and then the liquid (mostly water) is separated out to state 7. Since the working fluid, containing sulfur compounds, is allowed to condense in the HRSG and condenser, sulfuric acid will corrode those components. Thus acid-resistant materials are required in those components to protect the materials and as a result will significantly increase the cost of the cycle. After that 91% of the working fluid is recycled back up to the

compressor to be the diluting medium in the combustor. Then finally the excess working fluid is extracted in the bleed valve, sent to the CO_2 purification unit (CPU) and compressed up to 110 bars to yield a capture-ready carbon dioxide stream for EOR. The CPU removes the inert compounds from the working fluid (Ar & N_2) but before this, the sulfur compounds are also removed unlike the methane cycle because of EOR requirements. This SO_x removal system will be described in greater detail in section 4.4.1 because it is modeled at a much larger scale and is the critical component for the SO_x removal sour gas combined cycle discussed later.

The efficiency of this cycle with these conditions was found to be 45.2%. In comparison with the methane combined cycle described in section 3.2.1, which has the same layout but different fuel, this cycle has about a 0.7% efficiency decrease. The reason for this can be attributed to the fact that the methane cycle has a working fluid with a higher heat capacity (due to higher CO_2 fraction) and as such produces more work in the turbines, increasing the efficiency.

4.2.1   HRSG

When modeling the HRSG (and regenerator for the water cycle), the heat exchanger was divided up into two parts: a non-condensing section and condensing section. This was done to minimize the cost of acid resistance material needed in the HRSG since almost standard materials could be used for the non-condensing part and the expensive acid-resistant materials would only be required for the condensing section. As shown in Fig. 4-9, 'HRSG' represents the non-condensing heat exchanger and 'HRSG2' represents the condensing heat exchanger. The exit temperature of 'HRSG' was chosen and fixed at a temperature slightly above the dew point of the working fluid in order to prevent condensation there. The dew point of the working fluid (68% CO_2, 14% H_2O, 11% SO_2) is around 155°C therefore the exit temperature of 'HRSG' was chosen to be 160°C. A similar method for modeling the regenerator was done for the acid resistance water cycle described later in section 5.2.
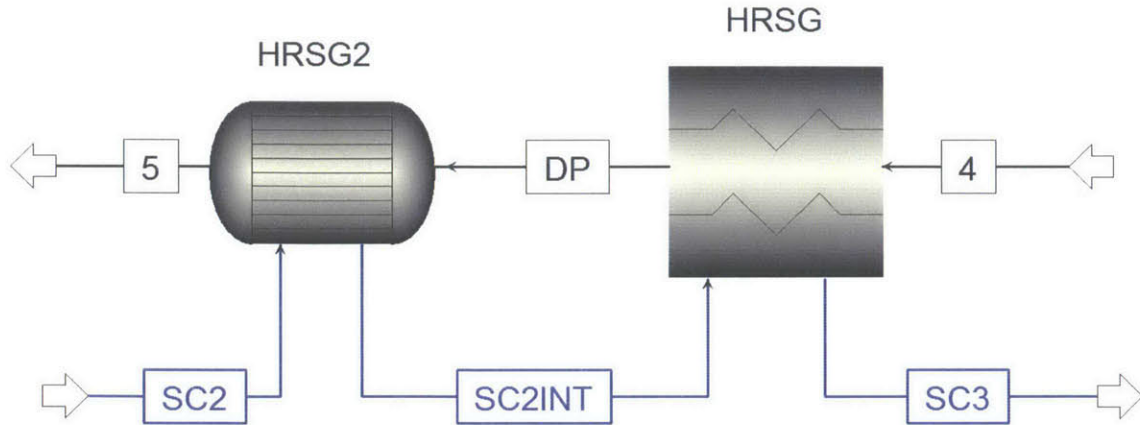
Figure 4-9: HRSG divided into a condensing, "HRSG2", and a non-condensing, "HRSG", heat exchanger

4.2.2 Sensitivity Studies

Combustor Pressure Sensitivity

A pressure sensitivity analysis was performed on the sour gas and methane combined cycles by varying the combustor pressure between 10-50 bar and observing its effect on some important cycle parameters. These results were for the cycles with the same modeling assumptions mentioned before but with varying operating pressure. The results are shown in Figures 4-10 to 4-16.

Figure 4-10 shows the effect of varying pressure on the net cycle efficiencies. The efficiencies of both cycles increase with pressure, as expected, and the methane cycle has about a 0.7% efficiency gain over the sour gas cycle, except for pressures below about 15 bar. It can also be seen that the methane cycle efficiency starts to level off at a pressure of around 40 bar (turbine pressure ratio = 35) which agrees with what is obtained in the literature [15, 14].

At the low combustor pressures, the sour gas cycle interestingly has a slight efficiency improvement over the methane case. This is because the bottoming steam cycle's net power output (per heating value of the fuel) for the sour gas cycle is initially much higher than that of the methane cycle which has the biggest effect on the efficiency difference. Even though the methane cycle's working fluid has a higher heat

139
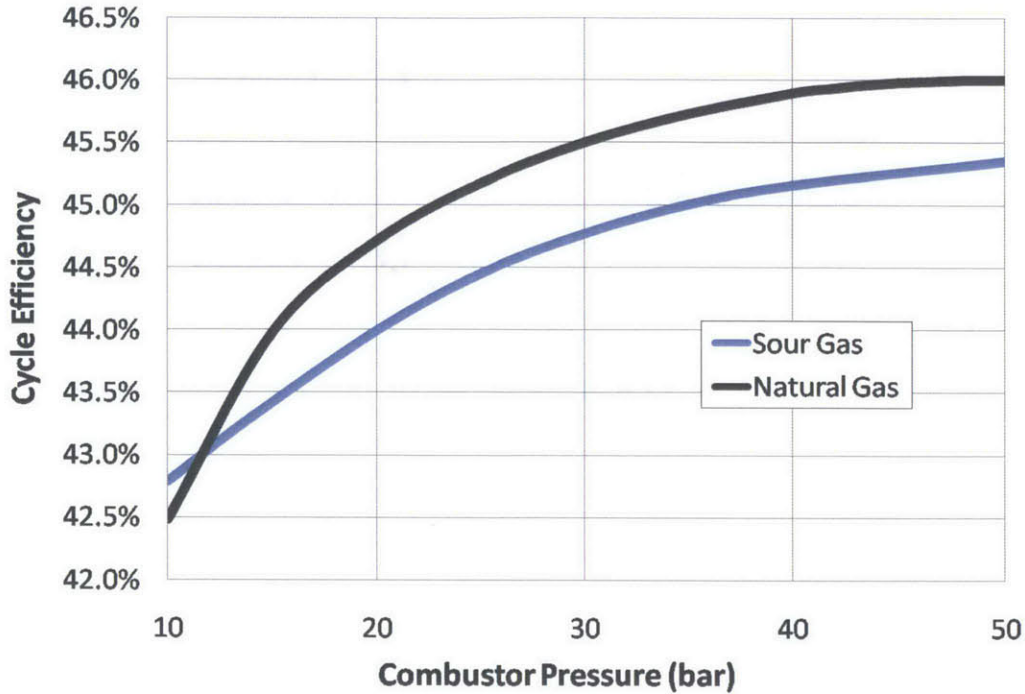
Figure 4-10: Effect of varying combustor pressure on the net cycle efficiency for the sour gas (acid resistance) and methane combined cycles

capacity which increases the HPT's power over the sour gas case, the steam cycle's power output difference has the bigger effect on the whole cycle's net efficiency at these lower pressures. More of this is shown on the next two figures.

Figures 4-11 and 4-12 show the power breakdowns for the two cycles with varying pressures. As mentioned, since the methane cycle has a higher heat capacity working fluid, it has a higher power output for every pressure. For both cycles, the HPT power increases with pressure due to a higher pressure ratio across the turbine. Similarly for the compressors as well. However the net steam cycle power output decreases with pressure because the mass flow rate through that cycle is decreasing in order to maintain the minimum temperature approach in the HRSG at 20°C. As the combustor pressure increases, the exit temperatures of the turbines decrease and as a result less heat is supplied to produce steam in the HRSG which decreases the steam cycle power output.

The recycle ratio was also found to increase with increasing pressure as can be
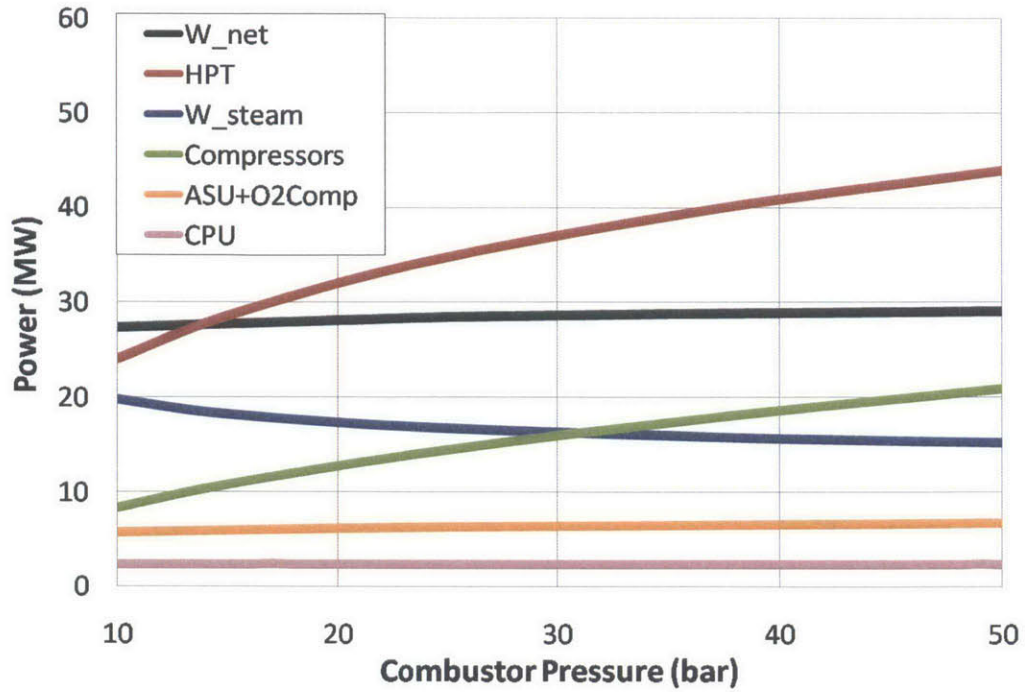
Figure 4-11: Effect of varying combustor pressure on power outputs and requirements for the sour gas (acid resistance) combined cycle components
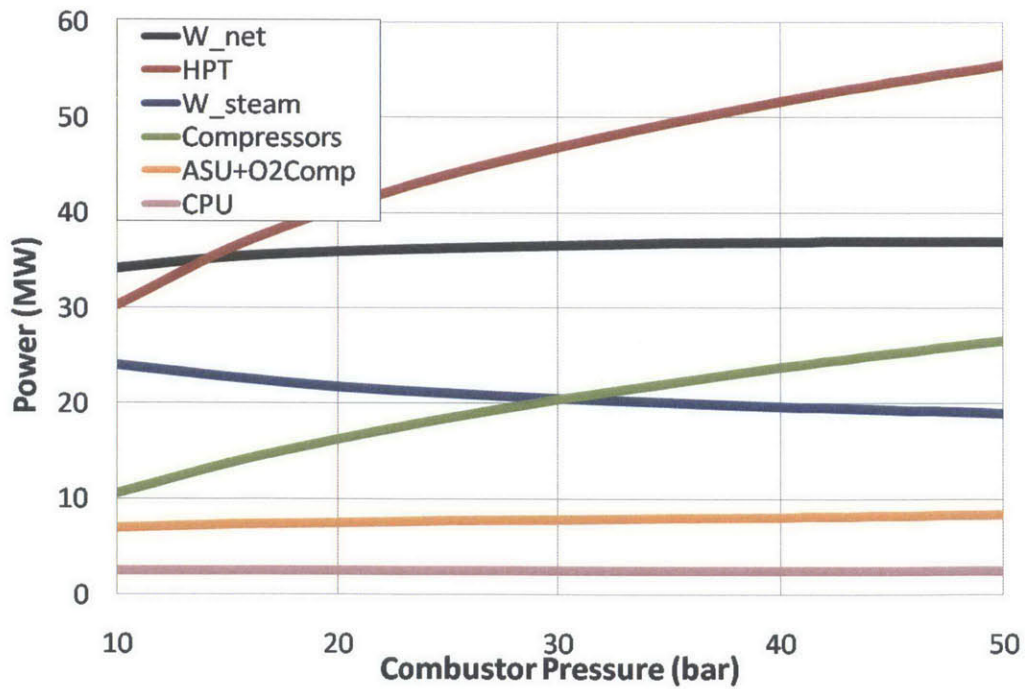
Figure 4-12: Effect of varying combustor pressure on power outputs and requirements for the methane combined cycle components
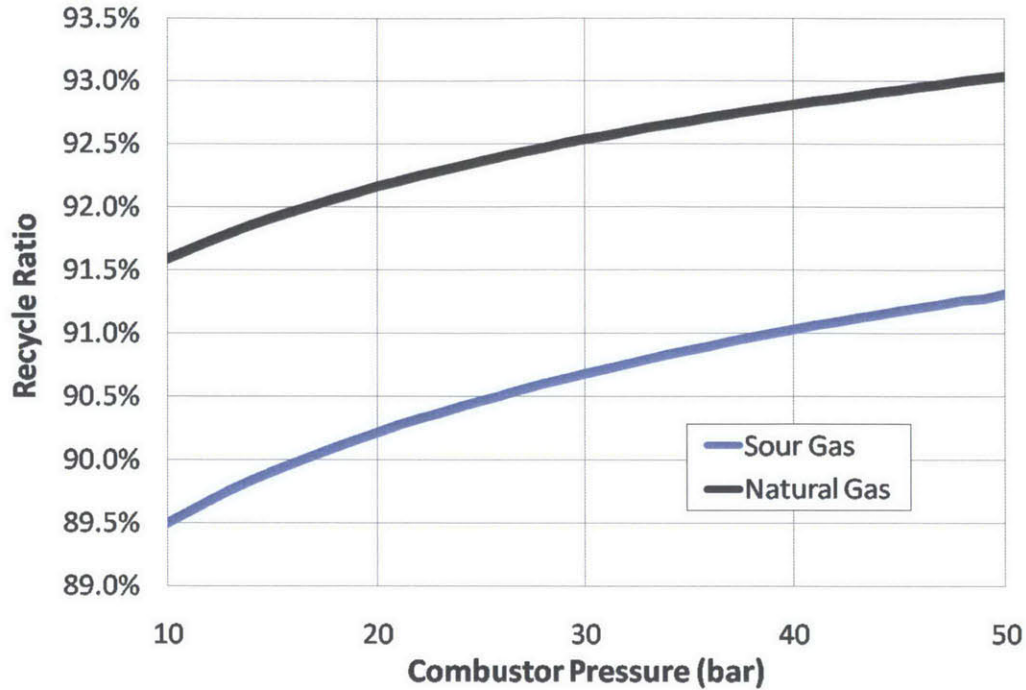
Figure 4-13: Effect of varying combustor pressure on the recycle ratio for the sour gas (acid resistance) and methane combined cycles

seen in Fig. 4-13. As the combustor operates at higher and higher pressures, the exit temperature of the compressor increases due to the increased pressure ratio across it. Therefore you would have a lower enthalpy difference across the combustor, and so the mass flow rate would have to go up in order to keep the heat input constant. The way to increase that mass flow rate is to increase the recycle ratio.

The recycle ratio for the methane cycle is also higher than the sour gas cycle. The reason for this is that the sour gas fuel already contains 15% CO_2 which acts as a diluting medium in the combustor, and so as a result will not require as much working fluid to be recycled as the methane cycle.

The working fluid compositions (at the exit of the combustor) did not vary much with pressure for both cycles and remained fairly steady. As shown in Fig. 4-14, the sour gas cycle's working fluid remained fairly the same at about 68% CO_2, 14% H_2O, 11% SO_2, 6% Ar and 1% N_2 (by volume). Similarly for the methane cycle, the working fluid stayed at about 77% CO_2, 15% H_2O, 7% Ar and 1% N_2 (by volume) as
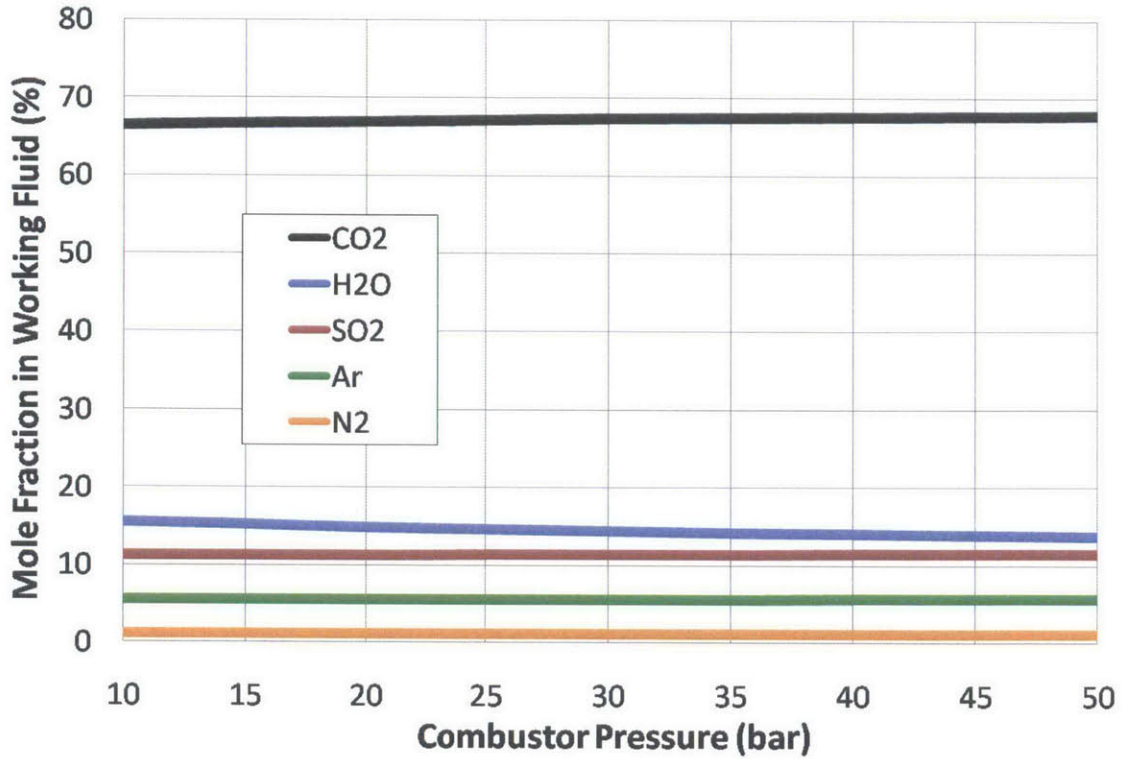
Figure 4-14: Effect of varying combustor pressure on emissions at combustor exit for the sour gas (acid resistance) combined cycle

seen in Fig. 4-15.

But for both cycles the H_2O mole fraction decreases slightly with pressure because of the increasing recycle ratio. As the recycle ratio is increased, more and more CO_2 is recycled to the combustor which eventually slightly decreases the fraction of the H_2O in the working fluid at the exit.

From Figure 4-16, the H_2SO_4 concentrations at both the condenser and HRSG exits decrease with pressure because the amount of H_2O in the working fluid is decreasing. Also, the concentration at the condenser exit is higher because it is at a lower temperature so more of the water has condensed and reacted with the SO_3 to produce H_2SO_4.
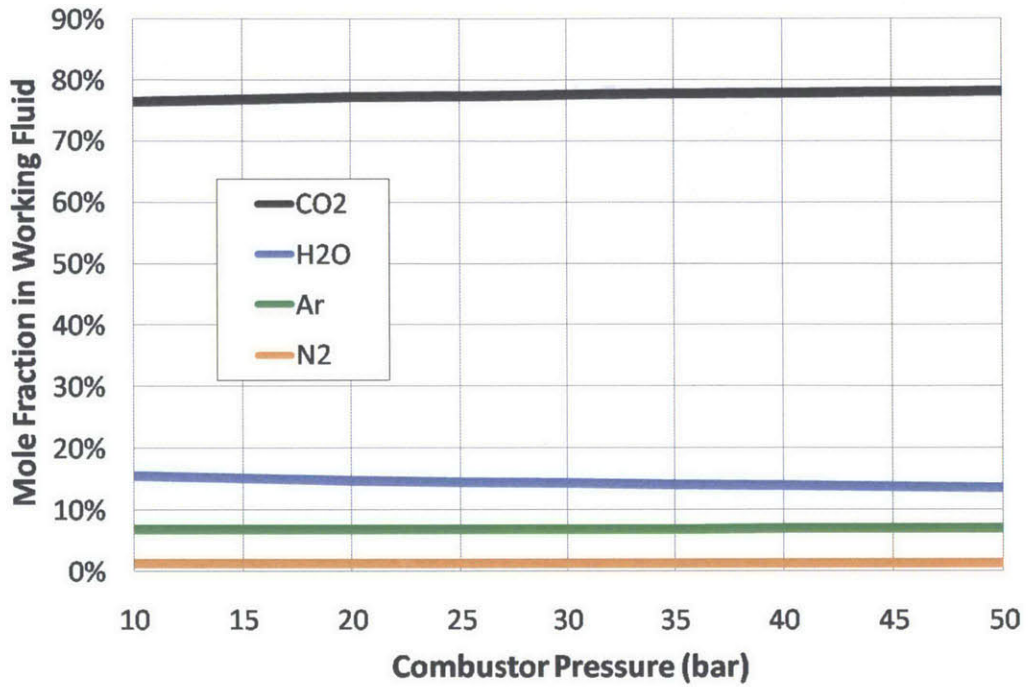
Figure 4-15: Effect of varying combustor pressure on emissions at combustor exit for the methane combined cycle
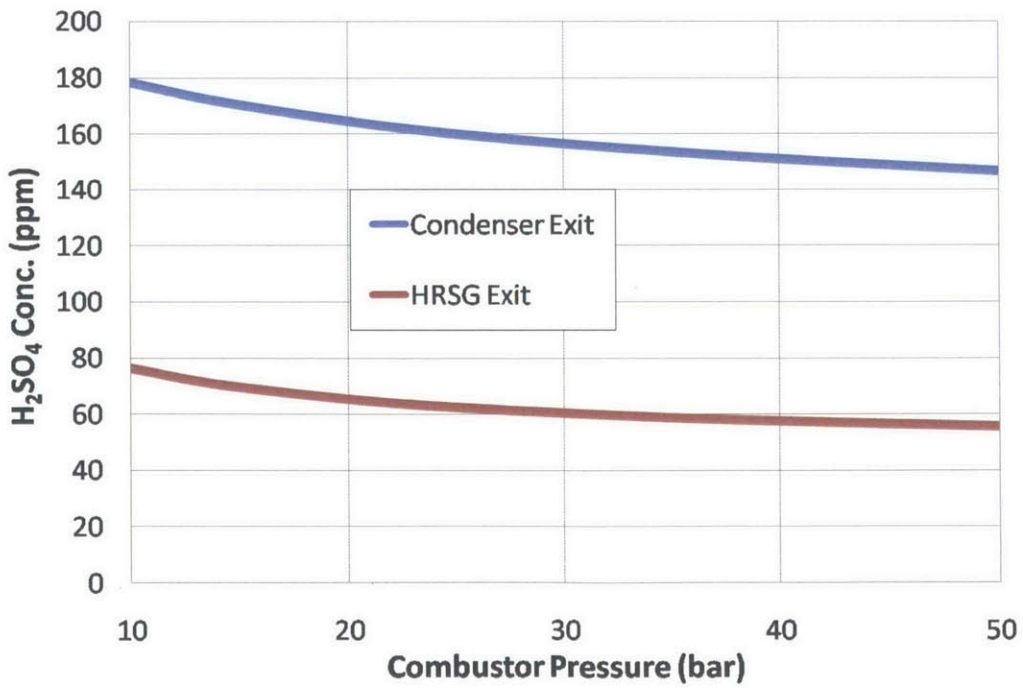
Figure 4-16: Effect of varying combustor pressure on sulfuric acid concentrations for the sour gas (acid resistance) combined cycle

4.3 No Condensation Cycle

The second type of the sour gas combined cycles that was modeled, was one which we call the "No Condensation Cycle". This cycle, as the name implies, is one where we don't allow the working fluid to condense in the main topping cycle. This type of cycle was modeled in order to see how the cycle performs and what the costs would be when the working fluid doesn't condense, thus the issue of corrosion would not be as prevalent as the previous acid resistance cycle. This would save on the costs of using the expensive acid-resistant materials but the performance is impacted as explained later on. Fig. 4-17 shows the cycle diagram and components for the no condensation sour gas combined cycle, with the corresponding T-s diagram in Fig. 4-18.

The working fluid, consisting of about 32% CO_2, 59% H_2O, 6% SO_2 (by volume), enters the main compressor (C1) at state 1 and is compressed up to a pressure of 40 bar. On the gas side, the oxygen stream from the air separation unit is sent to the combustor along with the fuel (70% CH_4, 15% H_2S, 15% CO_2), and the recycled working fluid. The recycled working fluid acts as a diluent in the combustor, and so the recycle ratio ($\dot{m}_1/\dot{m}_5$) of the working fluid fixes the combustor exit temperature at 1300°C. The combustor flue gases (32% CO_2, 59% H_2O, 6% SO_2 by volume) at 1300°C, state 3, are next expanded in the turbine to 1.12 bars to produce work. The lowest pressure in the cycle was chosen to be always greater than or equal to 1 atm to prevent any back flow when any of the fluid streams are extracted from the main cycle (ex. state 5).

Next, the main working fluid enters the HRSG at state 4 where it transfers thermal energy to the steam cycle while being cooled down to state 5. The steam bottoming cycle is quite similar to the steam turbine cycles of conventional combined cycle power plants. It is a double pressure Rankine cycle with reheat for better efficiency. In this case, the working fluid doesn't condense in the HRSG unlike the previous cycle. So a constraint was placed on the exit temperature of the HRSG to be higher than the dew point. The dew point of this cycle's working fluid (32% CO_2, 59% H_2O, 6% SO_2 by volume) was calculated using Aspen to be about 245°C.

145
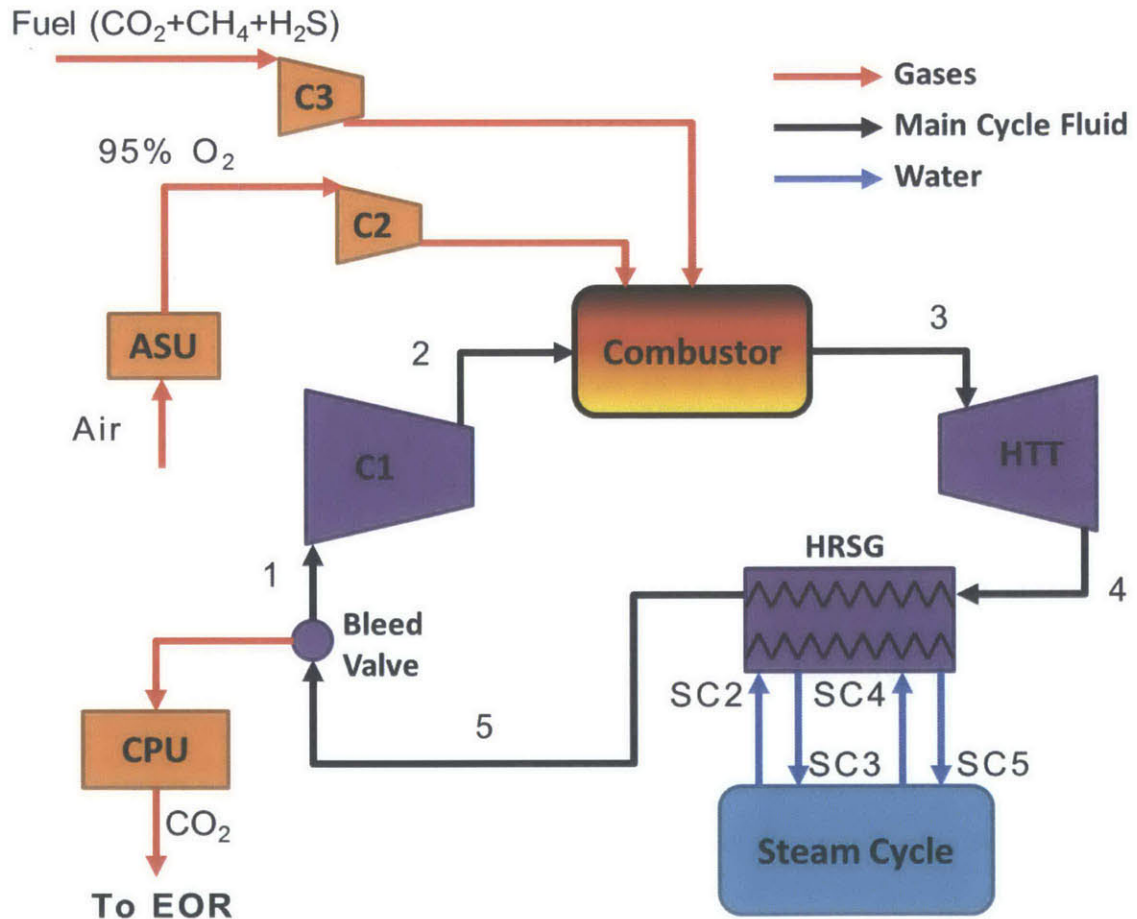
Figure 4-17: Overall process layout for the sour gas combined cycle with no condensation
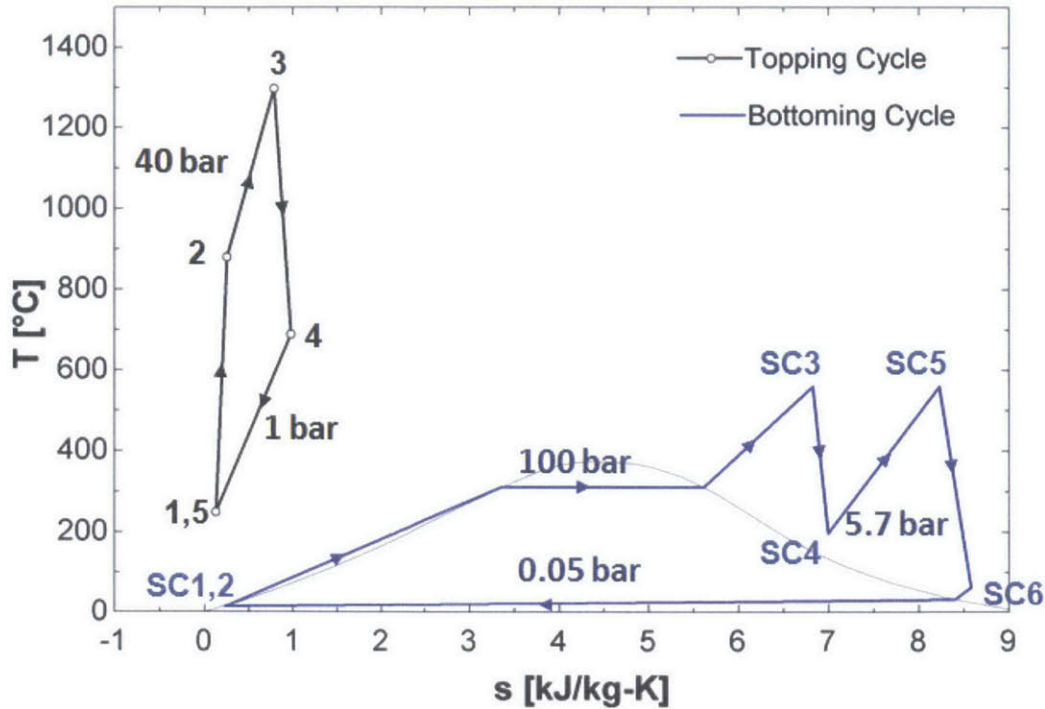
Figure 4-18: T-s diagram of the sour gas combined cycle with no condensation

Therefore when modeling the HRSG for this cycle, a couple of design parameters and constraints had to be met. From Table 4.1, the heat exchangers were designed to have a minimum internal temperature approach of 20°C and the exit temperature for the steam in the HRSG was fixed at 560°C. Also as mentioned the exit temperature of the gas was set to be at a temperature of 250°C in order to exit above the dew point and prevent condensation. The way to ensure this was to set a design specification for the HRSG where the mass flow rate of the steam cycle was varied until that gas exit temperature was reached. For this cycle, you can already see an efficiency penalty associated with this. Since the exit temperature of the HRSG is much higher than before, the calculated mass flow rate of the steam cycle is lower and thus reduce the power output of the steam turbines which will decrease the efficiency.

At the exit of the HRSG, state 5, 90% of the working fluid is recycled back up to the compressor to be the diluting medium in the combustor. Since the working fluid didn't condense, the temperature at state 5 is much higher than those of typical compressors. As such, the temperature at state 2 is also very high (∼900°C). Therefore

the mass flow rate of the cycle would have to increase as the enthalpy difference across the combustor has decreased, in order to keep the heat input across the combustor constant. This makes the work required for compressor C1 very high because of the high inlet temperature and the high mass flow rate of the working fluid. Adding intercooling would reduce that work in C1 but will result in a lower mass flow rate of the cycle because the temperature at 2 would be lower now (~600°C). This will in turn result in a lower mass flow rate of the steam cycle which will greatly impact the overall net work output and lead to a reduced efficiency. Therefore, through the results of an analysis that was done, it was found that the best option would be too keep the exit temperature of C1 high by not having intercooling. Doing this would help to reduce the exergy losses in the combustor because of the lower temperature difference and eventually lead to better performance results and cycle efficiency.

After the excess working fluid is extracted in the bleed valve, it is sent to the CO_2 purification unit (CPU) and compressed up to 110 bars to yield a capture-ready carbon dioxide stream for EOR. The CPU removes the inert compounds from the working fluid (Ar & N_2) but before this, the sulfur compounds are also removed, unlike the methane cycle, because of EOR requirements.

In the T-s diagram in Fig. 4-18, when comparing it to the acid resistance cycle, first of all they both have the same steam bottoming cycle plot. This is because the temperatures, pressures and all other intensive properties are fixed for all of the combined cycles, but the mass flow rate is what changes. Also, state 1 is different for the No Condensation cycle because we dont allow the working fluid to condense and so it is sent to the compressor at 250°C. As a result, the shape of the gas topping cycle (black plot) is smaller and shorter than the other cycle and from thermodynamic considerations we would expect and predict a lower cycle power output and lower cycle efficiency. Indeed the efficiency of this cycle with these conditions was found to be 35.6%. In comparison with the previous cycle, it can be seen clearly that there is a significant efficiency decrease of around 10%. Some of the reasons for this, which will be later discussed in greater detail, is the fact that the working fluid is not condensing in the HRSG and so it is not transferring its latent energy to the steam in the steam

148

cycle which would have produced more work.

4.4 SO_x Removal Cycle

The third and final type of the sour gas combined cycles, was one which we call the "SO_x Removal Cycle". This cycle, as the name implies, is one where we remove the SO_x compounds in the main topping cycle. This type of cycle was modeled in order to see how the cycle performs and what the costs would be when the SO_x compounds are removed from the working fluid before it is allowed to condense, thus acid corrosion would then not be an issue. This would also save on using the expensive acid-resistant materials. Fig. 4-19 shows the cycle diagram and components for the SO_x removal sour gas combined cycle, with the corresponding T-s diagram in Fig. 4-20.

The working fluid, consisting of 89% CO_2, 2% H_2O, 8% Ar (by volume), enters the main compressor (C1) at state 1 and is compressed up to a pressure of 40 bar. As can be seen, there is no SO_2 in the working fluid at this state because of the SO_x removal system. On the gas side, the oxygen stream from the air separation unit is sent to the combustor along with the fuel (70% CH_4, 15% H_2S, 15% CO_2), and the recycled working fluid. The recycled working fluid acts as a diluent in the combustor, and so the recycle ratio ($\dot{m}_1/\dot{m}_6$) of the working fluid fixes the combustor exit temperature at 1300°C. The combustor flue gases (78% CO_2, 13% H_2O, 1% SO_2 by volume) at 1300°C, state 3, are next expanded in the turbine to 1.6 bar to produce work. This pressure was chosen based on an analysis done to determine the optimal pressure entering the SO_x removal system in order to maximize efficiency. This will be explained in greater detail in the next section.

Next, the main working fluid enters the HRSG at state 4 where it transfers thermal energy to the steam cycle while being cooled down to state 5. The steam bottoming cycle is quite similar to the steam turbine cycles of conventional combined cycle power plants. It is a double pressure Rankine cycle with reheat for better efficiency. Once again, in this case, the working fluid doesn't condense in the HRSG. So a constraint was placed on the exit temperature of the HRSG to be higher than the dew point.
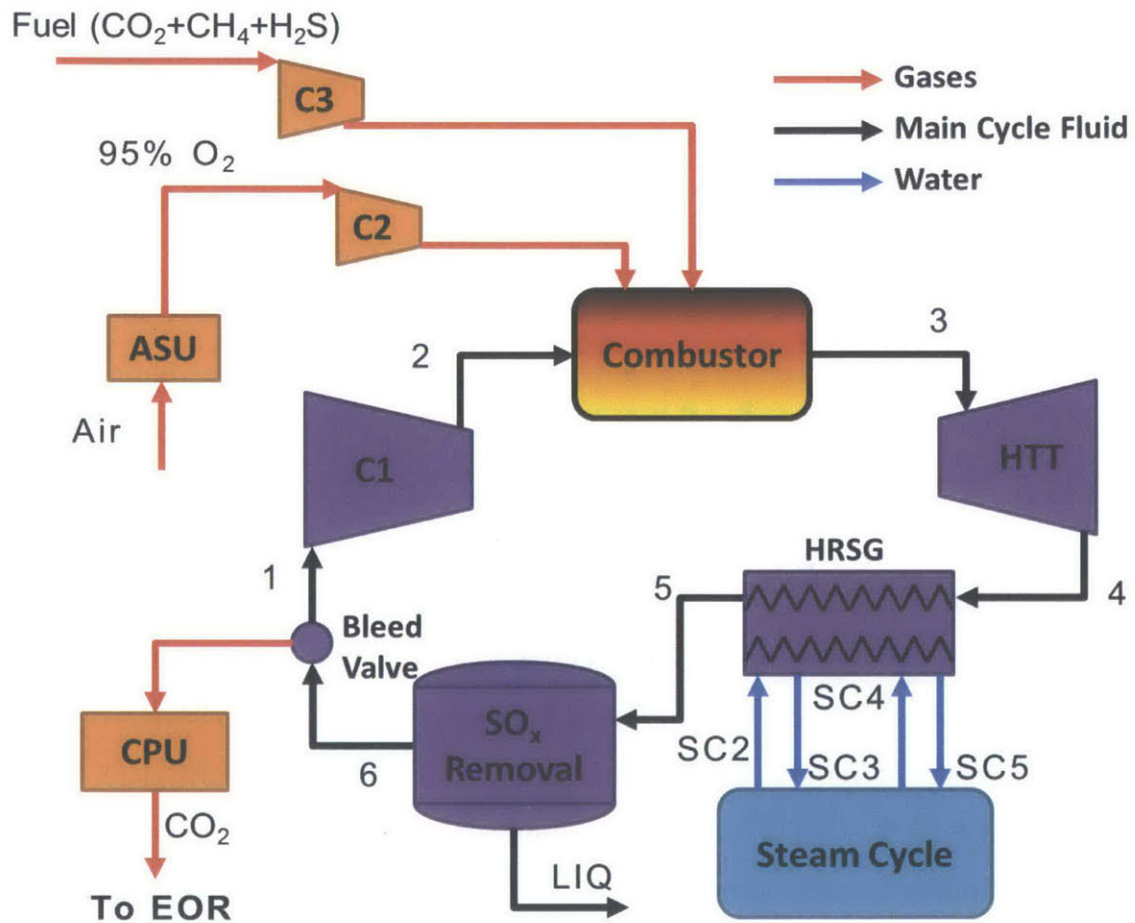
Figure 4-19: Overall process layout for the sour gas combined cycle with SO_x removal
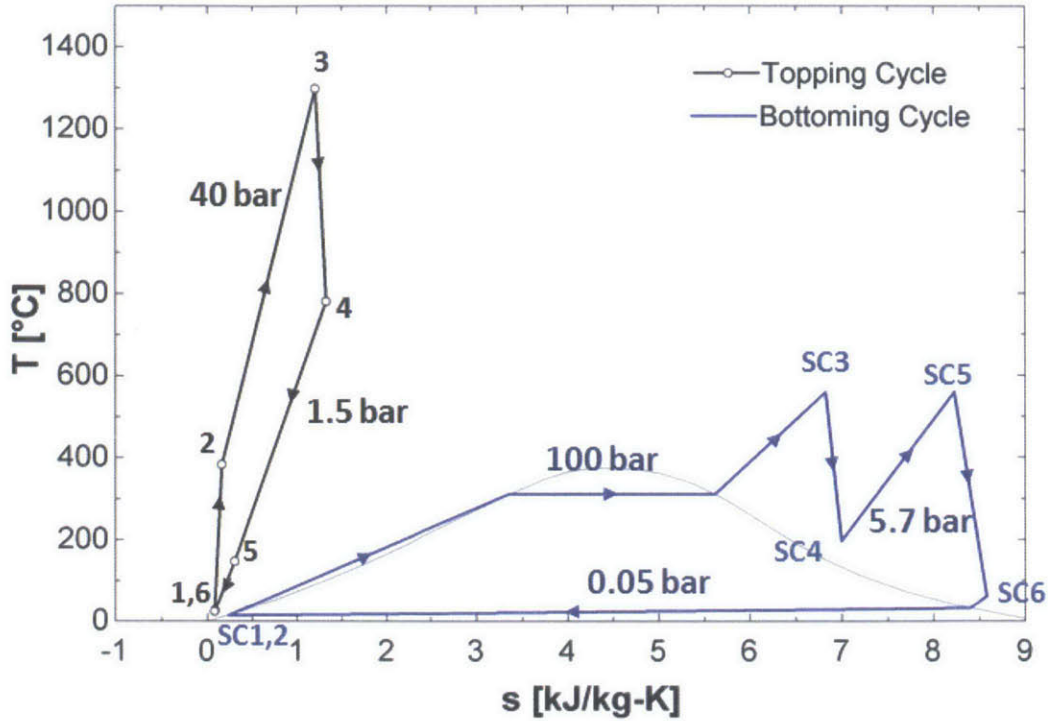
Figure 4-20: T-s diagram of the sour gas combined cycle with SO_x removal

The dew point of this cycle's working fluid (78% CO_2, 13% H_2O, 1% SO_2 by volume) was calculated using Aspen to be about 143°C.

Therefore when modeling the HRSG for this cycle, a similar approach to that described for the "No Condensation" cycle was used in order to fix the HRSG exit temperature at 148°C. However in this cycle, at the exit of the HRSG the working fluid is then sent to the SO_x removal system, and the exiting vapor stream now consists of mostly CO_2 with some Ar and N_2.

The SO_x removal system operates similar to traditional flue gas desulfurization systems found in coal power plants where the flue gases are sprayed with a mixture of lime (CaO) and water which condenses and neutralizes the effect of the acidic mixture. The SO_2 dissolves in the liquid and hence is separated from the gas stream. This will be explained in greater detail later on. The purified gas stream is then cooled down to the condenser temperature of 25°C before exiting the SO_x removal system.

At the exit of the SO_x removal system, state 6, 92% of the working fluid is recycled back up to the compressor to be the diluting medium in the combustor. After the excess working fluid is extracted in the bleed valve, it is sent to the CO_2 purification unit (CPU) and compressed up to 110 bars to yield a capture-ready carbon dioxide stream for EOR. The CPU removes the inert compounds from the working fluid (Ar & N_2). The efficiency of this cycle with these conditions was found to be 42.8%. In comparison with the previous cycles, this one had a better efficiency than the "No Condensation" cycle but lower than the "Acid Resistance" cycle. One reason for this, which will be later discussed in greater detail, is the fact that the turbine pressure ratio is slightly lower than the other two cycles and so the work output and efficiency decreases as a result of this.

4.4.1 SO_x Removal System

Traditional Flue Gas Desulfurization Systems

The SO_x removal system operates similar to traditional wet flue gas desulfurization (FGD) systems in that the flue gas is brought in contact with either a lime or limestone slurry in order to remove SO_2 and SO_3 from the flue gas. Lime (CaO) is more reactive and requires less capital equipment than limestone [60] and is therefore more widely used in practice. There are mainly two types of FGD technologies: wet FGD and dry FGD.

In wet FGD systems (shown in Figure 4-21), the gas to be cleaned enters the bottom of a cylinder-like tower and flows up while being sprayed by a lime slurry. The SO_2 is then absorbed into the spray and precipitated as wet calcium sulfite. The salt then settles to the bottom of the cylinder and is removed. More lime is added to the liquid in the reaction tank, to replenish any amount consumed in the process, before it is then pumped back up to the top of the cylinder to be sprayed on the gases once again.

For dry FGD processes, dry hydrated lime is injected directly into the flue gas to remove the sulfur products. The flue gas normally flows through the top of a
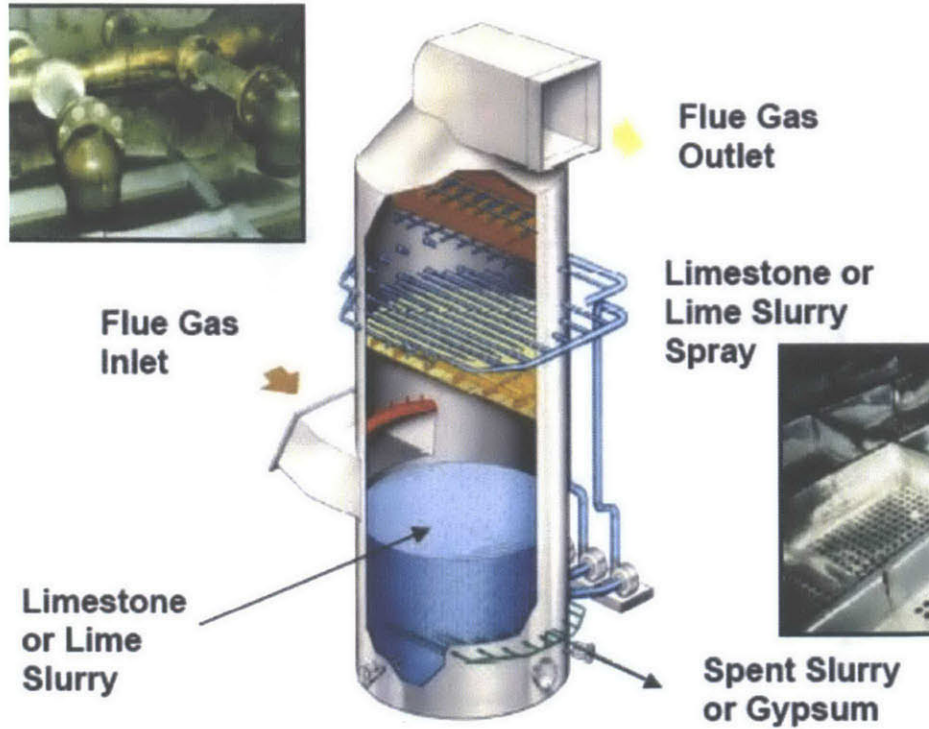
Figure 4-21: Wet flue gas desulfurization system [30]

cylinder-like vessel with a conical bottom. The cooled and purified flue gas flows out the bottom of the cylinder section while the unreacted lime and its reaction products fall to the bottom of the cone and are removed.

Wet FGD is mainly used for high sulfur fuels (>2%wt.) whereas dry FGD is used primarily for low sulfur fuels. The reagent utilization for a dry system is usually poorer compared to a wet system. The reagent stoichiometric ratio ($\frac{moles_{reagent}}{moles_{S-removed}}$) for dry FGD is higher than the ratio for wet FGD, so more moles of calcium are needed per mole of SO_2 removed. The reagent stoichiometry is about 1.02-1.03 for wet FGD and between 1.1-1.4 for dry FGD [61]. Typical power consumptions of these FGD processes are 1-2% of MW_{net} [61].

System Layout and Description

Figure 4-22 shows the system layout with all the components of the SO_x removal system. This system was modeled similar to the direct contact condenser described

153
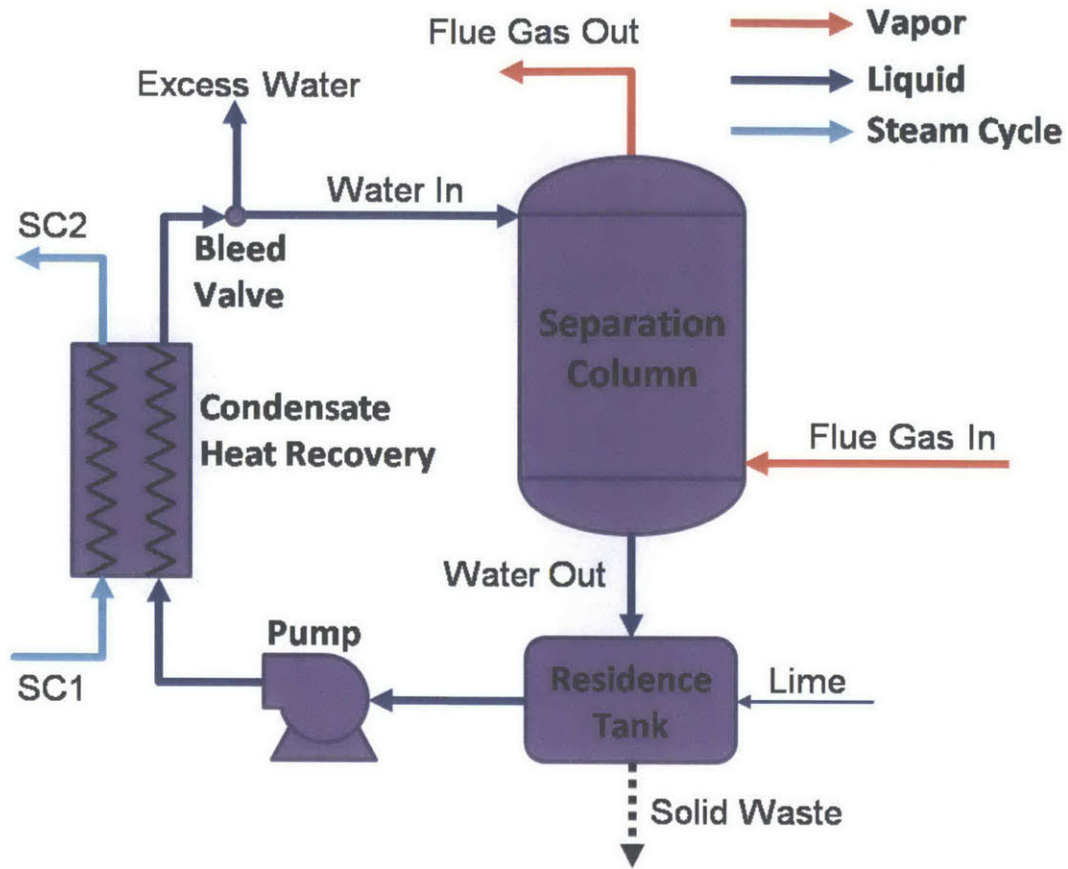
Figure 4-22: SO_x removal system process layout

by Zebian et al. [62]. The main two objectives for our whole system was to:

1. Keep the gas' exit SO_2 concentration < 100 ppm (EOR constratints [63])

2. Keep the liquid' exit pH $\simeq 7$

Flue gases from the HRSG enter the separation column and come in direct contact with recirculating water, containing lime (CaO), being sprayed from the top of the column. The recirculating water exits the column at an elevated temperature after absorbing the hot condensed water and acids from the original working fluid. The separation column was modeled using a RadFrac block in Aspen Plus [26]. The sulfur and lime reactions (shown in Figure 4-23) were provided as inputs to the simulation. The lime neutralizes the effect of the acid by reacting with the SO_2 and SO_3 dissolved in the water forming salts.

The gases flowing through the column experience a pressure drop that increases as the inlet pressure goes down. Therefore, as will be explained later, there is a compromise that needs to be made because if the inlet gases' pressure is too high there is a significant cycle efficiency decrease even though the pressure drop is low. The inlet gas stream's pressure was controlled by varying the turbine exit pressure in the main topping cycle.

The hot liquid leaving the column enters the residence tank and is given enough residence time to allow for the formation of calcium salts (ex. $CaSO_3$, $CaSO_4$). The solids settle in tank and are removed as waste. Also, fresh lime is added such that the pH of the system is kept neutral in order to avoid highly acidic or highly alkaline environments and protect the components' materials.

Next a pump is used to compensate for pressure losses in the process condensate recycle loop. Thermal energy is then transferred from the process condensate to the liquid of the steam cycle, preheating it before going to the HRSG; this thermal energy is the recovered thermal energy from the flue gas. This was done to minimize exergy losses from this whole process. After the heat recovery heat exchanger, the liquid stream is further cooled before being sent back to the separation column. The splitter is used to reject the extra process condensate. The split fraction in this bleed valve (96%) sets the flue gas exit temperature ($\sim 28°C$) because the higher the fraction the more water enters the column which cools the entering flue gases even further.

System Chemistry Modeling

The chemistry that was modeled for the separation column is shown in Figure 4-23 in the form of the reactions that were inputted to the model.

Before the CaO can react with the SO_2 and SO_3, both must be broken down into their respective ions. This is accomplished by dissolving the lime in water, which then dissociates into Ca^{2+} (through reactions 7 and 8), and then spraying it into the flue gases to dissolve the SO_2. When the SO_2 condenses into the water, it ionizes (through reactions 3 and 4) to form $SO_3{}^{2-}$. Similarly, when the SO_3 reacts with water it forms H_2SO_4 which then ionizes (reactions 5 and 6) and forms $SO_4{}^{2-}$. These ions then react

No.	Reaction	Rxn Type	Notes
1	$H_2O + SO_3 \leftrightarrow H_2SO_4$	Equilibrium	Sulfuric Acid Formation
2	$H_2O \leftrightarrow OH^- + H^+$	Equilibrium	Water Dissociation
3	$H_2O + SO_2 \leftrightarrow H^+ + HSO_3^-$	Equilibrium	
4	$HSO_3^- \leftrightarrow H^+ + SO_3^{2-}$	Equilibrium	
5	$H_2SO_4 \leftrightarrow H^+ + HSO_4^-$	Equilibrium	
6	$HSO_4^- \leftrightarrow H^+ + SO_4^{2-}$	Equilibrium	
7	$CaO + H_2O \rightarrow Ca(OH)^+ + OH^-$	Dissociation	Salt Dissociation (1st step)
8	$Ca(OH)^+ \leftrightarrow Ca^{2+} + OH^-$	Equilibrium	Salt Dissociation (2nd step)
9	$Ca^{2+} + SO_4^{2-} + 2H_2O \leftrightarrow CaSO_4.2H_2O$	Equilibrium	Salt Formation
10	$Ca^{2+} + SO_3^{2-} + 2H^+ + 2OH^- \leftrightarrow CaSO_3 + 2H_2O$	Equilibrium	Salt Formation

Figure 4-23: SO_x removal system reaction chemistry

with the Ca^{2+} and water to form salts (reactions 9 and 10).

A detailed and more accurate design and sizing of the column requires thorough modeling of phase and chemical equilibrium and possibly kinetic and residence times. However, herein only the aspects that were relevant to the power plant operation were considered.

System Operating Conditions and Results

As previously mentioned, one important parameter that needs to be analyzed is the pressure of the column. This is because it greatly impacts three important cycle parameters: compression & turbine work and column pressure drop. As shown in Fig. 4-24, the top stage pressure or the exiting gas' pressure is varied between ambient and 3 bar and its effect on net cycle efficiency and column pressure drop is analyzed. The inlet gas stream's pressure or bottom stage pressure is controlled by varying the turbine's exit pressure and the exiting gas stream's pressure is the pressure of the stream entering the compressor.

At lower pressures, there is a much higher pressure drop and also a higher compressor work and vice versa at higher pressures. But also at lower pressures the

156
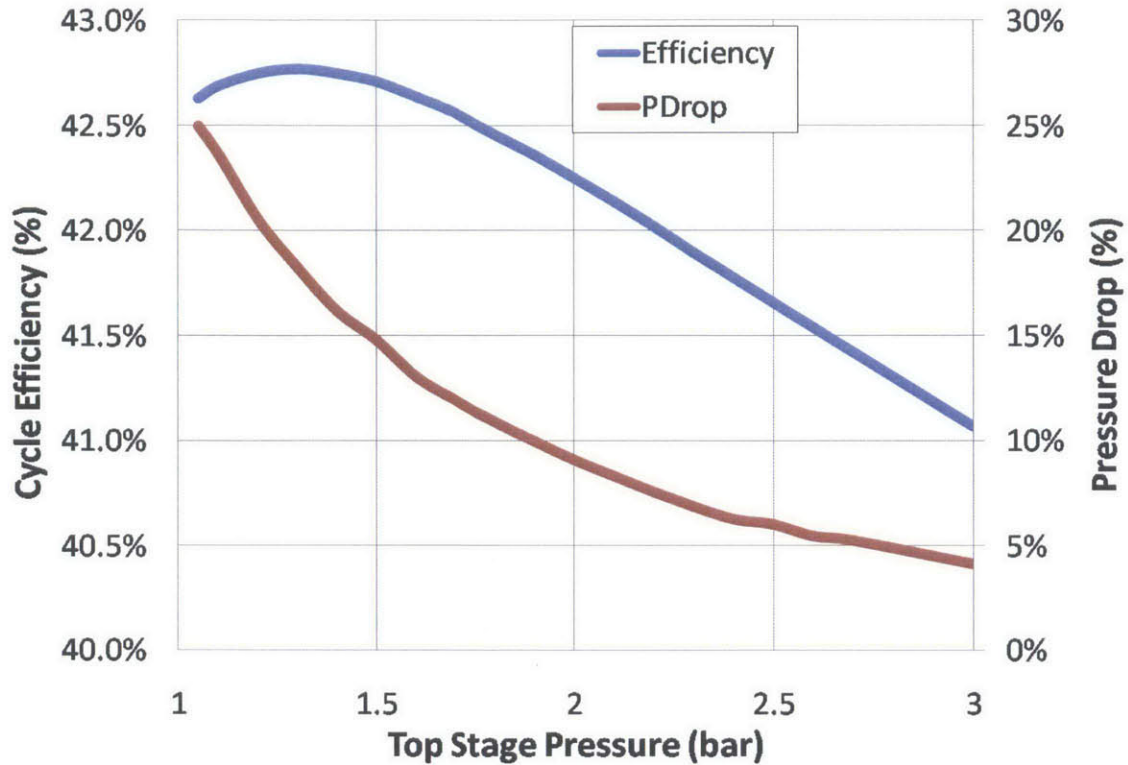
Figure 4-24: Effect of separation column's pressure on cycle efficiency

turbine work is greater because the original gases are allowed to expand down to lower pressures which produces much more work than at higher operating column pressures. Therefore, there exists an optimal value of the top column pressure which maximizes efficiency based on these two effects and it turns out to be around 1.3 bar. This corresponds to an inlet gas stream of 1.6 bar. These final optimal conditions and the other stream compositions are shown in Fig. 4-25.

The flue gas comes in directly from the exit of the HRSG in the main cycle and has a pressure which was determined from the above analysis. It then exits the column at a temperature of around 28°C before being cooled further down to the condenser (not shown) temperature of 25°C. The flue gas flow rate coming in, for this case is 53 kg/s. On the other side, the water (+ lime) enters the column at the top with a mass flow rate of 93 kg/s after 4% of it was removed as excess in the bleed valve. The exiting liquid mixture at 55°C is sent to the residence tank where lime is added and the solids are removed. The amount of lime necessary for this cycle with these
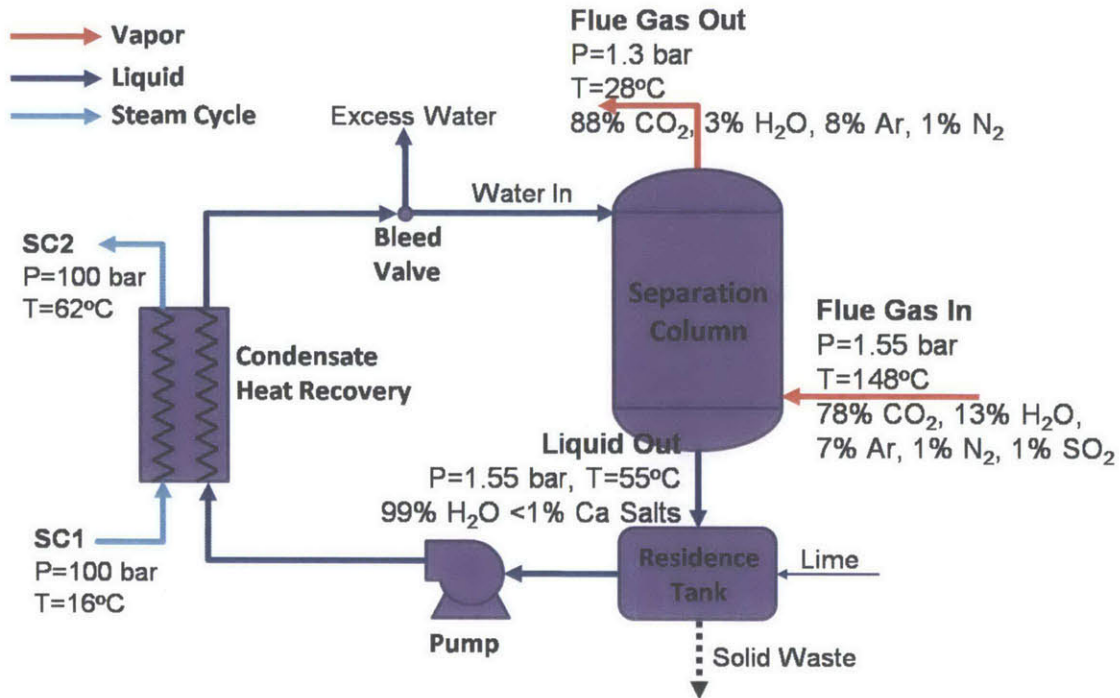
Figure 4-25: SO_x removal system showing the operating conditions

conditions was found to be 0.87 kg/s, this is the amount necessary for the "Liquid Out" stream to have a neutral pH. The reagent stoichiometry ($\frac{moles_{reagent}}{moles_{S-removed}}$) for our SO_x removal system was found to be 1.03 which is also exactly what traditional wet FGD systems operate at [61].

4.5 Performance Analysis and Cycle Comparisons

4.5.1 T-s Diagrams

When comparing the T-s diagrams of the three sour gas combined cycles, shown in Fig. 4-26, one can see that firstly they all have the same steam bottoming cycle. Therefore the only thing that changes between all of them is the mass flow rate of the cycle. State 1 is different for the "No Condensation" cycle because the temperature is maintained above the dew point of the working fluid before it is sent to the compressor at 250°C. Consequently, state 2 is also different and much higher. The shapes and
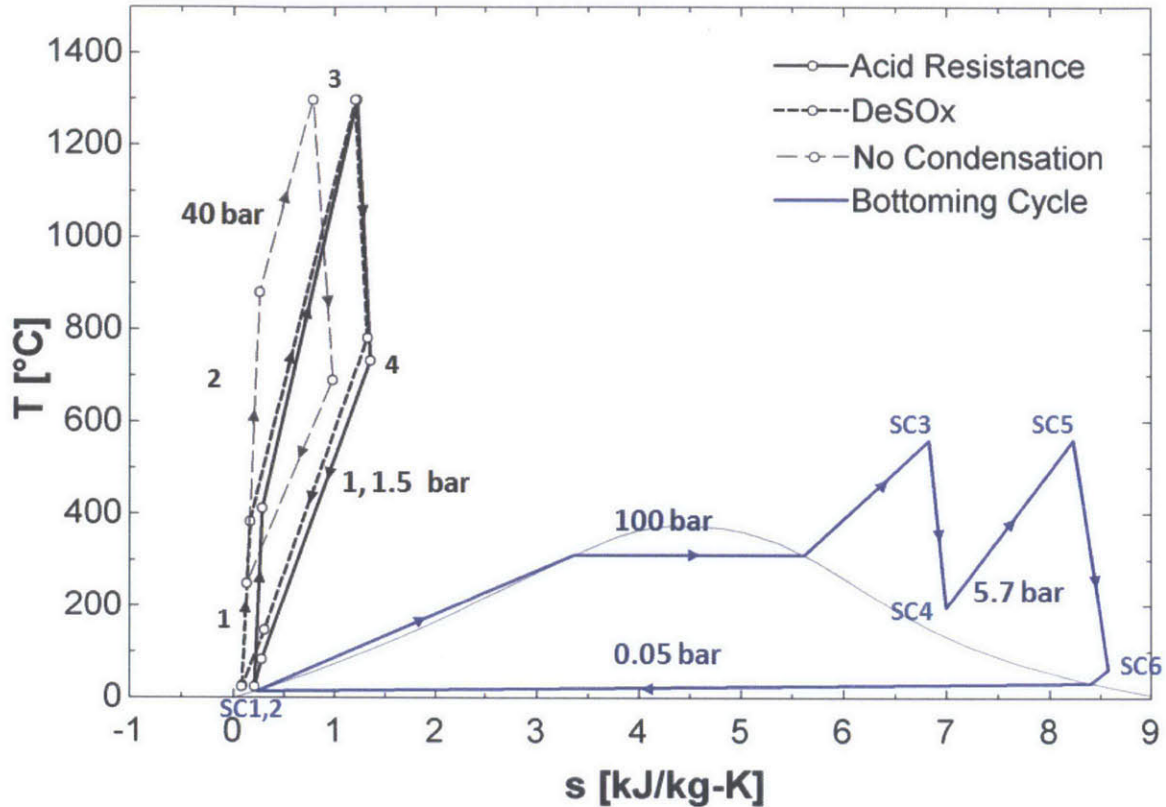
Figure 4-26: T-s diagrams of the sour gas combined cycles

areas of the plots for the other two cycles are also close which explains why the efficiencies are closer to each other than the No Condensation cycle. The T-s plot for that No Condensation cycle is shorter and narrower than the other two and so without even calculating it, we would expect the efficiency to be lower than the other two cycles and that is indeed the case. For the SO_x removal cycle, the low pressure line is slightly higher than the Acid Resistance cycle because of the slightly higher pressure required for the SO_x removal system (1.5 vs 1 bar).

4.5.2 Recycle Ratio Comparison

Figure 4-27 compares the recycle ratios for all of the three cycles. The recycle ratio is mainly dictated by the heat capacity of the working fluid. Higher heat capacity working fluids require less recycling to the combustor to achieve the same exit temperature. For these cycles, the SO_x removal cycle's working fluid had the lowest heat
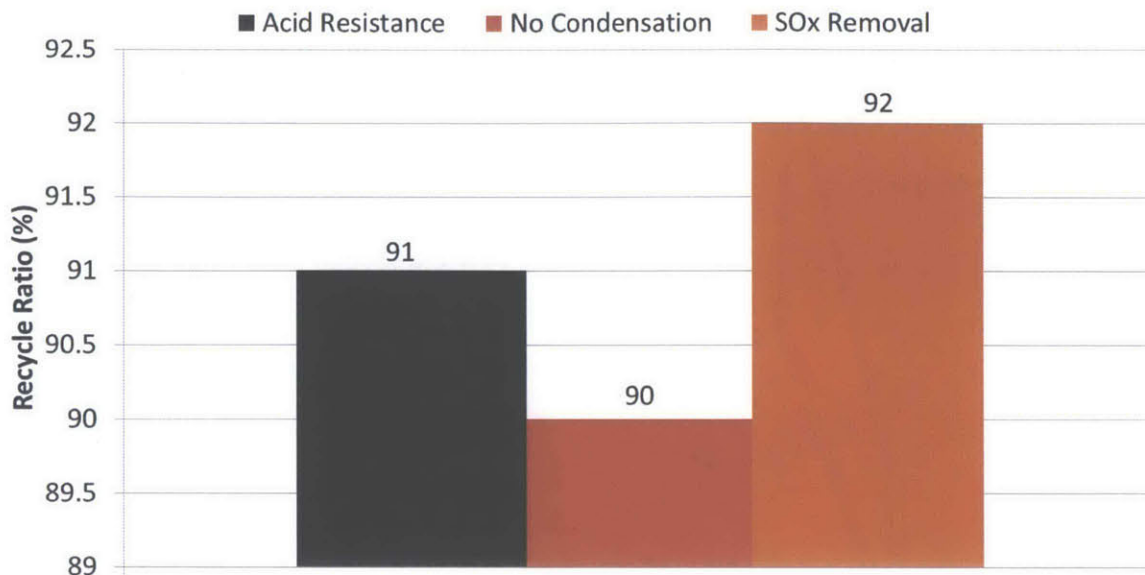
Figure 4-27: Recycle ratio comparison for the sour gas combined cycles

capacity, and therefore required slightly more recycling for the same combustor exit temperature (1300°C). On the other hand the No Condensation cycle had the highest capacity working fluid (due to the much higher amounts of H_2O) and so had the lowest recycle ratio at 90%.

4.5.3 Working Fluid Comparison

The working fluid at both the compressor entrances and combustor exits are examined for the cycles. Fig. 4-28 compares the working fluid composition at the compressor entrance. For the No Condensation cycle, much more H_2O is recycled back to the combustor (since the working fluid doesn't condense) and the working fluid composition doesn't change at all throughout the whole cycle, as can be seen on the next graph. Since the SO_x Removal cycle removes the SO_2 prior to entering the compressor, there is no SO_2 present at all in that working fluid. Also very little water is recycled as well so it is mainly CO_2 with some Ar and N_2. However for the Acid Resistance cycle both CO_2 and SO_2 are compressed and recycled to the combustor
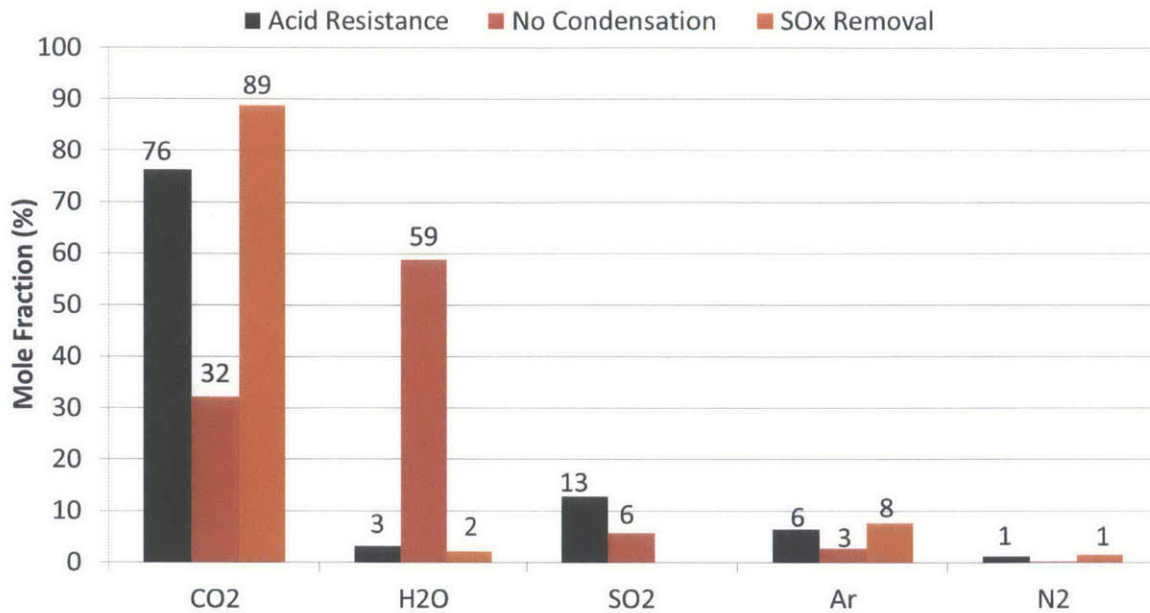
Figure 4-28: Working fluid comparison for the sour gas combined cycles (taken at compressor entrance)

which is why there is more SO_2 present in the working fluid.

Fig. 4-29 compares the working fluid composition at the combustor exit. As mentioned the cycle with No Condensation has the working fluid which stays the same throughout resulting in lower CO_2 concentrations after the combustor. Since no SO_2 is recycled to the combustor for the SO_x Removal cycle, only that produced by the combustion reaction exits, which in this case is only 1%.

4.5.4 Pressure Drop Sensitivity

The following analysis presents the results from a pressure drop sensitivity study that was done on the three cycles to determine its effect on the cycle efficiency. As can be seen from Fig. 4-30, the combustor pressure drop was found not to have a significant effect on the efficiency. The average slopes of the three graphs were determined to be -0.08, -0.13 and -0.17 Eff%/Pdrop% for the Acid Resistance, SO_x Removal and No Condensation cycle respectively. Therefore the No Condensation cycle had the largest efficiency decrease for every pressure drop increase. This is because since

161
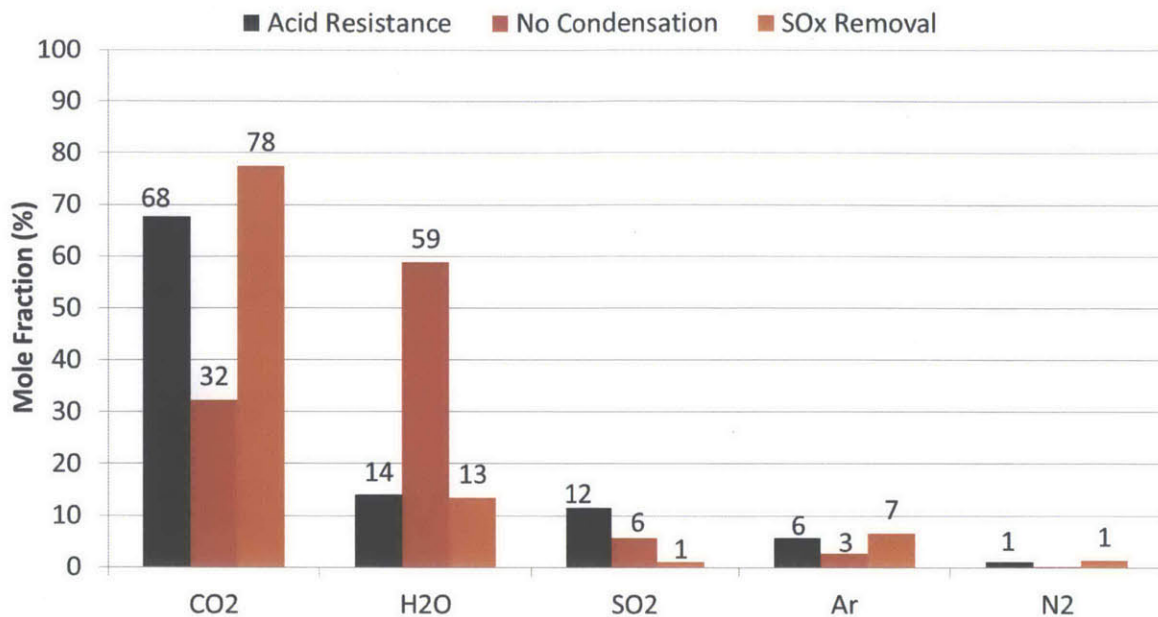
Figure 4-29: Working fluid comparison for the sour gas combined cycles (taken at combustor exit)

the working fluid for that cycle contains much more water than the other two, the enthalpy of the mixture exiting the combustor is more sensitive to pressure variations than those working fluids of the other two cycles. In our analysis and for the results shown next, the default value of the pressure drop was taken to be 5%. This is because typical combustor pressure drops for swirl-type combustors used for similar combustion reactions are between 3-5% and so in our case to be more conservative 5% was chosen.

4.5.5 Efficiency and Power Breakdown

The final and most important comparison of these cycles is the performance comparison shown in Fig. 4-31. Details of the power generated and consumed by the different components in the cycles are shown where they are expressed as a function of the (total) heat input to the cycle (based on the fuel's LHV) in order to non-dimensionalize the results. The heat inputs to all of the cycles were the same at 64 MW.

The first thing that is clearly noticeable is the unusually high red bars for the
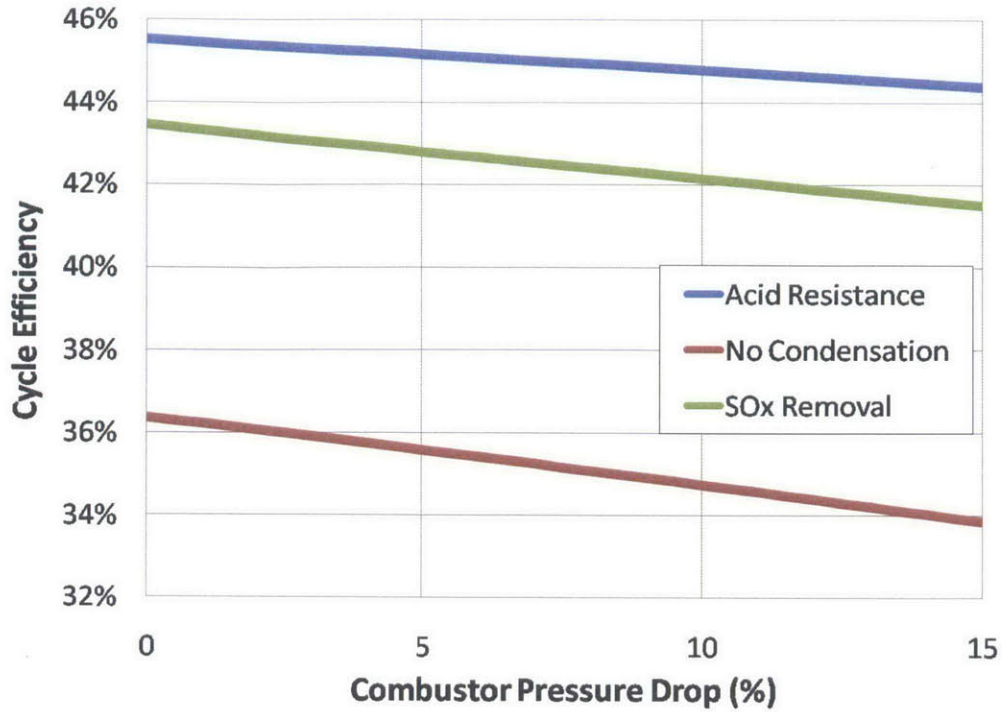
Figure 4-30: Effect of combustor pressure drop on net cycle efficiency for the sour gas combined cycles
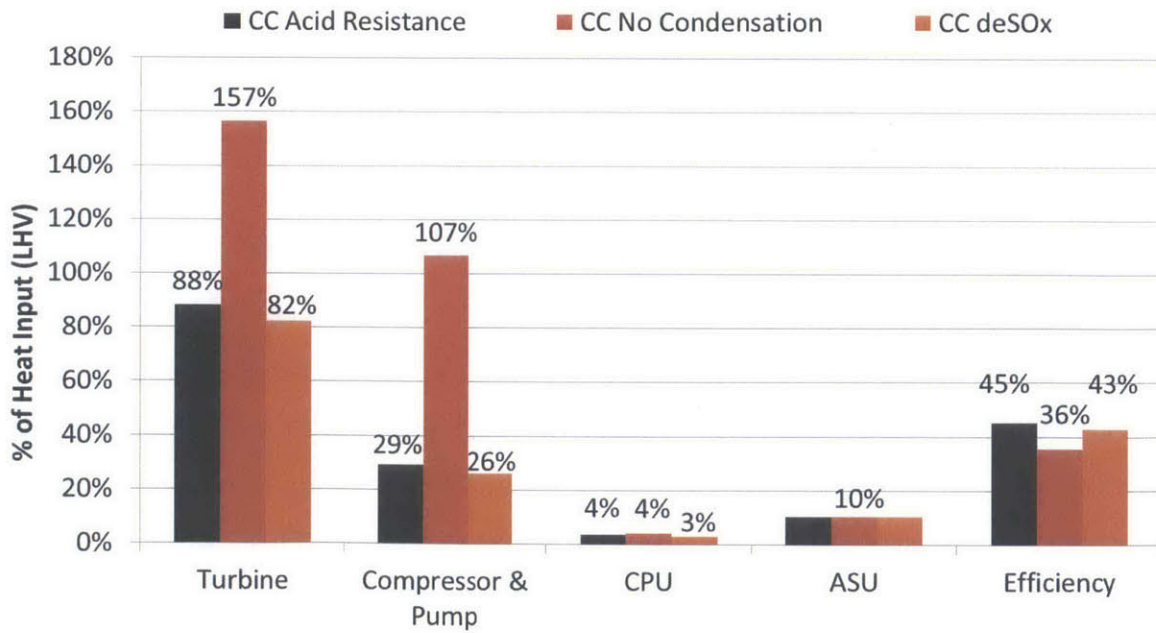
Figure 4-31: Power breakdown for the sour gas combined cycles

163

turbine and compressor works for the No Condensation cycle. The two bars are over 100% of the heat input which might seem like they violate the Second Law of Thermodynamics. But the difference between them (the "net" power) is less than 100% and so to produce that certain amount of power less than 100% of heat input is required and so there is no need to panic. The reason why these two bars are much higher than the other two cycles is because of the fact that the working fluid has a much higher heat capacity and so this cycle produces much more power in the turbine but also require a lot of power in the compressor to pressurize that working fluid to 40 bar. But as can be seen finally in the net efficiency this turns out to be the worst option.

Second of all, the turbine work for the SO_x Removal cycle is lower than the Acid Resistance cycle because the low pressure is 1.5 compared to 1.1 bar. So there is a smaller pressure ratio across the turbine and as a result less power is produced. The same is true for the compressor but this results in a lower power required since the pressure entering in the SO_x Removal case is 1.3 bar vs 1 bar for the Acid Resistance cycle.

The CPU (CO_2 Purification Unit) and ASU (Air Separation Unit) power inputs are fairly similar for all three cycles. But a slightly smaller power is required in the CPU for the SO_x Removal cycle because the SO_x compounds are already being removed in the main cycle before entering the CPU. Therefore, there is no further efficiency penalty associated with this process, unlike the other two cycles.

Also there is an efficiency decrease for the No Condensation and SO_x Removal cycles because of the inability to recuperate all of the latent energy from the topping cycle's working fluid in the HRSG. Since the working fluid doesn't condense in the HRSG for these two cycles, less heat is transferred to the steam bottoming cycle and so this leads to a smaller power output in the steam cycle. This results in another efficiency decrease for these two cycles.

Finally, all of these effects mentioned above combine to give the efficiency differences shown. The Acid Resistance cycle has the best efficiency at 45.2% followed by the SO_x Removal cycle at 42.8% and the worst cycle was the No Condensation cycle

164

with an efficiency of 35.6%.

4.6   Conclusions

The first type of the sour gas cycles were described and modeled: Acid Resistance, No Condensation and SO_x Removal. The Acid Resistance cycle had a configuration where the working fluid is allowed to condense in the main cycle components because an acid-resistant material is assumed to have been used in order to protect the components from corrosion. In the No Condensation, as the name implies, the working fluid is not allowed to condense in the main cycle components hence saving on the use of the expensive materials. In the SO_x Removal cycle, a SO_x removal system is employed which removes the sulfur compounds from the working fluid thereby greatly reducing the risk of corrosion from this exit stream as it makes it way through the rest of the cycle.

Pressure parametric studies were also done on the cycles in order to provide the optimal operating pressures, and to give a better understanding of the pressure dependence on the system performance. The SO_x removal system employed in these cycles, was explained and discussed in great detail and a sensitivity study was also done to determine what the impact of this system's operating conditions were on the overall cycle's performance. Then each of these three cycles were analyzed and compared, in order to determine how these cycle's perform and which cycle performs best. Out of the three combined cycles, the Acid Resistance cycle was found to have the highest efficiency followed by the SO_x Removal cycle then the No Condensation cycle. The main reason why the Acid Resistance cycle performed best was because of the fact that the working fluid is allowed to condense in the HRSG and so most of its latent heat is recuperated by producing steam for the steam cycle thus producing more work. The No Condensation cycle had the worst efficiency due to the fact that the working fluid doesn't condense, and also because the inlet temperature to the compressor for this cycle is high resulting in more power required to compress this stream up to the combustor pressure. A similar analysis will be discussed in the next

chapter for the water cycles and their results are also presented.

Chapter 5

Sour Gas Water Cycles

5.1 Modeling Assumptions

The important assumptions made when performing a thermodynamic analysis and modeling of the two sour gas water cycles are shown in Table 5.1. The same assumptions were applied to both of the water cycles: Acid-Resistance and SO_x Removal Cycles.

On top of the modeling assumptions made for the cycle components presented in section 3.3, similar to the sour gas combined cycles, additional modeling assumptions and components had to be considered due to the presence of sulfur compounds (ex. SO_2, SO_3..) in the working fluid. These were discussed in section 4.1, and the same modeling assumptions were used for the sulfuric acid formation, additional combustor models and heat exchangers.

5.2 Acid Resistance Cycle

The first type of the sour gas water cycles that was modeled, was one which we call the "Acid Resistance Cycle". This cycle has the same configuration as the methane water cycle described in section 3.2.2. Similar to the sour gas combined cycle, the only difference is the fuel (70% CH_4, 15% H_2S, 15% CO_2) and the fact that acid resistant materials are used for all the cycle components where condensation occurs.

	Sour Gas Water Cycles
Fuel	
Composition (mol%)	70% CH_4, 15% H_2S, 15% CO_2
LHV_{CH4}[a] (MJ/kg-CH_4)	50.1
LHV_{H2S} (MJ/kg-H_2S)	15.2
Combustors	
Operating Pressures (bar)	100 & 15 (Main & Reheater)
Pressure Drops (%)	10 & 6 (Main & Reheater)
Turbines	
TIT's[b] (°C)	600 & 1200 (HPT & LPT)
Isentropic Efficiencies (%)	87 & 90 (HPT & LPT)
Pumps	
Isentropic Efficiency (%)	75
Heat Exchangers	
MITA's[c] (°C)	20
Pressure Drops (%)	5
ASU	
Specific Power (kWh/kg-O_2)	0.225
O_2 Stream Composition (mol%)	95% O_2, 4.2% Ar, 0.8% N_2
O_2 Compression	
Isentropic Efficiency (%)	84
Compression Stages	3
Intercooler Temps (°C)	25, 25
Max Exit Temp (°C)	200
SO_x Removal System	
Gas Exit SO_2 Concentration	< 100 ppm
Liquid Exit pH	≈ 7
CPU	
CO_2 Delivery Pressure (bar)	110
Exit CO_2 Stream Composition (mol%)	> 99% CO_2 (EOR Ready)

Table 5.1: Sour gas water cycles modeling assumptions

[a]Lower Heating Value
[b]Turbine Inlet Temperature
[c]Minimum Internal Temperature Approach
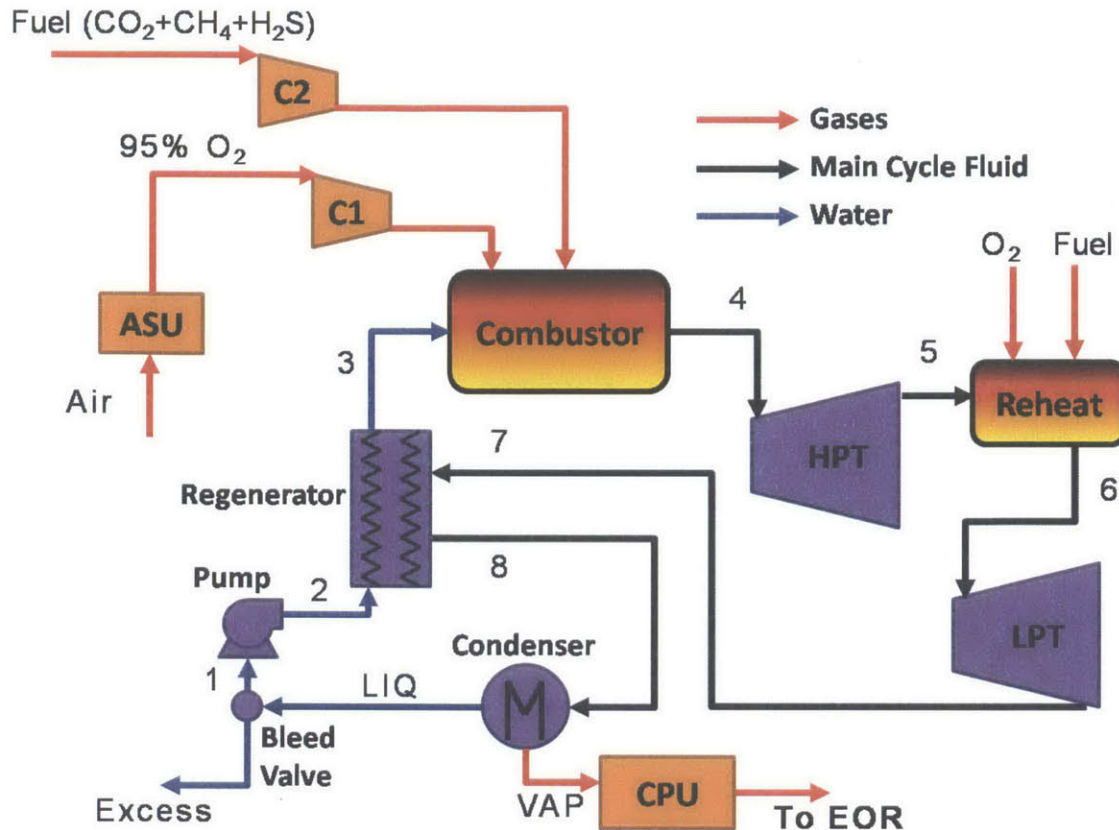
Figure 5-1: Overall process layout for the sour gas water cycle with acid resistance

Fig. 5-1 shows the cycle diagram and components for the acid resistance sour gas water cycle, with the corresponding T-s diagram in Fig. 5-2. It is based on a Rankine cycle with reheat and regeneration.

Firstly, water at state 1 is pumped up to a pressure of 100 bar where it is then preheated in the regenerator to about 247°C before entering the combustor. On the gas side, the oxygen stream from the air separation unit is sent to the combustor along with the fuel (70% CH_4, 15% H_2S, 15% CO_2), and the recycled working fluid (water). The water acts as a diluent in the combustor, and so the recycle ratio ($\dot{m}_1/\dot{m}_{LIQ}$) of the working fluid fixes the combustor exit temperature at 600°C. The main combustor flue gases (5% CO_2, 93% H_2O, 1% SO_2 by volume), state 4, are then expanded in the high pressure turbine (HPT) to 15 bars to produce power. The working fluid at state 5 is then reheated in the reheater where more fuel and oxygen are combusted

169

Figure 5-2: T-s diagram of the sour gas water cycle with acid resistance

to achieve a temperature of 1200°C. The reheater flue gases (10% CO_2, 88% H_2O, 2% SO_2, <1%Ar by volume), state 6, are then expanded again in the low pressure turbine (LPT) down to 0.1 bar.

Next, the hot working fluid enters the regenerator where it transfers its thermal energy to the water stream going to the combustor while being cooled down to state 8. Similar to the HRSG modeled for the Acid Resistance sour gas combined cycle, described in section 4.2.1, the regenerator was divided up into two parts: a non-condensing heat exchanger and condensing heat exchanger. This was done to minimize the cost of acid resistance material needed in the regenerator since near standard materials could be used for the non-condensing part and the expensive acid-resistant materials would only be required for the condensing section.

The remaining working fluid at state 8 is condensed to 25°C in the condenser and then the vapor is separated out to be sent for EOR. Since the working fluid, containing sulfur compounds, is allowed to condense in the regenerator and condenser,

sulfuric acid will corrode those components. Thus acid-resistant materials are required in those components to protect the materials and as a result significantly increases the cost of the cycle. After the condenser, 87% of the remaining liquid (water) is recycled back up to the pump to be the diluting medium in the combustor. Also, the vapor from the condenser is then sent to the CPU and compressed up to 110 bars to yield a capture-ready carbon dioxide stream for EOR. The CPU removes the inert compounds from the working fluid (Ar & N_2) but before this, the sulfur compounds are also removed unlike the methane cycle because of EOR requirements. This SO_x removal system was described in detail in section 4.4.1.

The efficiency of this cycle with these conditions was found to be 40.9%. In comparison with the methane water cycle described in section 3.2.2, which has the same layout but different fuel, this cycle has about a 0.5% efficiency decrease. The slight difference in efficiencies can be attributed to the fact that the methane cycle has a working fluid with a slightly higher heat capacity (due to higher CO_2 fraction) and as such produces more work in the turbines, increasing the efficiency.

5.2.1 Sensitivity Studies

Reheater Pressure Sensitivity

A pressure sensitivity analysis was performed to investigate the effect of reheat pressure variations on important cycle parameters. This analysis was performed on the sour gas and methane water cycles by varying the reheater pressure between 6-30 bars. The results were for the cycles with the same modeling assumptions mentioned before but with varying reheat pressure. The results are shown in Figures 5-3 to 5-7. The reheater pressure was varied, instead of the combustor, because it was found to have a bigger impact on cycle efficiency and parameters. Due to the higher pressure ratio across the LPT and the higher TIT than the HPT, a larger proportion of the power output came from the LPT.

Figure 5-3 shows the effect of varying pressure on the net cycle efficiencies. The efficiencies of both cycles increase with pressure initially until a maximum is reached at

171
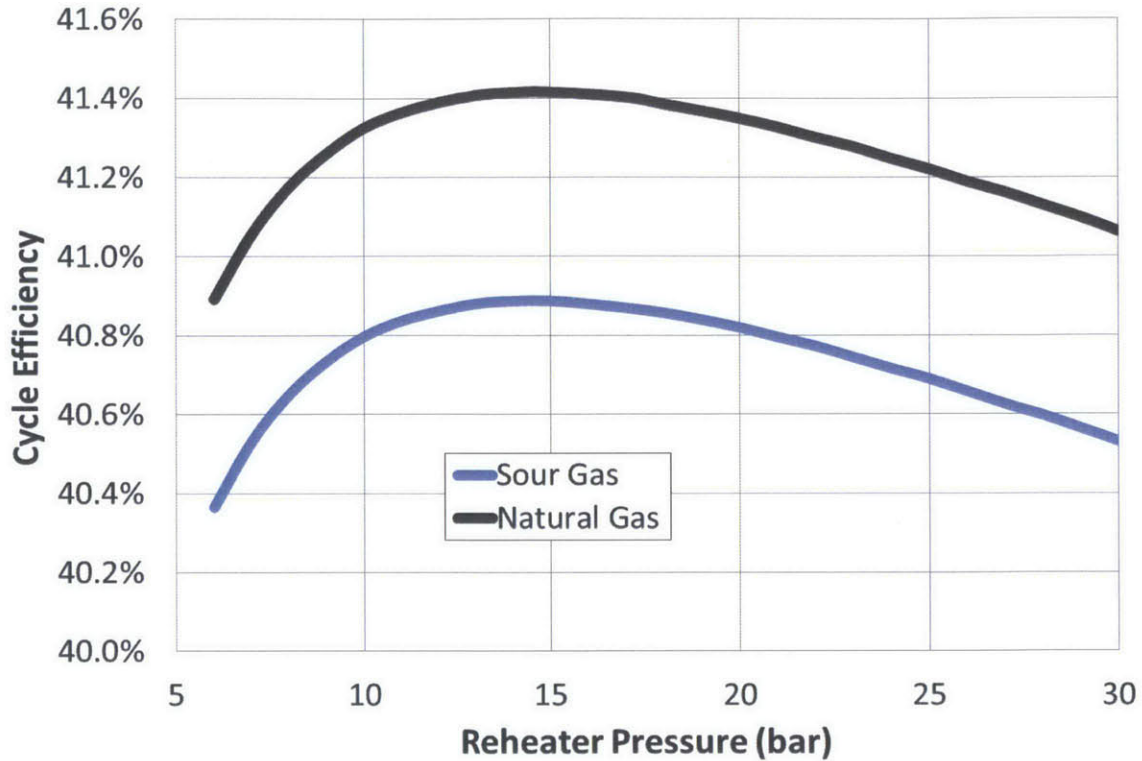
Figure 5-3: Effect of varying reheater pressure on the net cycle efficiency for the sour gas (acid resistance) and methane water cycles

about 15 bar, and then the efficiency starts to go back down. This is mainly because when reheat pressure is changing, the fuel flow rate (and oxidizer) is continuously adjusting in order to maintain a 1200°C reheat exit temperature. This then affects the total heat input to the cycle which in turn affects the efficiency. However, the pressure sensitivity analysis revealed that the efficiency did not vary by more than 0.5% when changing the pressure. The methane cycle also has about a 0.5% efficiency gain over the sour gas cycle which, similar to the combined cycles, is because the methane cycle's working fluid has a slightly larger heat capacity which produces more work and increases efficiency.

Figures 5-4 and 5-5 show the power breakdowns for the two cycles with varying pressures. As mentioned, since the methane cycle has a higher heat capacity working fluid, it has a higher power output for every pressure. For both cycles, the HPT power output was found to be more sensitive to pressure variations than the LPT,
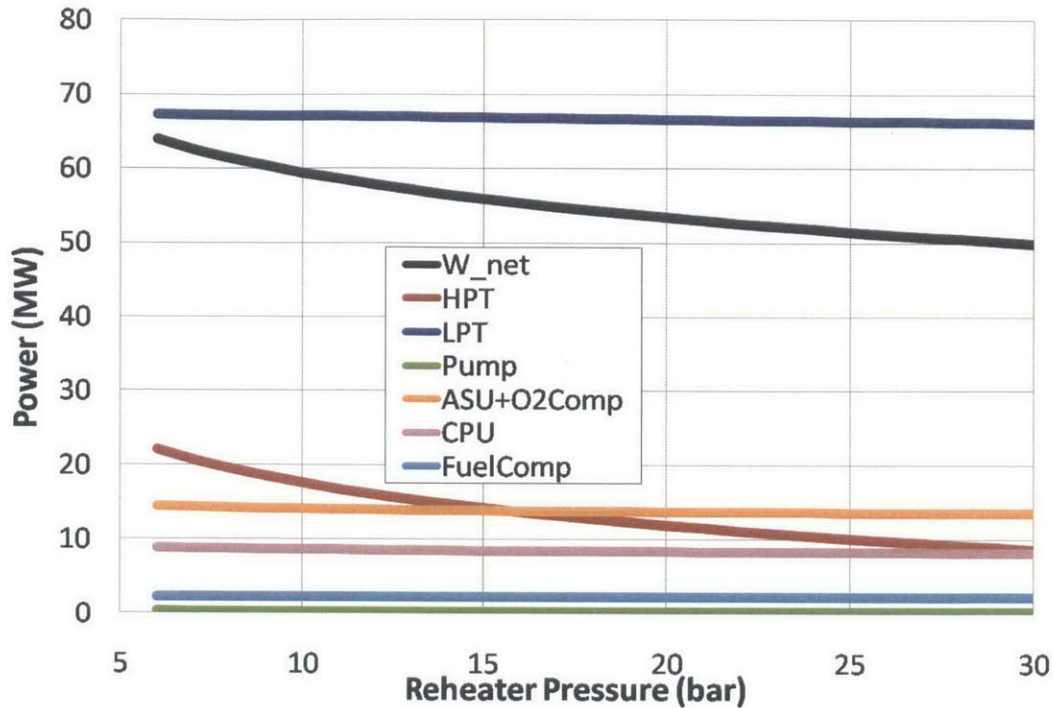
Figure 5-4: Effect of varying reheater pressure on power outputs and requirements for the sour gas (acid resistance) water cycle components

and the power output decreased with increasing pressure. This was due to the fact that the HPT had a lower pressure ratio across the turbine and that pressure ratio was decreasing with increasing reheat pressure and so the power output naturally decreases. The other components were found to be almost non-sensitive to increasing reheater pressure.

The recycle ratio for both cycles was found not to have a significant response to increasing pressure as can be seen in Fig. 5-6. The recycle ratio for the methane cycle is also lower than the sour gas cycle. Unlike the combined cycles where the methane cycle had the higher recycle ratio, for the water cycles, due to the high heat input in the combustor from methane combustion less of the methane cycle's working fluid needs to be recycled to achieve the same exit temperature. Also, for the water cycles, due to the much higher heat capacity of the recycled stream (liquid water), the main force that determines the recycle ratio is the amount of heat input (i.e. fuel) in the combustor. However, this was not the case for the combined cycles in the previous
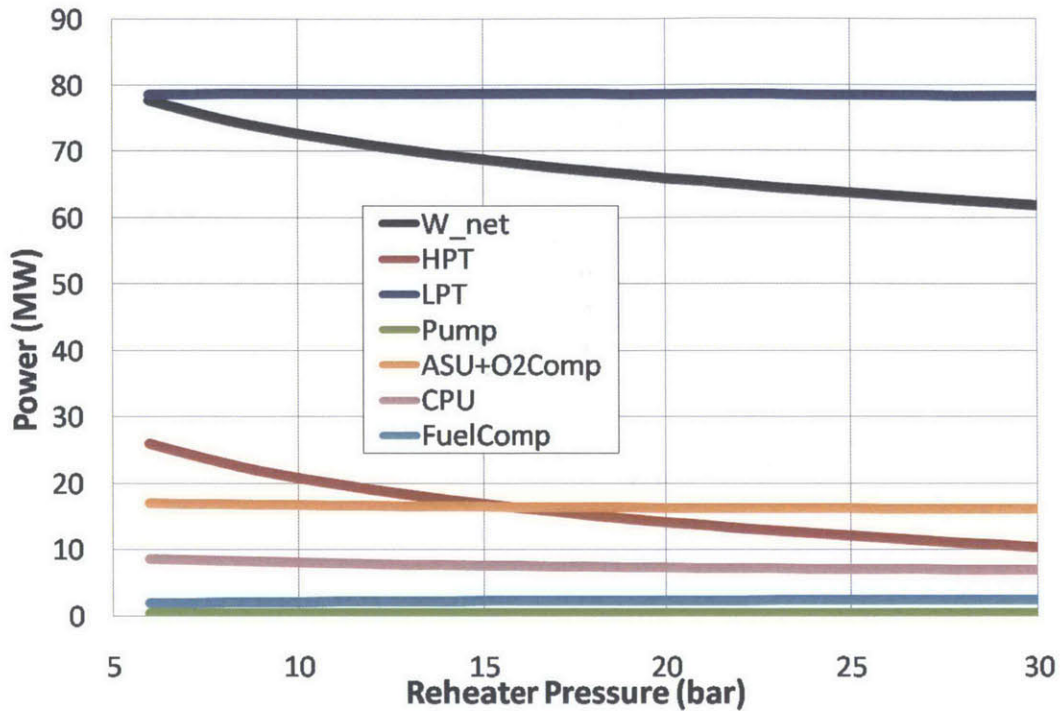
Figure 5-5: Effect of varying reheater pressure on power outputs and requirements for the methane water cycle components

chapter because the recycled working fluid had a low heat capacity and so for those the main driving force for the amount of recycle to the combustor was the amount of diluent entering the combustor, which was higher for the sour gas cycle.

From Figure 5-7, the acid concentrations at both the condenser and HRSG exits decrease with pressure because of the slight decrease in SO_3 concentration in the working fluid as the reheat pressure is increased. Therefore less of it reacts with the water and produces less sulfuric acid. Also, the concentration at the condenser exit is higher because it is at a lower temperature so more of the water has condensed and reacted with the SO_3 to produce H_2SO_4. The acid concentration at the condenser exit is also higher than that observed for the sour gas combined cycle in the previous chapter due to the much higher water content in the cycle working fluid.
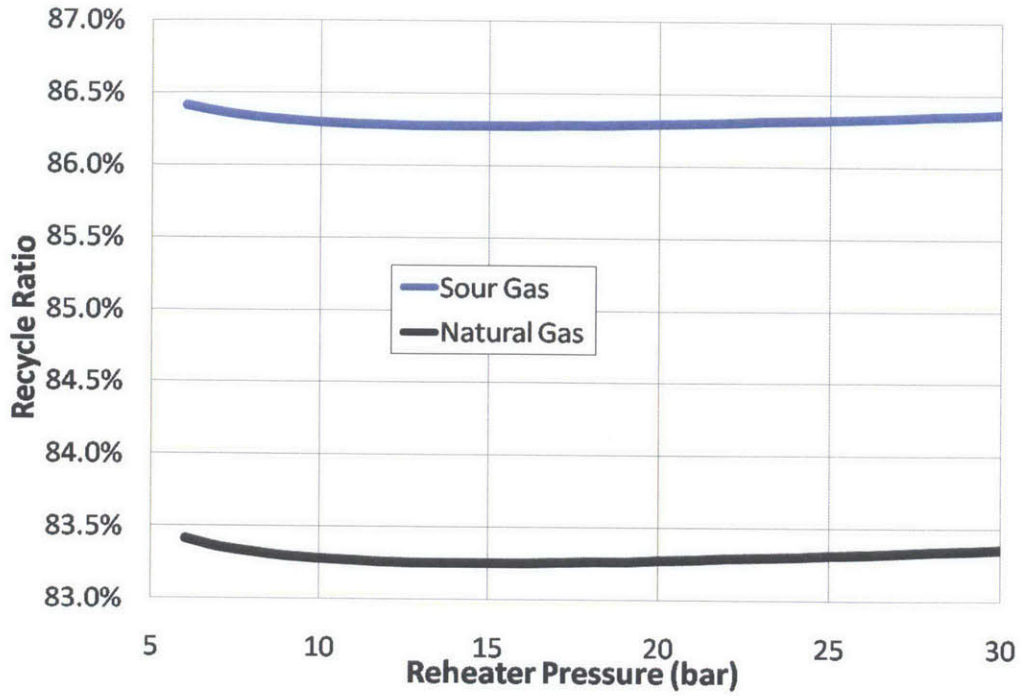
Figure 5-6: Effect of varying reheater pressure on the recycle ratio for the sour gas (acid resistance) and methane water cycles
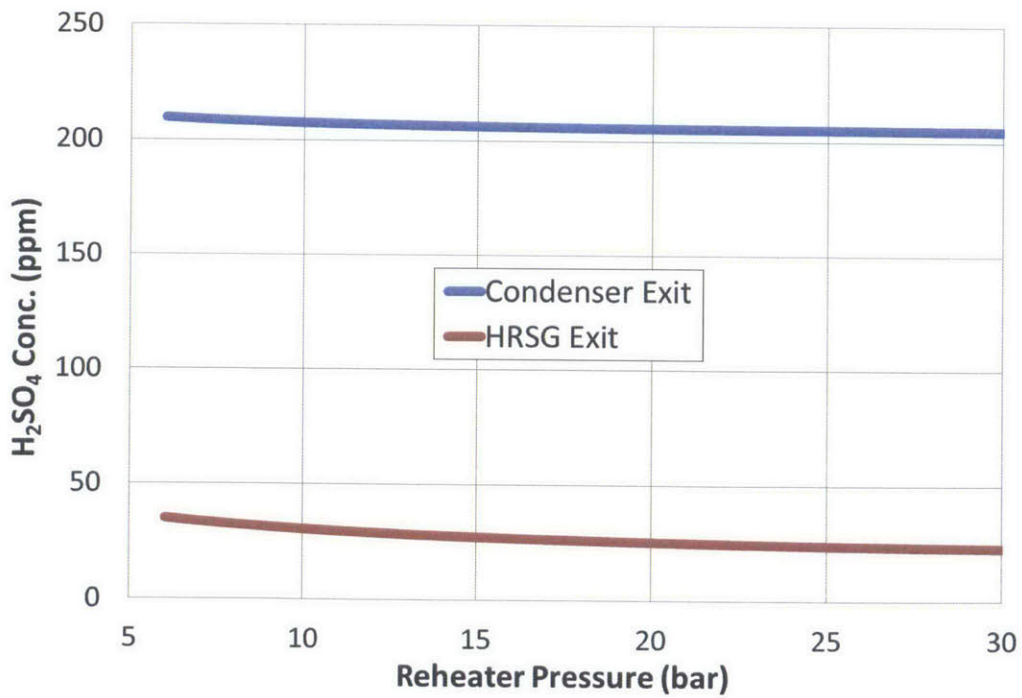
Figure 5-7: Effect of varying reheater pressure on sulfuric acid concentrations for the sour gas (acid resistance) water cycle
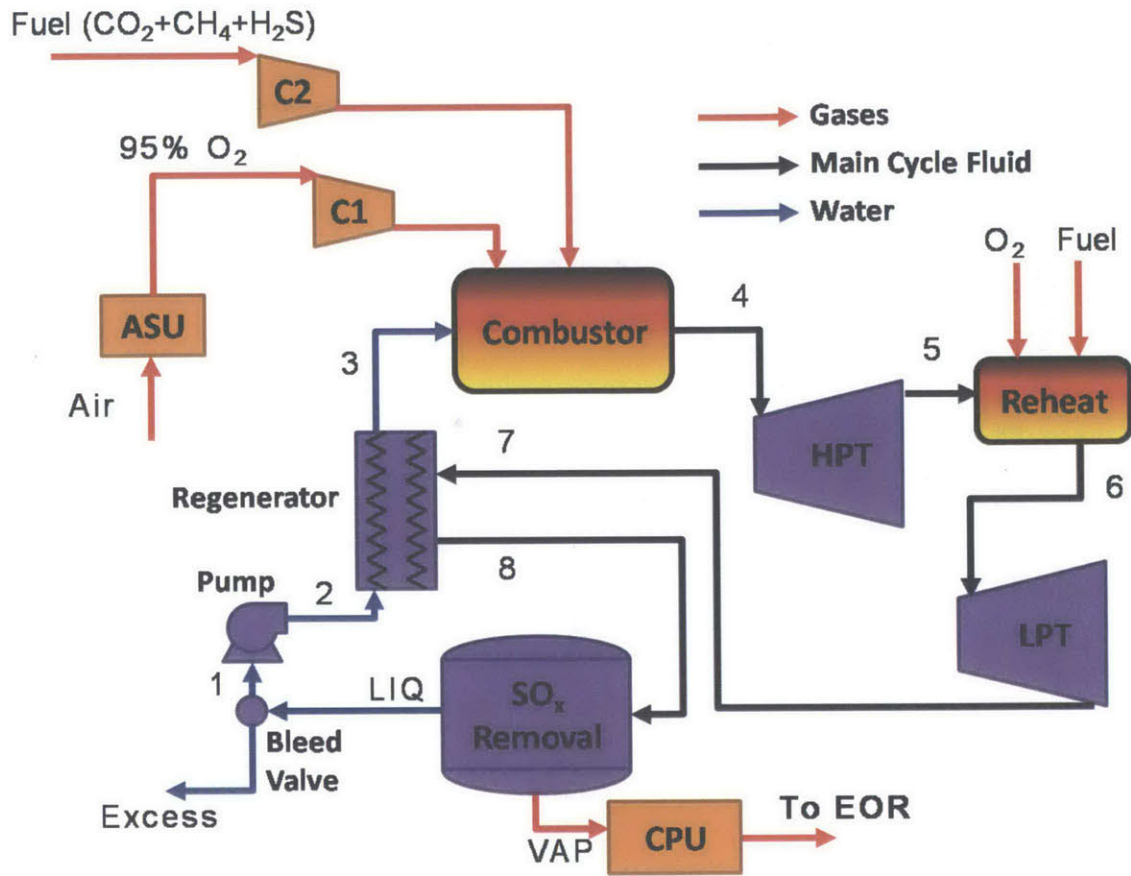
Figure 5-8: Overall process layout for the sour gas water cycle with SO_x removal

5.3 SO_x Removal Cycle

The other type of the sour gas water cycles, was one which we call the "SO_x Removal Cycle". Similar to the combined cycle, this cycle is one where we remove the SO_x compounds in the main cycle. This type of cycle was modeled in order to see how the cycle performs and what the costs would be when the SO_x compounds are removed from the working fluid before it is allowed to condense, thus acid corrosion would then not be an issue. This would also save on using the expensive acid-resistant materials in the main cycle components. Fig. 5-8 shows the cycle diagram and components for the SO_x removal sour gas water cycle, with the corresponding T-s diagram in Fig. 5-9.

Firstly, water at state 1 is pumped up to a pressure of 100 bar where it is then
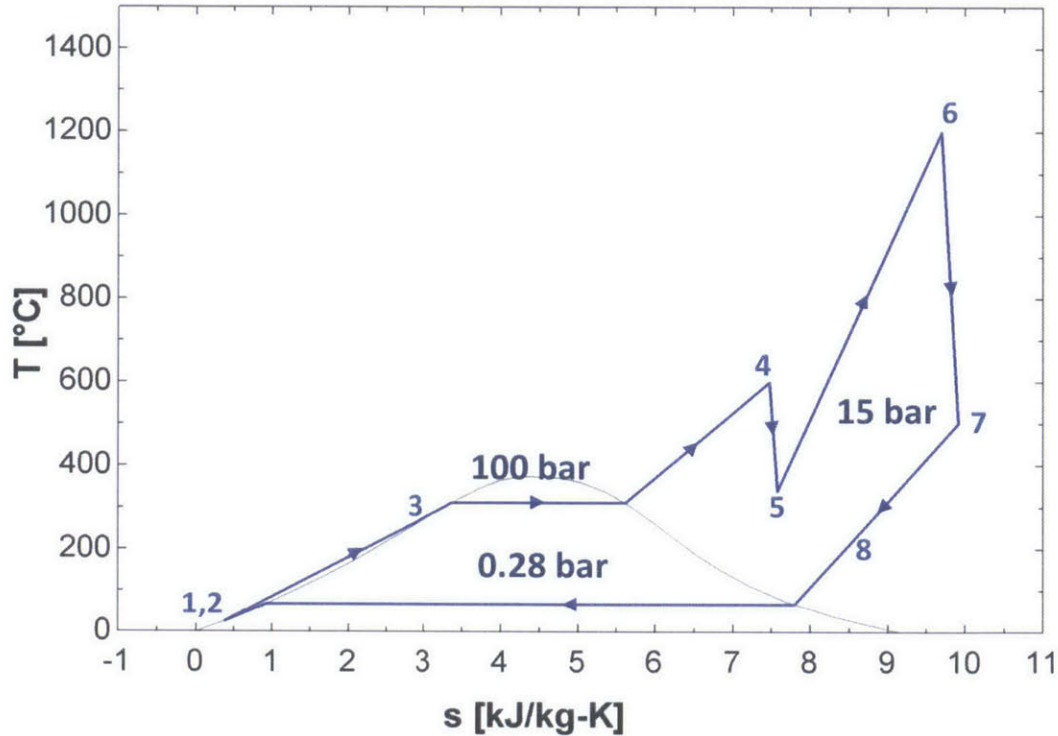
Figure 5-9: T-s diagram of the sour gas water cycle with SO_x removal

preheated in the regenerator to about 260°C before entering the combustor. On the gas side, the oxygen stream from the air separation unit is sent to the combustor along with the fuel (70% CH_4, 15% H_2S, 15% CO_2), and the recycled working fluid (water). The water acts as a diluent in the combustor, and so the recycle ratio ($\dot{m}_1/\dot{m}_{LIQ}$) of the working fluid fixes the combustor exit temperature at 600°C. The main combustor flue gases (5% CO_2, 93% H_2O, 1% SO_2 by volume), state 4, are then expanded in the high pressure turbine (HPT) to 15 bars to produce power. The working fluid at state 5 is then reheated in the reheater where more fuel and oxygen are combusted to achieve a temperature of 1200°C. The reheater flue gases (10% CO_2, 88% H_2O, 2% SO_2, <1%Ar by volume), state 6, are then expanded again in the low pressure turbine (LPT) down to 0.28 bar. Similar to the combined cycle, this pressure was chosen based on an analysis done to determine the optimal pressure entering the SO_x removal system in order to maximize efficiency.

Next, the hot working fluid enters the regenerator where it transfers its thermal

energy to the water stream going to the combustor while being cooled down to state 8. In this case, similar to the combined cycle, the working fluid doesn't condense in the regenerator. So a constraint was placed on the exit temperature of the regenerator to be higher than the dew point. The dew point of this cycle's working fluid (10% CO_2, 88% H_2O, 2% SO_2, <1%Ar by volume) was calculated using Aspen to be about 203°C. Therefore when modeling the regenerator for this cycle, the hot stream's exit temperature was fixed at 208°C and the cold stream's exit temperature was calculated such that the minimum internal temperature approach inside the heat exchanger was maintained at 20°C. Then at the exit of the regenerator the hot working fluid is then sent to the SO_x removal system, and the exiting vapor stream now consists of mostly CO_2 with some Ar and N_2.

5.3.1 SO_x Removal System

The SO_x removal system operates as was explained in section 4.4.1. The final optimal conditions and other stream compositions for the system are shown in Fig. 5-10. The flue gas comes in directly from the exit of the regenerator in the main cycle, with a pressure that was found in order to maximize cycle efficiency similar to the previous analysis done for the combined cycle. They exit the column at a temperature of around 49°C before being cooled further down to the condenser (not shown) temperature of 25°C. The flue gas flow rate coming in, for this case is 41 kg/s. On the other side, the water (+ lime) enters the column at the top with a mass flow rate of 625 kg/s after 4% of it was removed as excess in the bleed valve. The exiting liquid mixture at 54°C is sent to the residence tank where lime is added and the solids are removed. The amount of lime necessary for this cycle with these conditions was found to be 1.9 kg/s, this is the amount necessary for the "Liquid Out" stream to have a neutral pH.

At the exit of the SO_x removal system, 82% of the liquid water is recycled back to the pump to be the diluting medium in the combustor. The vapor stream exiting the SO_x removal system, is extracted then sent to the CO_2 purification unit (CPU) and compressed up to 110 bars to yield a capture-ready carbon dioxide stream for EOR.
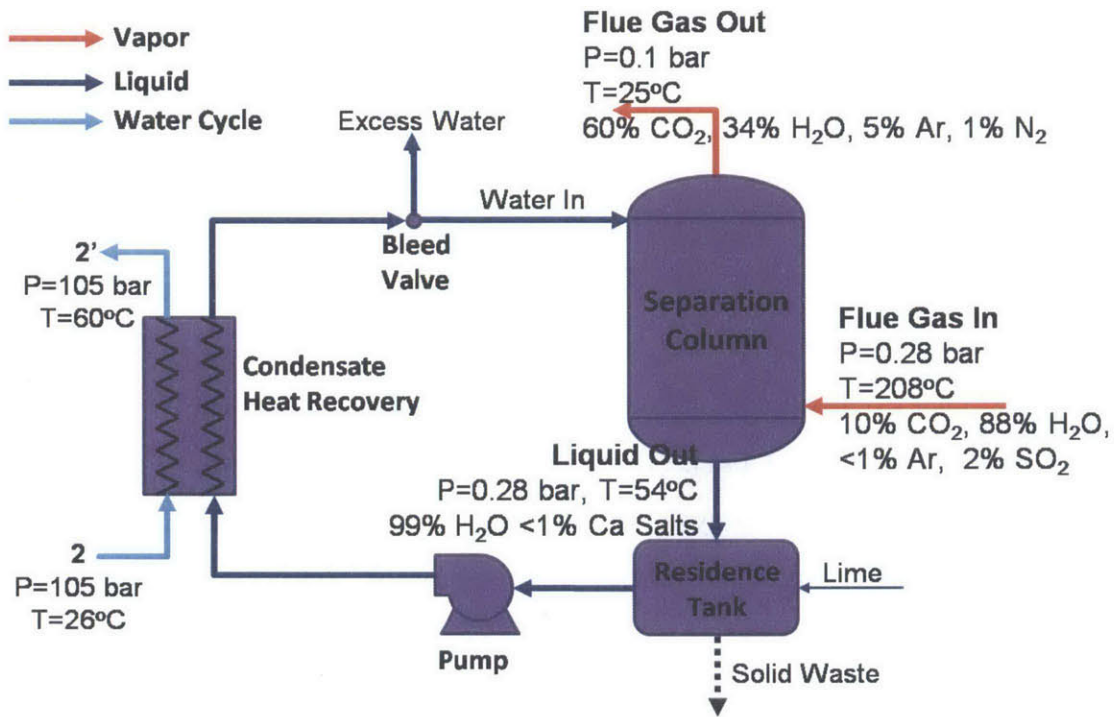
Figure 5-10: SO$_x$ removal system implemented in the water cycle showing the operating conditions

The CPU removes the inert compounds from the working fluid (Ar & N_2).

The efficiency of this cycle with these conditions was found to be 36.1%. In comparison with the previous water cycle, this one had a much lower efficiency, about a 4.5% efficiency drop. One reason for this, more of which will be discussed later, is from the fact that the LPT pressure ratio is slightly lower than the other cycle and so the work output and efficiency decreases as a result of this.

5.4 Performance Analysis and Cycle Comparisons

5.4.1 T-s Diagrams

When comparing the T-s diagrams of the two sour gas water cycles, shown in Fig. 5-11, one can see similar differences to those of the combined cycles in the previous chapter. For the SO_x removal cycle, the low pressure line is slightly higher than the Acid Resistance cycle because of the slightly higher pressure required for the SO_x removal system (0.3 vs 0.1 bar). Therefore as can be seen, the area inside the T-s diagram for the SO_x removal cycle is smaller and so even without calculating it, we would expect the efficiency to be lower than the other cycle and that's indeed the case.

5.4.2 Recycle Ratio Comparison

Figure 5-12 compares the recycle ratios for the cycles. The recycle ratio is mainly dictated by the heat capacity or enthalpy of the recycled working fluid. Higher enthalpy working fluids require less recycling to the combustor to achieve the same exit temperature. For these cycles, the SO_x removal cycle's recycled working fluid (water) had the higher enthalpy because it was at a higher pressure (0.3 bar), and therefore required less recycling to achieve the same combustor exit temperature (600°C). The temperature at the exit of the regenerator, state 3, and entering the combustor was also slightly higher for the the SO_x removal cycle (due to the added heat recovery from the the SO_x removal system). This also contributed to the decrease in amount

180

Figure 5-11: T-s diagrams of the sour gas water cycles

of working fluid recycled and the difference in recycle ratio.

5.4.3 Working Fluid Comparison

The working fluids at both the combustor and reheater exits are examined for the two cycles. Figures 5-13 and 5-14 compares the working fluid composition at the combustor and reheater exits. As can be seen the compositions are the same for both cycles. Since the same type of working fluid is being recycled (liquid water) the exits of the two combustors also have the same compositions. At the reheater exit, the working fluids had higher SO_2 and CO_2 concentrations because the product gases from the combustion of fuel and oxygen are high in those two compounds. So when it mixes with the incoming working fluid, the total mole fraction of SO_2 and CO_2 goes up and H_2O goes down at the exit.

181

Figure 5-12: Recycle ratio comparison for the sour gas water cycles
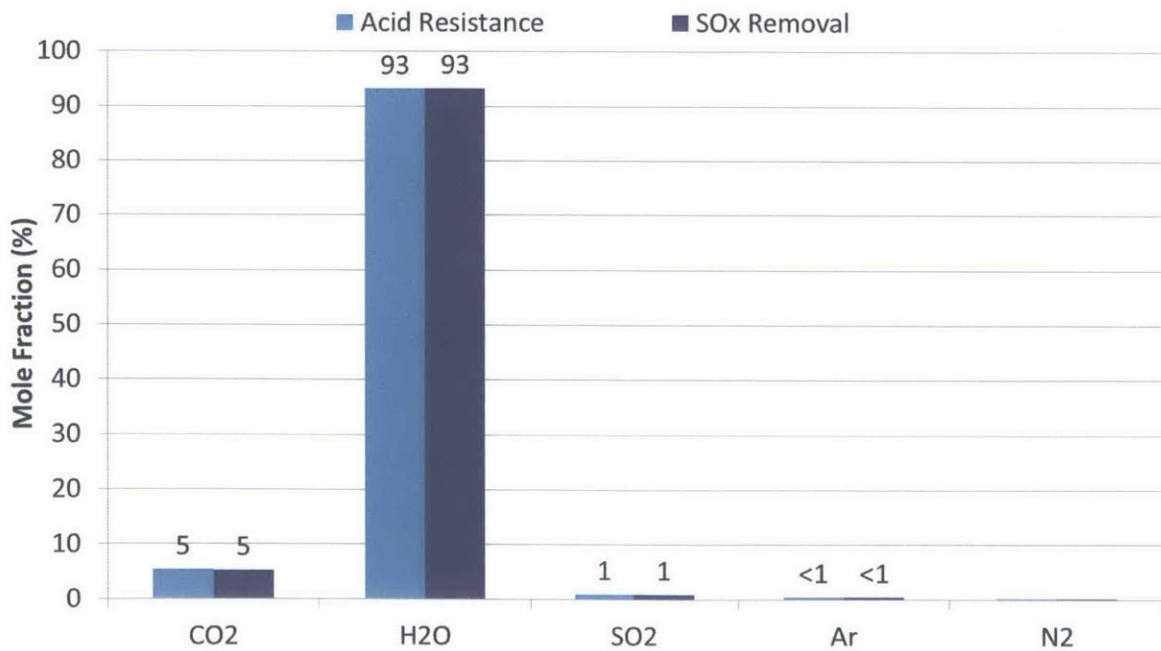
Figure 5-13: Working fluid comparison for the sour gas water cycles (taken at combustor exit)
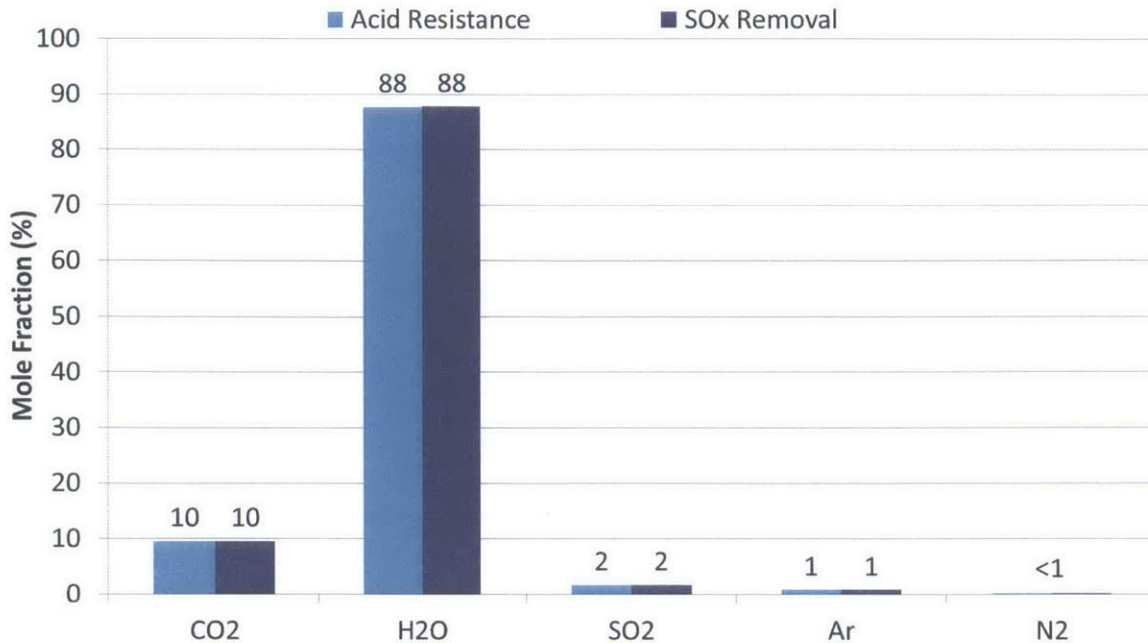
Figure 5-14: Working fluid comparison for the sour gas water cycles (taken at reheater exit)

5.4.4 Pressure Drop Sensitivity

The following analysis presents the results from a combustor and reheater pressure drop sensitivity study that was done on the two cycles to determine the effect on the cycles' efficiencies. As can be seen from Figures 5-15 and 5-16, the combustor and reheater pressure drops were found not to have a significant effect on the efficiency.

The average slopes of the two graphs for the combustor analysis were determined to be the same at about -0.02 Eff%/Pdrop%. For the reheater analysis, the values were different with slopes of -0.03 and -0.04 Eff%/Pdrop% observed for the Acid Resistance and SO_x Removal cycles respectively. As can be seen, the reheater pressure drop had a slightly bigger impact on the efficiency for the two cycles. This is because the LPT contributes more to the net power output and so varying its inlet pressure (by changing the reheater pressure drop), impacts the efficiency more significantly. In our analysis and for the results shown next, the default values of the pressure drops for the combustors and reheaters were taken to be 10% and 6% respectively. These values were chosen from specifications provided by CES as was mentioned earlier in
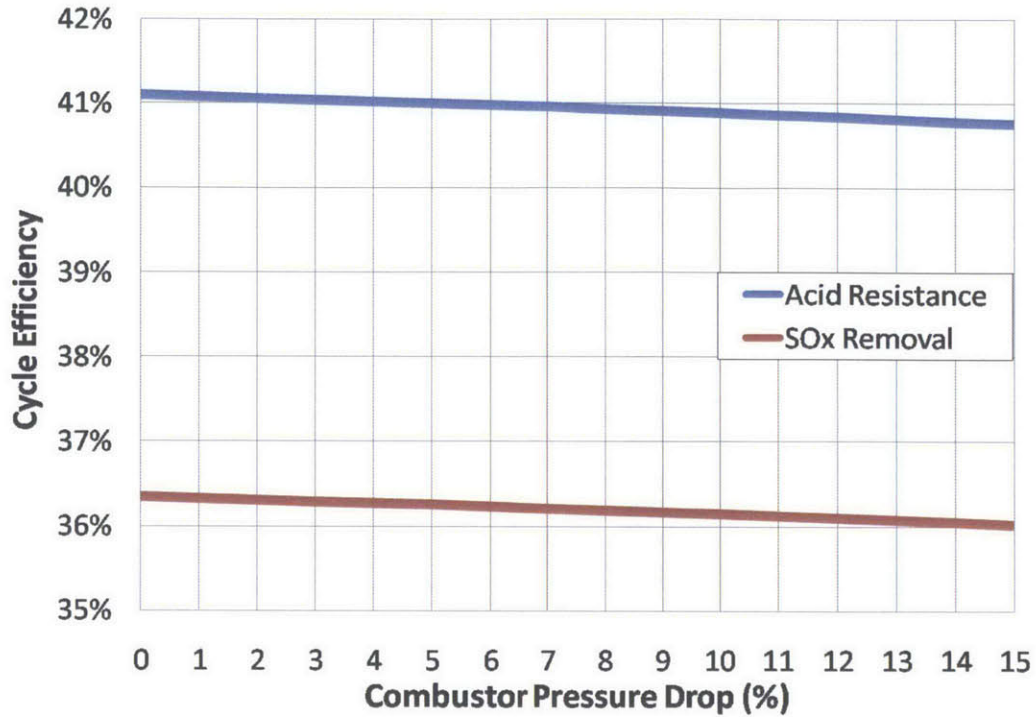
Figure 5-15: Effect of combustor pressure drop on net cycle efficiency for the sour gas water cycles

the document.

5.4.5 Efficiency and Power Breakdown

The final and most important comparison of these cycles is the performance comparison shown in Fig. 5-17. Details of the power generated and consumed by the different components in the cycles are shown where they are expressed as a function of the (total) heat input to the cycle (based on the fuel's LHV) in order to non-dimensionalize the results. The heat inputs to the two cycles were about 137 MW and 139 MW respectively.

The turbine work for the SO_x Removal cycle is lower than the Acid Resistance cycle because the low pressure is 0.3 compared to 0.1 bar. Therefore, there is a smaller pressure ratio across the turbine (LPT) and as a result less power is produced in the turbines. The compressors and pump works for the two cycles are both very low, only resulting in a 2% efficiency loss. This is because the recycled working fluid is
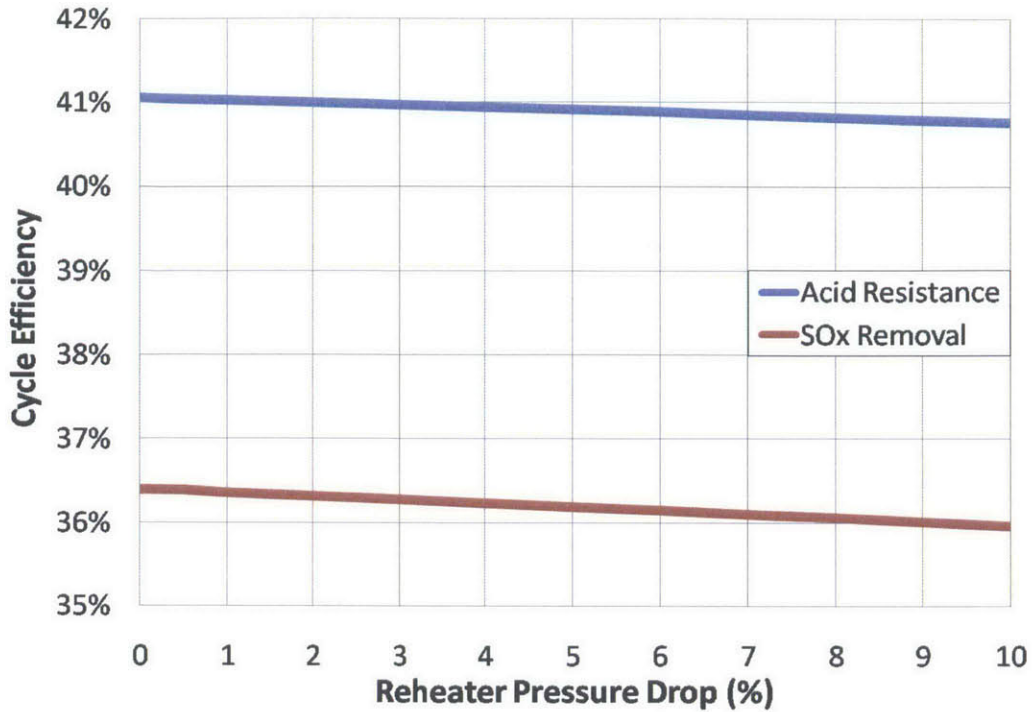
Figure 5-16: Effect of reheater pressure drop on net cycle efficiency for the sour gas water cycles
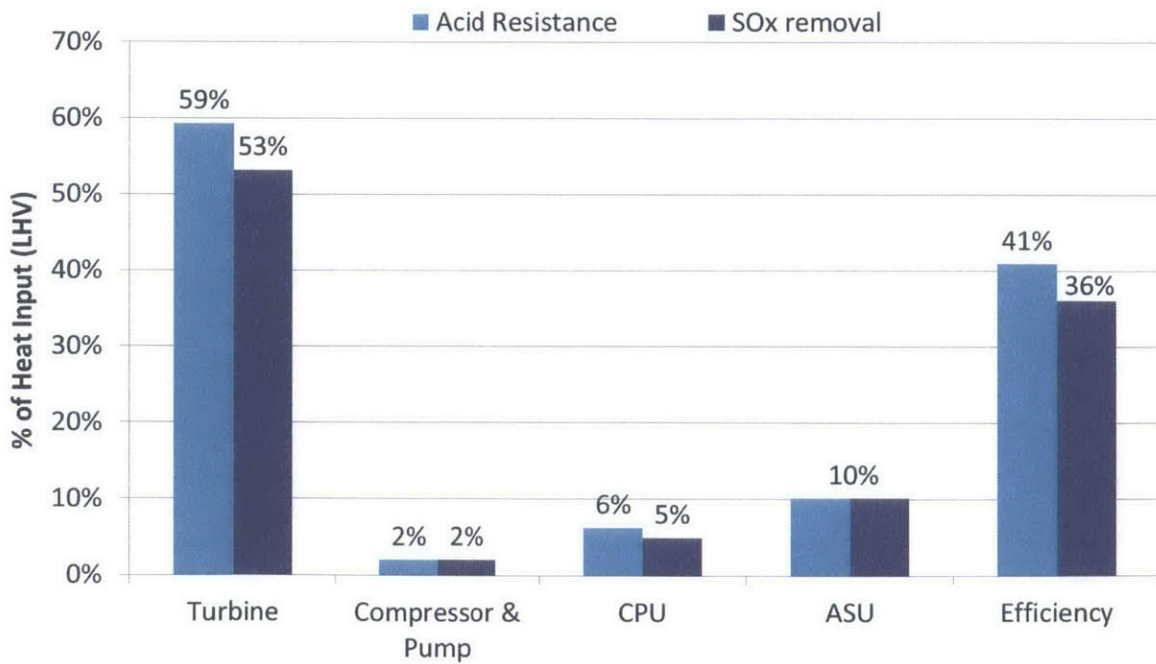
Figure 5-17: Power breakdown for the sour gas water cycles

liquid water and so pumping that up to the combustor pressure requires much less work than if it were a gas (as in the previous combined cycles).

The CPU (CO_2 Purification Unit) and ASU (Air Separation Unit) power inputs are fairly similar for all three cycles. But a slightly smaller power is required in the CPU for the SO_x Removal cycle because the SO_x compounds are already being removed in the main cycle before entering the CPU. Therefore, there is no further efficiency penalty associated with this process, unlike the other cycle.

Also there is an efficiency decrease for the SO_x Removal cycle because of the inability to recuperate all of the latent energy from the hot working fluid in the regenerator. Since the hot working fluid doesn't condense for this cycle, less heat is transferred to the liquid water being preheated and so this overall leads to a smaller net power output and also lower efficiency.

Finally, all of the above effects combine to give the efficiency differences shown. The Acid Resistance cycle once, again, has the best efficiency at 40.9% compared to 36.1% for the SO_x Removal cycle. As will be explained further in the next section, the SO_x Removal cycle had a much larger efficiency decrease from the Acid Resistance cycle for these water cycles than for the combined cycles. This is because the overall cycle pressure ratio decrease had a significantly bigger impact on the turbine work for the water cycle than the combined cycle.

5.5 Sour Gas Cycles Performance Comparisons

After comparing each of the cycles for the two cycle types separately, we now look at the differences between all five of the sour gas cycles that were modeled: Combined Cycle Acid Resistance, Combined Cycle No Condensation, Combined Cycle SO_x Removal, Water Cycle Acid Resistance, and Water Cycle SO_x Removal.

5.5.1 Recycle Ratio Comparison

Figure 5-18 compares the recycle ratios for all of the sour gas cycles. The recycle ratio is mainly dictated by the heat capacity or enthalpy of the recycled working

186
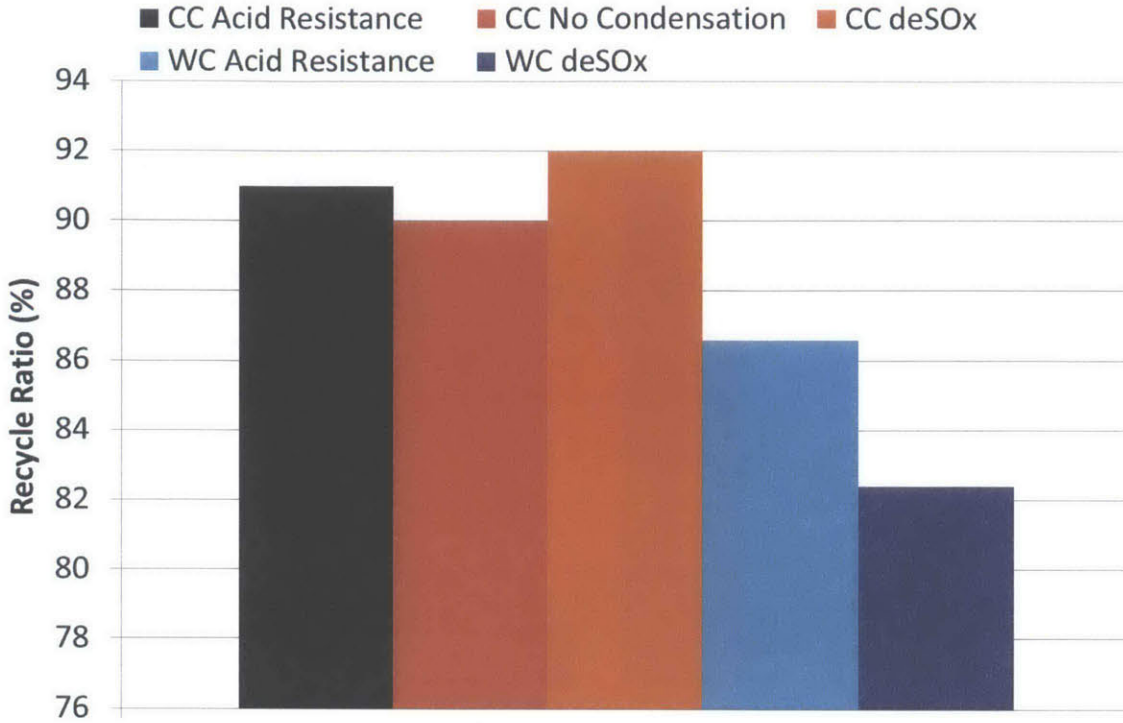
Figure 5-18: Recycle ratio comparison for all of the sour gas cycles

fluid. Higher heat capacity working fluids require less recycling to the combustor to achieve the same exit temperature. For these cycles, the two water cycles had the lowest recycle ratios because the recycled fluid, liquid water, had a much higher heat capacity than those of the combined cycles (gaseous CO_2). The No Condensation combined cycle also recycled mostly water but for that case it was in the form of a gas and so had a lower heat capacity than the liquid and therefore needed more recycling.

5.5.2 Working Fluid Comparison

The working fluid at the combustor and reheater exits are examined for all the cycles. Fig. 5-19 compares the working fluid composition at the combustor exit for the combined cycles and at the reheater exit for the water cycles. For the No Condensation combined cycle, much more H_2O is recycled back to the combustor (since the working fluid doesn't condense) than the other two combined cycles and so higher amounts
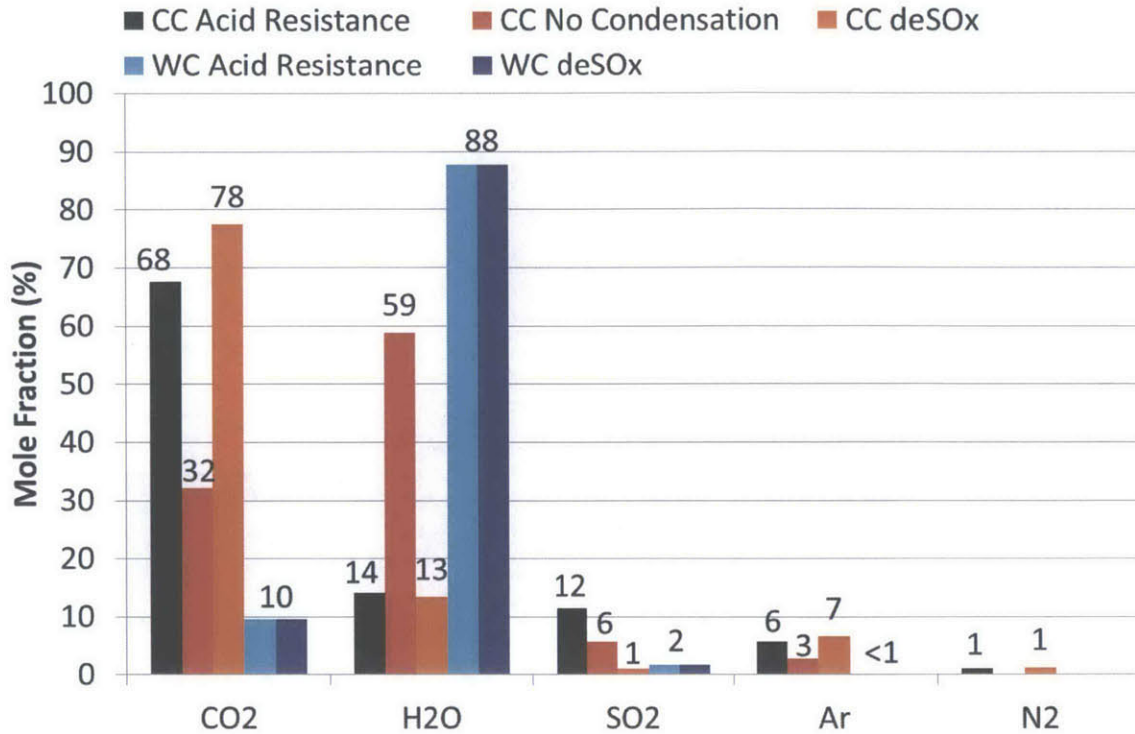
Figure 5-19: Working fluid comparison for all of the sour gas cycles (taken at combustor and reheater exits)

were observed at the exit of the combustor. Since the SO_x Removal combined cycle removes the SO_2 prior to entering the compressor, there is much less SO_2 present in the working fluid than the other two combined cycles. The water cycles recycle only H_2O back up to the combustor and so there is much more H_2O present in the working fluid than the rest of the sour gas cycles. Also since the same type of working fluid is being recycled (liquid water) for the water cycles they both have the same compositions.

5.5.3   Efficiency and Power Breakdown

Finally, the performance comparison of all these cycles are shown in Figures 5-20 to 5-22. Details of the power generated and consumed by the different components in the cycles are shown where they are expressed as a function of the (total) heat input to the cycle (based on the fuel's LHV), in order to non-dimensionalize the results.
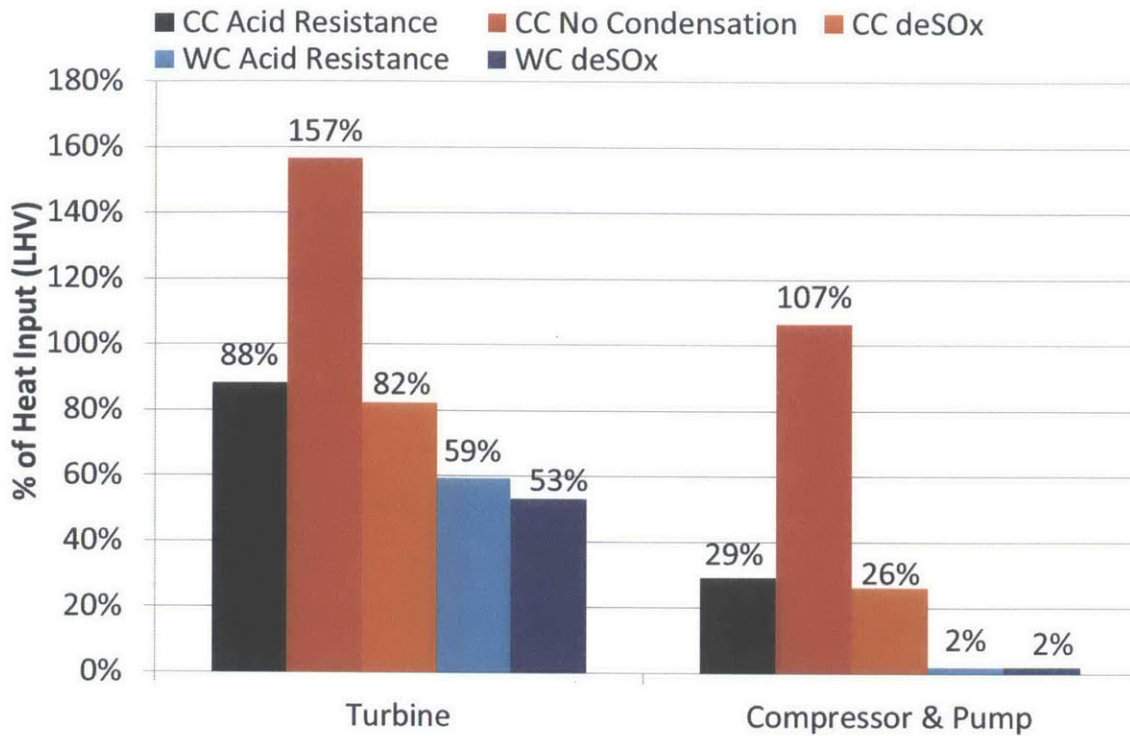
Figure 5-20: Turbine, compressor and pump power breakdowns for the sour gas cycles

The heat input to all of the combined cycles were the same at 64 MW, and the heat inputs to the two water cycles were about 137 MW and 139 MW respectively.

Fig. 5-20 shows the power breakdown for the turbines and compressors/pumps. The first thing that is clearly noticeable is the unusually high red bars for the turbine and compressor works for the No Condensation cycle. The reason for this is because of the fact that the working fluid has a very high heat capacity and so this cycle produces a lot of power in the turbine but also require a lot of power in the compressor to pressurize that working fluid to 40 bar.

Second of all, the turbine works for the two SO_x Removal cycles are lower than their equivalent Acid Resistance cycles because the low pressures were 1.5 and 0.3 bar compared to 1.1 and 0.1 bar. So there is a smaller pressure ratio across their turbines and as a result less power is produced. The same is true for the compressor for the combined cycle but this results in a lower power required since the pressure entering in the SO_x Removal case is 1.3 bar versus 1 bar for the Acid Resistance cycle.

The turbine power outputs for the water cycles are both much lower than the combined cycles, due to the nature of the cycles configurations and assumptions. In the water cycles, **liquid** water is fed to the combustor to act as a diluent and moderate the temperatures, whereas a gaseous working fluid is recycled to the combustor in the combined cycle cases. Therefore for the water cycles, part of the fuel's heating value is being used first for phase change to evaporate this liquid and then heating it up to the desired combustor temperature. Whereas in the combined cycles the heat input in the combustor is only used for heating up the gases. Since the heat input is fixed (fixed fuel flow rate), the only way to accommodate this recycled fluid's difference is to decrease the mass flow rate in the water cycle which in turn decreases the turbines power output. A second reason why we see the turbine power differences is from the fact that the water cycles, had higher pressure drops in the combustors and reheaters (10% & 6%) compared to 5% for the combined cycles. Therefore, this once again decreases the turbine power output.

The compressors and pump works for the two water cycles are also both very low compared to the combined cycles, only resulting in a 2% efficiency loss. This is because the recycled working fluid is liquid water and so pumping that up to the combustor pressure requires much less work than if it were a gas.

Fig. 5-21 shows the power breakdowns for the CPUs and ASUs. The CPU and ASU power inputs are fairly similar for all five cycles. But a slightly smaller power is required in the CPU for the SO_x Removal cycles because the SO_x compounds are already being removed in the main cycles before entering the CPU. Therefore, there is no further efficiency penalty associated with this process, unlike the other cycles. Also the water cycles have slightly higher power requirements in the CPU since the cycle operates at much lower condenser pressures than the combined cycles. So more work is needed to recompress that CO_2 stream for purification and EOR applications at the same pressure of 110 bar.

Also there is an efficiency decrease for the No Condensation and SO_x Removal cycles because of the inability to recuperate all of the latent energy from the topping cycle's working fluid in the HRSG, and from the hot working fluid in the regenerator

190
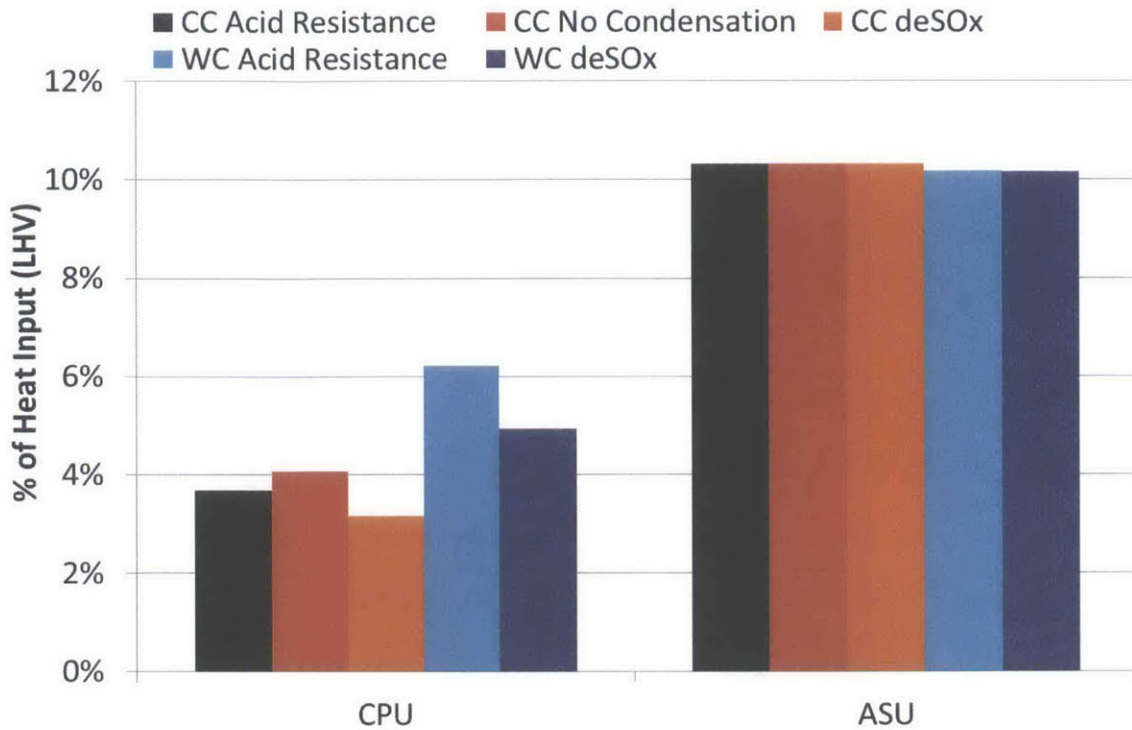
Figure 5-21: CPU and ASU power breakdowns for the sour gas cycles

for the water cycle. Since the working fluid doesn't condense in the HRSG for these two combined cycles, less heat is transferred to the steam bottoming cycle and so this leads to a smaller power output in the steam cycle. Also since the hot working fluid doesn't condense for the water cycle, less heat is transferred to the liquid water being preheated. This results in another efficiency decrease for these three cycles.

Finally, all of these effects mentioned above combine to give the efficiency differences shown in Fig. 5-22. The Acid Resistance cycles had the best efficiencies compared to their other cycle types. The water cycles also had lower efficiencies than the combined cycles except for the No Condensation cycle that had the worst efficiency at 35.6%. The SO_x Removal cycle had a much larger efficiency decrease from the Acid Resistance cycle for the water cycles than for the combined cycles. This is because the overall cycle pressure ratio decrease had a significantly bigger impact on the net power for the water cycle than the combined cycle. The SO_x Removal combined cycle had a benefit from this decreased pressure ratio in that the compressor

191
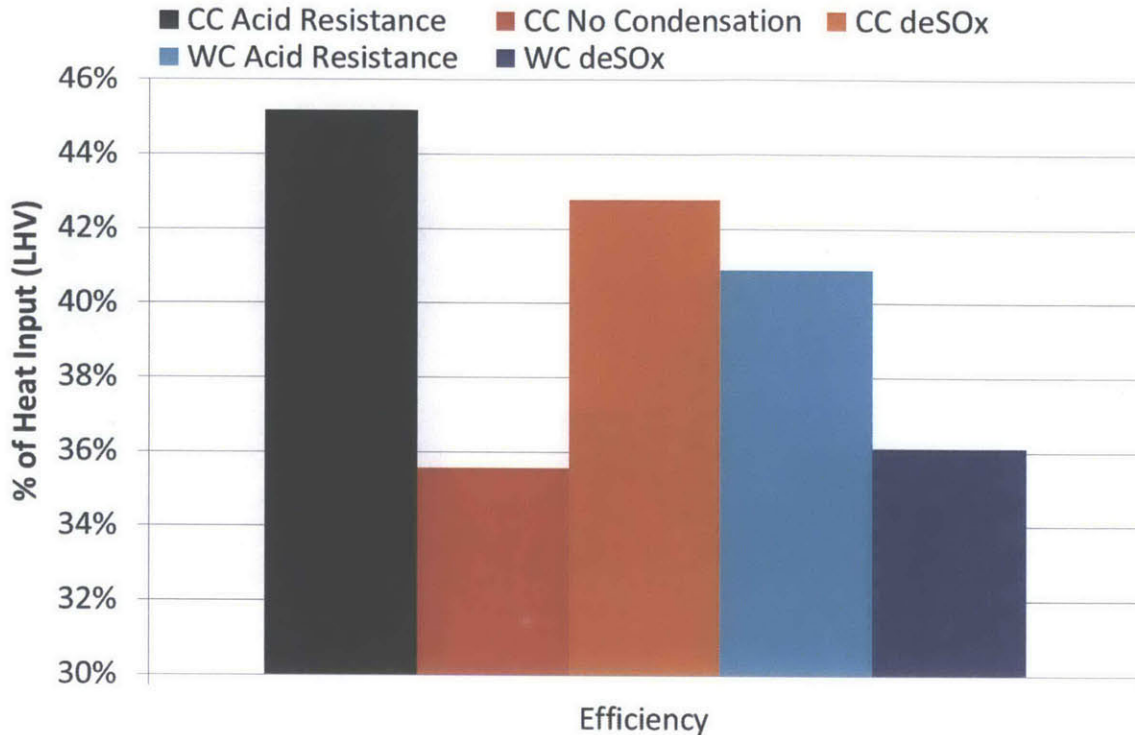
Figure 5-22: Efficiency comparison for the sour gas cycles

also had a smaller pressure ratio and so less work was required there. However, the SO_x Removal water cycle did not benefit from this because it relies on a pump for compression and the pump work is almost negligible compared to the turbine work.

5.6 Conclusions

Similar to the previous chapter, the second type of the sour gas cycles were described and modeled: Acid Resistance and SO_x Removal water cycles. The Acid Resistance cycle had a configuration where the working fluid is allowed to condense in the main cycle components because an acid-resistant material is assumed to have been used in order to protect the components from corrosion. In the SO_x Removal cycle, a SO_x removal system is employed which removes the sulfur compounds from the working fluid thereby greatly reducing the risk of corrosion from this exit stream as it makes it way through the rest of the cycle.

Pressure parametric studies were also done on the cycles in order to provide the

optimal operating pressures, and to give a better understanding of the pressure dependence on the system performance. The reheat pressure variation was found to produce an optimum point which maximizes efficiency and this value was used throughout the analysis. However, the efficiency did not vary much with only a 0.5% efficiency difference when changing the pressure between 6-30 bar.

A similar performance comparison was done for the two water cycles and it was found that once again, the Acid Resistance cycle had the better efficiency. Comparing all of the five cycles together now, the combined cycles on average performed better due to the fact that liquid water is being recycled in the water cycles which decreases the overall performance of these cycles. Therefore from a purely technical point of view, the performance ranking of these cycles were as follows: Combined Cycle Acid Resistance, Combined Cycle SO_x Removal, Water Cycle Acid Resistance, Water Cycle SO_x Removal, and then the worst was the Combined Cycle No Condensation.

Chapter 6

Cost Estimation

6.1 Overview

The five sour gas cycles have been evaluated from a technical performance perspective in the previous chapters. Thermodynamic analyses were conducted to understand the systems' performance and sensitivity to certain operating parameters. But as was mentioned before, these novel cycles will require new equipment and advanced processes that may or may not be available in the industry. As such, the following economic evaluation of these cycles is considered to be preliminary.

To be able to compare and thoroughly evaluate the sour gas cycles, a techno-economic performance evaluation needs to done in order to properly asses the viability of these cycles. The economic viability of the cycles will be discussed and presented in this chapter by performing a necessary cost estimation. Based on the results of this analysis, we can see which systems and sub-systems are the most cost-intensive and how they compare to the pure methane oxy-fuel cycles' costs breakdown.

6.2 Methodology

A bottom-up cost estimation approach was used in this analysis. Each cycle component's performance and process stream data's are transferred directly from Aspen Plus and then used to size and cost the equipment. The equipment sizing and cost

estimation is handled by Aspen Process Economic Analyzer which is integrated into Aspen Plus [26]. This program allows the user to select specific materials for the equipment, other than the default, and then the results are summed up to give the total equipment cost. Then the total equipment cost was used to calculate the levelized cost of electricity for each of the cycles in order to incorporate the effects of efficiency and fuel cost. In the forthcoming analysis and results, the equipment costs and the LCOE's were used to compare the cycles.

When estimating the equipment costs of the ASU (Air Separation Unit) and CPU (CO_2 Purification Unit) in our analysis, quotes from sources external to Aspen were used in order to get a better estimate for the costs. The ASU cost used was based on the quote by Air Liquide mentioned in the paper by Rezvani et al. [25]. The cost quotation for the ASU they were modeling had the same oxygen purity as our cycles (95 mol.%) and also came from a credible company and thus was considered reliable enough for our cost estimates.

Since the CPU that was modeled for the sour gas cycles was based on the model developed by Chukwunwike Ilocje [28], the cost estimation procedure and material selection for the non condensable gas removal process was also similar to those used by that same author.

6.3   Material Selection

A critical part of the cost estimation procedure, is the selection of the materials for the different components in all of the cycles. All of the sour gas cycles have SO_x present in the working fluid and sulfuric acid forms in the areas where this working fluid condenses. Therefore, in order to protect the equipment from corrosion, certain materials have to be used which would help reduce the chances of part failures. The corresponding materials for these equipment were determined based on literature recommendations and known properties of the selected materials. The same material recommendation was used for all of the sour gas cycles, and are discussed next where the equipment have been broken down into two subsections: the turbine and

196

compressor, and the acid equipment.

6.3.1 Turbines and Compressors

One of the biggest issues with the sour gas cycles' working fluid in the turbines and compressors is the problem of hot corrosion. Hot corrosion is defined as "the accelerated corrosion, resulting from the presence of salt contaminants, such as Na_2SO_4, that combined to form molten deposits, which damage the protective surface oxides" [64]. This Na_2SO_4 comes from the reaction of the SO_2 in the working fluid with the small concentrations of NaCl which is usually present in the combustion air if the plant is operated near a sea, or from other industrial pollutants present in the air. This reaction is shown below.

$$2\,NaCl + SO_2 + O_2 \longrightarrow Na_2SO_4 + Cl_2 \tag{6.1}$$

The problem of hot corrosion is mainly prevalent in the aircraft engine industry because the aircraft environment operates at high temperatures and the combination of this with sulfur contaminants in the fuel and the salty air from the oceans, result in the rapid consumption of the metal materials leading to catastrophic failures.

To combat this issue, it was found that increasing the chromium content in the metal alloys or coatings would significantly improve the resistance of the material. More specifically, nickel-based alloys with a chromium content greater than 15 wt.% were found to be more resistant to hot corrosion. The data also suggested that increasing titanium also helped improve the material's hot corrosion resistance [65].

Based on these results, the best available material from the ones listed in Aspen [66] was chosen for the turbines and compressors that had SO_2 in the working fluid. The most suitable material was found to be SS321. It contains 18% chromium and also some titanium [66] and was the highest chromium containing alloy that could withstand the high temperatures in the turbines and compressors. SS321 is also used in the aviation industry in aircraft exhaust stacks and jet engine parts [67, 68].

Another important material that needs to be chosen is the one for the fuel com-

pressors. Since the fuel contains high levels of H_2S, corrosion is an extremely serious issue for this component. Thomas et al. [69] suggested the use of the corrosion resistant alloy 20Cb-3 (Carpenter Alloy®), and the material's data sheet also recommends this alloy as having good corrosion resistance to sour gas [70].

6.3.2 Acid Equipment

The acid equipment refer to the components where the working fluid has condensed and sulfuric acid has formed. This is mainly for the condensing heat exchangers (condenser, HRSG, regenerator) and the absorber column in the SO_x removal system. The model results presented show that the pH levels in these systems are expected to be very low thus making their environments very aggressive. To combat the corrosion by the acid on these components' materials, a corrosion resistant material must be chosen that can withstand these extreme conditions. In a study by Shoemaker et al. [71], comparing the corrosion resistance of stainless steel metals, Alloy 686 (Iconel®) was found to be very stable in highly corrosive environments with sulfuric acid. As such, this material was chosen for the absorber shell cladding, and the shell and tube materials in the heat exchangers.

6.4 Cost Estimation Results

In the forthcoming section, the results of the cost estimation study are presented. The following cycle labels used in the graphs, are explained below:

CC AR	Combined Cycle with Acid Resistance
CC NC	Combined Cycle with No Condensation
CC SR	Combined Cycle with SO_x Removal
WC AR	Water Cycle with Acid Resistance
WC SR	Water Cycle with SO_x Removal

In all of the results presented in this chapter, the total cycle consists of these units: Turbines, Compressors/Pumps, Burners (if applicable), Heat Exchangers, ASU, CPU, and SO_x Removal System (if applicable). For the combined cycle layouts, similar to

what was done in the literature, the combustor costs were accounted for in the gas turbine costs since they are usually one unit in actual power plants. But for the water cycles, an extra 'burner' cost was added. For the two sour gas SO_x removal cycles, there is also a separate SO_x removal system cost, whereas for the other three cycles, the SO_x removal system's cost was accounted for in the CPU.

6.4.1   Cost Estimates

Methane Cycles

Figures 6-1 and 6-2 show the specific cost breakdown for two of the methane cycles modeled in the literature for each of the main components in the cycles. The specific cost is defined as the total equipment cost divided by the net power output. The values for these costs for the combined cycle and water cycle layouts were obtained from the paper by Rezvani et al. [25]. One important thing to note is that for the combined cycle, the gas turbine cost given also includes the combustor but also the compressor, which is the reason why the compressor/pump costs are very low.

In Figure 6-1, it can be seen that the turbine cost account for over a half of the cycle's total specific cost which is due to the gas turbine including the costs of the combustor and compressor thus increasing its share of the total. But it can also be seen that the other capital-intensive component is the ASU, which accounts for about a quarter of the plant's cost. This is true for a lot of the oxy-fuel power cycles, including coal. For the methane water cycle costs, shown in Figure 6-2, there is an extra 'burner' cost which was approximated according to a steam-injected combustor which they obtained. It can be seen that for the water cycle, since the condensing pressure is much lower, this results in large heat exchanger surface areas which increase their size and thus cost. Therefore, the heat exchangers have a bigger contribution to the total cost.
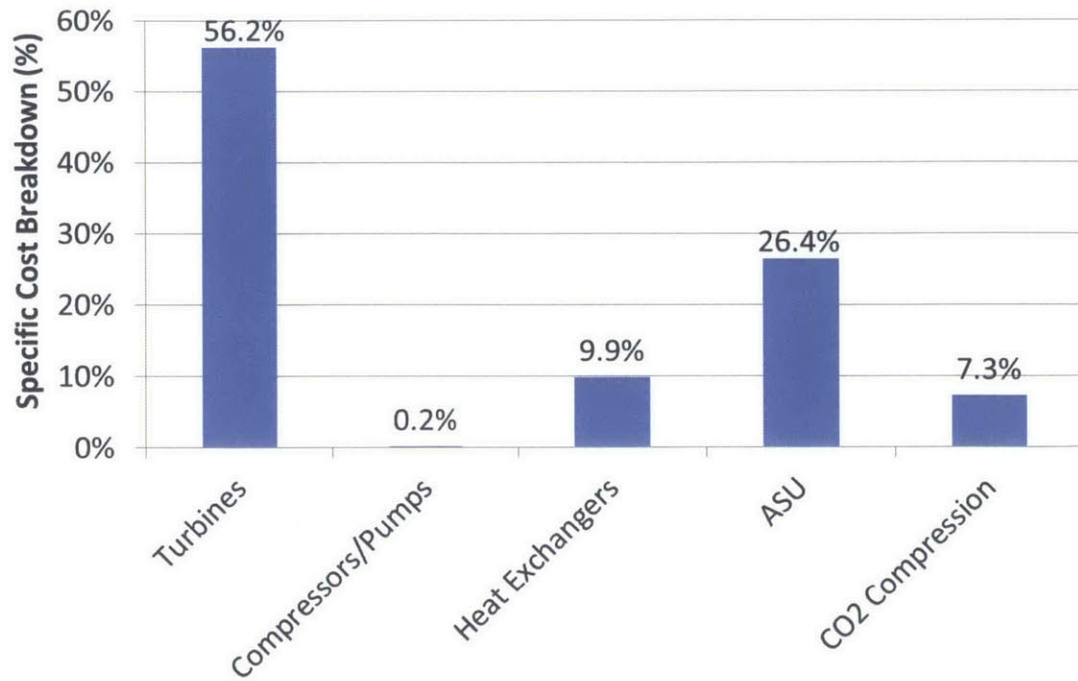
Figure 6-1: The breakdown of the specific costs for the methane combined cycle modeled by Rezvani et al. [25]
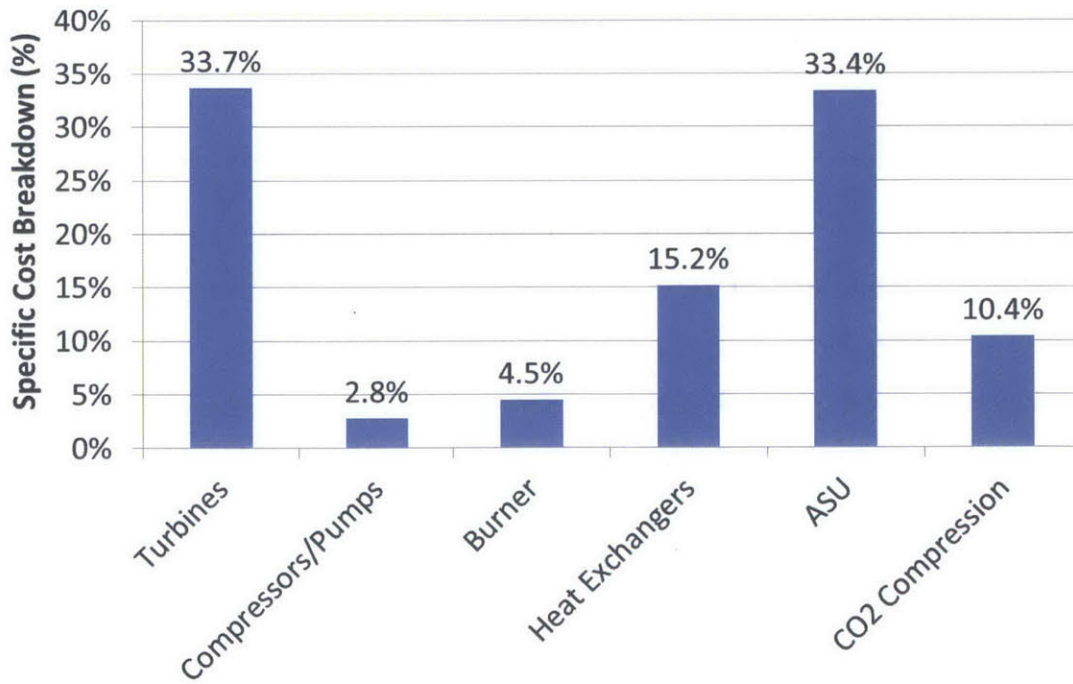
Figure 6-2: The breakdown of the specific costs for the methane water cycle modeled by Rezvani et al. [25]
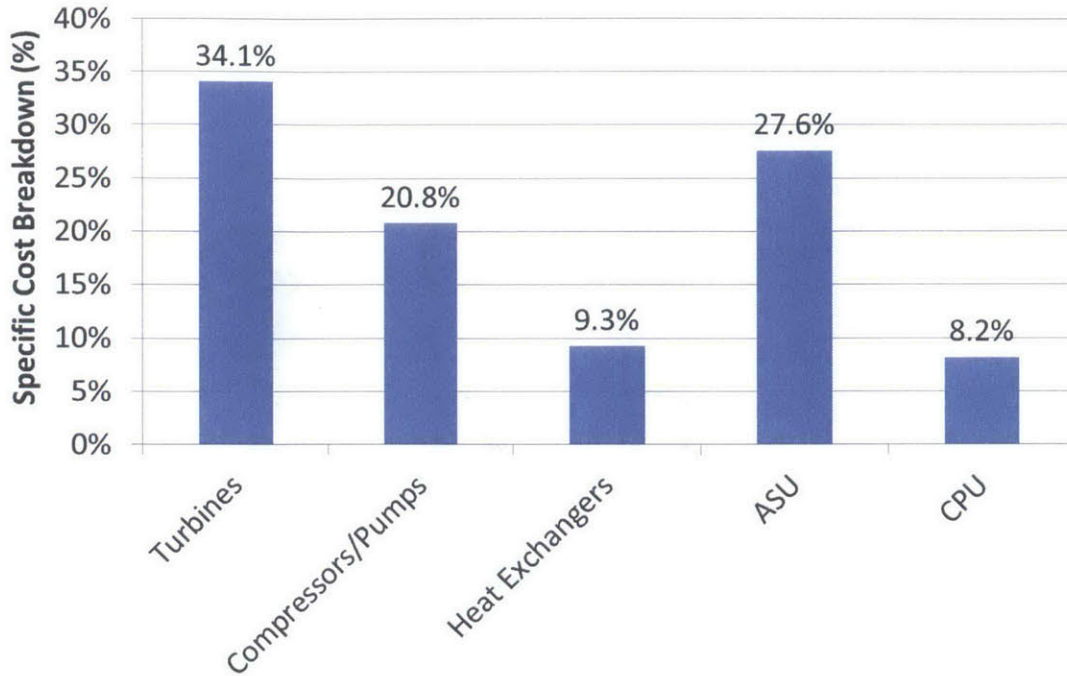
Figure 6-3: The breakdown of the specific costs for the sour gas acid resistance combined cycle

Sour Gas Acid Resistance Combined Cycle

Figure 6-3 shows the cost breakdown of the sour gas combined cycle with acid resistance. The turbines once again require the largest capital investment, out of all the other components in the cycle, especially since the gas turbine will require that special material to resist the hot corrosion. Similarly the compressor will also require the use of that material which increases its cost contribution. Similar to the methane cycles, the ASU is still one of the more capital-intensive components.

Sour Gas No Condensation Combined Cycle

Figure 6-4 shows the cost breakdown of the sour gas combined cycle with no condensation. For this cycle, since the working fluid doesn't condense, the temperature of the fluid entering the compressor is very high and has a high heat capacity due to the water content. Thus the flow rate of the fluid through the compressor is much higher resulting in a larger compressor size and cost. As can be seen from the graph where
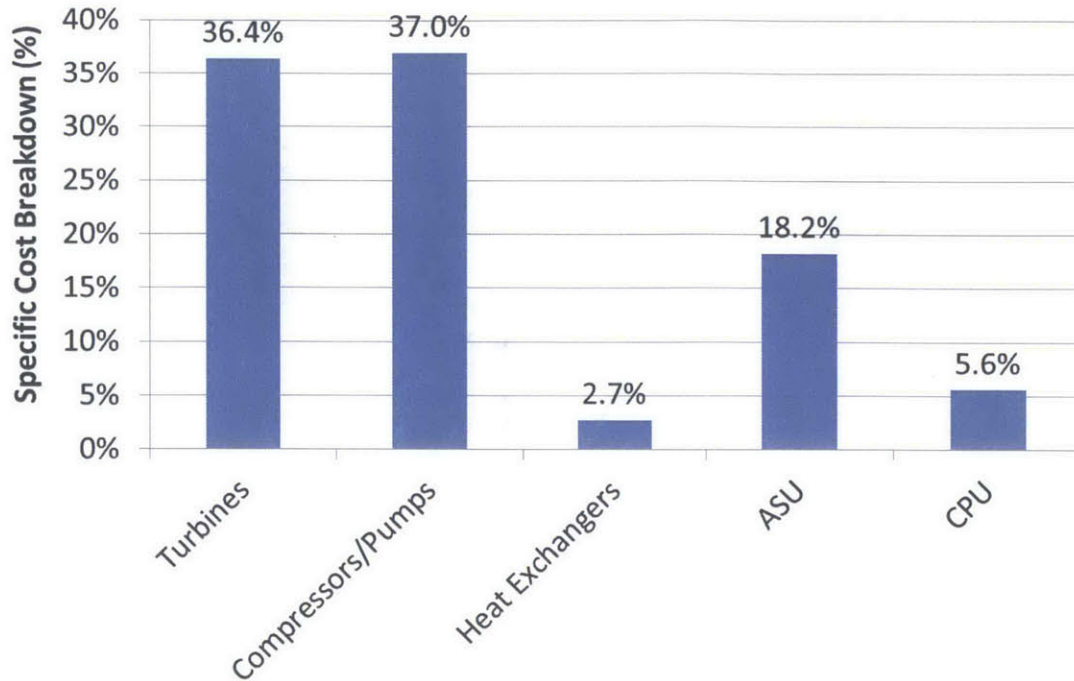
Figure 6-4: The breakdown of the specific costs for the sour gas no condensation combined cycle

the compressors and pumps for this cycle account for a much bigger contribution to the specific cost, compared to the methane cycle.

Sour Gas SO$_x$ Removal Combined Cycle

Figure 6-5 shows the cost breakdown of the sour gas combined cycle with SO$_x$ removal. Since this cycle removes the sulfur components from the working fluid before the compressor and before it is recycled to the combustor, the SS321 material wouldn't have to be used for the compressor because the probability of hot corrosion would be greatly reduced. Thus the proportion of the total cost by the compressor is decreased. Also the heat exchanger costs, which include the HRSG, are reduced because the expensive acid-resistant material also isn't being used for this cycle since the working fluid isn't condensing in the HRSG. The SO$_x$ removal system used in the main cycle, accounted for about 5% of the total specific cost which is still low compared to the larger capital-intensive processes in the ASU and turbines.
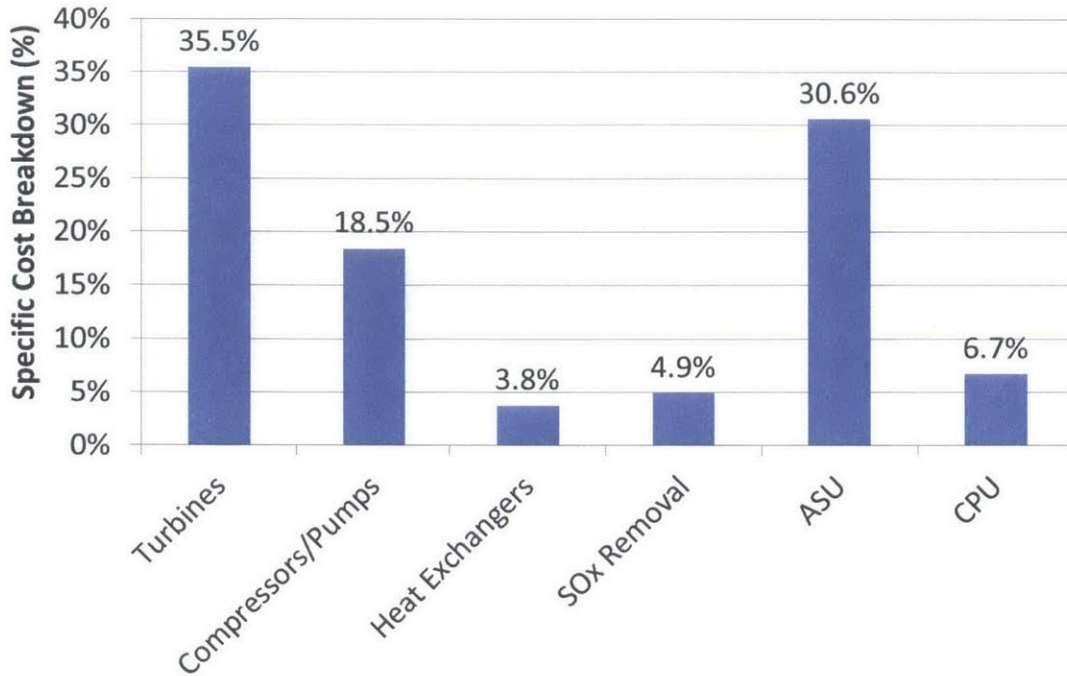
Figure 6-5: The breakdown of the specific costs for the sour gas SO_x removal combined cycle

Sour Gas Acid Resistance Water Cycle

Figure 6-6 shows the cost breakdown of the sour gas water cycle with acid resistance. Similar to the methane water cycle in Figure 6-2, the heat exchangers costs are higher than the combined cycles due to the lower condenser pressures and higher heat transfer areas. The compressors and pumps costs are also low considering that they're also one of the least power consumers in the cycle. Finally, the CPU costs for the sour gas water cycles account for a much larger share of the total cycle cost because of the low condenser pressures. The CPU will require larger compressors to recompress the CO_2 stream back up to the sequestration pressure and also, since the flow rate is very high, the SO_x removal system in the CPU is going to require larger equipment which further increase the capital costs.
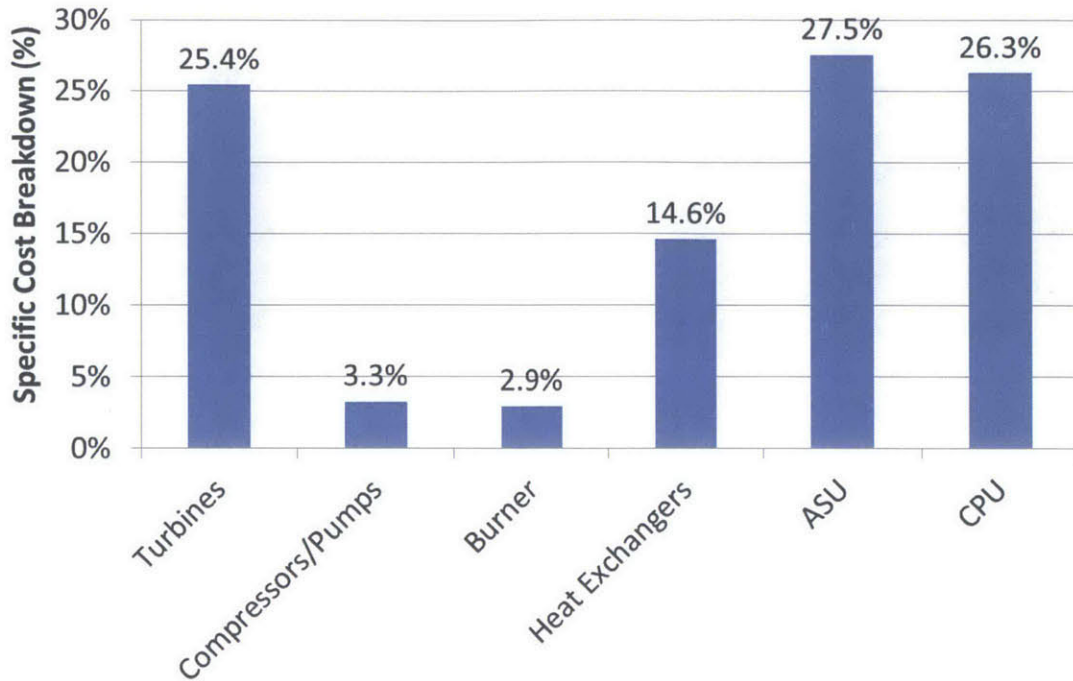
Figure 6-6: The breakdown of the specific costs for the sour gas acid resistance water cycle

Sour Gas SO_x Removal Water Cycle

Figure 6-7 shows the cost breakdown of the sour gas water cycle with SO_x removal. One glaringly unusual aspect of the cost breakdown for this cycle, is the fact that the heat exchangers have minimal impact on the total cost of the cycle. The heat exchangers include mainly just the regenerator, and since the working fluid isn't condensing, the expensive acid-resistant material isn't being used and so the costs are low. Once again for this cycle, the CPU costs are one of the more significant contributors to the cost of the whole cycle, since the cycle condenses down to low pressures and so will require larger compressors to recompress the stream for EOR applications.
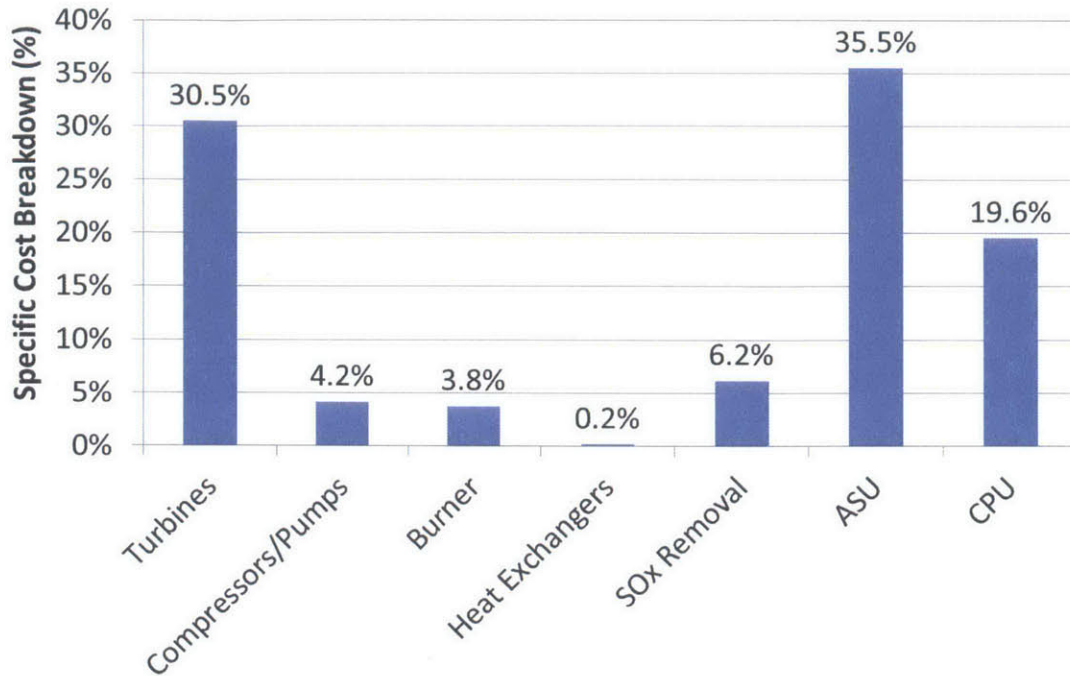
Figure 6-7: The breakdown of the specific costs for the sour gas SO_x removal water cycle

6.4.2   Comparative Cost Analysis

Equipment Costs

We have described how the specific cost of each of the cycles is broken down and what the contribution is by each component group. In order to get a better sense of how the cost estimates of these sour gas cycles compare to each other, the specific costs of each of the component groups in the cycles are presented together in Figures 6-8 to 6-11. The results are presented by taking the sour gas SO_x removal water cycle as a base cycle and all of the costs are shown as a ratio of that cycle's costs. Thus the results are normalized with respect to that cycle and this allow us to now compare all of the cycles to each other to determine which one will have the lowest cost. Just for reference, the total specific cost of that base cycle was found to be 2048 \$/kW.

Figure 6-8 shows the specific cost comparison for the turbines, compressors/pumps and burners component groups for all of the cycles. These components are some of the most capital-intensive equipments for all of the cycles as was seen in the previous

205

section. One noticeable characteristic of the CC-NC is the high compressor cost which is almost 17 times higher than the base WC-SR. The reason for this is that the inlet temperature to that compressor is very high since the working fluid doesn't condense in the cycle. As such the volume flow rate is very high, resulting in a large compressor, requiring a high amount of power to compress the working fluid. The high heat capacity of the working fluid for the CC-NC, also results in a larger turbine than the other cycles. However, for the rest of the cycles, the turbine costs are fairly similar considering they all use that same material to resist the hot corrosion.

The compressors/pumps costs for the cycles are significantly different however for all the cycles as can also be seen from Figure 6-8. We have already talked about the significantly higher cost for the CC-NC. The other combined cycles have higher costs for the pressurization equipment than the water cycles, since the water cycles only require liquid pumping and fuel compression which is less expensive than having larger compressors for the combined cycles' main cycle fluid. The CC-SR also was found to have a slightly lower compressor cost than the CC-AR because the SS321 material doesn't need to be used for the compressor in that cycle. Since the sulfur compounds are being removed from the main cycle fluid, there is no or very small probability of corrosion occurring in that compressor and so that higher cost material wouldn't have to be used, thus decreasing the overall compression cost for the CC-SR.

Next, the heat exchanger costs are compared for all of the cycles in Figure 6-9. The heat exchangers in general were not found to be large contributers to the total overall cost for all of the cycles, as was seen in the previous section, the heat exchangers only accounted for up to about 9% of the total specific cost. But notwithstanding, there were very significant differences in the heat exchanger costs for all of the cycles. As can be seen from the figure, the rest of the cycles had much higher heat exchanger costs than the base WC-SR. For all of the cycles where the working fluid doesn't condense, CC-NC, CC-SR and WC-SR, heat exchanger costs were lower because the expensive acid-resistant material did not have to be used for the regenerator and HRSG and the heat exchanger was smaller. The heat exchanger costs for the WC-AR is also much higher than its equivalent combined cycle, CC-AR, almost twice as expensive. This

206
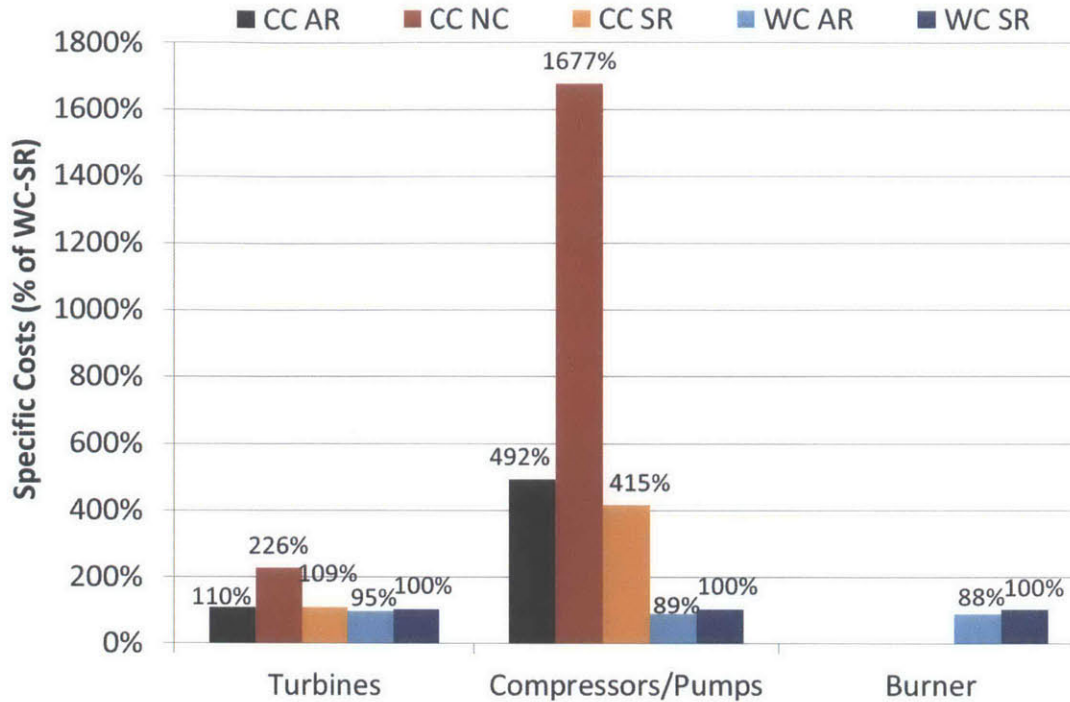
Figure 6-8: The turbine, compressor, pump and burner specific cost comparison for the sour gas cycles (as a % of the WC-SR cycle)

is because the water cycles expand down to much lower condenser pressures than the combined cycles and so the flow rate is higher resulting in large heat exchanger areas and thus higher costs. For that specific cycle this greatly increases the costs also because the amount of acid-resistant material that has to be used, goes up as well.

The SO_x removal system, ASU and CPU costs are now compared for all of the cycles in Figure 6-10. The SO_x removal system cost was only presented for the CC-SR and WC-SR cycles since that is a key feature of them. Whereas for the other cycles, the CPU cost has the SO_x removal process already included. As such the CPU costs for the cycles CC-AR and CC-NC are higher than for CC-SR, and similarly WC-AR was higher than WC-SR. The CPU costs for the water cycles were also found to be on average about 3 times higher than those of the combined cycles, since the condenser pressures are lower, the CO_2 stream requires more compression stages and thus a greater cost to get the stream up to the 110 bar for EOR.

The 'ASU' component includes the oxygen stream production and compression
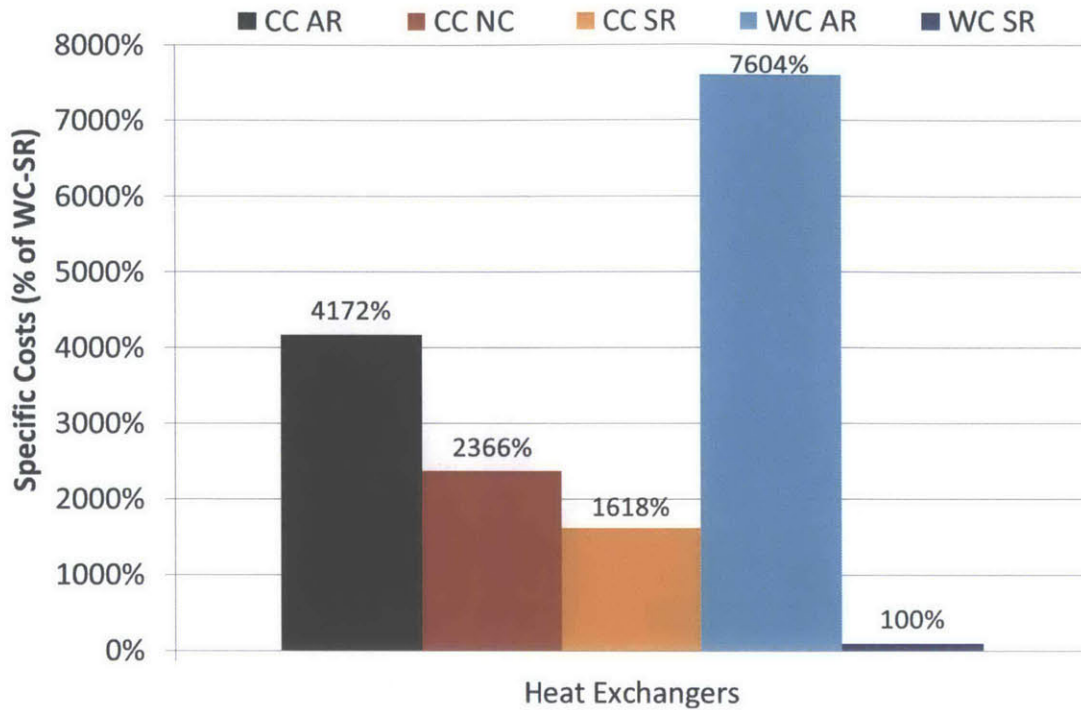
Figure 6-9: The heat exchanger specific cost comparison for the sour gas cycles (as a % of the WC-SR cycle)

up to the required operating pressure. It was found that the ASU costs for the water cycles were slightly higher than those of the combined cycles, similar to the CPU, the water cycles' combustors operate at higher pressures and so more compression of the O_2 stream is required which increases costs in the ASU. Comparing the two SO_x removal systems for the two cycles, it is seen that the water cycle's system has about 1.3 times the cost of the combined cycle. Once again, since the water cycle expands down to lower pressures, this increases the flow rate and leads to much greater amounts of water required in the SO_x removal system in order to condense and purify the vapor stream. This was shown in section 5.3.1. Consequently, bigger equipment are required and thus higher costs for the SO_x removal.

Finally the total specific costs were calculated and presented for all of the cycles as can be seen in Figure 6-11. All of the costs differences for each of the different component groups presented earlier, combine to give the total cost variations shown in the figure. As was expected earlier in the cycle analyses in the previous chapters,
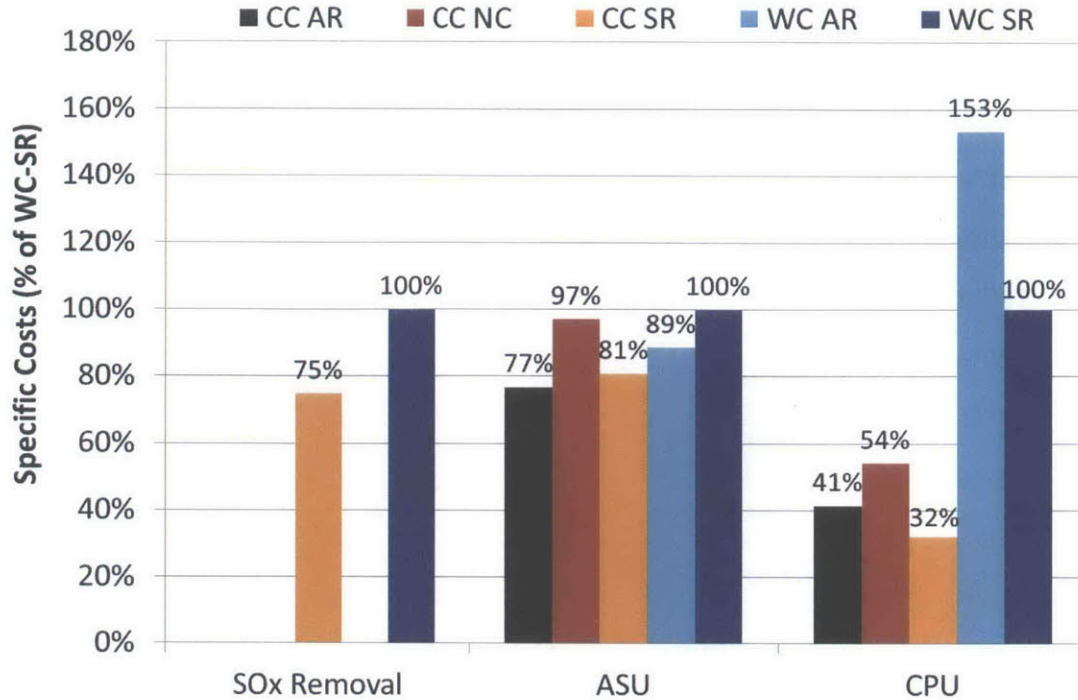
Figure 6-10: The SO_x removal system, ASU and CPU specific cost comparison for the sour gas cycles (as a % of the WC-SR cycle)

the two SO_x removal cycles were found to have overall lower costs than their acid resistance equivalents. Costs savings are achieved from the fact that the expensive acid resistant materials don't need to be used for these cycles since the working fluid doesn't condense. Also, as it turns out, although the acid resistance cycles have higher efficiencies than the SO_x removal ones, their cycle costs are slightly higher. Therefore a tradeoff would have to be made between cost and cycle performance. However for the CC-NC case, the cycle both has a low efficiency and high costs which means that it would probably not be the best option to use for this fuel. Ultimately the order of the cycles in terms of overall equipment cost from the cheapest to the most expensive is as follows: CC-SR $\rightarrow$ CC-Ar $\rightarrow$ WC-SR $\rightarrow$ WC-AR $\rightarrow$ CC-NC.

LCOE

The total equipment costs that were calculated before for the cycles, were used as the Bare Erected Costs (BEC) when calculating the Levelized Cost of Electricity (LCOE).

209
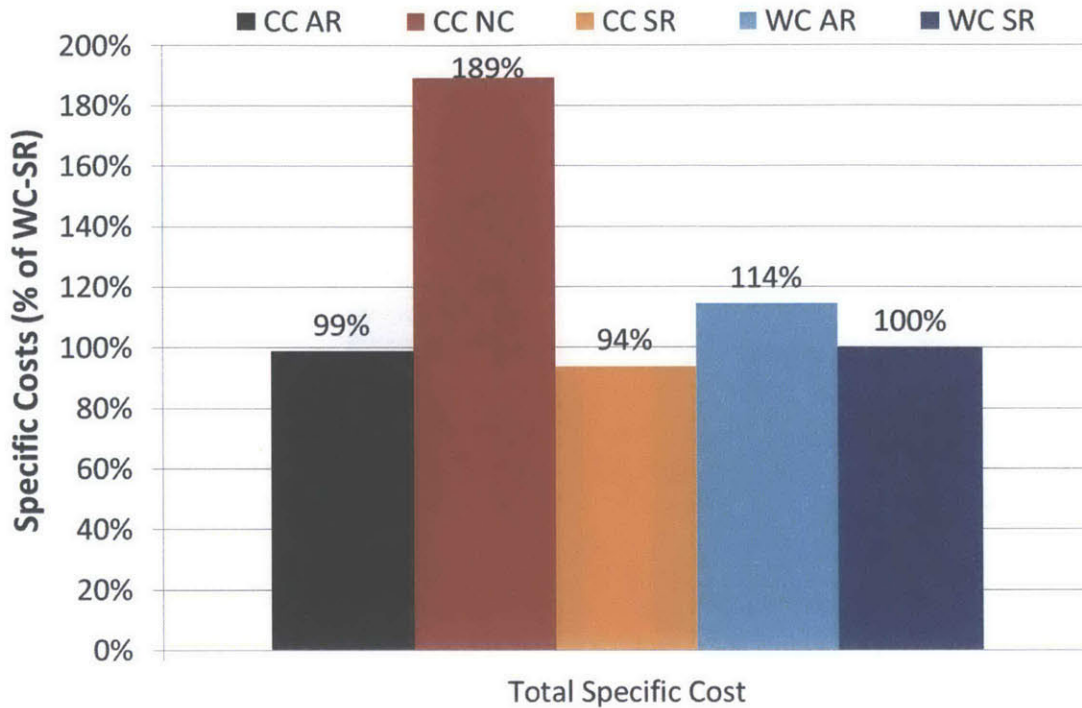
Figure 6-11: The total specific cost comparison for the sour gas cycles (as a % of the WC-SR cycle)

The LCOE calculation that was performed was based on the guidelines and assumptions discussed in the NETL report, Quality Guidelines for Energy System Studies: Cost Estimation Methodology for NETL Assessments of Power Plant Performance [72] and the assumptions that were used in this study are listed in Table 6.1. The results from this calculation are shown in Figure 6-12 were the LCOE is shown for all of the cycles. It can be seen that similar trends and relative results are observed to those in the previous section where the specific costs were compared. The difference here is that the impact of the cycle efficiency also plays a big role because the fuel cost is included in the LCOE calculations. The low efficiencies of the water cycles versus the combined cycles and the low efficiency of the CC-NC also contributes to higher LCOE's since the work output by those cycles are smaller than the others for the same fuel input. The CC-NC also had the highest equipment cost which along with the low cycle efficiency, further escalated the costs of this cycle resulting in a very high LCOE. Therefore a similar conclusion to before is drawn, in that the CC-SR has

Parameter	Value
Engineering, Procurement and Construction Cost (EPCC)	
Engineering, Procurement and Construction (EPC) Contractor Services	9% of BEC
Total Plant Cost (TPC)	
Process Contingency	30% of EPCC
Project Contingency	25% of EPCC + Process Contingency
Total Overnight Cost (TOC)	
Owner's Costs	17.5% of TPC
Global Economic Assumptions	
Operational Period	25 years
Plant Capacity Factor	90%
Internal Rate of Return on Equity	10%
Income Tax Rate	38% Effective
Capital Depreciation	25 years, 200% declining balance
Variable O&M Costs Factor	1.5% of EPCC
Fixed O&M Costs Factor	3.5% of EPCC
Fuel Cost (only natural gas)	3 $/MMBTU [73]
Escalation of COE (revenue), O&M Costs, Fuel Costs (nominal annual rate)	3%

Table 6.1: LCOE economic modeling assumptions

the lowest LCOE out of all of the other cycles and the CC-AR's LCOE is close but still higher. The CC-NC once again has the poorest economic performance with the highest LCOE out of all the cycles.

6.5 Conclusions

The preliminary cost analysis was performed on these cycles and provided a better understanding of how the costs are broken down and the key components that were the most capital-intensive were identified. The levelized cost of electricity was also calculated for these cycles to bring in the impact of cycle efficiency and a comparison was done in order to give a sense of the relative economic performance of these cycles and allowed us to identify the least and most expensive ones. The water cycles on average had higher costs than the combined cycles due to the fact that they condense
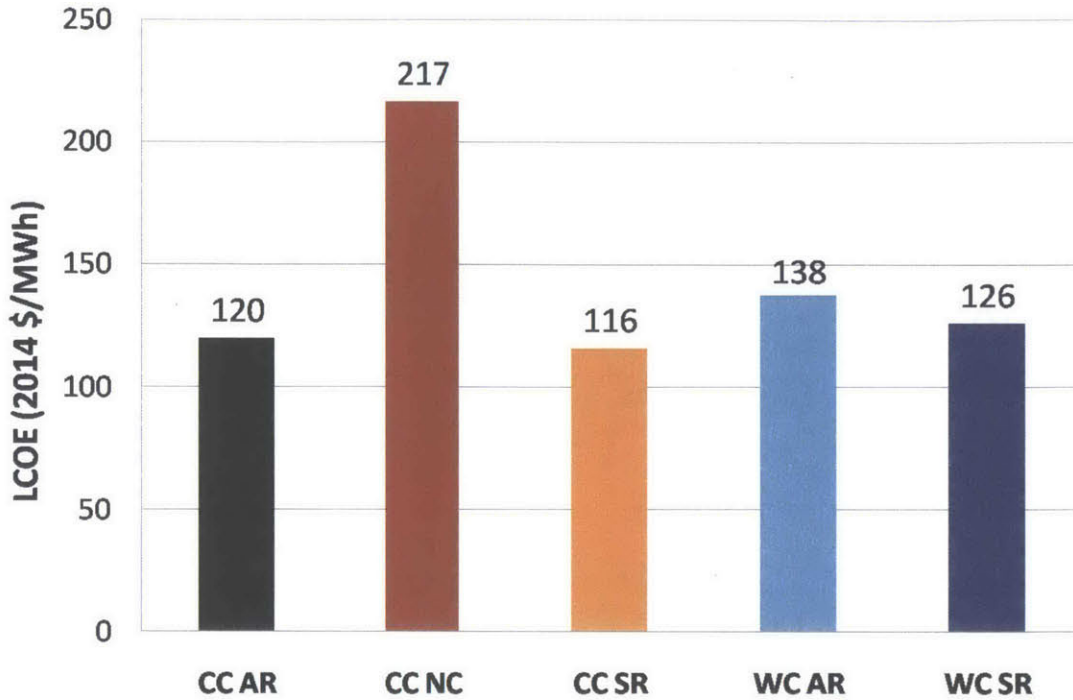
Figure 6-12: Levelized cost of electricity comparison for the sour gas cycles

down to lower pressures and so higher heat exchangers are needed which increases costs. Another issue with this low pressure is that in the CPU, more compression is needed to recompress the CO_2 for EOR which also results in further cost penalties. As was expected when first constructing the sour gas cycles, the SO_x Removal cycles turned out to have lower costs then their Acid Resistance equivalents due to the expensive materials being used in these cycles. Therefore those cycle configurations could be used but at the expense of lower efficiencies.

From a purely economic point of view, the performance ranking of these cycles were as follows: Combined Cycle SO_x Removal, Combined Cycle Acid Resistance, Water Cycle SO_x Removal, Water Cycle Acid Resistance, and then once again the worst was the Combined Cycle No Condensation.

Chapter 7

Conclusions

7.1 Summary

A detailed analysis of oxy-fuel power cycles utilizing sour natural gas as the fuel has been performed. A thorough literature review was done on gas fired oxy-fuel power cycles, but in all of the previous studies, pure methane was used as the fuel and sour gas was never looked at. The literature review allowed us to understand the different cycle layouts that are used for natural gas oxy-fuel cycles, and these would form the base cycles when constructing and analyzing the sour gas cycles. The semi-closed oxy-combustion combined cycle (SCOC-CC) and the water cycle were determined to be the simplest and most feasible cycles to use as the bases for the sour gas cycles. These two types of cycles (combined and water), were further subdivided into 2-3 more configurations, for the sour gas cycles, of addressing the issues and limitations due to the presence of sulfur compounds in these cycles.

For the combined cycle types, three further possibilities were modeled: Acid Resistance, No Condensation and SO_x Removal. Similarly for the water cycles, an Acid Resistance and a SO_x Removal cycle were considered. Pressure parametric studies were done on the two cycle types in order to provide the optimal operating pressures, and to give a better understanding of the pressure dependence on the system performance. The SO_x removal system employed in these cycles, was explained and discussed in great detail and a sensitivity study was also done to determine what the

impact of this system's operating conditions were on the overall cycle's performance. Then each of these five cycles were analyzed and compared with their corresponding cycle types and also all together, in order to determine how these cycle's perform and which cycle performs best. Out of the three combined cycles, the Acid Resistance cycle was found to have the highest efficiency followed by the SO_x Removal cycle then the No Condensation cycle. The main reason why the Acid Resistance cycle performed best was because of the fact that the working fluid is allowed to condense in the HRSG and so most of its latent heat is recuperated by producing steam for the steam cycle thus producing more work. The No Condensation cycle had the worst efficiency due to the fact that the working fluid doesn't condense, and also because the inlet temperature to the compressor for this cycle is high resulting in more power required to compress this stream up to the combustor pressure.

A similar performance comparison was done for the two water cycles and it was found that once again, the Acid Resistance cycle had the better efficiency. Comparing all of the five cycles together now, the combined cycles on average performed better due to the fact that liquid water is being recycled in the water cycles which decreases the overall performance of these cycles. Therefore from a purely technical point of view, the performance ranking of these cycles were as follows: Combined Cycle Acid Resistance, Combined Cycle SO_x Removal, Water Cycle Acid Resistance, Water Cycle SO_x Removal, and then the worst was the Combined Cycle No Condensation.

A preliminary cost analysis was also done on these cycles and provided a better understanding of how the costs are broken down and the key components that were the most capital-intensive were identified. The levelized cost of electricity was also calculated for these cycles to bring in the impact of cycle efficiency and a comparison was done in order to give a sense of the relative economic performance of these cycles and allowed us to identify the least and most expensive ones. The water cycles on average had higher costs than the combined cycles due to the fact that they condense down to lower pressures and so larger heat exchangers are needed which increases costs. Another issue with this low pressure is that in the CPU, more compression is needed to recompress the CO_2 for EOR which also results in further cost penalties.

214

From a purely economic point of view, the performance ranking of these cycles were as follows: Combined Cycle SO_x Removal, Combined Cycle Acid Resistance, Water Cycle SO_x Removal, Water Cycle Acid Resistance, and then once again the worst was the Combined Cycle No Condensation.

In conclusion, to bring this whole study together and going back to our project goals, one of the main objectives of this study was identifying the best possible cycle(s) to use for this new and unusual fuel (sour gas) from a techno-economic perspective. Since we are considering the fuel to be cheap, since no major processing and purifying steps need to be done to the extracted gas, sacrificing some efficiency points at the expense of a less costly system would not be a major issue. Therefore from this whole analysis it seems that the best process cycle to use is the Combined Cycle SO_x Removal followed by the Combined Cycle Acid Resistance.

7.2 Future Work

7.2.1 Optimization

Although some of the cycles' operating conditions were chosen to maximize efficiency, there is still room to optimize other design variables and performance parameters of the existing processes in order to maximize efficiency and also reduce the costs. This will make these cycles more viable and promising options for power plants with carbon capture and sequestration in the future.

7.2.2 Cost Estimation

The cost estimates presented in this study are still preliminary and require some updates and further verification. Aspen Plus is not well-known for costing power cycles, and specifically turbines and combustors, and so to achieve more reliable cost estimates, these issues need to be addressed by further literature investigations and possibly comparisons with other costing modules. Also some of the criteria for material selection was based on their availability in Aspen Plus and so this needs to

be validated by further comparisons with other published cost estimates for similar systems.

7.2.3 Detailed Combustor Modeling

Since there are not any studies in the literature on sour gas combustion and power cycles, after this cycle and performance analyses, the next step should be a detailed combustor design modeling. Determining the combustion characteristics of sour gas in a pure oxygen environment are vital to designing a combustor that can handle these conditions and give us better estimates of the emissions and pressure drops. A CFD modeling of oxy-fuel combustion of sour gas should be done looking at the effects of pressure on the combustion process and flame characteristics. The diluents for these cycles are also different, CO_2 vs H_2O. Therefore there are a lot of things that can be obtained from a CFD analysis on the oxy-fuel combustion of sour gas by looking at different operating conditions and how they pertain to the actual power cycles integration.

Bibliography

[1] United States Environmental Protection Agency (EPA). Global Greenhouse Gas Emissions Data. http://www.epa.gov/climatechange/ghgemissions/global.html, 2013.

[2] Energy Information Administration. International energy outlook, report doe/eia-0484,. 2013.

[3] Core Energy Holdings. Geologic CO2 Sequestration. http://coreenergyholdings.com/GeologicCO2Sequestration.html, 2013.

[4] Bert Metz, Ogunlade Davidson, HC De Coninck, Manuela Loos, and LA Meyer. Ipcc, 2005: Ipcc special report on carbon dioxide capture and storage. prepared by working group iii of the intergovernmental panel on climate change. *Cambridge, United Kingdom and New York, NY, USA, 442 pp*, 2005.

[5] Brentan R Alexander. *Analysis and optimization of the Graz cycle: a coal fired power generation scheme with near-zero carbon dioxide emissions*. PhD thesis, Massachusetts Institute of Technology, 2007.

[6] Jongsup Hong, Gunaranjan Chaudhry, JG Brisson, Randall Field, Marco Gazzino, and Ahmed F Ghoniem. Analysis of oxy-fuel combustion power cycle utilizing a pressurized coal combustor. *Energy*, 34(9):1332–1340, 2009.

[7] Arthur Darde, Rajeev Prabhakar, Jean-Pierre Tranier, and Nicolas Perrin. Air separation and flue gas compression and purification units for oxy-coal combustion systems. *Energy Procedia*, 1(1):527–534, 2009.

[8] Jongsup Hong, Patrick Kirchen, and Ahmed F Ghoniem. Laminar oxy-fuel diffusion flame supported by an oxygen-permeable-ion-transport membrane. *Combustion and Flame*, 160(3):704–717, 2013.

[9] US Energy Information Administration. Average national levelized costs for generating technologies in 2018. 2011.

[10] Daniel Fleig, Fredrik Normann, Klas Andersson, Filip Johnsson, and Bo Leckner. The fate of sulphur during oxy-fuel combustion of lignite. *Energy Procedia*, 1(1):383 – 390, 2009. Greenhouse Gas Control Technologies 9 Proceedings of the 9th International Conference on Greenhouse Gas Control Technologies (GHGT-9), 1620 November 2008, Washington DC, {USA}.

[11] Sang Hyun Tak, Sung Ku Park, Tong Seop Kim, Jeong Lak Sohn, and Young Duk Lee. Performance analyses of oxy-fuel power generation systems including co2 capture: comparison of two cycles using different recirculation fluids. *Journal of mechanical science and technology*, 24(9):1947–1954, 2010.

[12] Wolfgang Sanz, Herbert Jericha, Bernhard Bauer, and Emil GÄŗttlich. Qualitative and quantitative comparison of two promising oxy-fuel power cycles for co2 capture. *Journal of Engineering for Gas Turbines and Power*, 130(3):031702, 2008.

[13] F Franco, Theo Mina, G Woolatt, Mike Rost, and Olav Bolland. Characteristics of cycle components for co2 capture. In *Proceedings of 8th International Conference on Greenhouse Gas Control Technologies, Trondheim, Norway*, 2006.

[14] G Corchero, VP Timon, and JL Montanes. A natural gas oxy-fuel semiclosed combined cycle for zero co2 emissions: a thermodynamic optimization. *Proceedings of the Institution of Mechanical Engineers, Part A: Journal of Power and Energy*, 225(4):377–388, 2011.

[15] Olav Bolland and Philippe Mathieu. Comparison of two co2 removal options in combined cycle power plants. *Energy Conversion and Management*, 39(1618):1653 – 1663, 1998.

[16] C Gou, R Cai, and H Hong. An advanced oxy-fuel power cycle with high efficiency. *Proceedings of the Institution of Mechanical Engineers, Part A: Journal of Power and Energy*, 220(4):315–325, 2006.

[17] JD Overton T.W. and Patel S. Next generation of gas-fired power starts to take shape. *Power Magazine*, 2012.

[18] Roger Anderson, Fermin Viteri, Rebecca Hollis, Ashley Keating, Jonathan Shipper, Gary Merrill, Cora Schillig, Sachin Shinde, James Downs, Daniel Davies, et al. Oxy-fuel gas turbine, gas generator and reheat combustor technology development and demonstration. In *ASME Turbo Expo 2010: Power for Land, Sea, and Air*, pages 733–743. American Society of Mechanical Engineers, 2010.

[19] Clean Energy Systems. Advanced turbine developments for oxy-combustion trigen plants. *WESTCARB Business Meeting*, 2012.

[20] Olav Bolland, Hanne M Kvamsdal, and John C Boden. A thermodynamic comparison of the oxy-fuel power cycles water-cycle, graz-cycle and matiant-cycle. In *Power generation and sustainable development. International conference*, pages 293–298, 2001.

[21] Ovidiu Marin, Yves Bourhis, Nicolas Perrin, Pietro Di Zanno, Fermin Viteri, and Roger Anderson. High efficiency, zero emission power generation based on a high-temperature steam cycle. In *28th International Technical Conference on Coal Utilization and Fuel Systems, Clearwater, Florida*. Citeseer, 2003.

[22] Wolfgang Sanz, Herbert Jericha, Florian Luckel, and F Heitmeir. A further step towards a graz cycle power plant for co2 capture. *ASME Paper GT2005-68456, ASME Turbo Expo*, 2005.

[23] Herbert Jericha, W Sanz, J Woisetschläger, and M Fesharaki. Co2-retention capability of ch4/o2-fired graz cycle. *CIMAC Paper G*, 7, 1995.

[24] Wolfgang Sanz, Carl-W Hustad, and Herbert Jericha. First generation graz cycle power plant for near-term deployment. In *ASME 2011 Turbo Expo: Turbine Technical Conference and Exposition*, pages 969–979. American Society of Mechanical Engineers, 2011.

[25] S Rezvani, O Bolland, F Franco, Ye Huang, R Span, J Keyser, F Sander, D McIlveen-Wright, and Neil Hewitt. Natural gas oxy-fuel cyclespart 3: Economic evaluation. *Energy Procedia*, 1(1):565–572, 2009.

[26] Aspen Technologies Inc. Aspen Plus, 2012.

[27] Jongsup Hong. Techno-economic analysis of pressurized oxy-fuel combustion power cycle for CO2 capture. Master's thesis, Massachusetts Institute of Technology, Cambridge, MA, USA, 2009.

[28] Chukwunwike Ogbonnia Iloeje. Process modeling and analysis of CO2 purification for oxy-coal combustion. Master's thesis, Massachusetts Institute of Technology, Cambridge, MA, USA, 2011.

[29] Daniel Fleig, Mara. U. Alzueta, Fredrik Normann, Mara Abin, Klas Andersson, and Filip Johnsson. Measurement and modeling of sulfur trioxide formation in a flow reactor under post-flame conditions. *Combustion and Flame*, 160(6):1142 – 1151, 2013.

[30] Marsulex Environmental Technologies. Flue Gas Desulfurization System, 2011.

[31] Erika De Visser, Chris Hendriks, Maria Barrio, Mona J Mølnvik, Gelein de Koeijer, Stefan Liljemark, and Yann Le Gallo. Dynamis co2 quality recommendations. *International Journal of Greenhouse Gas Control*, 2(4):478–484, 2008.

[32] Total France. Sour gas: A history of expertise. 2007.

[33] W.F.J. Burgers, P.S. Northrop, H.S. Kheshgi, and J.A. Valencia. Worldwide development potential for sour gas. *Energy Procedia*, 4(0):2178–2184, 2011. 10th International Conference on Greenhouse Gas Control Technologies.

[34] Hanne M. Kvamsdal, Kristin Jordal, and Olav Bolland. A quantitative comparison of gas turbine cycles with capture. *Energy*, 32(1):10 – 24, 2007.

[35] Mark Maslin. *Global warming: a very short introduction*. Oxford University Press, 2008.

219

[36] NOAA ESRL Global Monitoring Division. Mauna Loa CO2 Annual Mean Data. `ftp://ftp.cmdl.noaa.gov/ccg/co2/trends/co2_annmean_mlo.txt`. Accessed: 01-07-2013.

[37] NOAA National Climate Data Center. Global Surface Temperature Anomalies. `http://www.ncdc.noaa.gov/cmb-faq/anomalies.php`, 2012.

[38] Kyoto Protocol. United nations framework convention on climate change. 2010.

[39] ICO2N. Enhanced Oil Recovery a significant economic opportunity to help jump-start Carbon Capture and Storage. `http://www.ico2n.com/wp-content/uploads/2011/08/ICO2N-EOR-Fact-Sheet.pdf`, 2011.

[40] National Enhanced Oil Recovery Initiative (NEORI). Carbon dioxide enhanced oil recovery: A critical domestic energy, economic, and environmental opportunity. 2012.

[41] Olav Bolland and Henriette Undrum. Removal of co2 from natural gas fired combined cycle plants. volume 99, 1999.

[42] Lei Chen, Sze Zheng Yong, and Ahmed F Ghoniem. Oxy-fuel combustion of pulverized coal: Characterization, fundamentals, stabilization and cfd modeling. *Progress in Energy and Combustion Science*, 38(2):156–214, 2012.

[43] DOE. Clean Coal Technology & The Clean Coal Power Initiative. `http://www.fossil.energy.gov/programs/powersystems/cleancoal`, 2012.

[44] Chao Fu and Truls Gundersen. Using exergy analysis to reduce power consumption in air separation units for oxy-combustion processes. *Energy*, 44(1):60–68, 2012.

[45] Paul N Dyer, Robin E Richards, Steven L Russek, and Dale M Taylor. Ion transport membrane technology for oxygen separation and syngas production. *Solid State Ionics*, 134(1):21 33, 2000.

[46] Rohan Stanger and Terry Wall. Sulphur impacts during pulverised coal combustion in oxy-fuel technology for carbon capture and storage. *Progress in Energy and Combustion Science*, 37(1):69 – 88, 2011.

[47] H. Li, J. Yan, J. Yan, and M. Anheden. Impurity impacts on the purification process in oxy-fuel combustion based {CO2} capture and storage system. *Applied Energy*, 86(2):202 – 213, 2009. {IGEC} {III} Special Issue of the Third International Green Energy Conference (IGEC-III), June 1820, 2007, Vsters, Sweden.

[48] R Anderson, H Brandt, and H Mueggenburg. A power plant concept which minimizes the cost of carbon dioxide sequestration and eliminates the emission of atmospheric pollutants. *Greenhouse Gas Control Technologies*, page 59, 1999.

[49] Roger E Anderson, Scott MacAdam, Fermin Viteri, Daniel O Davies, James P Downs, and Andrew Paliszewski. Adapting gas turbines to zero emission oxy-fuel power plants. In *ASME Turbo Expo 2008: Power for Land, Sea, and Air*, pages 781 791. American Society of Mechanical Engineers, 2008.

[50] G. Woollatt and F. Franco. Natural gas oxy-fuel cyclespart 1: Conceptual aerodynamic design of turbo-machinery components. *Energy Procedia*, 1(1):573 580, 2009. Greenhouse Gas Control Technologies 9 Proceedings of the 9th International Conference on Greenhouse Gas Control Technologies (GHGT-9), 1620 November 2008, Washington DC, {USA}.

[51] Drew Robb. Special report: Supercritical co2the next big step? *Turbomachinery International*, 53(5):22, 2012.

[52] EI Yantovskii, KN Zvagolsky, and VA Gavrilenko. Computer exergonomics of power plants without exhaust gases. *Energy Conversion and Management*, 33(5):405–412, 1992.

[53] DP Hochstein. Carbon dioxide power cycle. *Soviet Boiler and turbine construction*, (10):420–423, 1940.

[54] Carl-W Hustad. Optimization of thermodynamically efficient nominal 40 mw zero emission pilot and demonstration power plant in norway. In *ASME Turbo Expo 2005: Power for Land, Sea, and Air*, pages 271–278. American Society of Mechanical Engineers, 2005.

[55] Herbert Jericha, Emil Gottlich, Wolfgang Sanz, and Franz Heitmeir. Design optimisation of the graz cycle prototype plant. In *ASME Turbo Expo 2003, collocated with the 2003 International Joint Power Generation Conference*, pages 113- 121. American Society of Mechanical Engineers, 2003.

[56] H Jericha, W Sanz, E Gottlich, and F Neumayer. Design details of a 600 mw graz cycle thermal power plant for co2 capture. In *ASME Turbo Expo 2008: Power for Land, Sea, and Air*, pages 507–516. American Society of Mechanical Engineers, 2008.

[57] National Energy Technology Laboratory. Quality guidelines for energy system studies: Process modeling design parameters. *U.S. Department of Energy*, 2012.

[58] Clean Energy Systems. http://www.cleanenergysystems.com. Accessed: 02-24-2014.

[59] Ravi K Srivastava and Wojciech Jozewicz. Flue gas desulfurization: The state of the art. *Journal of the Air & Waste Management Association*, 51(12):1676–1688, 2001.

[60] National Lime Association. Flue Gas Desulfurization, 2012.

[61] R Gaikwad, WL Boward, and W DePriest. Wet flue gas desulfurization technology evaluation. *Sargent and Lundy, LLC, prepared for National Lime Association, project*, (11311-000), 2003.

[62] Hussam Zebian, Nicola Rossi, Marco Gazzino, Danila Cumbo, and Alexander Mitsos. Optimal design and operation of pressurized oxy-coal combustion with a direct contact separation column. *Energy*, 49:268–278, 2013.

[63] U.S. Department of Energy National Energy Technology Laboratory. Advanced oxy-combustion technology development and scale-up for new and existing coal-fired power plants. (DE-FOA-0000636), 2012.

[64] N Eliaz, G Shemesh, and RM Latanision. Hot corrosion in gas turbine components. *Engineering failure analysis*, 9(1):31–43, 2002.

[65] George Y Lai. *High-temperature corrosion and materials applications*. ASM International, 2007.

[66] Aspen Technologies Inc. Aspen Icarus Reference Guide, 2013.

[67] eMachineShop. Stainless Steel Alloys. http://www.emachineshop.com/machine-shop/Stainless-Steel-Alloys/page515.html. Accessed: 04-06-2014.

[68] CN Alloys Ltd. http://www.cnalloys.co.uk/stainless-steel. Accessed: 04-06-2014.

[69] David Thomas and Sally Benson. *Carbon Dioxide Capture for Storage in Deep Geologic Formations-Results from the CO2 Capture Project: Vol 1-Capture and Separation of Carbon Dioxide from Combustion, Vol 2-Geologic Storage of Carbon Dioxide with Monitoring and Verification*. Elsevier, 2005.

[70] Carpenter. 20Cb-3 Stainless Technical Data Sheet, 2011.

[71] LE Shoemaker and James R Crum. Experience in effective application of metallic materials for construction of fgd systems, 2010.

[72] National Energy Technology Laboratory. Quality guidelines for energy system studies: Cost estimation methodology for netl assessments of power plant performance. *U.S. Department of Energy*, 2011.

[73] US Energy Information Administration. Natural gas. 2014.